OCULAR ACCOMMODATION CONTROL AND ADAPTIVE OPTICS

The development of monocular and binocular adaptive optics instrumentation for the study of accommodation and convergence, and study of the monocular accommodative response to rapid changes in dioptric stimuli

Alistair Paul CURD

Submitted for the degree of
Doctor of Philosophy

Bradford School of Optometry and Vision Science
School of Life Sciences
University of Bradford

2014

Abstract

Ocular accommodation control and adaptive optics

Alistair Paul Curd

Keywords: Ocular accommodation control, adaptive optics, aberrations, latency, instrumentation, convergence, myopia

The relationship between accommodation and myopia has been under investigation for many years, and the effort to understand it is ongoing.

In this thesis, an introduction to the state of myopia research is given first, with particular reference to studies of accommodation and higher-order ocular aberrations, which feature in the subsequent chapters.

Following a brief introduction to the general technique of aberrometry and visual stimulus control using adaptive optics, the development of a monocular adaptive optics instrument for this purpose is described. The instrument is used to vary a dioptric stimulus and record the accommodation response in pilot studies and a detailed experiment, which has also been published elsewhere. It is found, among other things, that accommodation can respond to more than one different input level during its latency period, and that such inputs can be stored until components of the accommodation control system are free to process them. Indications of a minimum halting time for accommodation, of around 0.6 s, are presented.

In later chapters, the development and testing of a new, binocular adaptive optics apparatus will be found. As well as binocular aberrometry and adaptive optics control of stimulus aberrations, this instrument displaces images to allow for and stimulate ocular convergence in binocular accommodation experiments. It is the first instrument in the world with its combined functionalities.

Finally, the contribution of this thesis is summarised, and further instrumentation development and experiments are put forward for the continuation of this branch of accommodation and myopia research.

Acknowledgements

First, credit where credit is due, and unending thanks and praise to God, for the beauty and order of things—even if the world has been subjected to increasing entropy for a while—and for my exciting journey to Bradford and to this time of study! Let us not be those who “see, but never perceive” what You have done.

To Joy: Thank you for caring for us so well, especially when the pressure has been on.

Many thanks to my supervisors, Prof. Mallen and Dr. Cufflin, for pointing me in the right directions. In particular, thanks to Ed for many good hours in the lab, his garage and outside. It would have taken a lot longer without his metalwork and electronics! Thanks too for probably a good bathful of coffee, and perhaps a paddling pool’s worth of beer.

Many thanks also to Dr. Karen Hampson for all her work in designing the systems before my work started on them, and on the code.

To the whole department—it’s been great to be here with you.

To my friends in G39: it has been fun! Good times. I’m not going to list you all, but you all know who you are! See you again soon (but please, let’s not go to Lahore this time).

Contents

List of figures

List of tables

1 Context

1.1 Introduction

1.1.1 The myopia problem

Recent research on myopia has been driven by a compound concern. First, myopia is common in most industrialised countries, and widespread in some (Kempen et al., 2004; Pan et al., 2012a); in East Asia, clinicians write of "an epidemic" (Grosvenor, 2003; Saw, 2003; Morgan and Rose, 2005). Quek et al. (2004) found myopia (spherical equivalent refraction, SER ≤ −0.50 D)* in 74% of 946 Singaporean students, aged between 14 and 19 years; 6% were highly myopic (SER ≤ −6.00 D). Lee et al. (2013) found 86% of 5,048 male 18 to 24 year-olds were myopic in Taiwan; 21% of their population sample was highly myopic (same definitions).

Second, the prevalence of myopia appears to have increased significantly over recent decades. In the USA, prevalence† among persons aged 12–54 years increased from 25% to 42% between 1971–1972 and 1999–2004; the prevalence of myopia beyond SER of −7.9 D increased eight-fold, from 0.2% to 1.6% (Vitale et al., 2009). This increase is visible around much of the world (Morgan and Rose, 2005), and is discussed further in section 1.2.2.

Myopia is an economic and social burden to countries and individuals: spectacles, contact lenses and refractive surgery cost money. The direct cost of myopia correction, per year, had risen to at least $3.8 billion in the USA in 2002 (Vitale et al., 2006), and is approximately $755 million in Singapore (Zheng et al., 2013). There is also a social cost, where fewer people are able to choose

* SER = spherical error + (cylindrical error ÷ 2)

† Myopes were defined as those wearing a right-eye prescription with SER < 0, or with a measured refraction of SER < 0 if presenting VA ≤ 20/50.

certain careers, and carry out certain critical roles, e.g. in the fire service, police or army (Edwards, 1998; Association of Optometrists, 2014).

A major part of the concern is the sight-threatening pathologies associated with high myopia in particular, including maculopathies, retinal detachment and other chorioretinal conditions (Saw et al., 2005; Hayashi et al., 2010; Morgan et al., 2012). The thickness of the subfoveal choroid has been found to decrease in both adults and children with increasing myopia (Ho et al., 2013; Read et al., 2013; Wei et al., 2013) and is thinner in the more myopic eye in myopic anisometropia (Vincent et al., 2013). This thinning may lead to a lack of nourishment to the retina, and there is an association between glaucoma and myopia, particularly high myopia (Marcus et al., 2011), that has been postulated to be causal, at least for high myopia (Ma et al., 2014).

1.1.2 Myopia development and eye growth

Children generally begin life with hyperopia (Saunders, 1995), which decreases as the eye grows (Sorsby et al., 1961; Sorsby and Leary, 1970). To compensate for growth of the axial length of the eye, the focussing powers of the cornea and crystalline lens decrease; this process is termed “emmetropisation”. The average eye is still mildly hyperopic when it stops growing, aged around 14 years (Sorsby et al., 1961; Sorsby and Leary, 1970). At this point, the average eye length is about 23 mm and the focussing power is about 60 D.

If axial length and focussing power develop to be mismatched, the result is a spherical refractive error. As axial length increases, the eye will become myopic if there is an insufficient reduction in optical power (see Figure 1-1, for instance). Myopia can also develop after the normal emmetropisation period of

about 14 years; it must then be due to a further lengthening of the eye or an increase in the power of the cornea and lens. Myopia is sometimes classified accordingly as early-onset or late-onset myopia, with Goldschmidt (1968).

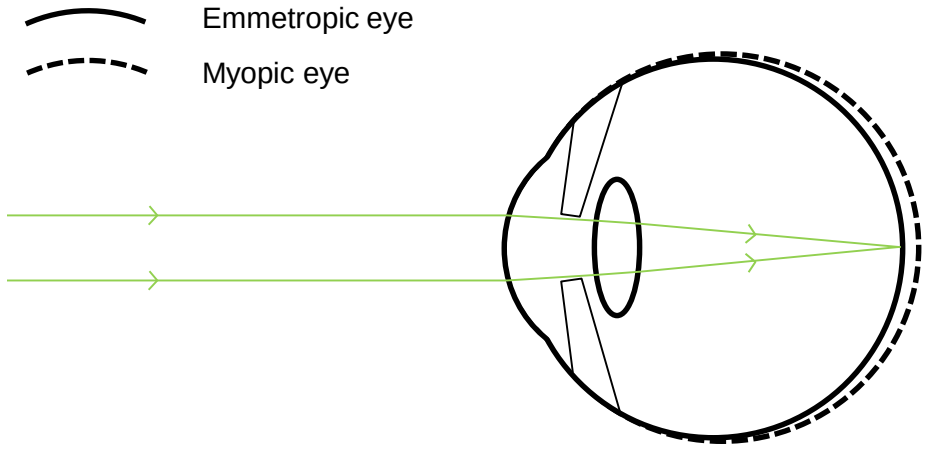

Figure 1-1: Schematic emmetropic and myopic eyes, with accommodation relaxed. The myopic eye has grown, such that light from a distant object is now focused in front of the retina.

On average, the axial length is greater in myopes than in emmetropes (Carroll, 1981; Mallen et al., 2005; Mutti et al., 2007), while lower focussing power does not seem to be associated with myopia[*]; the difference in axial length is nearly all attributable to a deeper vitreous chamber (Jones et al., 2005). Axial length is also known to increase rapidly in children developing myopia, compared with those remaining emmetropic (Mutti et al., 2007).

Both Carroll (1981) and Mallen et al. (2005) found a regression coefficient of around an extra ⅓ mm of axial length per −1 D of spherical refractive error. Observations reviewed by Wang and Ciuffreda (2006), and recently made again by Kollbaum et al. (2012), show that blur is often noticeable for less than 0.25 D of myopic defocus. We therefore find that the length of the eye needs to be correct to just a small fraction of a millimetre for clear vision.

[*] For a survey of biometry relating to myopia (up to 1998), see Wildsoet (1998). In more recent publications, it appears a more powerful cornea (by about 0.25 D) may be balanced by a less powerful crystalline lens in myopes. These differences in power increase following myopia onset (Jones et al., 2005; Mutti et al., 2007; Iribarren et al., 2012; Mutti et al., 2012).

1.2 Evidence for nature and nurture in myopia

1.2.1 Nature

Much effort has gone into identifying genes that are responsible for myopia, reviewed up to 2010 by Baird et al. (2010). In the past, genetic associations found in one study have not been replicated in others, indicating only tenuous links. However, some recent studies now agree on the association of myopia and axial length with a variation in at least one base pair of the genome (Kiefer et al., 2013; Schache et al., 2013; Verhoeven et al., 2013).

The relationship between myopia in parents and children is striking. Mutti et al. (2002) looked at several risk factors for myopia in the Orinda study in the USA. They found that children with one or two myopic parents were three or six times more likely to be myopic than children with no myopic parents (myopia: beyond −0.75 D in both meridians). The analysis took account of differences in intelligence, and time spent on nearwork or playing sports. In urban Chinese children, there was a similar difference between myopia prevalence among the groups: no myopic parents, 68.2%; one myopic parent, 83.3%; two myopic parents, 88.9% (Xiang et al., 2012a) (myopia: SER ≤ −0.5 D). Xiang et al. (2012b) also found that the prevalence of high myopia (SER ≤ −6 D) in children increased with the severity of parental myopia.

Twin studies have also pointed towards the genetic influence on myopia. For instance, in the GEM (GEnes in Myopia) study in Australia, Dirani et al. (2006) found significantly higher correlation of SER within 345 monozygotic pairs (r = 0.82) than within 267 dizygotic pairs (r = 0.36).

While arguing for an environmental cause for most myopia, and in all populations, Morgan and Rose (2005) did concede a possible genetic

susceptibility in some East Asian populations. A “founder effect” may explain the speed of the increase of myopia among the Inuit from one generation to the next (Morgan et al., 1975; Morgan and Rose, 2005), discussed further in the next section.

1.2.2 Nurture

While research has not shown that the environment (including behaviour) is solely responsible for myopia, its role is indicated in the following four areas.

1.2.2.1 Increased prevalence of myopia

In Morgan and Rose (2005), an increase in myopia across most of the world was documented. Table 1-1 shows a sample of the increases presented in that review.

Table 1-1: Examples of increases in prevalence of myopia, as gathered by Morgan and Rose (2005).

Country/ region	Details of participants	Date of earlier recording	Prevalence of myopia	Date of later recording	Prevalence of myopia
Japan[s]	17-year-old students	1984	49.3%	1996	65.6%
Vietnam[u] (urban)	6- to 17-year-old students	1964	5.2%	1999	32%
Vietnam[u] (rural)	6- to 17-year-old students	1964	1.0%	1999	11.8%

[s] Same definition of myopia used for the two measurements (Matsumura and Hirai, 1999).
[u] Definition of myopia unpublished in at least one case: difference in definition between the two time points is not known.

A review of Finnish literature on the prevalence of myopia in the twentieth century also showed a large increase over time (Parssinen, 2012). The prevalence appeared to double among 15-year olds, to about 20%, and more than double among adults to 20–30%. (Cut-off points for myopia ranged from < 0.0 to ≤ -0.5 D.) In the USA, prevalence[*] increased from 25% to 42%

[*] Myopes were defined as those wearing a right-eye prescription with SER < 0, or with a measured refraction of SER < 0 if presenting VA ≤ 20/50. There were several thousand participants at both time points.

between 1971–1972 and 1999–2004; the prevalence of myopia of at least 7.9 D (SER) increased eight-fold, from 0.2% to 1.6% (Vitale et al., 2009). In Singapore, Seet et al. (2001) documented a rise in prevalence among military conscripts, from 26% to 83%, over about twenty years up to the late 1990s (myopia: SER < −0.5).

The increase in myopia among the Canadian Inuit (Morgan et al., 1975) was briefly mentioned in section 1.2.1. Goldschmidt (2003) also noted a similar increase in Greenland Inuit, citing Skeller (1954) and Alsbirk (unpublished). According to them, the prevalence of myopia was 1.2% in 1950, rising to 12% in 1982 (unknown definitions of myopia). Between these dates, housing, diet and schooling all underwent significant changes (Goldschmidt, 2003).

Of the Inuit studies, Goldschmidt (2003) concluded, *"*These studies strongly indicate that environmental factors are important, because in a stable homogeneous population, gene frequencies cannot change much from one generation to the next*".* Rose et al. (2002) drew the same conclusion from the Singaporean case.

1.2.2.2 Prevalence depends on environment, within an ethnic group.

A diaspora can change refractive error, relative to the population of its country of origin, as can be seen in the Indian population in Singapore. Morgan and Rose (2005) attempted to draw conclusions from different studies in the two countries, with a higher myopia prevalence (SER ≤ −0.5 D) in Indian conscripts to the Singaporean army (69%; aged 16–25 years; method: non-cycloplegic autorefraction) than in children in India (8–11%; aged 15 years, including rural and urban; method: cycloplegic retinoscopy) (Dandona et al., 1999; Wu et al.,

2001; Dandona et al., 2002; Murthy et al., 2002)[*]. Also tellingly, Pan et al. (2012b) found the prevalence of myopia (SER < −0.5 D) and high myopia (SER < −5 D) to be significantly greater in second-generation (or higher) immigrants (30% and 4.8%) than in first generation immigrants (23% and 2.5%) (method: non-cycloplegic autorefraction and subjective refinement). These data indicate that Singaporean culture has an effect on refractive error.

Grosvenor (2003) also commented on the importance of a study on rural Sherpa children and Tibetan children (both groups aged 7–18 years) in Kathmandu (Garner et al., 1999). These children are genetically similar, because of their common ancestry, but Garner et al. found the prevalence of myopia (SER ≤ −0.50D) among the rural Sherpa children was 3% (method: cycloplegic retinoscopy), and that among the urban Tibetan children was 22% (method: non-cycloplegic autorefraction) [†]. There is a genetic similarity, combined with a clear difference of environment between the two communities; this pointed towards an environmental effect on myopia prevalence.

In a related phenomenon, a higher prevalence of myopia and high myopia has often been observed in urban, as opposed to rural, populations, for instance in Wu et al. (2013).

1.2.2.3 Myopia and occupation

An association between myopia and nearwork has been observed many times. It can be seen in different rates of myopia among different occupations or habits. Adams and McBrien (1992) found that 49% of 251 microscopists experienced onset or progression of myopia after entry into their occupation.

[*] Prevalences and age data are taken from the original articles; there is some discrepancy with the summary of Morgan and Rose (2005).
[†] Other cut-off points for the definition of myopia show a similarly striking difference in this study (Garner et al., 1999).

Zylbermann et al. (1993) found that males in the teenage, orthodox Jewish education system were significantly more myopic than females in the orthodox system and all teenagers in "general schools" (mean SER of −2.90 D, compared with −0.90 or −0.50 D for the other groups). This was attributed to the study habits of the male orthodox group, which included many more hours of nearwork, a habit of swaying whilst reading, and reading very small print. In general, children educated to a higher level, or who read more, are found to be more myopic (Zadnik and Mutti, 1998; Mutti et al., 2002; Saw et al., 2002). Finally, Simensen and Thorud (1994) found that eight out of eleven female factory workers who checked weaving patterns at 30 cm became myopic (requiring spectacles), more than six months after beginning their roles.

There are other environmental variables that may correlate with both myopia and nearwork. Intelligence, parental myopia, sports activity and diet are some examples, and there may be other confounding variables that have not yet been considered. Careful studies with appropriate multivariate analyses have been carried out; some can be found in section 1.3.

1.2.2.4 Animal models

Experiments on animals have shown that a change in the visual environment can cause increased lengthening of the eye, and thus myopia. A clear inducement of myopia is found where "form deprivation" is imposed by the use of a diffuser over the eye of an animal, or by closing the eyelids. Smith (1998a) reviews these observations, dating back to Hubel et al. (1976). Refractive error has also been investigated among humans with ocular anomalies that reduce visual acuity, such as cataract and optic atrophy. People with these conditions were found to be more myopic than the controls (Rabin et al., 1981).

When lenses are used to induce defocus, animals again respond with change in refraction. In response to hyperopic defocus, the axial length of the eye increases, resulting in myopia in monkeys (Smith, 1998b), chicks (Irving et al., 1991) and other species. This could be explained by the eye not receiving a cue to stop growing from clear, or myopic, distance vision (Morgan, 2003). Also, the growth of the animal's eye slows in response to myopic defocus, including in chicks (Irving et al., 1991) and monkeys (Smith, 1998b). It seems that form deprivation functions similarly to a hyperopic defocus signal for eye growth in some visual systems.

Taken together with the lag of accommodation at near (see section 1.4.1.1), these results could indicate that hyperopic blur at near drives the eye towards longer axial length, and myopia. However, the relevance of these results to most myopia in humans has not yet been established. First, the myopic shift of the animals can be inhibited by short intervals of normal viewing (Napper et al., 1995; Smith et al., 2002), and reversed by removal of the blurring mechanism (Troilo and Wallman, 1991; Smith, 1998b). Further, the blurring in these experiments is extreme compared with what most people encounter, before or during myopia development (Smith, 1998a).

Application of this hyperopic blur theory to myopia in humans was also complicated by Chung et al. (2002). They found that 47 myopic children (SER ≤ −0.5 D, initial age: 9–14 years, ethnicity: Chinese or Malay) undercorrected by 0.75 D progressed significantly faster than another 47 who were fully corrected (progression: −1.00 D vs. −0.77 D over 24 months). Axial lengthening was also increased in the undercorrected group according to ANOVA (p = 0.04), but was

not significantly different at all of the four time points (every six months)[*]. They suggested that any retinal blur (from hyperopic or myopic defocus) would lead to axial lengthening. However, other studies have found no significant differences in myopia progression as a result of undercorrection (Adler and Millodot, 2006).

Initially, animal research focused on infants. Now, adolescent and adult animals have been studied, and they also show susceptibility to form-deprivation myopia (Siegwart and Norton, 1998; Troilo and Nickla, 2005; Zhou et al., 2007). The susceptibility decreases with age (Siegwart and Norton, 1998; Troilo and Nickla, 2005; Zhou et al., 2007), but the rate of recovery from the myopia, when severe blurring is removed, also decreases with age, at least in marmosets (Troilo and Nickla, 2005).

1.3 Studies of risk factors for myopia

It is difficult to separate out the effects of potential risk factors for myopia, because they are closely related. For instance, nearwork and time spent indoors might be put forward as risk factors, but hours of reading in a week might be expected to correlate strongly and negatively with hours spent outdoors. Many researchers have studied large numbers of participants, in order to find the most important environmental factors in myopia development, that is, what causes the eye to lengthen beyond its emmetropic axial length.

1.3.1 Diet

Cordain et al. (2002) suggested that diet is a key factor in communities developing a high prevalence of myopia. They proposed that hyperinsulineamia is responsible, as Western diets of refined starch and sugar are taken up,

[*] The differences at individual time points are not given, but the published error bars indicate that there was not a significant difference at least at the 6-month and 24-month points.

accounting for changes such as those observed in Inuit (Morgan et al., 1975) and Nepalese (Garner et al., 1999) communities.

Against this hypothesis, Lim et al. (2010) surveyed 851 Chinese Singaporean children and found that refractive error was not associated with any nutrient, including total energy intake, carbohydrate and sugar. They did find that greater axial length was associated with both greater saturated fat consumption and greater cholesterol consumption.

1.3.2 Nearwork

An association of nearwork with myopia has been observed and studied for centuries (Rosenfield and Gilmartin, 1998). At the same time, it has been noted that there are confounding factors in this relationship; perhaps it is not the nearwork itself which causes myopia, but correlated behaviours and surroundings. For example, children may share all of genes, a love of reading, intelligence (leading to more nearwork), a certain level of outdoor activity, and myopia with their parents, and it cannot simply be said that nearwork has caused the myopia (Mutti et al., 2002).

The effect of nearwork could be related to known effects of defocus on animal models (section 1.2.2.4). In this theory, chronic blur, or specifically hyperopic defocus, caused by lag of accommodation, causes axial lengthening of the eye (Gwiazda et al., 1993).

Some correlation has been found between myopia and different measures of nearwork in cross-sectional studies. For instance, Mutti et al. (2002) found a statistically significant odds ratio for the likelihood of myopia (beyond −0.75 D in both principal meridians) of 1.02 per dioptre-hour of nearwork in children, aged about 14 years. Saw et al. (2002) found a statistically significant odds ratio of

1.04 (for SER ≤ −3 D) when comparing dioptre-hours above and below the median (8.7 dioptre-hours per week) in children aged about 8 years. These ratios are after controlling for parental myopia, education and other factors. A higher, significant odds ratio of 3.05 was found for myopia when comparing the number of books read per week, above and below the median (2 books). There also appeared to be a stronger response towards myopia in Chinese than other ethnicities.

Jones-Jordan et al. (2011) appeared to clarify the association to some extent. Once a year, they surveyed time spent on nearwork of various forms and on outdoor or sports activities, along with refractive error, for children aged 6 to 14 years. Each child provided data for between one and nine years. Children who became myopic (beyond −0.75 D in both meridians) over this time were compared with children who were emmetropic throughout the study. It was found that “became myopes” did more overall nearwork than emmetropes (measured in dioptre-hours) from one year before myopia onset, and onwards. Specific nearwork activities were also identified which occupied “became myopes” and emmetropes for different numbers of hours per week, from myopia onset (for the “became myopes”), and onwards. These activities were reading, watching TV, playing computer games; for time spent studying, there was a difference only in the single year of myopia onset. However, in a paper from the same overarching study, Mutti et al. (2007) had found that axial length and refractive error of emmetropes and “became myopes” diverged significantly, 3–4 years before myopia onset. Because the divergence in refractive error and axial length occurred before the change in nearwork for “became myopes”, Jones-Jordan et al. (2011) concluded that a difference in dioptre was not the cause of myopia development.

This result does not, however, rule out nearwork as an important factor in the observed development of myopia. It does not argue against nearwork leading to myopia for a “became myopes” population with a greater susceptibility than “remained emmetropes”, for other environmental or genetic reasons. Further, for susceptible individuals, there may be a threshold for myopia development that is below the levels of nearwork investigated in such studies.

1.3.3 Peripheral refraction

Hyperopic peripheral refraction also is under investigation as a risk factor for myopia.

When a diffuser or negative lens covers half of the field of vision in chicks and monkeys, the defocused half of the eye is known to enlarge, resulting locally in myopia (Wallman et al., 1987; Smith et al., 2009a; Smith et al., 2010). Furthermore, blurring only the peripheral visual field with a scattering diffuser increases axial length, and causes myopia, in chicks and monkeys (Smith et al., 2005; Stone et al., 2006). Stone found, however, that the enlargement did not always result in myopia in chicks (Stone et al., 2006). Hyperopic defocus of the peripheral visual field has also been found to increase axial length in monkeys (Smith et al., 2009b). A defocusing lens was used, with a central aperture to provide clear vision.

Relative peripheral refraction (RPR)—the difference between peripheral and foveal refractions, as in Figure 1-2—is currently of much interest. In adult humans, Chen et al. (2010) and Ehsaei et al. (2011) both found that myopes had a hyperopic RPR while emmetropes had a relatively consistent refraction into the periphery (measuring up to eccentricities around 40° and 30°, respectively). Chen et al. also found that hyperopes had a myopic RPR, and

that in children, fewer differences between refractive error groups were significant. Spherical equivalent RPR ranged from a mean of −2.0 D for hyperopes (+0.50 < SER ≤ +2.00 D) in the superior field at 35° to +2.0 D for moderate myopes (−3.00 > SER ≥ −6.00 D) in the nasal field at 40° (higher myopes were not investigated). Ehsaei et al. (2011) found a mean spherical equivalent RPR of about +2 D in myopes (−2.00 ≥ SER ≥ −9.62 D) at 30° eccentricity in horizontal, vertical and oblique meridians.

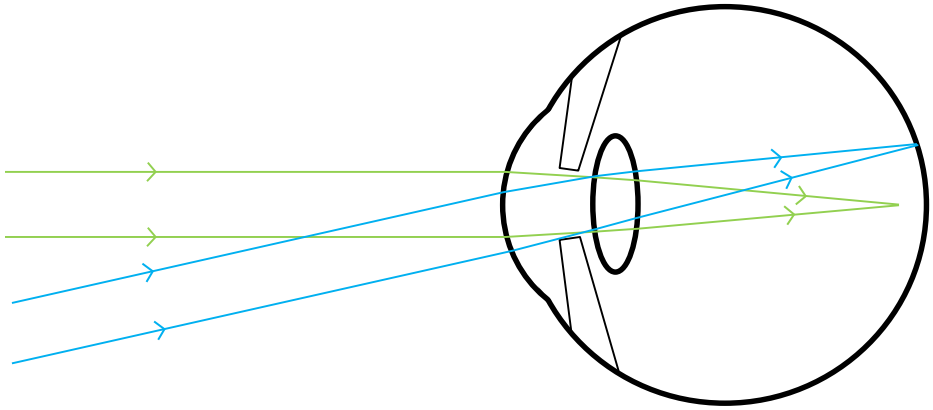

Figure 1-2: A schematic eye with axial myopia, but which is emmetropic for the direction of the blue rays. Its relative peripheral refraction is therefore hyperopic.

In a longitudinal human study, Mutti et al. (2007) measured axial refraction, axial length and refraction at 30° temporal to the fovea. They compared the RPR of children who became myopic (beyond −0.75 D in both meridians) with that of children who remained emmetropic. The spherical equivalent RPR for the two groups only became significantly different, with a more hyperopic spherical equivalent RPR in incipient myopes, *after* the axial length and axial refraction had become significantly different. Therefore, they concluded that hyperopic defocus in the periphery was not the most important factor in myopia development. The spherical equivalent RPR of “became myopes” was 0.7 D more hyperopic than that of persistent emmetropes, following myopia onset.

Other longitudinal studies have also found no, or very weak, association between RPR and myopia onset and progression (Mutti et al., 2011; Sng et al., 2011; Lee and Cho, 2013). However, Faria-Ribeiro et al. (2013) found a significantly more hyperopic RPR in 32 progressing myopes compared with 30 stable myopes, in the nasal peripheral retina, among young adults. The mean difference in spherical equivalent RPR increased to 1 D and above at 30° and 35° eccentricity.

Randomised controlled trials (RCTs) of optical treatments which reduce relative peripheral hyperopia have had some success in retarding myopia progression, as reviewed by Smith (2013). Such treatments have included multifocal spectacles, multifocal contact lenses and orthokeratology, compared against single-vision spectacles or contact lenses as control corrections[*].

In a systematic review and meta-analysis of RCTs of treatment for myopia control, Walline et al. (2011) found that multifocal spectacle designs resulted in slightly slower myopia progression than single-vision controls. The overall difference was clinically insignificant, but Smith (2013) reviews larger effects produced by more recent studies, particularly of multifocal contact lenses and orthokeratology.

1.3.4 Outdoor activity

Studies in Sydney (Rose et al., 2008) and Singapore (Dirani et al., 2009) looked at the refractive errors of children, with respect to their outdoor activity. Correcting for nearwork, intelligence quotient, age, ethnicity, parental myopia, and parental education and employment, these studies found an association

[*] The COMET studies (e.g. Gwiazda et al., 2003), contributed to these findings, although they initially concerned the possible control of myopia by reduction of accommodative demand at near, using progressive addition lenses.

between refraction and outdoor activity. For instance, Rose et al. (2008) found that among both 6-year and 12-year old children, children who spent more than 2.7 hours outdoors per day (the highest tertile) had a mean SER about 0.2 D less myopic than that of those who spent less than 1.7 hours outdoors per day (the lowest tertile). In teenagers, Dirani et al. (2009) found a regression coefficient of +0.18 D in SER, per hour outdoors per day.

Jones-Jordan et al. (2011) showed that children who became myopic (beyond −0.75 D in both meridians) had spent less time in outdoor/sports activities than those who remained emmetropic. The difference in outdoor/sports activity was present four and five years before myopia onset. As discussed in section 1.3.2, Mutti et al. (2007) had previously found that refraction and axial length of "became myopes" began to be significantly different from that of emmetropes, three or four years before onset. Jones-Jordan et al. (2011) therefore reported a link between outdoor/sports activity and myopia onset. They found that less outdoor activity, by 1.1–1.8 hours per day, was associated with the development of myopia of at least 0.75 D. However, the distribution of refractions of the "emmetropic" and "became myopic" groups are not given; the difference between them is not known.

Jones-Jordan et al. (2011) did not differentiate between outdoor and indoor sport activity, but Dirani et al. (2009) and Rose et al. (2008) and their colleagues found that indoor sports were not associated with refractive error.

Higher illuminance during outdoor activity, or lower illuminance during indoor activity, has been proposed as a relevant factor in refractive error development. Indeed, in animal research, primates have also been found to become more hyperopic in high ambient light and to exhibit relative form-deprivation

hyperopia, rather than myopia (Smith et al., 2012). On the other hand, the chromaticity of ambient light can induce and reverse myopia and hyperopia development in chicks (Foulds et al., 2013); a difference in colour between indoor and outdoor light may be relevant to myopia.

1.4 Accommodation and myopia

To summarise so far, it seems that some environmental factors, combined with genetics, introduce a likelihood of becoming myopic; outdoor activity appears to mitigate the risk to some degree.

There is still a need for more knowledge concerning the effect of nearwork on the eye. Research could lead to the exclusion of nearwork as an important cause of myopia, or to possible steps towards the mitigation of myopia.

Some responses of the eye to nearwork can be measured as they occur, and are candidates for relatively quick study in the laboratory. There are changes in convergence, accommodation, pupil diameter and axial length (see section 1.4.2). Particular details or defects of these responses may, over time, contribute to the development of a refractive error.

1.4.1 Cues to accommodation and inaccurate accommodative response

The accommodation system can respond to cues including monochromatic aberration of the retinal image[*], convergence of the eyes in binocular vision, chromatic aberration of the retinal image*, angular size of a stimulus, and perception of the proximity of a stimulus (Fincham, 1951; Fincham, 1953).

[*] Monochromatic aberration refers to a blurring of the image for all wavelengths of incident light, owing to the imperfect geometry of the optical system. Chromatic aberration refers to different images and image distances for different wavelengths, owing to the dispersion of the optical materials.

The presence of some of these cues can override, conflict with, or remove the need for others. For example, convergence of the eyes will stimulate accommodation, without blur of the retinal image, when an object is viewed binocularly, through pinholes (Fincham, 1953). Alternatively, the vergence of light from a stimulus can be altered, without changing convergence of the eyes, using lenses. This will cause blur of the retinal image, and the accommodation system is stimulated to refocus the image on the retina (Fincham, 1953).

An individual may have an inaccurate response to a cue to accommodation, or to a combination of cues, which results in a displacement of the plane of best focus from the retina. The retinal image will then be blurred. Given the results from animal models, it is possible that this blur results in a signal for eye growth (see section 1.2.2.4), depending on the environment and genetic make-up of an individual. Outdoor activity may then provide a counterbalance (see section 1.3.4).

In the remainder of section 1.4, it will also be useful to bear in mind that Rosenfield and Abraham-Cohen (1999) found a significantly higher mean blur threshold among myopes (0.19 D, −1.00 ≥ SER ≥ −5.75 D) than among emmetropes (0.11 D, +0.50 ≥ SER ≥ −0.50 D), and also significantly greater variability of the blur threshold among the myopes (N = 12 in both groups). Such a difference in blur threshold would be expected to at least contribute towards some of the phenomena discussed below. However, the experiment was performed under cycloplegia, at 4 D, using a near addition to the participants' refractive correction; it is not completely clear what these thresholds would translate to when accommodation is active (but see the correspondence with findings in higher-order aberrations in section 1.5.6).

1.4.1.1 Lag of accommodation

The accommodative response is known to lag up to 1 D behind the stimulus during nearwork (Gwiazda et al., 1993; Harb et al., 2006). Abbott et al. (1998) found that progressing myopes (PMs) demonstrated a greater lag than stable myopes (SMs) and emmetropes, in adults aged 18–31 years. PMs had a significantly lower accommodation stimulus response curve (ASRC), compared with SMs and emmetropes, and a greater mean lag, by 0.5 D for a 4 D stimulus, for example. However, this difference was only present when negative lenses were used to bring an image of a distant target nearer to the participants. In the case of a positive lens series decreasing the accommodative stimulus of a near target, and in the case of physically moving the target, without an interposed lens, no significant difference was found between the three refractive groups. Gwiazda et al. (1993) also compared the ASRC and found that myopic children demonstrated larger lags of accommodation than emmetropic children (all aged 5–17 years) when the accommodative stimulus was increased using a negative lens series, but did not when a near target and a positive lens series were used. Other studies have found no difference between refractive error groups when using targets at different positions, with no imaging lens (Seidel et al., 2005), and when using positive imaging lenses (Jiang and Morse, 1999). We will return to these results as higher-order aberrations of the eye are discussed in section 1.5.5.1.

The lag—the inaccurate response to the cues from the stimulus—results in hyperopic blur, which induces myopia in animal models (see section 1.2.2). However, infant animal models have recovered quickly from myopia induced in this way (see section 1.2.2).

1.4.1.2 Accommodative adaptation

When an individual performs nearwork over some duration, and then changes to focus on the distance, the accommodative system takes time to adapt to the change in the stimulus (Ehrlich, 1987; Wolffsohn et al., 2003). The accommodative power decreases over seconds or minutes to best focus on infinity, depending on the nearwork activity and duration. The defocus during this slow response is sometimes also called "nearwork-induced transient myopia" (NITM)[*].

During the protracted return to clear vision, the retinal image of the target at distance is blurred over seconds or minutes (Wolffsohn et al., 2003); animal studies have associated blur with myopia development (see section 1.2.2.4). Ciuffreda and Wallis (1998) found that adult myopes experienced greater defocus on the transition to the far target (mean of 0.35 D) than emmetropes (0.1 D) and hyperopes (0.01 D). The residual defocus of late-onset myopes (LOMs, onset after 15 years of age) took longer to decay to within 0.1 D of its pre-adaptation value (63 s, from an exponential fit) than that of early-onset myopes (EOMs, 35 s). The adaptation task was ten minutes' reading at 20 cm. In monocular vision (without a cue from convergence), Vera-Diaz et al. (2002) also found that adaptation was stronger (mean: 0.33 D vs. 0.17 D), 10 s after a reading task at 25 cm and more persistent (mean: 0.25 D vs. < 0.1 D, 30 s post-task) in PMs than in SMs. No significant differences were found between EOMs and LOMs.

Wolffsohn et al. (2003) also found that cognitive effort during near and far tasks significantly affected the accommodative adaptation over the 180 s following

[*]It can be said that accommodative adaptation is not a true myopia, because the accommodative stimulus at near still appears to be affecting the system. As this internal, stimulus-induced signal decays, the accommodation relaxes (Rosenfield, 1998).

presentation of arithmetic calculations at 4.50 D, in 18 participants. The mean residual adaptation was 0.55 D when the calculations were performed during the near task (active), but only read at distance (passive), compared with 0.43 D when moving from either active or passive to active tasks. The size of this effect also depended on the observer's refractive error and its history (if and when they became myopic). The decay time of the accommodative adaptation was not affected by the cognitive demand of the tasks. Such effects of cognitive effort may be relevant to considerations of the interaction between education and myopia.

Although it has been studied as a possible cause, it is not clear that repeated NITM could produce a myopic shift. The defocus of the retinal image is myopic during the adapted, defocussed time period. Referring to section 1.2.2.4, animal models have found myopic defocus to result in hyperopia. Also discussed there, Chung et al. (2002) reported that undercorrection of myopes may accelerate myopia progression, but others have found a small, and statistically insignificant, effect (Adler and Millodot, 2006). In addition, the duration of the defocus is small, compared with normal vision; animals models indicate this may have a strong, mitigating effect on any potential myopia development.

Accommodation when visible cues are absent, or "tonic accommodation" (TA), is also affected by nearwork. The adaptation of the level of accommodation in a dark environment was investigated in 12 emmetropes by Ebenholtz (1983) (pre-adaptation mean: 1.58 D). It increased significantly by a mean of 0.34 D following 8 minutes' fixation at the near point, and decreased significantly by a mean of 0.21 D following fixation at the far point. McBrien and Millodot (1987) found that LOMs (onset after 15 years of age, SER < −0.25 D) demonstrated a

+0.4 D shift in TA (dark environment) after 15 minutes' reading and performing calculations at 5 D, while EOMs and emmetropes did not demonstrate a significant shift[*]. Interestingly, the +0.4 D adaptive shift brought the mean TA level of the LOMs into agreement with that of the EOMs and emmetropes (both with baseline 0.9 D).

1.4.2 Axial length change during accommodation

Partial coherence interferometry has allowed detailed measurement of the structure of the eye in vivo (Drexler et al., 2001); axial length can be measured in this way while an observer responds to visual stimuli (Drexler et al., 1998; Santodomingo-Rubido et al., 2002). Drexler et al. (1998) observed an elongation of the eye, when focus moved from the far to the near point. The mean elongation was 13 µm among 23 emmetropes and 5 µm among 23 myopes (SER < −1 D). Mallen et al. (2006) found mean elongation in the same refractive groups (N = 30 in both groups, using SER <> −2 D) of 37 µm and 58 µm, respectively, when moving the stimulus from 0 to 6 D[†]. Even though the elongation was reversed by focus at the far point, it suggests that prolonged nearwork could possibly lengthen the eye over time.

Read et al. (2010) found an elongation of a similar magnitude when subjects were exposed to hyperopic and diffuse defocus; there was also a decrease in axial length of similar magnitude during myopic defocus. Together with a

[*] Ebenholtz did find adaptation of TA in emmetropes after 8 minutes' fixation on a cross-hair at the near point or the far point. One difference in the protocols was the use of the near and far points of each participant by Ebenholtz, while McBrien and Millodot used the same stimulus positions for each participant.

[†] Any difference inherent to the choices of accommodative stimulus, between the elongations observed by Drexler et al. and Mallen et al., are expected to be exaggerated by the instrument used by Mallen et al. (Atchison and Smith, 2004). The Zeiss IOLMaster uses an average refractive index for the eye (1.3549), and does not take into account increased lens thickness during accommodation, which would increase optical path length through the eye, even if the axial length remained constant. The data of Drexler et al. included lens thickness and took account of changes in it accordingly. This exaggeration of axial length was acknowledged by Mallen et al.

lengthening during accommodation (Drexler et al., 1998; Mallen et al., 2006), a lag of accommodation (Gwiazda et al., 1993), and analogies in animal studies (see section 1.2.2.4), this defocus-dependent length change does point towards a stress on eyes during prolonged nearwork, which could be influential in the development of myopia (Read et al., 2010).

Evidence of heredity (see section 1.2.1), and from studies of nearwork (section 1.3.2) and outdoor activity (section 1.3.4) as risk factors for myopia, could indicate:

- This stress on the eye, if prolonged and repeated, may be a cause of myopia, through axial lengthening of the eye.
- An individual can have an inherited resistance to the lengthening effect of the stress, or partly counter it with outdoor activity. Outdoor activity may aid relaxation of the stress through prolonged distance vision. Higher illuminance or shorter-wavelength ambient light may be beneficial (see animal models mentioned in section 1.3.4).

1.4.3 Microfluctuations

The optical power of the eye is known to fluctuate constantly, even during fixation on a stationary target (Campbell et al., 1959). Recordings of accommodative power showing these fluctuations are shown in Figure 1-3. Note the amplitude of the fluctuations, compared with the 0.5 D scale bar on the left-hand side. These “microfluctuations” of accommodation will be visible in the data of this thesis and will affect the analyses.

The power spectra on the right-hand side of Figure 1-3 illustrate two components to the fluctuations. First, there is a low-frequency component (LFC, ≤ 0.6 Hz), which increases in amplitude as the stimulus to accommodation is

degraded. This increase has been demonstrated with decreasing luminance (Gray et al., 1993; Day et al., 2009) or contrast of the stimulus (Niwa and Tokoro, 1998), and increasing depth of field (Stark and Atchison, 1997; Day et al., 2009). The fluctuations also increase with accommodative load, with root mean square (RMS) amplitude increasing from around 0.2 D at distance to about 0.3 D when fixating at 25 cm (Day et al., 2006). It has long been hypothesised that the visual system uses the feedback resulting from the fluctuations to control accommodation (Campbell et al., 1959). Second, there is a higher-frequency peak (high-frequency component, HFC) that is correlated with arterial pulse; it appears to be an effect of other physiological activity, rather than under neurological control (Winn and Gilmartin, 1992).

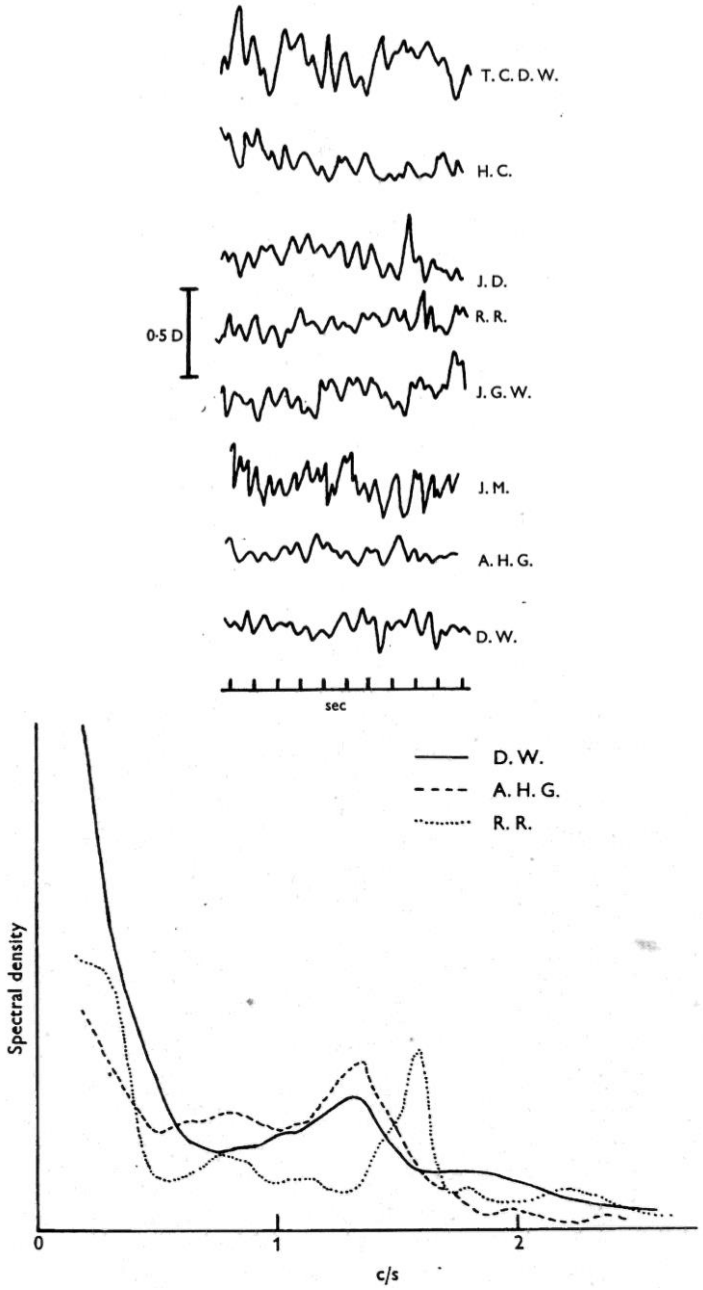

Figure 1-3: Fluctuations in the "static" accommodation response, from Campbell et al. (1959). The left-hand plot contains recordings of the accommodation response to a static stimulus at 1 D, with dilated pupils. The right-hand plot shows the power spectrum of the fluctuations recorded, for three of the subjects. Reproduced with permission from John Wiley and Sons.

There is a relationship between myopia and the amplitude of the microfluctuations of accommodation. Day et al. (2009) found that the RMS amplitude of the fluctuations was higher in myopes (SER < −0.5 D) than emmetropes, over various stimulus luminances and depths of field (controlled by varying the diameter of a pinhole). The largest fluctuations were in myopes in

a dark environment (mean RMS amplitude: 0.55 D), and the largest mean difference between myopes and emmetropes was for a target luminance of 0.002 cd m^{-2} (mean difference in RMS amplitude: 0.1 D). The total RMS amplitude (Day et al., 2006) and the power of the LFC (Seidel et al., 2003) were also greater in LOMs (onset after 15 years of age) than in EOMs and emmetropes. The largest difference in RMS amplitude was 0.05 D, between LOMs and EOMs/emmetropes.

When *not* using a Badal arrangement for viewing the target, Seidel et al. (2005) found that differences between the refractive groups were no longer statistically significant (to $p < 0.05$). This was true in both monocular and binocular vision. They concluded that the LOMs had a higher depth of field, but were assisted by the other "real-world" cues for proximity of a target.

The binocular accommodation traces in Campbell (1960) show a close correlation (at least at lower frequencies) between the fluctuations of the two eyes, in binocular viewing of a target at 2 D. Coherence analysis of the aberrometry of Chin et al. (2008) also revealed a stronger correlation over time of the LFC of defocus in the two eyes of participants, compared with correlations between the eyes in the HFC and the total frequency range (0.08–10.25 Hz). The two eyes appear to share the same control instructions for the low-frequency microfluctuations.

The analysis of Seidel et al. (2005) found no significant difference in the microfluctuations (total RMS amplitude, LFC or HFC), between monocular and binocular viewing conditions.

1.4.4 Modelling the accommodative control system

In efforts to understand the effects of nearwork, models of the control system for accommodation have been constructed (some are discussed below and in chapter 6). They attempt to numerically simulate the accommodation response (AR) using hypothesised or deduced control processes and limits within the biological system. There are several phenomena which should be taken into account by such a model.

Most simply, the accommodation system does respond to changes in the distance to a stimulus, normally leading to clear vision of stimuli within the accommodative amplitude.

We know that there are a lead and lag of accommodation at far and near (Abbott et al., 1998), which are likely to be influenced by the depth of field of the eye and spherical aberration, in particular (Plainis et al., 2005; Lopez-Gil and Fernandez-Sanchez, 2010).

There are also the microfluctuations during the response to a static accommodative stimulus, which appear to be controlled and provide feedback to the accommodation system (section 1.4.3). The fluctuations appear to be driven so that they can detect changes in blur, or rates of change of blur in the retinal image. Their increased amplitude (in the low frequency domain) in response to a degraded stimulus would then be an effort to maintain a constant level of feedback (Gray et al., 1993).

With a dynamic stimulus, accommodation displays further complexity. There is a latency of around 370 ms following a step-change in dioptric stimulus (Campbell and Westheimer, 1960). This delayed response is exemplified in

Figure 1-4. It is now known that the ciliary muscle can in fact respond after 0.3 s, as Shao et al. (2013) found, using optical coherence tomography.

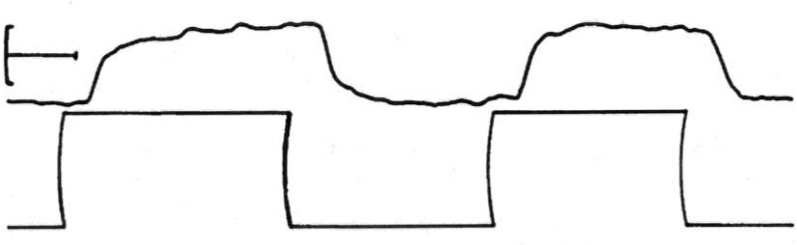

Figure 1-4: Record of accommodation responses (upper line) to 2 D steps in stimulus, starting at distance. The lower line traces the stimulus. The vertical scale marking represents 1 D, and the horizontal 1 s. Reproduced from Campbell and Westheimer (1960), with permission from John Wiley and Sons.

Campbell and Westheimer (1960) also tested AR to shorter pulses in dioptric stimulus, including where the stimulus stepped and returned to its original position within the latency period. These trials resulted in an attenuated pulse in accommodation compared with pulses of longer duration, and sometimes in the absence of an accommodative response.

Hung and Ciuffreda (1988) found that responses to gradual changes in dioptric stimulus have complex step and ramp behaviour, depending on the speed of the ramp in stimulus. Examples are shown in Figure 1-5. They also found that the latency of the response to a ramp in dioptric stimulus also depends on the speed of the ramp. When accommodation undergoes a step-change in response to a ramp in dioptric stimulus (after a static latency period), it appears to use a prediction of the level of the changing stimulus as the destination of the step.

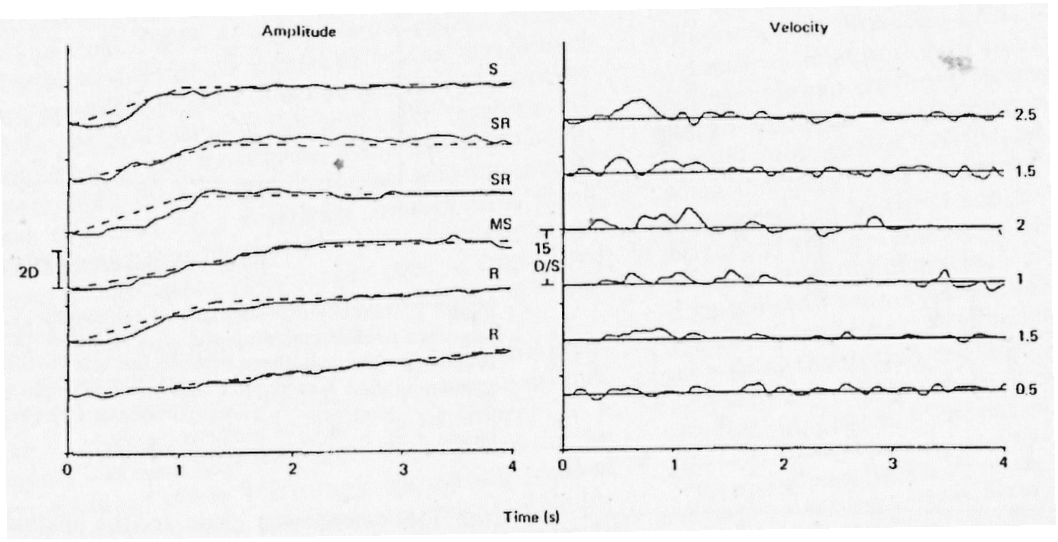

Figure 1-5: Representative accommodative responses (solid lines, left-hand plot) to ramps in dioptric stimulus (dashed lines). The ramp velocities range from 0.5 to 2.5 D s^{-1}. The responses were identified as step (S), ramp (R), step–ramp (SR), ramp–step (RS) or multiple-step (MS). The right-hand plot shows the velocities of the accommodation responses. Reproduced from Hung and Ciuffreda (1988) with permission from John Wiley and Sons.

These observations indicated that accommodation has two modes:

1. A fast-moving response, which responds to fast, or large, changes in retinal blur, after a delay. This fast movement depends on previous levels of blur, rather than the current level. It is referred to as “preprogrammed” or “open-loop”.
2. A slower response which continuously fine-tunes accommodation in response to slower changes in blur (“closed-loop”).

Using this insight, and following previous attempts, Khosroyani and Hung (2002) were able to simulate known accommodative responses to pulses, steps, ramps and sinusoidal variations of dioptric stimulus (Figure 1-6). (These simulations did not include the microfluctuations in steady-state accommodation.)

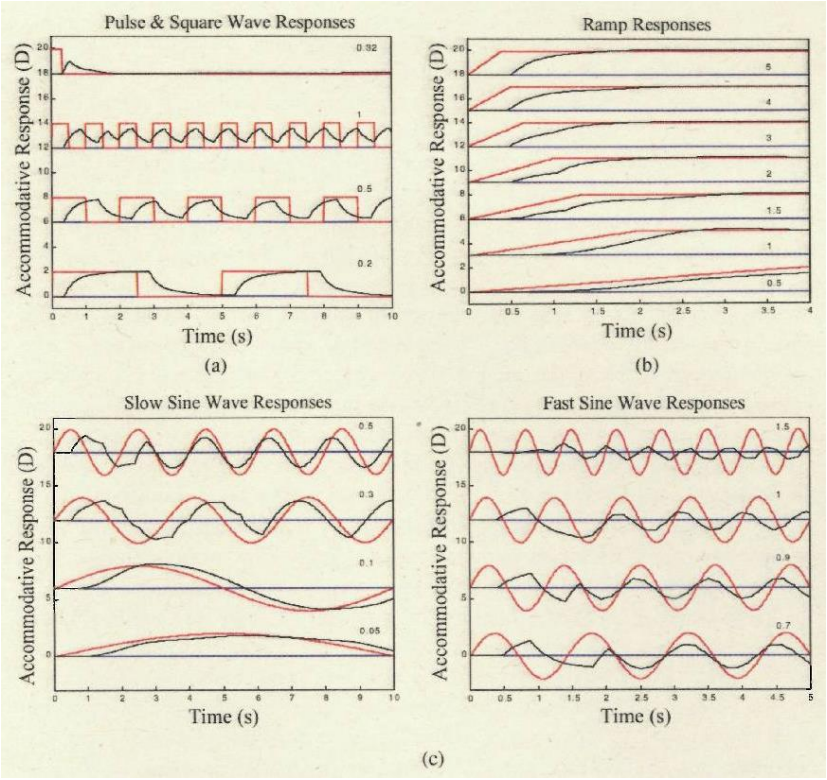

Figure 1-6: Simulations from Khosroyani and Hung (2002) of (a) pulse and square wave stimuli, (b) ramp stimuli, and (c) sine wave stimuli. The simulated stimuli are marked in red, and the responses in black. Reproduced with permission from John Wiley and Sons.

Schor and Bharadwaj (2005; 2006) developed a related, two-component model to closely simulate step-changes of accommodation and disaccommodation. They found that a compound signal from the accommodation controller to effect a pulse in acceleration and a step in velocity could result in simulations closely matching their experimental results. Their analysis of experimental accommodation responses revealed that the peak velocity of a response depended on the magnitude of the change in stimulus, for accommodation (Bharadwaj and Schor, 2005), or the starting position, for disaccommodation (Bharadwaj and Schor, 2006b; Bharadwaj and Schor, 2006a). These dependencies in the pulsed signal to accelerate accommodation were included in the models.

However, these matters are not fully resolved. Kasthurirangan and Glasser (2005), found the peak velocity of both accommodation and disaccommodation

to be affected by the starting point, and less strongly, by the magnitude of the step. One difference in their analysis is that Kasthurirangan and Glasser first fitted an exponential curve to the accommodation response over time, while Bharadwaj and Schor (2005) calculated instantaneous velocities, and applied a smoothing function later. We may expect smoothed instantaneous velocities to represent accommodation more accurately than the exponential model, but hypothesising such a model may be useful for future understanding.

The relatively slow response of deformations of the crystalline lens, following contraction or relaxation of the ciliary muscle, is an important feature in these recent models. It does not account for the latency of accommodation, but is used to inform the control systems in the simulations which result in the characteristic curves of Figure 1-6(a), for instance.

With reference to the Badal arrangement of the instruments of this thesis, Bharadwaj and Schor (2005; 2006a) also found that the presence of a size cue in the changing stimulus increased the velocity of accommodation, and did not affect the trends observed in disaccommodation.

1.5 Higher-order, or general, aberrations

1.5.1 General aberrations—beyond spherocylindrical refractive error

The aberration of a beam of light is a deviation from its 'ideal' properties. For a monochromatic beam of light which we have attempted to collimate, an aberration is a deviation of the shape of the wavefront from a flat plane[*]. For a beam which we have attempted to focus to a point, an aberration is a deviation from a spherical wavefront centred on that point. Such a deviation will prevent

[*] The surface describing the wavefront is the surface of constant phase across the beam. An alternative phraseology would be to talk in terms of the variations of phase of the beam over a given surface, i.e. a plane perpendicular to the beam.

the entire beam from coinciding at one point of best focus; an image being conveyed using such a beam will be blurred.

When an aberration of a beam of light is caused by transmission through an optical system, we also call that the aberration of the optical system[*]. For a beam incident on the eye, the aberration of the eye is the deviation of the wavefront within the eye from a spherical surface centred on a point on the retina. Considering a point source of light at the retina, the aberration of the eye would be the deviation of the resultant external beam from a plane wavefront, if the eye is fixating on a distant target.

Defocus is one familiar type of aberration. It is the difference between the actual optical power and the ideal optical power of a system. A myopic eye, at distance, has positive defocus, because the focal length is shorter than the distance to the retina; the optical power is greater than is ideal. Ocular defocus and astigmatism are commonly corrected with spherocylindrical lenses.

Aberrations which cannot be corrected by spherocylindrical lenses are known as “higher-order aberrations” (HOAs). The total HOA can be broken down into components arising from particular properties of the geometry (or dispersion) of the optical system.

One commonly discussed component of HOA is spherical aberration (SA). When a collimated beam of light meets a spherically curved boundary between refractive indices, how well it is focused to a point depends on the width of the beam. Rays meeting the spherical surface at a large angle of incidence (AOI) will not cross the optic axis of the system at the same point as rays incident with

[*] The finite size of apertures in an optical system will cause diffraction, which also blurs images. Here, we are just considering the imperfect geometry of the system (and dispersion, in the case of chromatic aberration).

a small angle. So a wide beam, having a variety of AOIs across its width, will not be well focussed (Figure 1-7). We would expect an optical system whose surfaces are curved to display this kind of aberration, in general, although aspheric surfaces can be designed to eliminate it.

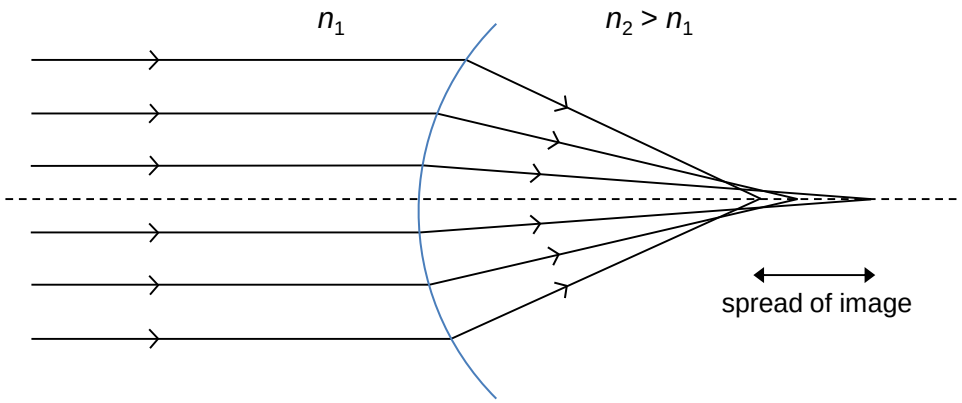

Figure 1-7: Spherical aberration. The blue boundary is spherical, resulting in different image positions for the rays. Refractive index (*n*) increases across the boundary.

Techniques for studying the aberrations of the eye involve analysing a beam or image reflected from the retina. On leaving the eye through the pupil, this beam carries information about the optics it has passed through. The overall shape, or total aberration, of the wavefront leaving the pupil is commonly measured at a Shack-Hartmann wavefront sensor, as described in section 2.2.2. Analysis is then carried out on properties of this total aberration. For instance, defocus, astigmatism or SA may be extracted and analysed. Sections 2.2.3 and 2.2.4 describe the common use of the Zernike series of polynomials, in the decomposition of the total aberration.

1.5.2 Aberrations in the population

Population studies of aberrations have shown that nearly all of the aberration of the eye is usually spherocylindrical, with spherical defocus being dominant (Porter et al., 2001; Castejon-Mochon et al., 2002; Thibos et al., 2002c). Using the Zernike decomposition of the total aberration (see sections 2.2.3 and 2.2.4),

Thibos et al. (2002b) and Porter et al. (2001) found that the mean SA was significantly different from zero (RMS amplitude about +0.1 μm over a 6 mm pupil, corresponding to a defocus error of 0.3 D). Thibos et al. (2002b) also found other HOAs to be significantly different from zero (*n* = 100, under cycloplegia), while Porter et al. (2001) did not (*n* = 109, without cycloplegia). Both populations had mean SER ≈ −3 D.

The magnitude of the aberrations of an individual's left and right eyes appear to be correlated to some extent, with evidence of mirror-imaging of aberrations between the two eyes (Porter et al., 2001; Castejon-Mochon et al., 2002; Thibos et al., 2002c; Hartwig and Atchison, 2012). This correlation was subject-dependent, however, and sometimes very weak. Chin et al. (2008) found.

1.5.3 Sources of aberrations, and compensation and adaptation within the visual system

The surfaces of both the cornea and the crystalline lens can introduce optical aberrations to the eye. It appears that astigmatism and some HOA components of the cornea are compensated by those of the lens, to some extent, whether by optimisation during development or passive genetic instruction (Artal et al., 2001; Kelly et al., 2004; Artal et al., 2006). Such compensation can theoretically be achieved by lateral positioning and tilting of the crystalline lens, relative to the axis of the cornea and the pupil (Kelly et al., 2004; Artal et al., 2006). This intraocular compensation of aberrations appears to decrease with the severity of myopia (Artal et al., 2006), total aberration (He et al., 2003) and age (Artal et al., 2002).

Artal et al. (2004) also found that rotating the aberrations of the eye by 45°, and multiples thereof, increased the perceived blur level of a stimulus (right eye, five participants). The participants adjusted the magnitude of the aberrations to achieve similar blur levels in successive images, unaware of the orientation of the aberrations in each case; lower aberration magnitudes were required for rotated aberration patterns to achieve the same subjective blur as with the natural aberration orientation. There was therefore evidence for neural adaptation to the higher-order ocular aberrations.

1.5.4 Fluctuations of higher-order aberrations

Just as accommodation is known to fluctuate during fixation on a static target (see section 1.4.3), fluctuations in HOAs have been observed.

Hofer et al. (2001) initially measured these variations, using a wavefront sensor (see chapter 2). They found that the fluctuations in HOAs were measurable, but weaker than those in defocus, and their power spectrum against frequency was not systematically correlated with that of defocus. Zhu et al. (2004) however did find similar power peaks in HOA fluctuations to those in accommodation, perhaps assisted by the removal of low frequency defocus drift and application of a band-pass filter (0.1–1.5 Hz) to their data. Zhu et al. (2006) were later able to confirm that HOA fluctuations were lenticular and not corneal, by comparing videokeratoscopy and wavefront sensing data.

In binocular vision, Chin et al. (2008) found that correlation of the fluctuations in HOAs of both eyes over time was subject-dependent and weak on average ("coherence value" < 0.2), while Mira-Agudelo et al. (2009) found slightly stronger fluctuations in HOAs in binocular viewing than in monocular viewing, for a near target (0.25 m), but not a far target (5 m).

1.5.5 Aberrations and accommodation

1.5.5.1 Interactions between higher-order aberrations and accommodation

Wilson et al. (2002) found that observers could distinguish between blur due to different signs of defocus. Accommodation was paralysed and a target (point source or letter) was moved away from the position of best focus, either towards or away from the observer. Positive and negative levels of defocus were not expected to result in different retinal images, but the total aberration of the eye did result in an ability to distinguish between myopic and hyperopic blur, particularly for larger artificial pupil sizes. With 5 mm pupils, average discriminability (fraction of correct responses beyond chance level) of the sign of defocus was around 0.6. It was therefore suggested that the form of the retinal image may be used as one cue to guide accommodation. Lopez-Gil et al. (2007) provided a theoretical understanding of the source of the difference in the images, using the Zernike decomposition of the total aberration (see section 2.2.3): an aberration of the ideal wavefront with an even degree of rotational symmetry would be expected to result in different images, depending on the sign of defocus, but an aberration with odd rotational symmetry would not. Both parities are expected in the total HOA.

The presence of aberrations degrades the retinal image, but it does lend the eye an increased depth of field (Marcos et al., 1999). As well as providing satisfactory images over a less restricted range of distances, a greater depth of field may reduce the demand for precision, and therefore the calculative load, on the accommodation system.

He et al. (2000) found in eight subjects that RMS total aberration of the eye, and the amplitudes of HOAs (5^{th}–7^{th}-order Zernike terms) decreased as the stimulus

moved in from infinity, but increased again after reaching a minimum. He et al. related this minimum to the position of tonic accommodation. This connection is interesting, but the mean RMS total aberration was constant for an accommodative stimulus of 1–3 D, there was no clear minimum for the “coma” aberrations (within the 3rd-order Zernike terms) and SA did not share the same position for the minimum in RMS amplitude as the 5th–7th-order Zernike terms.

Given that the eye has aberrations even when defocus is minimised, accommodation may be expected to work to provide the best image quality, rather than result in the focal power we would normally calculate for a spherical lens. In particular, SA of the eye is in general positive at distance, and decreases and becomes negative as the level of accommodation increases, as the lens changes shape (Plainis et al., 2005). When this change in SA is considered in terms of the effect on image quality, it could explain a lead and lag of accommodation at far and near (Plainis et al., 2005; Lopez-Gil and Fernandez-Sanchez, 2010).

Returning to the relationship between lag of accommodation and myopia in section 1.4.1.1, we can include HOAs. Various studies have found higher lags at near for PMs (progressing myopes), compared with SMs (stable myopes) and emmetropes, when negative lenses are used to stimulate accommodation, but no significant difference when using natural targets (no imaging lens) or a positive imaging lens to view a target. Assuming accommodation always resulted in the best image quality (smallest point-spread function, with a certain depth of field), we may be able to explain the results with a difference in HOAs between the refractive groups.

Modifying an accommodative stimulus using negative spherical lenses will add negative SA to the optical system of eye + external lens, with the SA of the eye also becoming more negative with increasing accommodation (Plainis et al., 2005). These SA components will therefore add, to contribute to a greater depth of field; the greater depth of field would allow a lag of accommodation, assuming the visual system will find the most relaxed position within the range providing the least blur. The positive lenses may have resulted in the low accommodative errors by cancelling out the negative SA of the accommodated eye and reducing depth of field during accommodation. A more negative SA in PMs, or possibly other differences in HOAs, may explain the greater lag at near, when using negative lenses.

Since these experiments are carried out using corrected vision, extra negative lenses are present for the myopes, which may compound any effect of negative SA on the AR (Cheng et al., 2003). However, the difference observed is in PMs vs. SMs and emmetropes, with no difference between SMs and emmetropes. It seems the variation of the negative imaging lens is more important than the presence of the constant correcting lens.

Aberrometry of corrected myopes is similarly confounded; there are higher angles of refraction for light passing through the peripheral cornea, introducing more positive SA to the measurement, when compared with emmetropes focussing on the same stimulus (Cheng et al., 2003). This SA is further modified by the correcting lenses, although Cheng et al. found the SA of the correcting lenses to be < 3% of that of myopic eyes

Buehren et al. (2005) did find a greater increase in RMS amplitude of HOAs following nearwork for PMs than emmetropes, including within the fourth-order

Zernike terms (which include SA*). For a 5 mm pupil, myopes (SER < −0.5 D, mean: −3.84 D) had 4th-order Zernike aberrations with mean RMS amplitude of 0.098 μm, compared with 0.071 μm in emmetropes (SER within ±0.25 D). Following 2 hours' reading, the mean 4th-order RMS amplitude in myopes increased by 0.04 μm, which was significantly greater than the increase of approximately 0.01 μm in emmetropes. RMS amplitude of 0.1 μm in SA over a 5 mm pupil corresponds to a defocus error of 0.4 D.

1.5.5.2 Accommodation and experimental manipulations of higher-order aberrations

Following advances in adaptive optics (AO), as reviewed by Roorda (2011), the effect on accommodation of experimentally correcting or modifying the total aberration of the eye has been of interest.

We might expect that correcting the aberrations would reduce the inaccuracy in accommodation and reduce the depth of field. Gambra et al. (2009) observed the lag of accommodation at near to be reduced in four out of five subjects, when HOAs were corrected. A static correction of pre-trial aberrations was used.

Changes and fluctuations in lens shape (see section 1.4.3) during accommodation will affect the total aberration, as observed by Hofer et al. (2001) and Zhu et al. (2004); dynamic correction is desirable to further investigate the importance of HOAs.

When Chen et al. (2006) and Chin et al. (2009b) investigated accommodation under dynamic correction and inversion (Chin et al.) of the HOA they found that

* There are also higher-order Zernike terms which contribute to a complete calculation of spherical aberration; they are smaller, but can become non-negligible, e.g. contributing > 0.5 D to the accommodative amplitude in some participants (López-Gil and Fernández-Sánchez, 2010).

the effect of the correction was subject-dependent, and that responses in accommodation to step-changes in dioptric stimulus were sometimes absent or in the incorrect direction, particularly for a decreasing step in dioptric stimulus. Caveats here are that Chen et al. could only correct the aberration at a frequency of 1 Hz (not much faster than the relevant fluctuations of accommodation, as in section 1.4.3), and Chin et al. used a step of 0.5 D, which is a relatively small change in dioptric stimulus, comparable with the depth of field of the eye (Marcos et al., 1999; Collins et al., 2006). However, the non-spherocylindrical aberration, and changes and fluctuations in it, was indicated as a cue to accommodation, with its importance varying between individuals.

1.5.6 Aberrations and myopia

Some studies have compared the total aberration of myopic eyes against emmetropic eyes, or examined aberrations as a function of refractive error. The question is whether higher-order aberrations in the retinal image (uncorrectable with spherocylindrical lenses) could be linked to myopia or myopia progression.

Studies without cycloplegia* generally indicate that the myopic eye has greater HOAs than the emmetropic eye. As noted in section 1.5.5.1, Buehren et al. (2005) found significantly greater RMS HOA in corrected myopes than in emmetropes, at distance and after reading. Paquin et al. (2002) found a significant increase in RMS HOA with refractive error, of 0.02 μm / −1 D SER, for a 5 mm pupil. Such an increase in HOAs with myopia may explain the higher blur threshold found among myopes by Rosenfield and Abraham-Cohen (1999) (see section 1.4.1).

* Paralysing accommodation is likely to affect the shape of the lens in general; studies using cycloplegia are less directly relevant to questions of myopia and real-world vision.

Given that blur is an important input to emmetropisation, HOAs can be expected to affect the process, either contributing to possible blur cues to halt or continue growth, or masking those cues. That HOAs also change with accommodation, affecting the accommodation response for best image quality (see section 1.5.5), further involves them in considerations of the relationship between myopia and nearwork.

In a final note, Han et al. (2007) found a significant effect of deliberate narrowing of the palpebral aperture on RMS aberration and SA. The eyelids were found to modify the shape of the cornea. Han et al., like Buehren et al. (2005), noted a link between the narrower palpebral aperture of myopes when reading and their ocular aberrations. They also noted the smaller palpebral aperture of Asians, relative to Caucasians, possibly implying a link to the high prevalence of myopia in South-East and East Asia. Buehren et al. (2007) went on to link the change in HOAs caused by partial lid closure to a hyperopic displacement of the best image plane at distance. As discussed earlier, such defocus is considered to be a possible factor in increasing axial length and the development of myopia.

1.6 Contribution and synopsis of this thesis

This thesis contains the development of two new AO and aberrometry systems for investigating the accommodative response, and an experiment investigating accommodation control. The instruments provide unique capabilities to control stimuli to accommodation and convergence, and to record the response of the eye or eyes. Data demonstrating the performance of these apparatus are documented.

Introductions to techniques used in data collection and analysis are provided in chapter 2.

Chapter 3 describes the development of a monocular AO and aberrometry system, which follows on from previous work at the University of Bradford (Chin, 2009; Hampson et al., 2009). This system has two aberrometry channels, which allow separate measurement of the eye's aberrations and those introduced by the AO control element (a deformable mirror, DM). The system was improved by the replacement of two optical elements, and was thoroughly realigned and calibrated, including further development of the optical mounting and adjustment techniques.

Chapters 4 and 5 contain a pilot study on the AR to rapid changes in dioptric stimulus, and improvement of the experimental protocol using the monocular apparatus.

In chapter 6, an experiment using the monocular AO and aberrometry apparatus is reported. Rapid changes in dioptric stimulus, above and below a baseline (one period of a square wave), were presented to participants. The AR was analysed with reference to existing knowledge and models of accommodation control, also considering similar work on the saccadic system. The data and much of the analysis have also been published as Curd et al. (2013a) and presented as Curd et al. (2013b).

Chapter 7 describes the development of a new, binocular AO and aberrometry instrument. In this system, as well as using DMs to provide control of the aberrations of a stimulus to both eyes, rotating mirrors are used to stimulate convergence. It is therefore possible to investigate the AR in binocular vision,

including both convergence and HOA control. It is also possible to put the stimuli to accommodate and converge into conflict. This is a new combination of capabilities for an AO system, requiring building, alignment and calibration of a complex optical system, and the concurrent development of complex control software (developed by Dr. Karen Hampson, at the University of Bradford).

In chapter 8, the performance of the binocular AO and aberrometry system is demonstrated. Data were collected from trials on two participants presented with a step-change in both AS and retinal disparity (stimulus to converge). In half of the trials, HOAs were also corrected, before the step-change in the stimulus. At the time of writing, a manuscript is in preparation for submission to a peer-reviewed optics journal, reporting the developments of chapters 7 and 8.

Finally, the thesis is concluded in chapter 9. Experimental findings and the capabilities of the instruments now available for future development and research are summarised, with suggestions of experiments which now present themselves for investigation.

2 Introduction to measurement and control of ocular and stimulus aberrations

2.1 Schematic arrangement for simultaneous aberration measurement and control

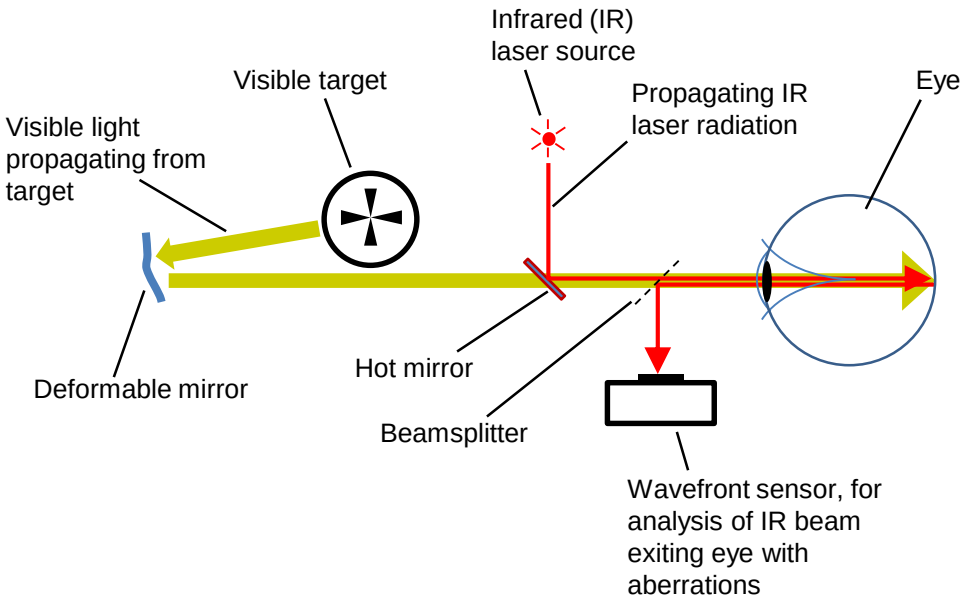

Figure 2-1: Simplified schematic arrangement of a system for simultaneously controlling the aberrations of a stimulus and detecting the aberrations of the eye.

The studies of this thesis involve control of a stimulus to accommodate and measurement of the response of the eye. Not only distance to the accommodative stimulus, but also higher-order aberrations (see section 1.5) are controlled. Similarly, the accommodation response, astigmatism and HOAs are recorded by the apparatus.

Figure 2-1 shows one simplified example of a system where aberrations of a target can be controlled, using the deformable mirror (DM), and measurement of the ocular aberrations can be performed simultaneously. A hot mirror is used here to combine the infrared (IR) and visible beams, so that they can both enter the eye; a beamsplitter allows the aberration measurement beam to be directed towards the detector. Sections 2.2 and 2.3 provide further introduction to the IR

aberrometry and visible stimulus control; more detail will be found in chapters 3 and 7 on the particular instruments in this thesis.

In a practical system, many other optical components are required, as will be apparent in chapters 3 and 7. In particular, relay optics are required to form images of the aberrations at different points within the system. The controlled aberrations of the deformable mirror are imaged onto the pupil, to provide a known condition for the stimulus as light enters the eye; the pupil is also imaged onto the wavefront sensor, so that aberrations at the detector are an image of those in the IR beam exiting the eye.

2.2 Aberration measurement

2.2.1 The aberrometry beam

If we consider light from a point stimulus, the aberrations of the eye are the difference between the wavefront within the eye, and a perfectly spherical wavefront converging on the retina. This difference results in a blur of the image of the stimulus.

Now let us consider a hypothetical point source of light at the retina. If an aberration-free eye were perfectly focussed on a particular location in space, light from a point source on the retina would be focussed to that location. If the eye were focused at infinity, light from the retinal point source would leave the eye as a plane wave. Not considering diffraction, the aberrations of a real eye would be the difference between the real wavefront and a plane wave[*].

[*] Diffraction is neglected, since the ocular pupil diameter was > 5 mm, which is several thousand times the wavelength of the IR radiation, producing an Airy disk with an angular radius of less than 1 mrad. The resultant blur in the image at the wavefront sensor is insignificant compared with that owing to other aberrations of the eye and instrument.

It is currently impossible to measure the aberrations from inside the eye in vivo, so we attempt to place a point source of light at the retina and measure the aberrations externally. Since the retina is a diffusely reflecting surface, an approximation to a point source can be provided by sending a beam of light into the eye, to be focused on the retina. This beam is kept to a small diameter, to minimise the size of the focussed spot on the retina*.

Since the retina scatters and absorbs incident light, a laser is required in practice to achieve the necessary power and area of the beam. Also, an invisible beam is required which will not stimulate pupil miosis. In the instruments of this study, an IR laser was used to form the point source at the retina, and some of the radiation scattered at that point returned back to and exited the pupil, propagating with the ocular aberrations.

An image of the IR wavefront leaving the eye was formed at the wavefront sensor by relay optics: curved mirrors and lenses. The information from the wavefront sensor was analysed to investigate the components of the aberration of the beam leaving the eye.

2.2.2 The Shack-Hartmann wavefront sensor

In both instruments of this thesis, a Shack-Hartmann wavefront sensor is used to measure the shape of the wavefront. Such a sensor consists of a lenslet array and an intensity pattern detector (Platt and Shack, 2001). The intensity detector was a CCD camera chip in the instruments described here.

In a Shack-Hartmann wavefront sensor, the intensity detector is placed in the focal plane of the lenslets. The beam covers multiple lenslets, and each lenslet

* Aberrations become manifest (and focussed spot size increases) as beam area increases. (Consider a pinhole system, where the light no longer needs focussing.) However, diffraction also becomes more important as beam size decreases; a diameter of around 3 mm achieves a useful trade-off.

focusses its portion of the beam to produce an intensity peak on the detector. The position of the intensity peak for each lenslet corresponds to the average slope of the wavefront across that lenslet. Therefore, if the beam is a plane wave at the lenslet array, an array of intensity peaks will be produced with the same lattice dimensions as the lenslet array. If the beam is converging, for instance, the intensity peaks will be closer together. Figure 2-2 illustrates this principle.

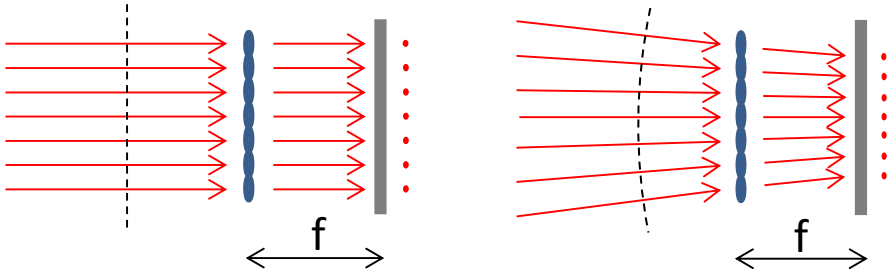

Figure 2-2: Spots formed in the focal plane by a lenslet array for a collimated beam of light and a converging beam. The spots are closer together for the converging beam. The dashed lines show the shape of the wavefront.

Any shape of a wavefront, down to the resolution of the lenslets, can be detected in principle. In practice, a searching algorithm must be used to find the position of the intensity peaks, and the properties of the searching algorithm may limit the wavefront shapes that can be accurately measured. In the control software for these instruments, one intensity peak is expected within an area on the detector corresponding to that of one of the lenslets (a “search block”). If a large wavefront curvature produces zero or two peaks within a search block, the searching algorithm often does not succeed in identifying the positions of the intensity peaks*.

* There is a trade-off between dynamic range and sensitivity, for a detector with a given resolution. The dynamic range (the maximum slope that can be measured) increases as the numerical aperture of the lenslets increases, while sensitivity to the slope of the wavefront decreases.

2.2.3 Calculation of aberrations; Zernike decomposition of total aberration

The Shack-Hartmann sensor (section 2.2.2) provides information about the total aberration of a beam, or the shape of the wavefront. This shape can be analysed as a combination of analytical aberrations such as defocus, astigmatism, spherical aberration, etc.

A popular decomposition of the total aberration for analysis is the Zernike series of polynomials (Thibos et al., 2002a). These expressions are a family of circular polynomials, with increasing angular and radial frequencies. The lower order terms can be understood as familiar aberrations (see Figure 2-3) and the whole series is orthogonal. I.e., the various terms, and their contributions to any given circular function, are independent of one another: adding, say, vertical coma to a function does not alter the level of astigmatism it contains, using the terminology of Figure 2-3, and so on.

Given the exact shape of a wavefront, a coefficient can therefore be calculated for any Zernike term, independent of all other coefficients. That is, the equation

$$Wavefront\ shape = \sum Zernike\ polynomials \times their\ coefficients \quad (1)$$

can be solved uniquely for the coefficients, whichever Zernike terms are included*.

* By multiplying both sides by each chosen Zernike polynomial, and integrating over the circle (pupil area).

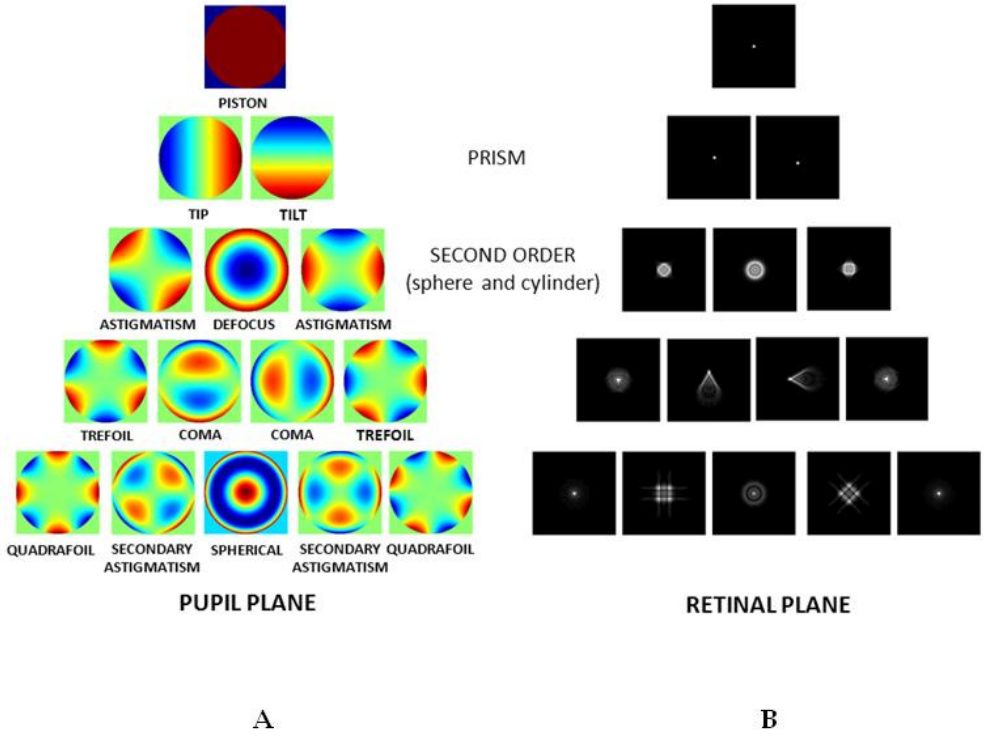

Figure 2-3: (A) The lower order Zernike polynomials, corresponding to particular aberrations of a wavefront. Colour indicates relative phase of that part of the beam. (B) The point spread function (e.g. at the retina) resulting from each aberration. From Vera-Díaz and Doble (2012), with permission.

The coefficients of the Zernike modes describe the relative contributions of the Zernike modes to the total shape of the wavefront. The relative phase of the wavefront at a location across the beam is usually measured in microns, and so this is usually the unit of the coefficients. It is often helpful to understand the contributions in terms of optical power for defocus and astigmatism, and the values of the Zernike coefficients can be converted into dioptres, where appropriate. For instance, defocus in dioptres is

$$\frac{4\sqrt{3}}{(beam\ radius\ in\ mm)^2} \times c_4$$

where c_4 is the Zernike coefficient for defocus, in microns[*] (Applegate et al., 2003).

2.2.4 Limitations of the aberrometry technique

Use of a Shack-Hartmann wavefront sensor and the Zernike polynomials allows us to describe aberrations imaged onto the lenslet array of the sensor. However, there are approximations and limitations within the technique.

First, the Shack-Hartmann wavefront sensor only provides information about the shape of the wavefront down to the resolution of the lenslet array. Second, we have information about the average *slope* of the wavefront over a lenslet, but not the actual phase of that part of the wavefront. Using the slopes to return to a single estimate of the phase at each lenslet would be a further approximation, with a potentially serious impact on accuracy.

Using the slopes, instead of the phase, equation (1) (page 47) for the Zernike coefficients becomes

$$\begin{aligned} &Sampled\ average\ slopes\ of\ wavefront \\ &= \sum Sampled\ average\ slopes\ of\ Zernike\ polynomials \\ &\times their\ coefficients \end{aligned} \tag{2}$$

Now, the derivatives of the Zernike polynomials are not orthogonal[†], so as well as introducing approximations from the averaging of slopes across the lenslets, solving this equation will not in general lead to unique solutions, and there will be some coupling between coefficients, which will decrease

[*] We might call this result "Zernike defocus". A better estimate of the true defocus, or spherical equivalent error, can be found by including coefficients of higher-order, circularly symmetric modes (Thibos et al., 2004; Lopez-Gil and Fernandez-Sanchez, 2010). This is taken into consideration in chapters 6 and 8.

[†] For instance, the integral of Zernike defocus ($2r^2 - 1$) × spherical aberration ($6r^4 - 6r^2 + 1$) is zero, but the integral of the product of their derivatives is not.

the precision of the estimates of the coefficients (Cubalchini, 1979)[*]. In our system, a single estimated value is computed for each coefficient, which may therefore be misleading. The coupling is minimised by including fewer Zernike terms and coefficients in the calculation, relative to the number of sampling points. That is, fewer parameters must describe a defined surface, so coupling between the parameters will be restricted in range.

2.3 Stimulus control

2.3.1 Visible target

In these studies, a black Maltese cross on a colourless background was back-illuminated with a tungsten-halogen lamp to provide a visible target (as in Figure 2-4). The observer fixated on an image of the target, while the IR beam and Shack-Hartmann sensor interrogated the optics of the eye.

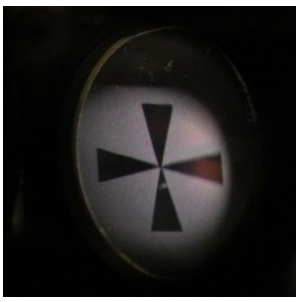

Figure 2-4: A photograph of the target, taken from the participant's point of view, in the monocular apparatus of chapters 3–6. The edge of a parabolic mirror is visible. The faint red patch visible with the camera is not visible to eye; the background appears a much warmer white colour to the eye.

2.3.2 Dynamic control of the target

In the instruments developed, DMs were used to control the aberrations of the stimulus to the participants.

A series of deformations of the DMs were used with the Shack-Hartmann sensor to calibrate the effect of the deformations on the aberrations of a beam

[*] As one illustration, Cubalchini found a correlation between coma and tilt. The variance of the estimate for the tilt aberration was degraded by more than a factor of 2, when the comatic terms were included.

passing through the system. The DMs could then be used to cancel out any aberrations present from inaccurate positioning, and inherent properties, of the many optical components. Finally, the calibration allowed controlled changes to be made to the stimulus during fixation, using deformations of the mirrors. This process is described in more detail in chapter 7, with reference to the development and performance of the binocular adaptive optics system.

The aberrations of the stimulus can be modified with considerable flexibility, based on the selection and combination of Zernike terms. Most simply, the vergence of the target at the eye can be changed very rapidly by a DM. The higher-order aberrations of the eye, and components of them, measured using the Shack-Hartmann wavefront sensor, can also be corrected or modified, for example by inversion (Chin et al., 2009b). Combinations of even- or odd-order Zernike terms can be chosen, for instance (ibid.). Further, since fluctuations in these aberrations, and accommodative power, are being measured over time with a certain frame rate, they can also be dynamically corrected or modified as the systems allow (ibid.). Changes in the accommodative response owing to such changes may provide new insight into the accommodation control system, and potentially, the development of myopia (see chapter 1).

3 Monocular adaptive optics instrumentation and development

3.1 Design

3.1.1 Overview

Figures 3-1 to 3-3 (pages 55–57) illustrate the monocular apparatus for studying accommodation dynamics. The general principles of such an adaptive optics (AO) aberrometer for the eye have been discussed in chapter 2. As described there, this system features a visible stimulus, a deformable mirror (DM) as the AO element for stimulus control, a Shack-Hartmann wavefront sensor, and means to simultaneously provide the visible stimulus and perform infrared (IR) aberrometry on the eye.

The instrument was based on that originally developed by Hampson et al. (2009), and also see Chin (2009), containing one main modification: the pair of parabolic mirrors close to the eye replaced a pair of lenses that had previously performed the same functions (see sections 3.1.2 and 3.1.3). Reflections from the surfaces of those lenses had resulted in stray light in the system which was difficult to filter from the signal. The stray light made it difficult to collect reliable data, although it was possible to perform experiments (Chin et al., 2009a; Chin et al., 2009b; Hampson et al., 2010). The parabolic mirrors[*] were designed to focus beams incident at 45°.

Thorough realignment of the whole apparatus was necessitated by the replacement of these components, and also by the temporary removal of the system from the laboratory for essential building work, prior to the work towards this thesis. In the process of realignment, several modifications were made to

[*] Edmund Optics, part numbers: NT83-973, NT47-099; diameters: 25.4 mm; focal lengths: 203.2 mm, 101.60 mm.

mounting and positioning accessories for the optics. In particular, the arrangement of components of the “stroke amplification relay” (see Figure 3-1) was redesigned and assembled (see section 3.2.1). These changes allowed improvements to the alignment process, making it more systematic, and progress can be seen when comparing the calibration results of Chin (2009) and those in section 3.3.

The remainder of section 3.1 describes the optical design of this apparatus. Sections 3.2 and 3.3 relate the development and alignment processes, and the calibration of the instrument.

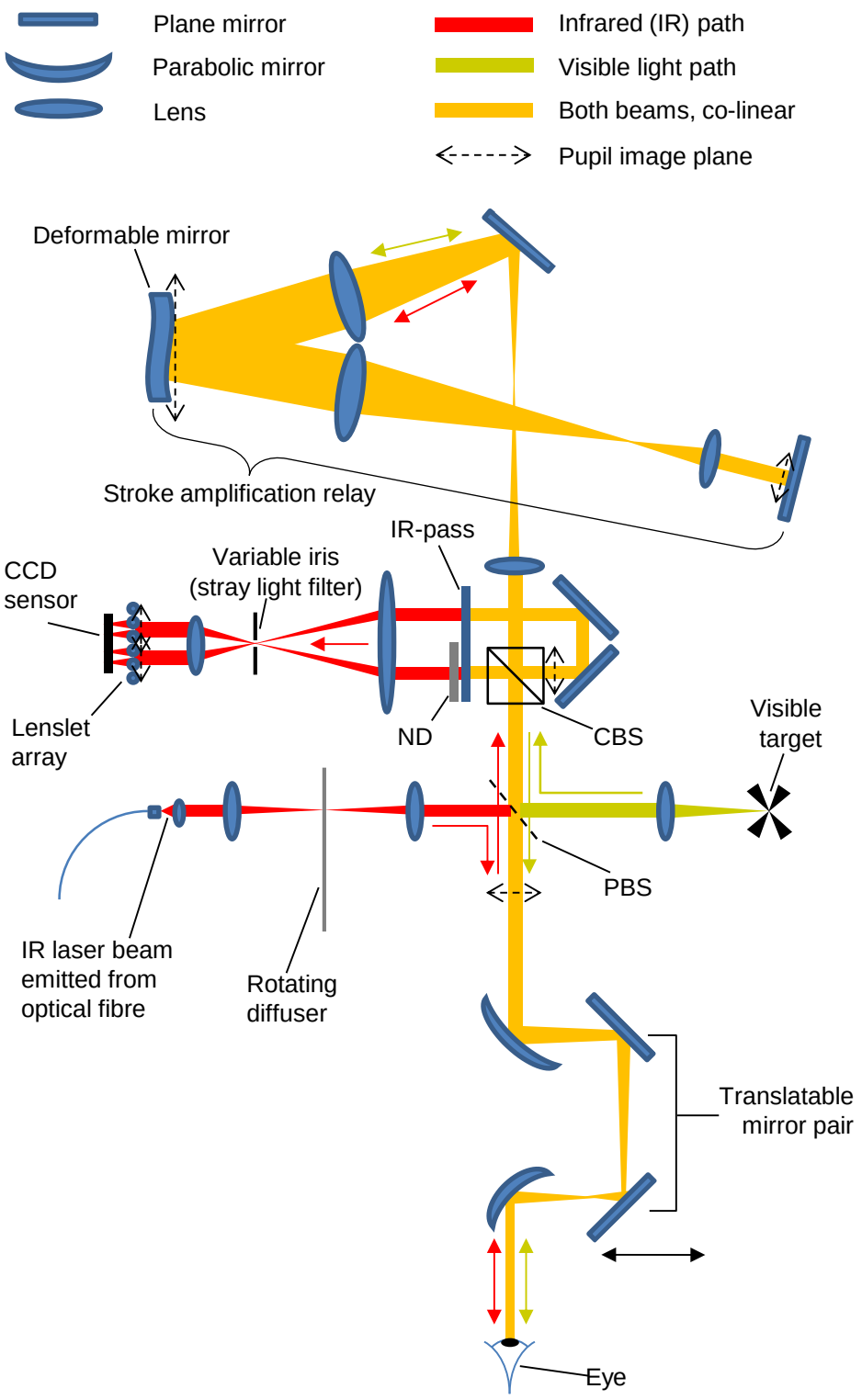

Figure 3-1: Diagram of the monocular adaptive optics apparatus.
IR-pass: filter blocking visible radiation (below 715 nm); ND: neutral density filter;
CBS: cube beamsplitter; PBS: pellicle beamsplitter

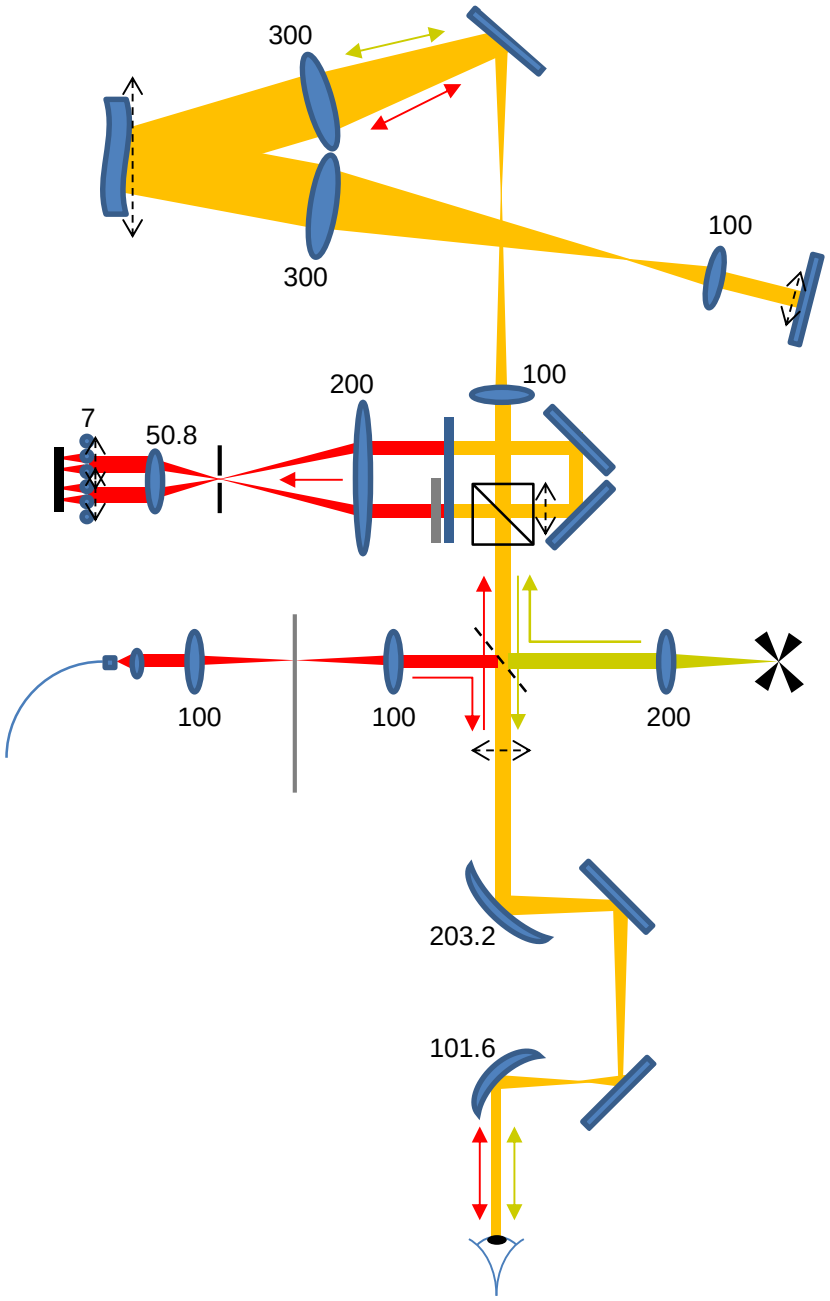

Figure 3-2: The instrument of Figure 3-1 (same legend), showing the focal lengths of the focussing elements in mm. Separations between elements are described in sections 3.1.2 and 3.1.3; the ocular pupil plane is imaged at the deformable mirror and the lenslet array.

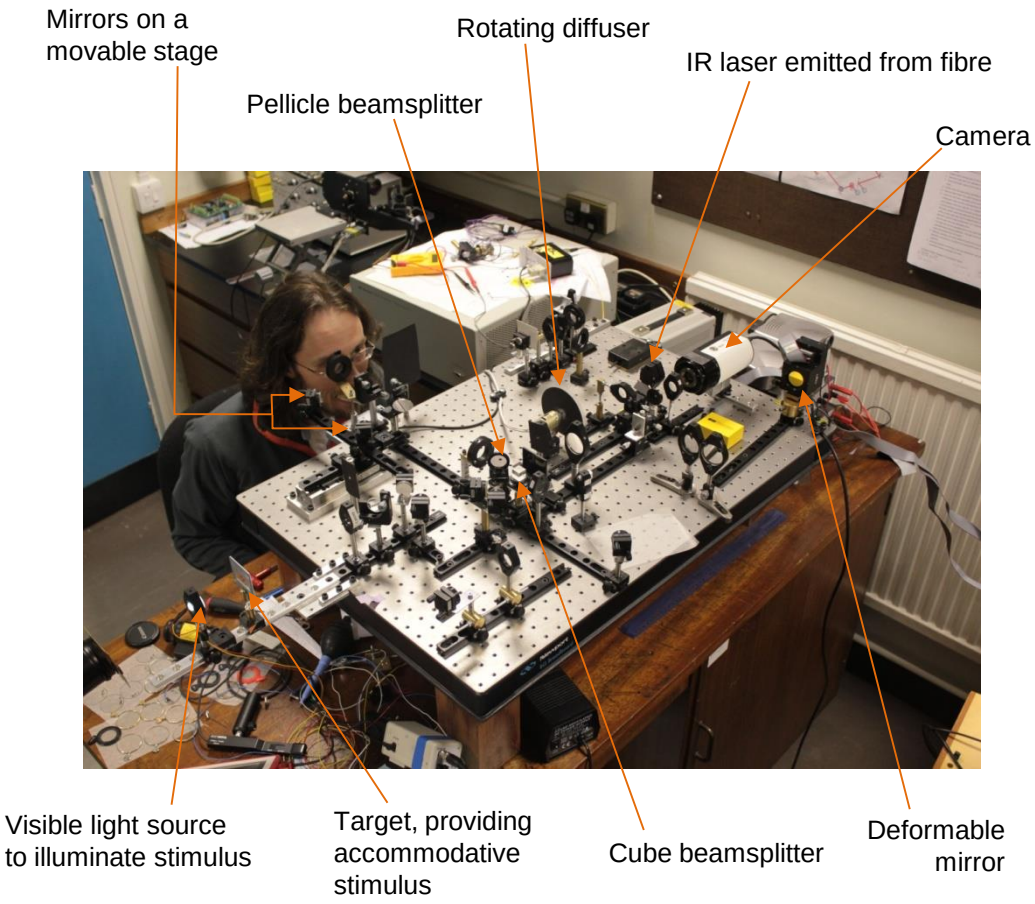

Figure 3-3: Photograph of the monocular adaptive optics apparatus.

3.1.2 Visible stimulus

A black Maltese cross on a colourless background, the "stimulus object" was back-illuminated to provide the accommodative stimulus (shown in Figure 2-4, page 51). This pattern is a commonly used accommodative target, containing high-contrast edges in a variety of orientations. The observer fixated on an image of the pattern, while the IR beam and Shack-Hartmann sensor interrogated the optics of the eye.

Light from the stimulus object was collimated, and then reflected at the pellicle beamsplitter (PBS, Figure 3-1). Travelling through the cube beamsplitter (CBS), the light was relayed to the deformable mirror (DM) as a collimated beam. It was made to reflect twice at the DM by the "stroke amplification" relay lenses and mirror. It was finally relayed to pass back through the CBS and PBS, and

through the parabolic mirrors, to provide an image of the stimulus object to the observer.

The translatable mirror pair of Figure 3-1 was mounted on a rail, so that the distance between the two parabolic mirrors could be varied. An image of the stimulus object could be provided at optical infinity, when object was one focal length from its closest lens, and the distance between the parabolic mirrors was set to the sum of their focal lengths. The baseline image (before modification by the DM) could be brought closer to the participant by moving the pair of plane mirrors closer to the parabolic mirrors.

With the pupil of the eye at the focal point of the nearest parabolic mirror, the change in angular size of the stimulus was minimised with respect to mirror position, as in Badal's optometer[*].

During fixation, the distance to the accommodative stimulus was modulated by the DM. Through the stroke amplification relay, the DM was made conjugate with itself, to double its modifications of the phase across the beam, as in Webb et al. (2004) (see also section 3.1.4). Along the stimulus path from the DM to the parabolic lens furthest from the eye, the distance between lenses (or between lens and parabolic mirror) was the sum of their focal lengths. Curvature of the wavefront by the DM was imaged at the pupil, producing movement of the visible stimulus, towards or away from the participant.

There were irrelevant or undesirable visible light paths, such as those diverted towards the camera by the CBS. Those paths were absorbed by an IR-pass

[*] There is a small change in image size as the dioptric stimulus is varied, since the image formed between the two parabolic mirrors is magnified differently for different image positions. Angular size was calculated to increase by 16%, when moving from 0 to 4 D, the stimulus range in chapters 4–6.

filter, to prevent them interfering with recording of the IR intensity pattern at the camera chip.

3.1.3 Two-channel infrared aberrometry

830 nm radiation from a diode laser was emitted from an optical fibre, and collimated. It was first focused onto a rotating diffuser, which caused the laser speckle pattern from the roughness of the retina to be rapidly varied over time, and averaged over the camera exposure time. This averaging prevented distortion of the positions of the intensity maxima at the camera, and misinterpretation of the intensity pattern, for instance in overestimation of total RMS aberration (Hofer et al., 2001).

Propagating from the rotating diffuser, the beam was recollimated and reflected towards the eye by the PBS. It passed through a pair of parabolic mirrors, which minified the beam. Sending a small beam through the cornea and crystalline lens reduced aberrations in the desired point focus on the retina (see section 2.2.1). The smaller the IR spot on the retina, the narrower the range of directions in the IR beam reflected from the eye, producing less blur of the intensity maxima at the camera. The smaller the spots at the wavefront sensor, the more precise the measurement of the wavefront slope. The measured power of the laser at the cornea was set to 0.33 mW. This is approximately half the maximum permissible exposure of the eye at this wavelength of 0.7 mW, for 8 hours' continuous viewing (British Standards Institution, 2009).

After the IR beam was scattered at the retina, some of the radiation passed back through the crystalline lens, the pupil and the cornea. Following the return through the two parabolic mirrors, if the eye were free from aberrations, the IR beam would have been a plane wave, since the visible beam had originally

been collimated before meeting the parabolic mirrors. For the real observers, responding to the visible stimulus, a lead or lag of accommodation and higher-order aberrations (HOAs) of the eye were now encoded in the shape of the wavefront of the IR beam.

Longitudinal chromatic aberration, resulting in different vergences of IR and visible radiation leaving the eye, was considered negligible, since adjustment of the stimulus object to relax accommodation also resulted in a focussed IR spot, visible as a red spot to the observer. Further, the measures of static accommodation were as expected (see for instance the long pulses in chapter 5), within the natural inaccuracy of accommodation (Abbott et al., 1998). It will be apparent that any small difference in the focussing power of the eye for the white light of the stimulus and that for the 830 nm radiation has little bearing on the conclusions of chapter 6. Achromatic doublet lenses were used to minimise chromatic aberration within the instrument.

The cube beamsplitter acts to provide two aberrometry channels for the system. One half of the beam is directed straight away towards the Shack-Hartmann wavefront sensor (the “eye channel”); the other half is passed on to the DM before it is eventually relayed to the wavefront sensor (the “DM channel”). The brightnesses, at the sensor, of the eye channel and DM channel are balanced by the ND filter. Sections 2.2.2 and 3.1.5 contain further description of the wavefront sensor.

Along both IR paths, from the parabolic mirror furthest from the eye to the lenslet array of the wavefront sensor, all distances between lenses (or lens and parabolic mirror) were the sum of their focal lengths, relaying the image of the pupil onto the DM and onto the wavefront sensor. The DM is one focal length

from both lenses closest to it. The lenslet array and the plane mirror of the stroke amplification relay are both one focal length from their respective closest lenses.

The eye channel beam arrived as the upper beam at the lenslet array in Figure 3-1, which produced the Shack-Hartmann intensity maxima at the camera chip, one focal length from the lenslets. With the pupil conjugate to the lenslet array, the intensity pattern could be analysed (see section 2.2.3) to describe the shape of the wavefront of the IR beam as it exited the eye (having been scattered at a point on the retina). Magnification of the wavefront between the pupil and lenslet array was taken into account.

After a convoluted path via the DM, the stroke amplification relay, the CBS and its closest two plane mirrors, the DM channel beam arrived at the lenslet array as the lower beam in Figure 3-1. The DM channel was useful for observation and calibration of the action of the DM, using a model eye (a lens with f = 19.0 mm and a white card retina).

The eye channel provided the wavefront from the eye, without the confounding effect of the DM. Other systems using DMs for AO control of the stimulus wavefront do not have these independent channels (Fernandez and Artal, 2005; Chen et al., 2006; Fernandez et al., 2009; Gambra et al., 2009; Sabesan et al., 2012). In control and analysis of those systems, it is necessary to take account of the interaction of the wavefront returning from the eye with the controlled shape of the deformable mirror.

In both the eye channel and the DM channel, the beam passed through an iris at the focal point of the penultimate relay lens. The closing of this iris blocked

stray light from Purkinje-Sanson images and other reflections from reaching the sensor.

3.1.4 Deformable mirror

The DM was a 30 mm diameter, 37 channel, piezoelectric DM (Flexible Optical B.V., The Netherlands). In this mirror, the 37 piezoelectric actuators were bonded to the rear of a deformable plate, which had a reflective coating. They had a maximum specified stroke of 8 μm, which was effectively doubled by the stroke amplification system labelled in Figure 3-1. Therefore, the maximum relative displacement the DM could introduce across a wavefront was 32 μm[*]. The USB digital-to-analogue converter (DAC) from the same company was used to convert computer-generated signals to voltages which were amplified and applied to the actuators. The DAC was specified to have a typical refresh rate of 1 kHz.

The DM was used to cancel out inherent aberrations of the system and vary the accommodative stimulus from its baseline setting. In the previous developmental stage of this apparatus, the DM was also used to modify HOAs of the stimulus (Chin, 2009; Chin et al., 2009b).

A small angle of incidence at the DM was required to maximise the aperture of the DM and the effective stroke of the actuators, and also to maintain accuracy of the stroke amplification relay. If the angle of incidence were too great, the DM would be too far from being conjugate with itself, through the stroke amplification relay, in some regions. Imaging of the wavefront from the DM to the pupil would also be less accurate. We would expect a reduction in the

[*] 8 μm × 2 for path difference in reflection × 2 with stroke amplification.

accuracy of DM calibration (see section 3.3, and section 7.3.2 for the binocular AO system) in this case.

3.1.5 Wavefront sensor

The Shack-Hartmann sensor (see section 2.2.2) consisted of a square lenslet array of pitch 0.2 mm and a CCD camera (Retiga EXi Fast 1394, from QImaging, Canada) with resolution 1392 × 1040 pixels and chip dimensions 8.98 mm × 6.71 mm. The CCD pixels were square and there were therefore approximately 31 pixels[*] available in each direction for sensing of the wavefront slope at each lenslet.

The focal length of the lenslet array was 7 mm. Therefore, the maximum wavefront slope at a lenslet that could be detected was 1.6°[†]. Beyond this angle, a lenslet's focussed intensity maximum would pass into the "search block" on the CCD chip that corresponded to an adjacent lenslet in the array (see section 2.2.2). At the edge of a 5 mm pupil, 2 D of defocus resulted in slopes close to the limit of the system.

Figure 3-4 shows the intensity maxima produced by the lenslet array at the camera chip, using a model eye.

[*] 1392 pixels × 0.2 mm ÷ 8.98 mm
[†] $\tan^{-1}$(0.2 mm ÷ 7 mm)

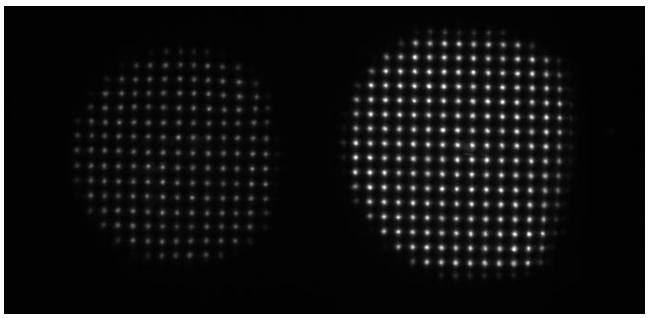

Figure 3-4: Shack-Hartmann intensity maxima at the camera chip, output to a PC monitor. A pattern from each channel is visible, with some vignetting of the beam. A model eye was used, with a collimated beam incident on the lens of the eye, and the deformable mirror set to cancel out aberrations of the apparatus. The beam resulting in the left-hand image has lost energy in an extra reflection at the cube beamsplitter and other smaller losses in the DM channel; the ND filter was not in place in this case.

3.1.6 Dynamic stimulus control and wavefront analysis

A workstation controlled the voltages sent to adjust the DM and recorded the intensity pattern from the camera. Software built by Dr. Karen Hampson at the University of Bradford was used for this control and acquisition, as in Hampson et al. (2009) and Chin (2009). The software converted the intensity pattern at the CCD chip into Zernike polynomials describing the wavefront exiting the eye (see sections 2.2.3 and 2.2.4), including the magnification factor between the pupil and the lenslet array.

The fastest rate at which data could be captured in this control loop, and settings applied to the DM, was 20 frames s^{-1} (to the nearest frame s^{-1}). It was limited mainly by the exposure time or readout time of the CCD camera. For the exposure times used in calibration, and in the data acquisition of chapters 4–6, the total frame time was 50 ms, limited by the readout time. It was increased from around 100 ms (as in the binocular AO instrument of chapters 7 and 8) by binning pixels together in groups of four for readout.

3.2 Development

3.2.1 Optical alignment

Following the work of Hampson et al. (2009) and Chin (2009) with the previous generation of this apparatus, it had been necessary to remove the apparatus from the laboratory, for essential building work at the University of Bradford. When the apparatus was returned to the laboratory, it required thorough realignment, and the parabolic mirrors replaced a pair of lenses, as discussed in section 3.1.

Alignment included adjusting all components so that the optical paths were the correct lengths and focussed images were obtained: images of the pupil plane at the camera, and of the DM at the pupil, as described in sections 3.1.2 and 3.1.3. The visible and IR beams were centred on the optical elements to minimise aberrations and maximise tolerance of alignment without vignetting of the beams. It was necessary for the visible and IR beams to be collinear.

Using the naked eye, an IR viewer, IR cameras, and scattered reflections, pieces of paper and lens tissues to view beam locations, the following steps were among those taken. Alterations often necessitated checks and adjustments of the alignment of other components.

- The PBS and the visible beam were moved so that the IR and visible beams were concentric on the PBS and on points within the collimating optics for both the IR source and stimulus object. The location of the beams on the PBS needed to be accurate such that the beam returning from the eye was not occluded by the PBS mount. (The beam is expanded by the parabolic mirrors on its return from the eye, with the 1” PBS mount at 45° to the beam.)

- The lenses and plane mirror of the stroke amplification relay were set to the correct distances, with an angle offset, such that two images of the stimulus object could be seen at the same distance between the lenses. Mounting was improved such that the joint axis of the mirror and its closest lens (f = 100 mm) could then be rotated to bring the reflected beam back to collinearity with the incident beam. The DM and the two lenses with f = 300 mm also required alignment without optical rails, to achieve the small angle of incidence desired at the DM (see section 3.1.4).
- Using a model eye (a lens with f = 19.0 mm and a white card retina), the IR and visible beams were made concentric at the stimulus image formed within the stroke amplification relay. They were also checked for collinearity at the image point upwards from the CBS in Figure 3-1 and other locations within the system.
- The angles of the parabolic mirrors and translatable plane mirrors were adjusted such that movement of the plane mirrors did not move the beams incident on the pupil.
- The angle of the CBS was adjusted so that reflections from its outer surfaces were sufficiently misaligned with the signal beam, such that those reflections did not pass through the stray light filter. The combination of the CBS and its two closest plane mirrors required accurate alignment to achieve this filtering of stray light, whilst retaining the signal beam.

3.2.2 Diagnosis and repair of the DM voltage amplifier

During alignment and calibration, one and then two actuators of the DM became irresponsive to control voltages from the computer. When various electrical

connections between the computer and the DM were tested, the fault was found to lie within the voltage amplifier supplied by the DM manufacturer.

The enclosure for the amplification circuitry was opened, and testing revealed that connections in the amplification circuitry had melted. The resulting disconnections were between the input and output to the relevant actuators.

The DM was specified by the manufacturer to take an input of 400 V, to move an actuator to one extreme of its 8 μm range. However, the voltage amplifier supplied was in an enclosure containing only a single fan, above a stack of two circuit boards (controlling half the actuators each). Connections on the lower circuit board had melted. When insufficient cooling had been diagnosed, the connections in the amplifier circuitry were resoldered and a new enclosure was made. It used a more powerful fan and the circuit boards were arranged side by side. Normal function of all actuators was regained and not subsequently lost. Two high-voltage supplies were used to power the amplifier (with 225 V each); their stability was checked in the repaired control arrangement.

3.2.3 Control software

Development and testing of the software was an important part of the preparation of this apparatus. The C++ code was written by Dr. Karen Hampson.

3.3 Calibration

The model eye (lens and white card retina), was used for calibration of the instrument. The position of the retina was adjustable along the axis of the lens. It was set so that the model eye was measured to be emmetropic by retinoscopy and have a refractive error of plano/−0.25x136 with a Shin-Nippon SRW-5000 autorefractor.

During calibration, a +2 D lens was often in place, near to the pupil plane, to correct the system for the model eye, because the baseline vergence at the eye was set to −2 D, in preparation for experiments (see chapter 6).

3.3.1 Defocus and astigmatism of the model eye, observed in both channels

The eye channel measured 1.7 D of astigmatism from the model eye, probably mainly owing to beam size and eccentricity at the parabolic mirrors and other components. This aberration was also present in the DM channel, and was too severe for the DM to be well calibrated and to correct for it. The astigmatism was partially corrected with a +1.5 DC trial lens, also close to the pupil plane. At this point, measurements of the eye channel and DM channel gave close spherocylindrical errors (e.g. eye channel: −0.06/−0.25x127, DM channel: −0.28/−0.14x137).

After calibrating the effect of moving each actuator of the DM in both directions from their mid-point (see sections 2.3.2 and 7.3.2), the DM was set to cancel out aberrations in the DM channel. The remaining spherocylindrical error in the DM channel was typically plano and in the eye channel was typically −0.1 DS/−0.3 DC.

To check the calibration of the measurement of defocus, various powers of trial lens were used in front of the model eye. The Zernike coefficients calculated by the measurement and control software were recorded, and the defocus coefficient was converted into dioptres (see section 2.2.3). The change in spherical defocus returning from the eye was proportional to the change in trial lens power, as shown in Figure 3-5.

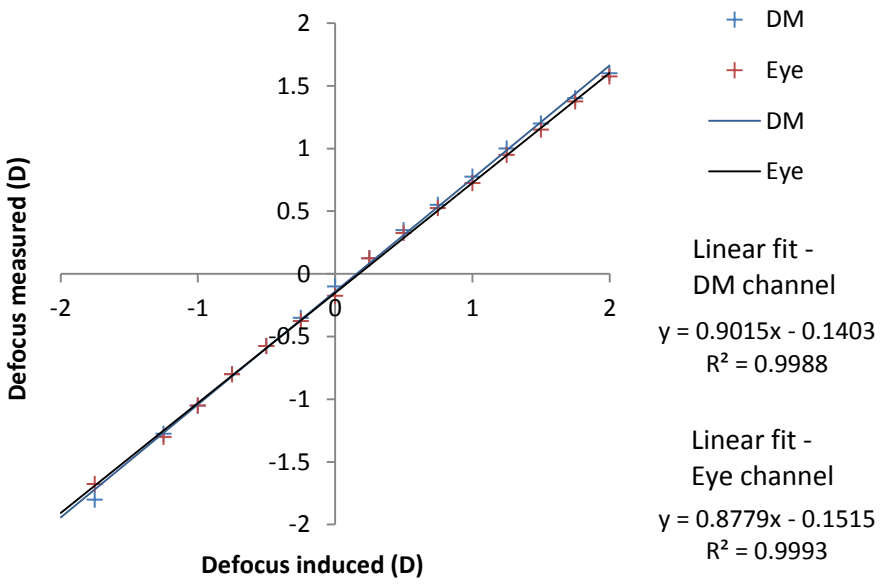

Figure 3-5: Calibration of defocus detection, using trial lenses in front of a model eye. The linear fit was calculated in Microsoft Excel. The trial lenses were in imperial units of power.

The changes in measured and imposed defocus would ideally have been equal, but there was an unknown optical path length between the lenslet array and the camera chip. The lenslet array was attached to a mount which was screwed into a thread in the camera casing, and the distance concerned was not directly measureable, and may not have been equal to the focal length of the lenslets (7 mm). A factor within the software could have been adjusted to correct for this, but it was sufficient for the analysis of chapter 6 in particular that the measurement is linear with the defocus imposed and the gradient ≈ 1.

The measurement of cylindrical defocus from the eye was also checked. Cylindrical trial lenses were introduced near to the plane of the model eye, and the spherocylindrical aberration detected by the control and analysis software was compared with predictions carried out in MATLAB (Mathworks, 2011). The MATLAB code for adding cylindrical aberrations to the residual system aberration was provided by Dr. Karen Hampson at the University of Bradford, and was based on decomposition into spherical and cylindrical lens powers, as

found in Thibos et al. (1997). The results are shown in Table 3-1 and show agreement, to within 0.1 DS/0.1 DC, and usually within 0.05 DS/0.05 DC. This agreement is good, especially given that the axis of the trial lens was positioned at 45° without the use of gradations on the lens holder, introducing imprecision to the comparison.

The use of the parabolic mirrors and realignment of the system considerably improved the performance of this AO apparatus. Stray light and associated alignment difficulties had previously limited the calibration range to ±0.75 DS and DC (Chin, 2009; Hampson et al., 2009); following the developments of this chapter, a range of approximately ±2 D could be used.

Table 3-1: Predictions and measurements of spherocylindrical aberration of the model eye with additional cylindrical lenses.

Trial lens (cylindrical dioptres at x45)	Spherocylindrical aberration			
	Eye channel		DM channel	
	Predicted	Measured	Predicted	Measured
0	–	−0.06/−0.25x127	–	−0.28/−0.14x137
−1.50	−0.30/−1.26x47	−0.28/−1.28/x43	−0.42/−1.36x45	−0.38/−1.40x47
−1.00	−0.30/−0.76x48	−0.27/−0.77x42	−0.42/−0.86x45	−0.34/−0.95x44
−0.75	−0.30/−0.51x49	−0.27/−0.53x52	−0.41/−0.61x45	−0.37/−0.65x51
−0.50	−0.30/−0.26X52	−0.28/−0.28x58	−0.42/−0.36x45	−0.40/−0.39x53
−0.25	−0.27/−0.07x86	−0.24/−0.13x86	−0.42/−0.11x44	−0.41/−0.14x56
+0.25	+0.19/−0.50x131	+0.19/−0.49x123	−0.03/−0.39x136	−0.04/−0.37x130
+0.50	+0.43/−0.74x132	+0.40/−0.72x123	+0.22/−0.64x135	+0.19/−0.61x129
+0.75	+0.68/−1.00x133	+0.67/−0.98x125	+0.47/−0.87x131	+0.45/−0.87x131
+1.00	+0.93/−1.24x133	+0.86/−1.14x133	+0.72/−1.14x135	+0.68/−1.10x141

3.3.2 Pulses of defocus, generated and observed in the DM channel

Using the IR beam reflected from a model eye, the action of the DM can be observed in the DM channel at the wavefront sensor.

Figure 3-6 and Figure 3-7 report the results of testing control of the DM. Following calibration, the control software was repeatedly used to send

instructions to the DM to deform after set numbers of camera frames, such that it should effect a specific pulse in defocus at the eye; the resultant Zernike defocus in the DM channel was extracted and converted to dioptres. Figures 3-6 and 3-7 show small variations in the pulse baseline values and height, as the tests were carried out, but the steps in defocus, for a stimulus passing via the DM, were generated as required for the studies of chapters 4–6. Pulses of intermediate duration to those of Figure 3-6 showed the same characteristics.

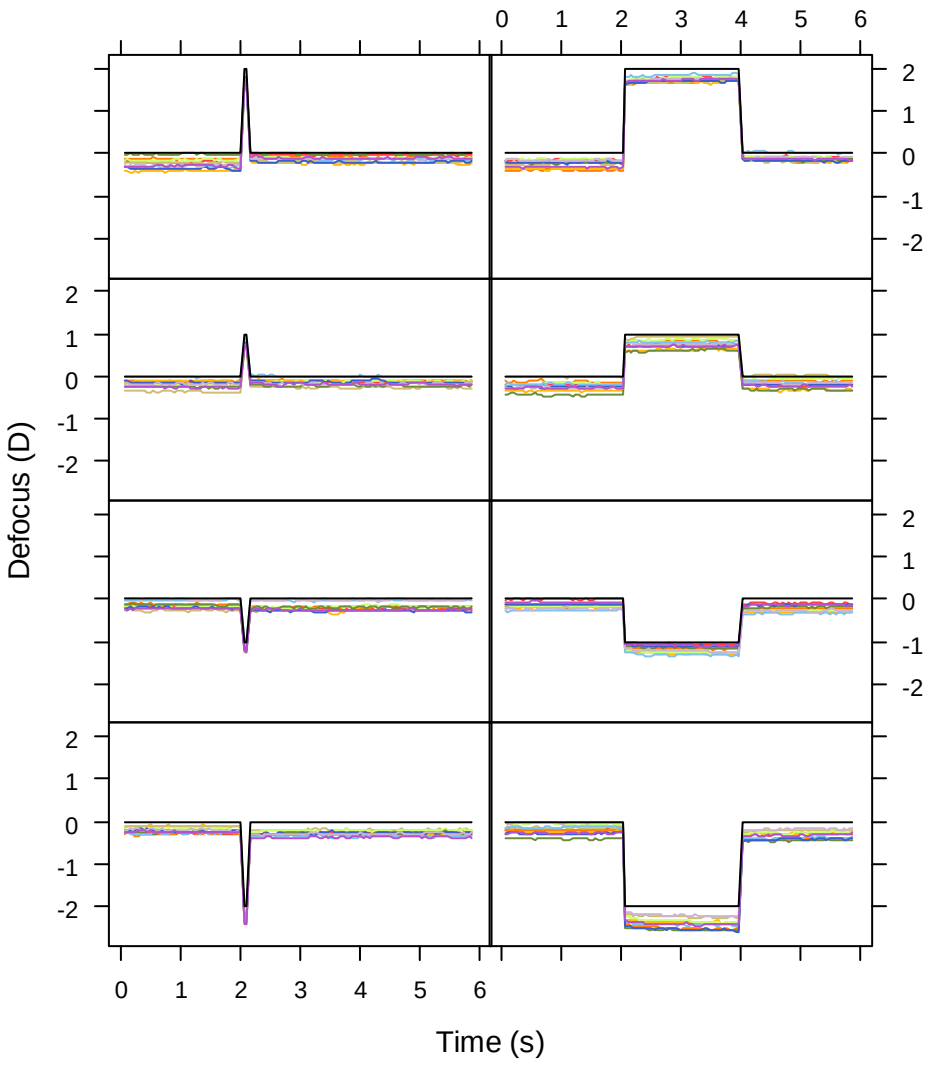

Figure 3-6: Tests of the DM in producing a pulse in defocus at the wavefront sensor. Two different durations of the pulse (2 frames, 40 frames) and four pulse heights (−2, −1, +1 and +2 D) were tested ten times. The black lines are the ideal response of the system. This figure was plotted using the "lattice" package (Sarkar, 2008) in R (R Development Core Team, 2012).

Note that the pulse with the single-frame duration (Figure 3-7) shows no plateau to the defocus recorded. In reality, the spike portrays a square pulse; aberrations are calculated for the total exposure of each frame, resulting in one data point per frame.

These trial pulses again illustrate the improvement in performance of the apparatus. Previously, experiments were limited to reliable steps of ±0.5 D in the stimulus to accommodate.

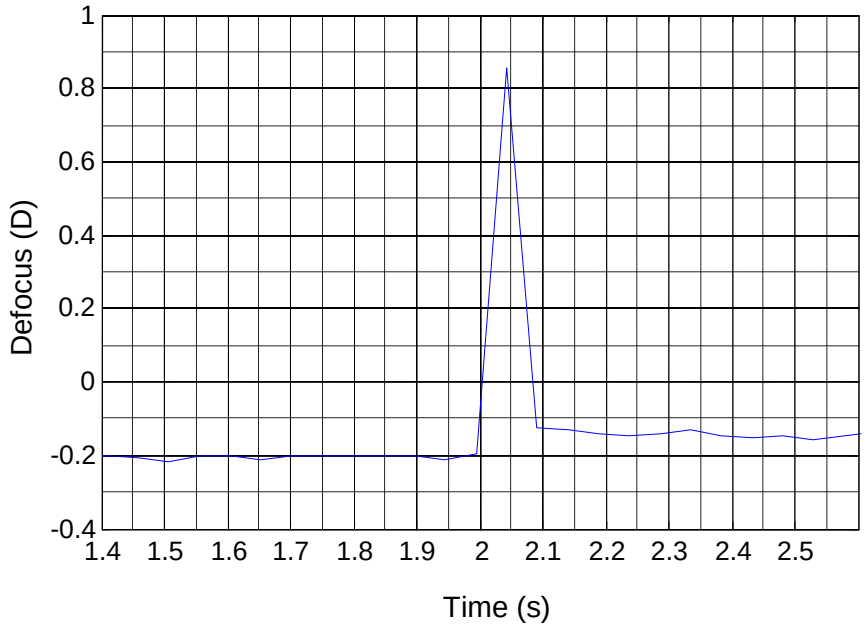

Figure 3-7: Defocus in the DM channel, using the model eye, for a dioptric pulse of 1D, with duration of a single frame of exposure at the camera. The frame length of the apparatus was 50 ms. This graph was plotted in MATLAB (Mathworks, 2008).

4 Pilot study: The monocular accommodative response to a brief pulse in dioptric stimulus

4.1 Introduction

To test the monocular apparatus of chapter 3, a pilot study was carried out with one participant. Data were collected on the monocular accommodative response (AR) to a brief pulse in dioptric accommodative stimulus (AS), with pulse durations between 0.05 and 0.40 s.

As introduced in section 1.4.4, Campbell and Westheimer (1960) studied the AR to variations in AS, including a pulsed stimulus. Since then, experiments have continued on step changes in dioptric stimulus (Kasthurirangan et al., 2003; Schor and Bharadwaj, 2005; Bharadwaj and Schor, 2006a), but little has been done to explore the response to short-duration pulses of the stimulus. More recently, Bharadwaj et al. (2009) have considered the adaptive effect of modifying a step change in AS with a brief period of an intermediate or overshooting level of AS, but pulse dynamics themselves remain little explored.

Campbell and Westheimer (1960) used a pulse of 2 D in the stimulus, starting with a “far stimulus”. They found the reaction time of the AR had an average value of 0.37 s. The reaction time was still around this value, even when pulses of only 80–100 ms were used, although some responses were absent at these durations. After the pulse, accommodation decayed approximately to the baseline level.

Khosroyani and Hung (2002) developed a model which simulated the AR to the pulsed AS of Campbell and Westheimer, as well as other dynamic ARs. This model, or further developments of it, may be valuable as part of understanding the response of the eye to its environment.

In particular, Khosroyani and Hung found that a model using a two-stage response to defocus was successful in simulating the AR to a range of dynamic dioptric stimuli. The form of the model was originally proposed by Hung and Ciuffreda (1988); it included a rapid, open-loop response to larger levels of defocus (with no feedback on accuracy during the response) and a slow, closed-loop response, with constant feedback, active when the rapid, open-loop response was not required. The range of simulated dynamic stimuli included pulses, steps, ramps and sinusoids in AS.

4.2 Methods

4.2.1 Data acquisition

The single participant in this study was male, aged 38 years, with a refractive error of −6.00/−0.50x90 in his right eye (left eye: −6.75 DS). He used his right eye, which was his dominant eye[*], and wore his habitual contact lens correction. The experiment was approved by the Life Sciences Research Ethics Committee at the University of Bradford, and was carried out with informed consent of the participant.

The apparatus used was the monocular adaptive optics (AO) system described in chapter 3. A bite bar maintained the participant in one position, so that the pupil image continuously covered the area of the sensor used for aberrometry.

The vergence of the stimulus at the corrected eye was set to zero, using the two plane mirrors on a movable stage, as described in section 3.1.2 (without the +2 D trial lens in place, mentioned in section 3.3). The deformable mirror (DM) was calibrated and used to cancel out aberrations within the instrument (see section 3.3.1).

[*] Determined by the choice of the eye for viewing a target through an aperture.

The DM was used to provide a pulse in AS, i.e. a step away from and back to the baseline AS of 0 D. Pulses of height 0.5 and 1 D (increases in AS) were used; pulse durations were 0.05, 0.10, 0.20, 0.30 and 0.40 s. The exposure time of the sensor was set to 12 ms, providing a high signal to noise ratio. Examples of the pulsed AS, recorded using a model eye, were shown in Figures 3-6 and 3-7, in section 3.3.2. The participant was instructed to attempt to keep the image clear at all times during each trial.

The aberrations of the eye were recorded (see section 3.1.3) at each of the ten pairs of parameters (two pulse heights × five pulse durations), with seven repeats. The ten parameter settings were randomised, using a MATLAB (Mathworks, 2011) script, with a new permutation for each repeat. Each trial was 8 s long, with the pulse beginning 2 s from the start of data collection. The participant was also instructed not to blink; any trial during which the participant blinked was discounted, and a repeat of the trial was carried out at a later point in the sequence.

4.2.2 Data analysis

The aberrations of the eye were recorded and analysed as a sum of Zernike polynomials (Thibos et al., 2002a) for each of the 160 frames in a trial.

In the Zernike description of a circular function, the curvature of a spherical wavefront is approximately described by a single term (Thibos et al., 2004), usually called “defocus”, as introduced in section 2.2.3. The calculated value of this Zernike defocus coefficient was extracted for each frame of each trial, following analysis of the intensity pattern detected by the Shack-Hartmann wavefront sensor (see section 2.2.4). When multiplied by a normalisation

factor*, the defocus coefficient gives the vergence in dioptres of the infrared beam exiting the eye, neglecting weaker, higher-order aberrations (Thibos et al., 2004). The normalised defocus term for each frame therefore described the dynamic AR over a trial.

In some trials, there was no pulse in the AR to the pulsed dioptric stimulus. Such trials were identified by eye, by inspection of the accommodation traces in section 4.3. In the cases where there was a pulse, the maximum value of the AR was found using MATLAB (Mathworks, 2011), from the normalised values of the Zernike coefficient of defocus.

4.3 Results

Figure 4-1 shows a typical AR over the full 8 s of a trial, with a pulse in dioptric stimulus after 2 s. Accommodation is seen to respond to the pulse in AS and decay approximately to baseline, with an offset to the results.

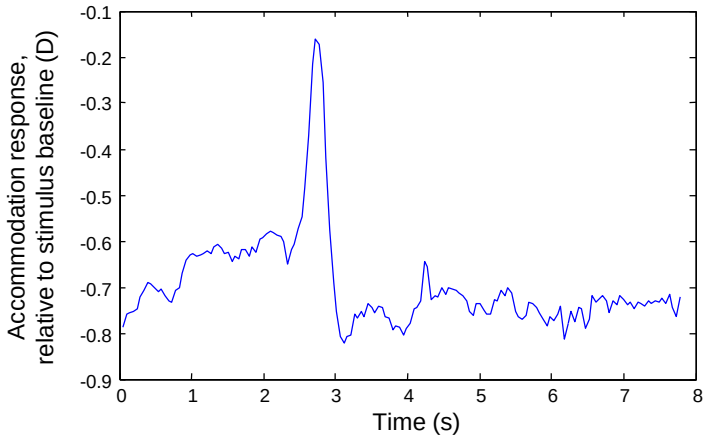

Figure 4-1: One recording of accommodation over 8 s. Microfluctuations of accommodation and the response to the pulse in the dioptric stimulus after 2 s are clearly visible.

Figure 4-2, over seven pages, shows the entire dataset, between time points at 1 s and 4 s during each trial; this interval includes the pulse and any clear

* The normalisation factor is $4\sqrt{3} \div (\text{beam radius in mm})^2$ when the Zernike coefficient is in microns, as it is in the software output.

response to it. Peaks in AR are usually visible, after a latency period following the initial step in AS. There is a variable offset of the baseline AR between trials.

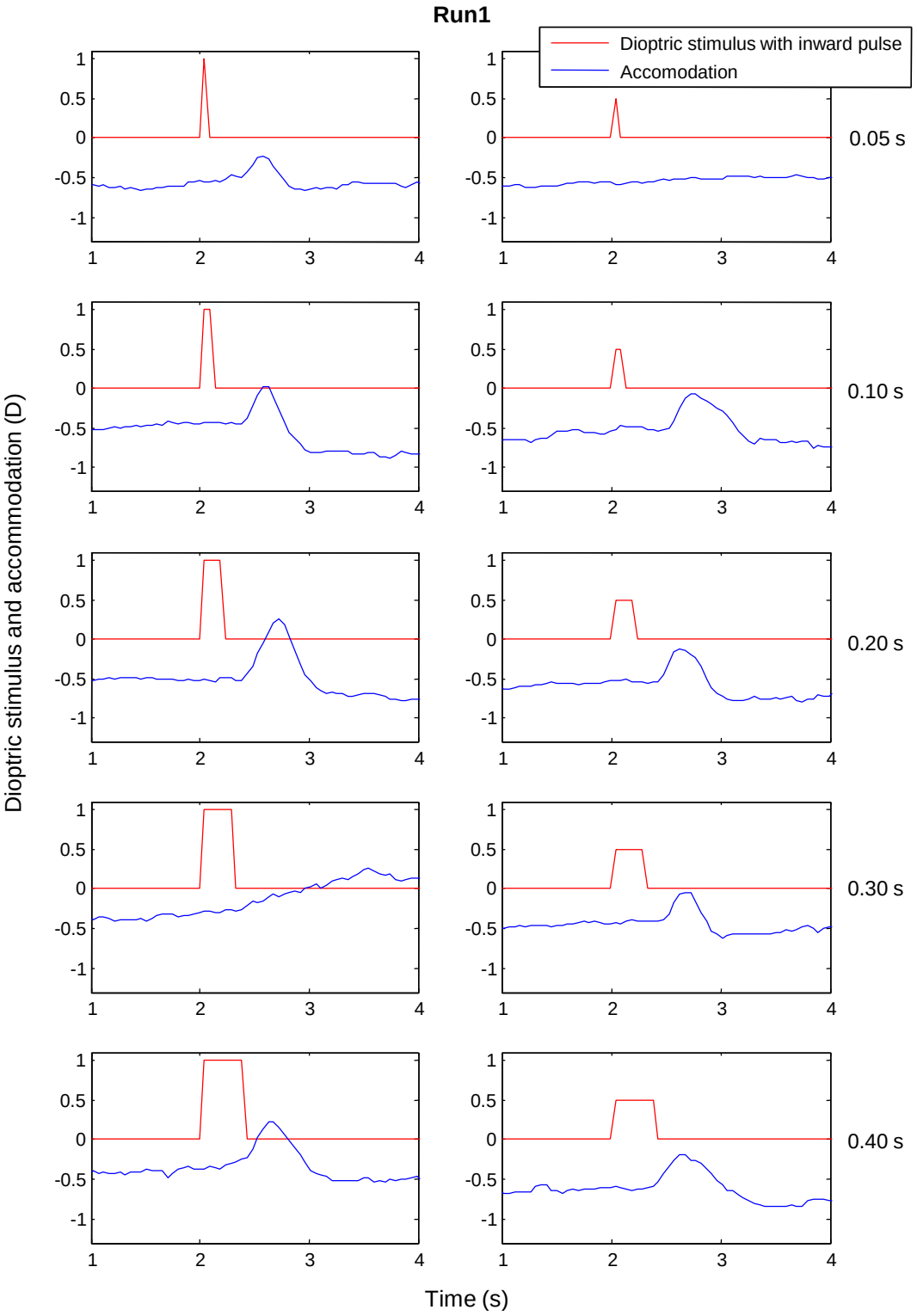

Figure 4-2: The AR in the seven runs through the parameter space for the pulses in AS (this and the following six pages). The pulse duration is given to the right of each row.

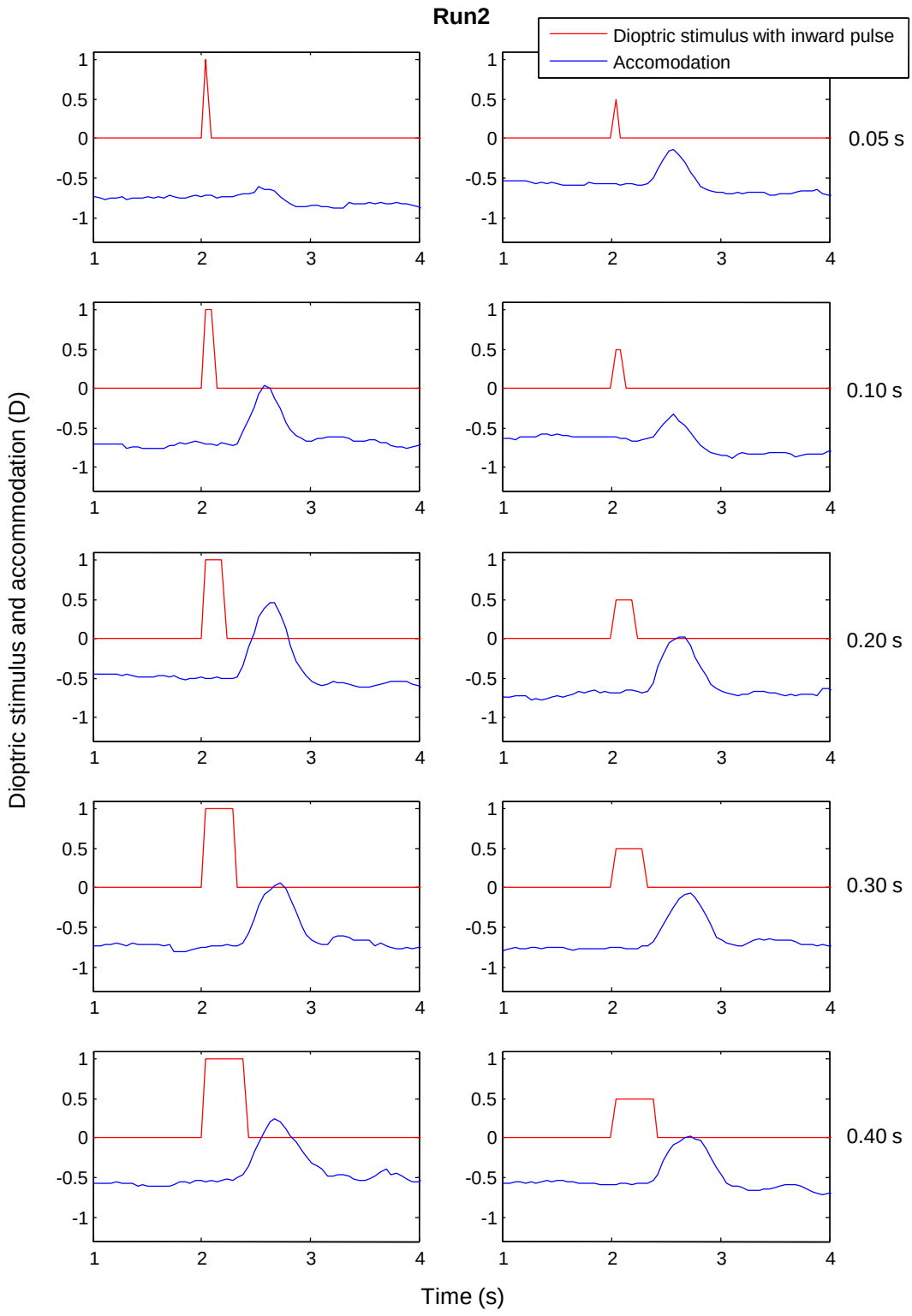
Run2
Dioptric stimulus with inward pulse
Accomodation
0.05 s
0.10 s
0.20 s
0.30 s
0.40 s
Dioptric stimulus and accommodation (D)
Time (s)

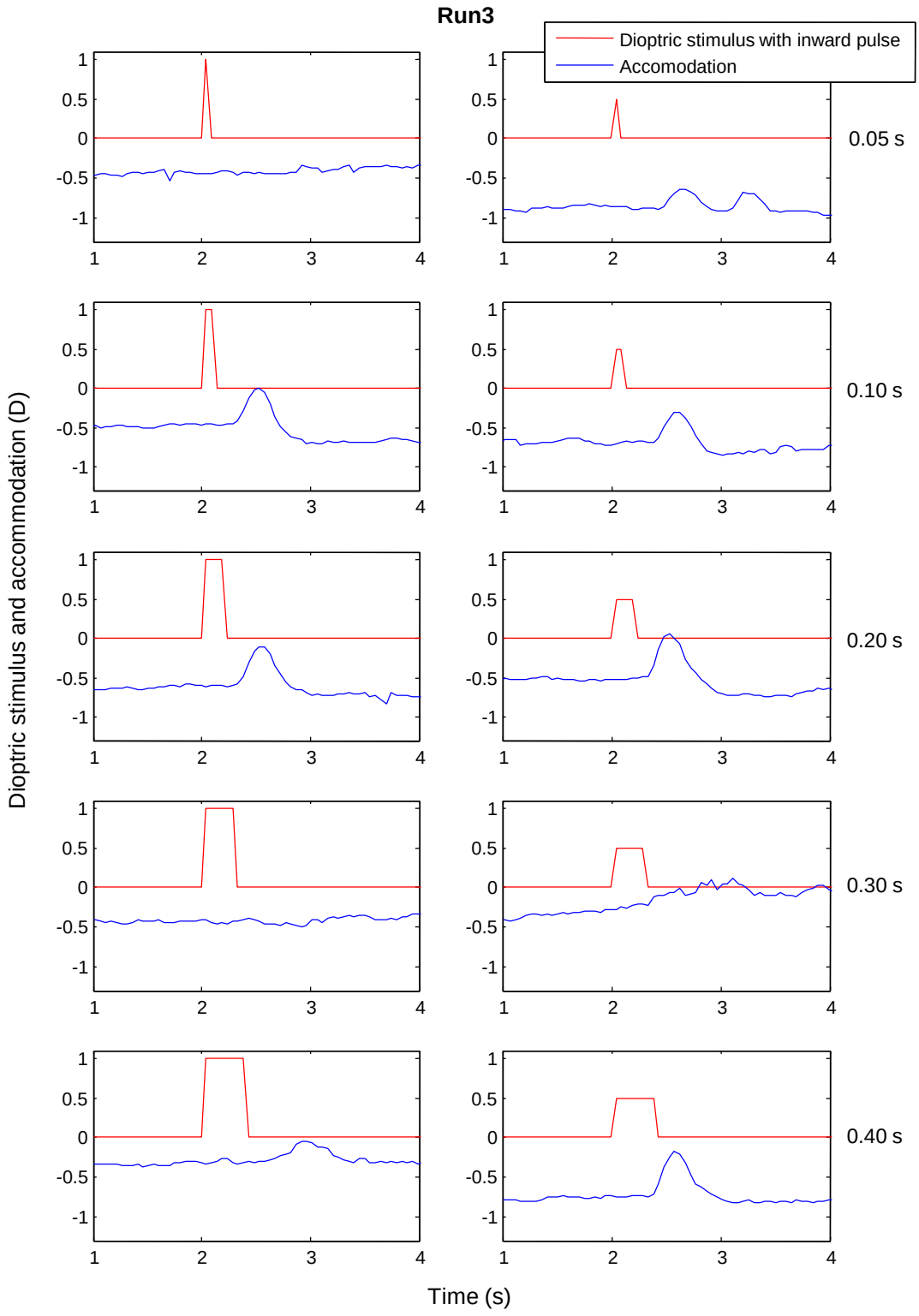
Run3
Dioptric stimulus with inward pulse
Accomodation
0.05 s
0.10 s
0.20 s
0.30 s
0.40 s
Dioptric stimulus and accommodation (D)
Time (s)

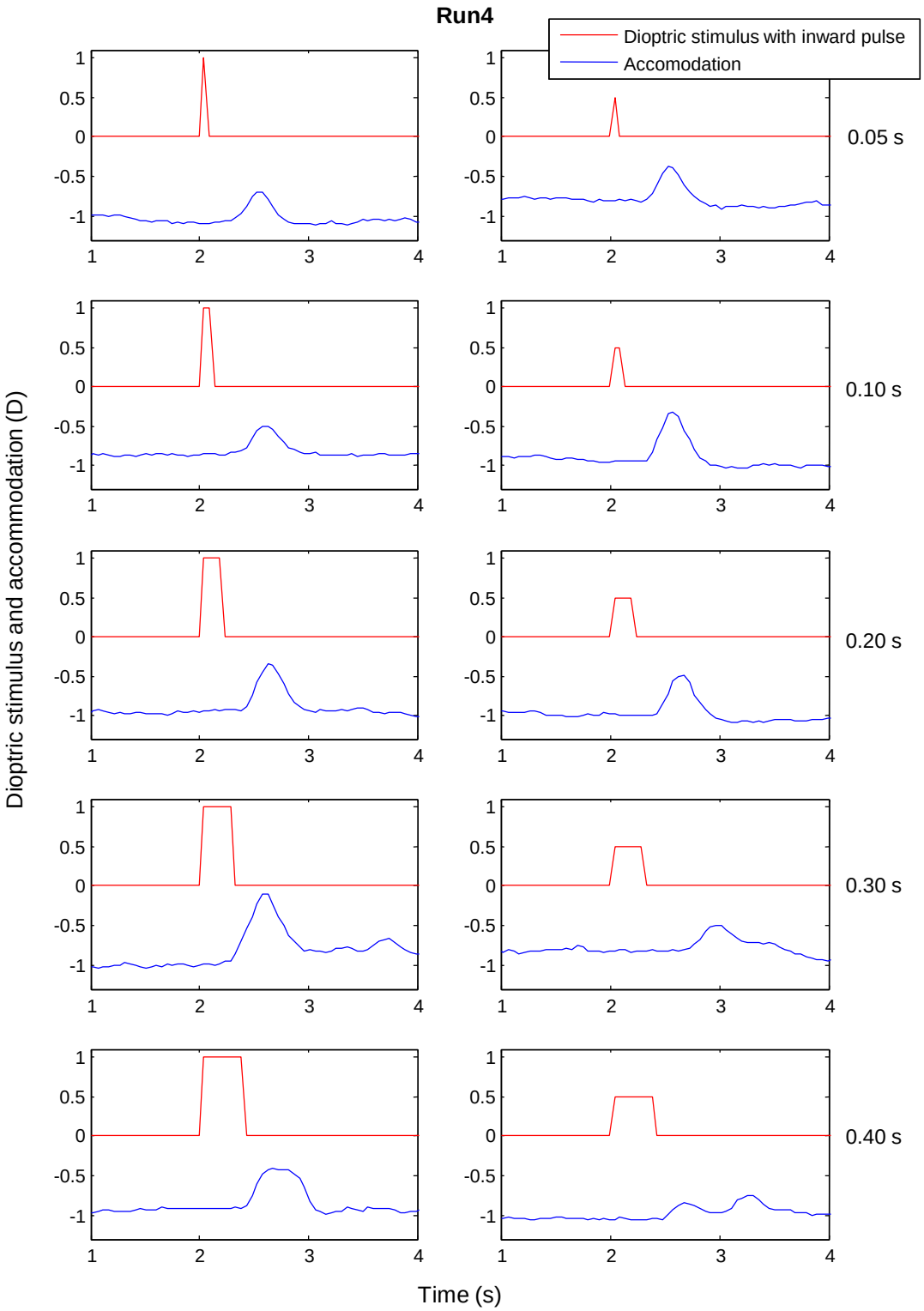
Run4
Dioptric stimulus with inward pulse
Accomodation
0.05 s
0.10 s
0.20 s
0.30 s
0.40 s
Dioptric stimulus and accommodation (D)
Time (s)

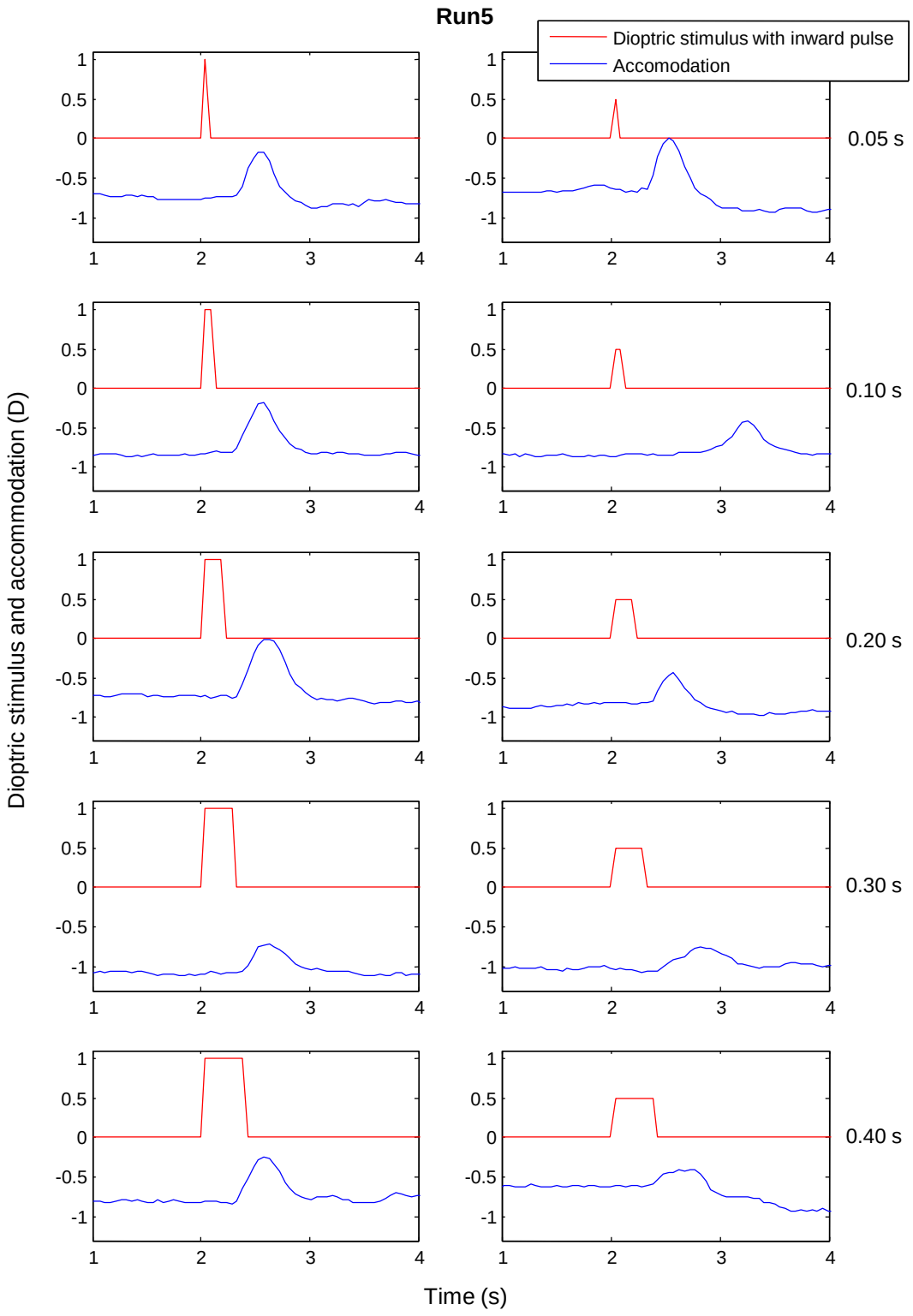
Run5
Dioptric stimulus with inward pulse
Accomodation
Dioptric stimulus and accommodation (D)
Time (s)
0.05 s
0.10 s
0.20 s
0.30 s
0.40 s

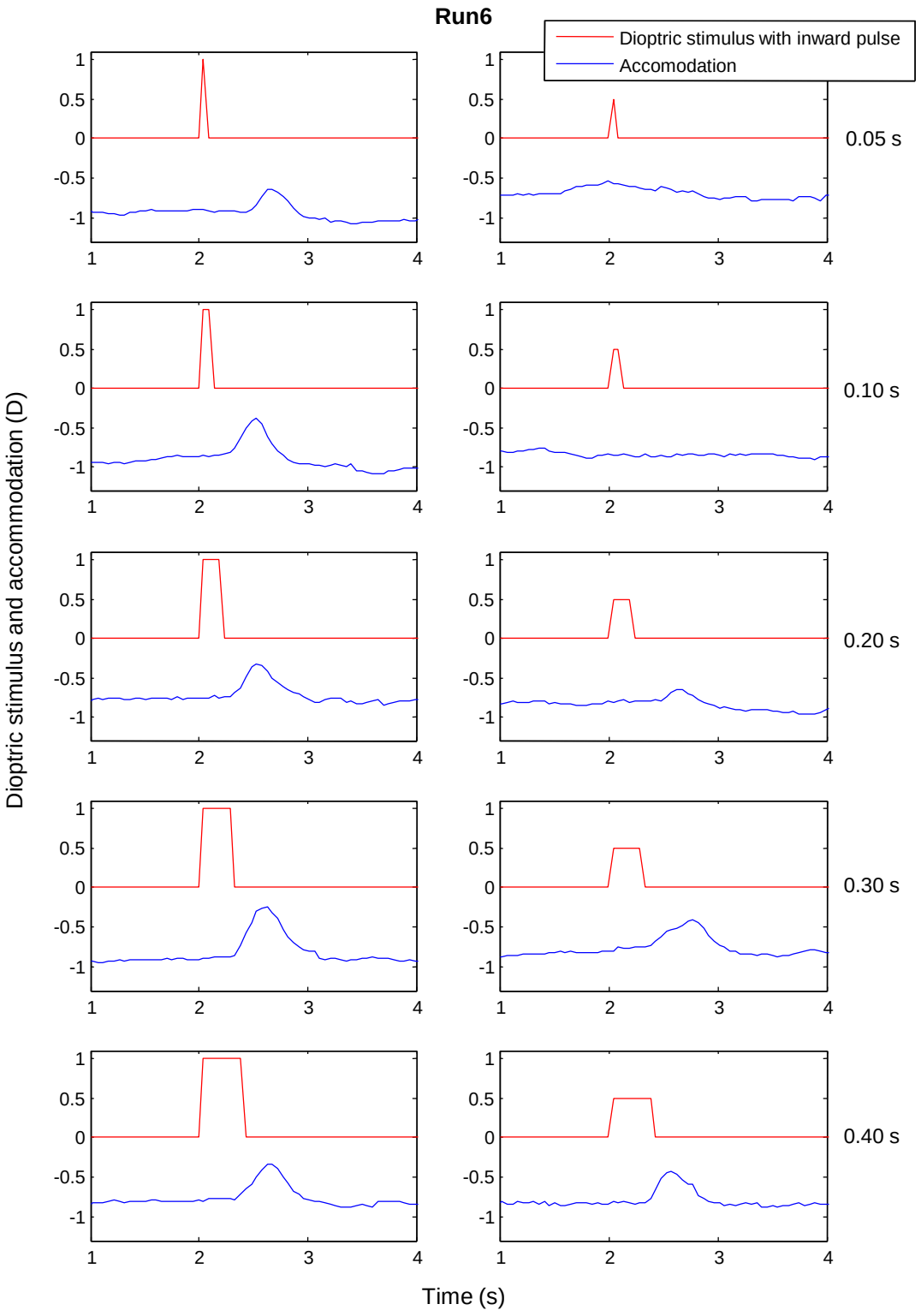
Run6
Dioptric stimulus with inward pulse
Accomodation
0.05 s
0.10 s
0.20 s
0.30 s
0.40 s
Dioptric stimulus and accommodation (D)
Time (s)

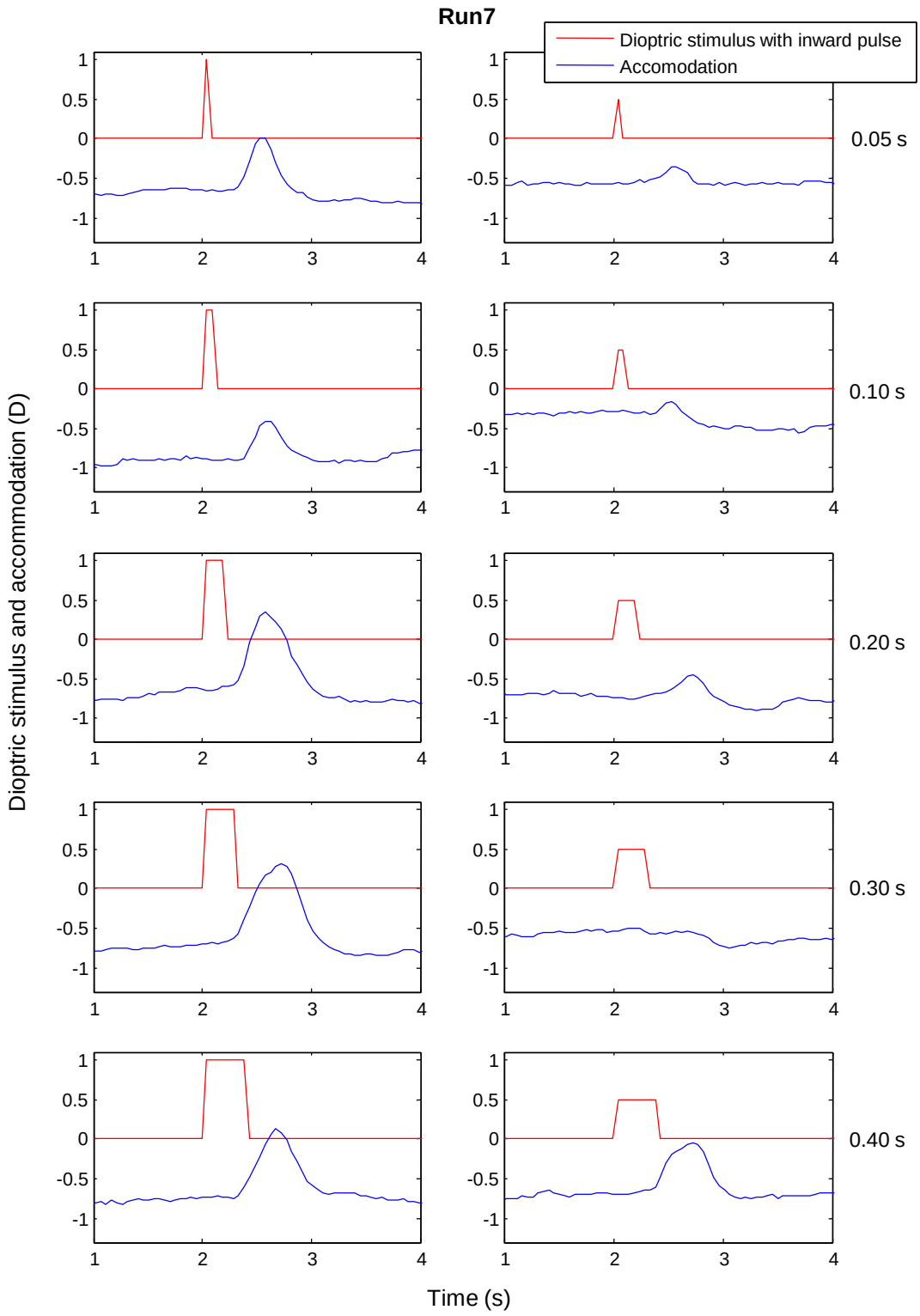
Run7
Dioptric stimulus with inward pulse
Accomodation
0.05 s
0.10 s
0.20 s
0.30 s
0.40 s
Dioptric stimulus and accommodation (D)
Time (s)

Figure 4-3 shows the mean AR for each pair of AS pulse parameters (step height and duration). A baseline AR was found for each trial, which was the mean defocus over the first 40 frames (the frames before the pulse in AS). The baseline was subtracted from each trial, leaving a relative AR; the mean relative AR is plotted.

The plots of Figure 4-3 all show a similar time-width to the mean response, as is also seen in Figure 4-2 (previous seven pages); peak amplitude of the responses is discussed further with reference to Figure 4-4. Timing and peak amplitude of the AR are both discussed in section 4.4.1.3.

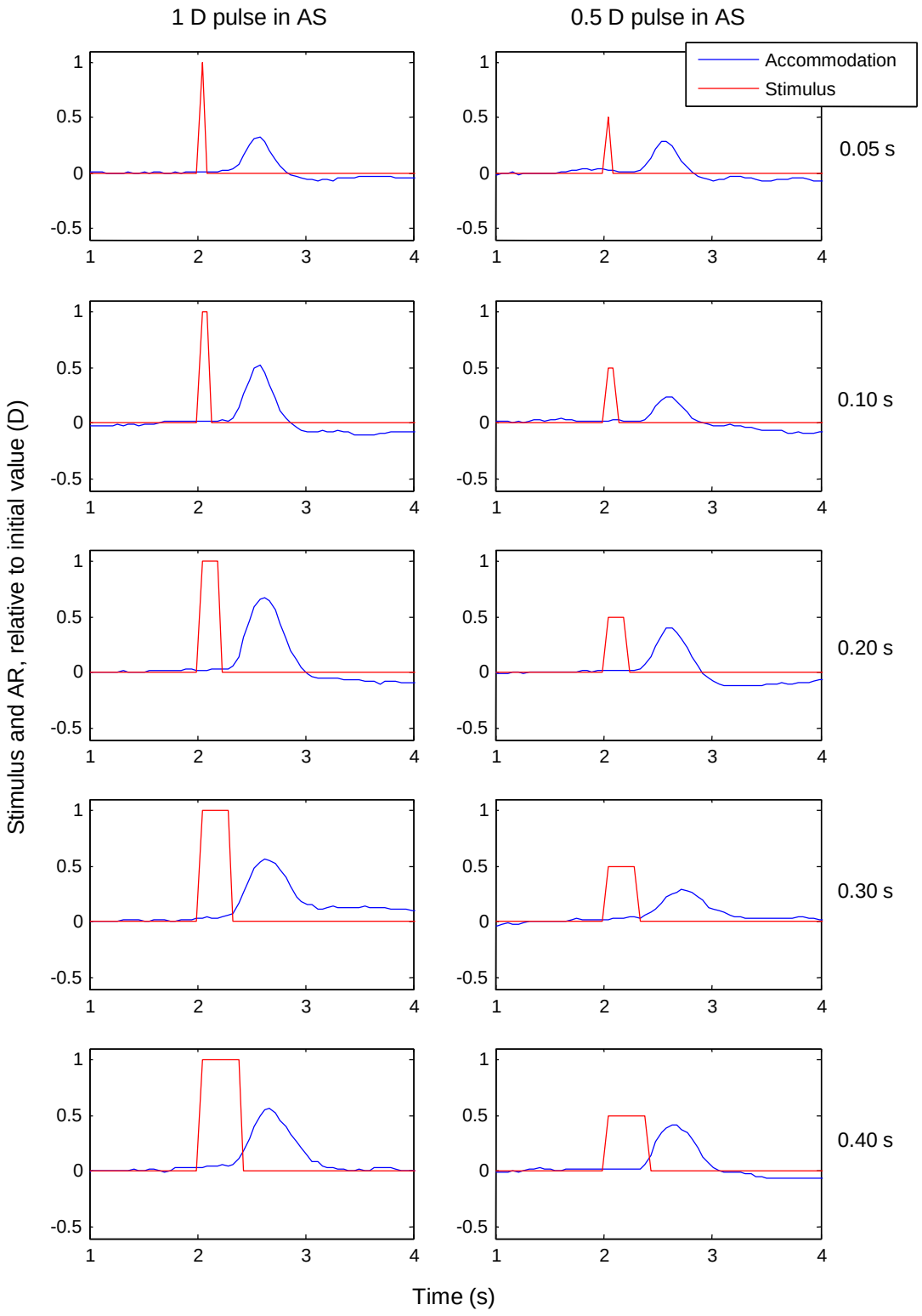

Figure 4-3: The mean relative AR for the ten settings of the pulsed AS.

Figure 4-4 shows the maximum AR to the pulses in AS. For 8 of the 70 trials (5 pulse durations × 2 pulse heights × 7 repeats) there was no pulse in the AR. The runs without a pulse in AR were excluded from the analysis in Figure 4-4.

See also Table 4-1, which shows the number of trials where there was a pulse in AR, out of the seven trials at each parameter setting.

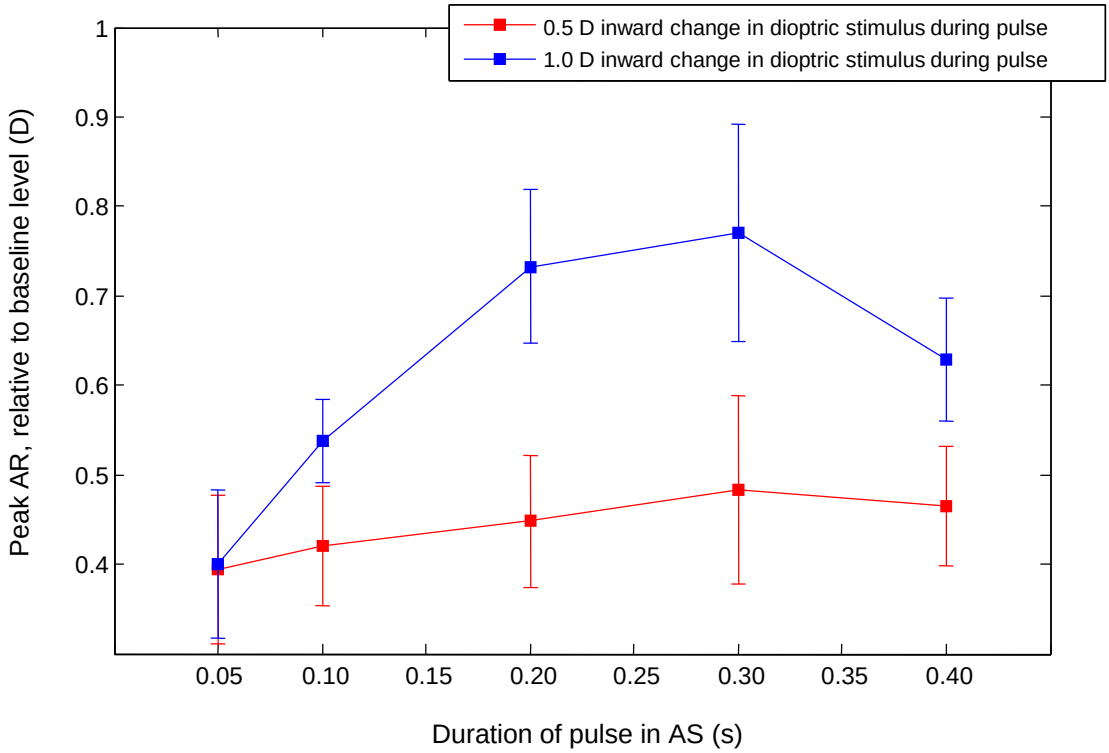

Figure 4-4: The peaks in the pulsed AR to pulses in AS. Error bars are the standard error of the mean. Trials where there was no pulse in AR were excluded. (Between zero and two runs out of seven were excluded at each pulse height and duration, see Table 4-1.) The baseline for AR was the average accommodation over the 2 s prior to the pulse in AS.

Table 4-1: The number of trials where there was a pulse in AR, at all AS pulse parameter settings. There were seven trials in total at each setting.

	0.5 D	**1.0 D**
0.05 s	5	6
0.10 s	6	7
0.20 s	7	7
0.30 s	5	5
0.40 s	7	7

For the briefest pulses (0.05 s), the peak ARs to a 1 D pulse and a 0.5 D pulse in stimulus were very similar (mean difference 0.006 D, standard error 0.1 D); the amplitudes of the responses diverged as duration increased. With an AS

pulse height of 1 D, peak AR tended to increase with increasing duration of the pulse in AS, except at the longest duration of 0.40 s. With an AS pulse height of 0.5 D, peak AR remained consistent over the range of pulse durations, within one standard error of the mean.

4.4 Discussion

4.4.1 The accommodative response

4.4.1.1 Replication of AR data from Campbell and Westheimer (1960)

The AR data appear qualitatively to repeat similar measurements taken by Campbell and Westheimer (1960). Figure 4-5 is an illustration from their paper of an AR to a 2 D pulse of duration 0.32 s. Figure 4-6 shows a corresponding trial from this experiment.

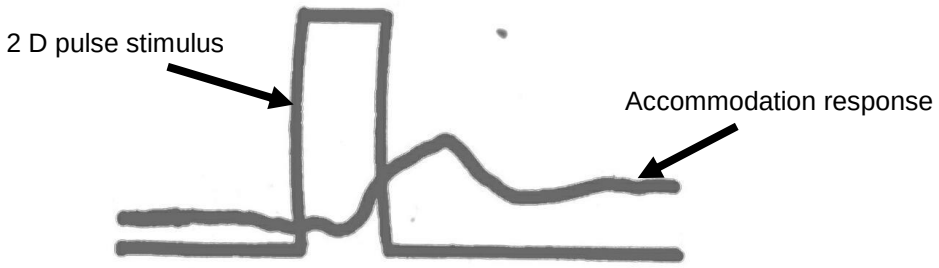

Figure 4-5: "Accommodation response to a 2D pulse stimulus of 0.32 sec duration" (Campbell and Westheimer, 1960). Reprinted with permission from John Wiley and Sons. Text and arrows added for clarity.

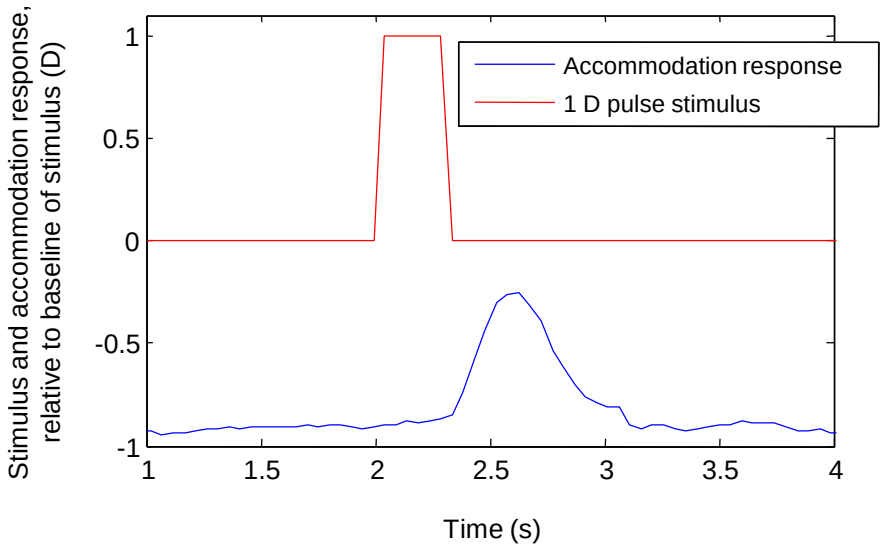

Figure 4-6: An AR to a 1 D pulsed stimulus of 0.30 s duration, from this pilot study.

4.4.1.2 Absent pulses in AR

There was no clear AR in 8 out of 70 trials. An example can be seen in the top left of Figure 4-2 (Run 1), page 78. Campbell and Westheimer (1960) observed such absences of a response, for AS pulse durations of 100 ms or shorter. They also found ARs were sometimes absent for pulses of longer duration, when using a negative pulse height in AS.

The absence of responses for pulses of 0.30 s does not appear to have been observed by Campbell and Westheimer for pulses of increasing AS. One possible explanation is that the pulses in the current study were 1 D and 0.5 D in amplitude, while Campbell and Westheimer's pulses were 2 D in amplitude. The lower level of defocus caused by the pulse may have been less likely to stimulate a response. Another possible explanation is that the illumination source used here was a "white" LED, which is relatively deficient in long-wavelength light, compared with the automobile headlamp used by Campbell and Westheimer. The chromatic aberration cue to accommodation used by some people (Fincham, 1951) may therefore be reduced. A further

explanation is that there is a variability in response between participants that is not accounted for by the six participants in their study.

In general explanation of trials with absent AR, there may be a trigger level of defocus, as in Khosroyani and Hung (2002)*. Such a trigger level may have varied between trials, perhaps linked with the state of the natural microfluctuations of accommodation.

4.4.1.3 Amplitude and duration of the pulse in AR

Campbell and Westheimer (1960) found that pulses in AR began after a time delay, and began to return to the pre-pulse baseline level one pulse duration after accommodation onset. That is, if a pulse was 0.30 s in duration, then after the onset of a response, accommodation began to relax back to its initial state after 0.30 s. Therefore, the pulse in AR "increases in amplitude and duration with increasing pulse duration" (Khosroyani and Hung, 2002).

The current experiment may shed further light on the pulsed response. Firstly, the trend in increasing peak response to pulses in AS of height 1 D can be seen, except for the longest pulses at 0.40 s (Figure 4-4). In the pulses of height 0.5 D, however, all mean peak responses were within one standard error of each other. This relative uniformity of the mean peak AR could indicate a minimum response to a pulse in AS, in cases when an AR is triggered by an initial signal of defocus information. The equality of the peak response to pulses of 1 D and 0.5 D at 0.05 s duration may also indicate this minimum response. To increase the AR beyond this minimum level may require a second measurement to provide an input to the accommodation system; such a measurement may not have been above threshold for further accommodation

* Although the open-loop component of this model is relevant here, which uses a velocity signal as the trigger, a difference in defocus must be detected in order to imply a velocity.

control in the cases of AS pulses of 0.5 D or 0.05 s. The dual-mode model of Hung and Ciuffreda (1988) and Khosroyani and Hung (2002) also includes different modes of recognition of defocus information and subsequent accommodation control. Chapter 6 will further discuss measurements taken and processed by the accommodation system.

Secondly, responses to the briefer pulses in AS, such as that in Figure 4-7, do not seem to follow the deduced rule of equal latency of accommodation for both edges of the pulse (Campbell and Westheimer, 1960; Khosroyani and Hung, 2002). The beginning of the relaxation of accommodation shown in Figure 4-7 begins around 0.2 s after accommodation onset, well beyond the expected interval of 0.05 s. In fact, the widths of the pulses in AR do not differ greatly among stimulus pulses with durations between 0.05 and 0.40 s (see Figure 4-2, all runs). Campbell and Westheimer also included pulses in AS of duration greater than 1 s, and described the increase in accommodation as proceeding for a time interval “of the order of” the duration of the AS pulse, before accommodation began to relax (Campbell and Westheimer, 1960). When pulses from 80 ms to greater than 1 s are considered, this description may appear accurate, but examining the results in detail at short pulse durations may show a minimum duration of the AR to a pulsed stimulus.

Comparison of more data with the model of Khosroyani and Hung (2002) is found in chapter 6.

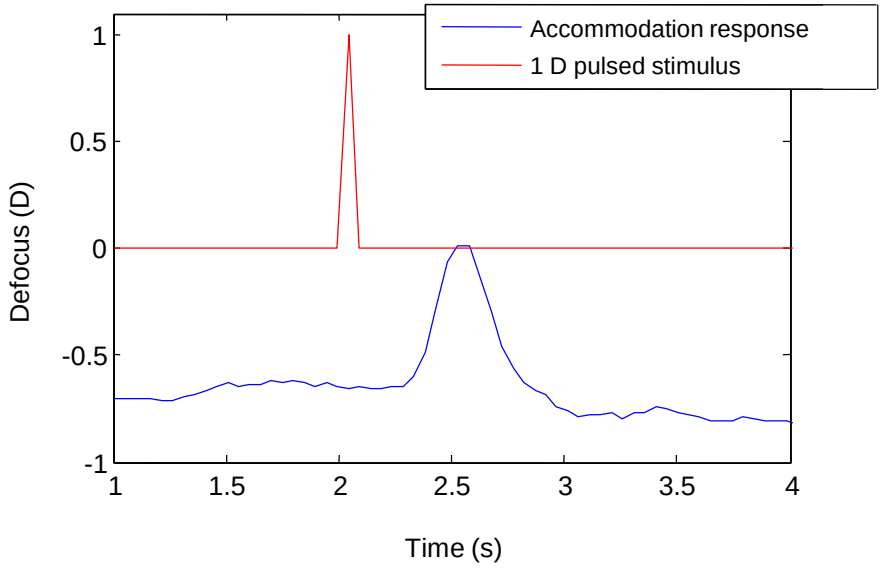

Figure 4-7: An AR to a 0.05 s pulse in AS, plotted relative to the stimulus baseline.

4.4.2 Sources of bias and improvements made to data acquisition

Noise from the piezoelectric DM was considered as a source of bias in the experiments, possibly resulting in the unexpected consistency of the AR. When the steps in AS were effected, the action of the DM was clearly audible to the participant as a click. The click of the DM could have been a strong cue to accommodate, especially after conditioning of the participant to expect such a noise followed by a change in accommodation.

It should be added that pulses were sometimes accidentally provided during which the vergence of the stimulus at the eye was +0.5 or +1 D, i.e. the stimulus was “beyond” the far point and stimulation of accommodation was not expected. This occurred when the incorrect sign for pulse height was input to a dialogue box in the software. Even in these cases, the responses were consistent with those of section 4.3 in direction, amplitude and duration, which further implicated a common cue to all trials, which was possibly auditory.

To remove the auditory cue to accommodate, participants in further data acquisition with this apparatus wore headphones, which attenuated laboratory

noise. Through the headphones, they listened to music or spoken word, which masked the attenuated laboratory noise. The click of the DM was inaudible to participants following this modification. A microphone was introduced, in order to speak to the participant through the headphones; a switch temporarily silenced the auditory masking input, allowing the participant to hear the experimenter clearly.

It is also possible that the data were similarly biased by the uniform time before the pulse in AS. Each time, after the participant was instructed not to blink, they heard a mouse-click. After the mouse-click, there was an interval of about 2 s before the pulse in AS. Since this interval was always the same, the participant could learn when the pulse would occur, which may have affected the AR.

To remove this timing cue, when a participant was asked not to blink at the start of future trials, the experimenter waited for 1, 2 or 3 s before clicking the mouse to begin data collection, at which point the mouse-click was attenuated and masked through the headphones. The different waiting times were in random order in future trial sequences, in computer-generated permutations.

To make firmer and quantitative conclusions about the AR to brief pulses in AS, more participants would clearly be required. Finally, the analysis of the vergence of the light leaving the eye could include higher-order Zernike terms, including spherical aberration, to describe defocus with greater accuracy (Thibos et al., 2004; Tarrant et al., 2010).

4.5 Conclusions

A pilot investigation involving one participant was undertaken, to test the instrumentation described in chapter 3, and to begin the study of the response of the accommodation system to brief pulses in AS.

The experiment replicated similar results from a previous study (Campbell and Westheimer, 1960), and also used pulses of shorter duration and different amplitude.

One of the replicated findings is that the accommodation system sometimes does not respond to dioptric pulses of short duration. An AR was absent in 8 out of the 70 trials in which AS increased during the pulse. There appears to be a varying state of the accommodative system at the point of the pulse in AS, which may be linked to the natural microfluctuations of accommodation.

It also appears there may be a minimum amplitude of the AR to a brief pulse in AS. This was indicated by the approximately constant mean peak response of 0.4–0.5 D, for a pulse in AS of amplitude 0.5 D. That is, for a 0.5 D pulse in AS, the peak AR did not decrease significantly for briefer pulses. For a 1.0 D pulse in AS, the peak AR did decrease as pulse duration decreased (see Figure 4-4). The consistency in the low amplitude case may indicate that the visual system has recognised a disturbance, and triggered an AR, but a further measurement of the disturbance must give a result above a certain value for finer control to be applied to the AR.

The similar time-widths of all of the pulsed responses may reveal a minimum duration for a pulse in AR. The rising AR to the 0.05 s pulse in AS was not halted after 0.05 s. It may be that once a step change in accommodation has

been triggered, further control over accommodation is not applied during a certain, fixed, time interval.

These questions of accommodation control will be revisited in the analysis of chapter 6.

Sources of bias have been identified; it is felt the data of this chapter may be used to form hypotheses, but not to draw firm conclusions. More participants, and the removal of auditory and timing cues, appear essential to clear investigations of such ARs, although the non-visual conditioning of accommodation is also interesting (see section 9.3.1.6).

Most significantly for the remainder of this thesis, this study showed that the instrument of chapter 3 could be used to provide and manipulate the AS to a participant as desired, and to measure the consequent AR.

5 Further pilot data acquisition using the monocular adaptive optics apparatus, with improved protocol

5.1 Review of improvements to the protocol

As the pilot study of chapter 4 was carried out, using the apparatus of chapter 3, improvements to the data acquisition protocol appeared necessary, as discussed in section 4.4.2. The auditory cue from changes in the deformable mirror (DM) was attenuated and masked by music or spoken word played through headphones. A consistent timing cue for a change in the accommodative stimulus (AS) was removed by introducing an unpredictable waiting time, randomly chosen from 1, 2 or 3 s, between asking the participant not to blink and signalling to the software to begin a trial.

5.2 Method

Data were collected from one female participant, aged 26 years, with refractive error −0.50/−0.75x12 in her right eye (left eye: −0.50/−0.75x10). Data collection was approved by the Life Sciences Research Ethics Committee at the University of Bradford, and was carried out with informed consent of the participant.

The apparatus used was the monocular adaptive optics (AO) system of chapter 3, with a bite bar maintaining the participant in one position. Auditory and timing cues to changes in AS were removed, as reviewed in section 5.1. The participant used her right eye, which was her dominant eye.

The vergence of the stimulus at the eye was set to zero, using the two plane mirrors on a movable stage, as described in section 3.1.2., with a +2 D lens in place at the model eye (as mentioned in section 3.3). The deformable mirror

(DM) was used to cancel out aberrations within the instrument (see section 3.3.1).

With the +2 D trial lens removed, the DM was set to return the AS to 0 D (by adding +2 D of defocus), and the stimulus object was moved slightly, to its furthest point from the participant for which the participant reported a clear image. This ensured that no more than 4 D of accommodation was demanded, and the stimulus was not moved beyond the far point.

The DM was used to provide a pulse in AS, as in the pilot study of chapter 4. The accommodative response (AR) was extracted as the normalised Zernike defocus term, also as described there.

Pulses in AS of height −2, −1, +1 and +2 D were used (positive values signifying an increase in accommodative demand), and pulse durations were 0.20, 0.35, 0.50, 1.00 and 2.00 s. Thus, some trials pulses briefer than the latency of accommodation (0.37 s) were used, since they were of scientific interest, but longer pulses also provided comparison of results with the expected AR. Five repeats were carried out at each of the twenty parameter settings (four pulse heights × five pulse durations), making a total of 100 trials.

The exposure time of the sensor was set to 7 ms, for a high signal to noise ratio. The best exposure time was reduced from 12 ms in chapter 4 by removing the ND filter in the eye channel; it was not required to balance the brightness of the two channels at the sensor, since the measurements in the DM channel were not needed for analysis.

In this protocol, the order of the parameter settings was randomised over all 100 trials in the sequence*, using an R (R Development Core Team, 2012) script, including the random waiting time before the software was instructed to begin a trial (see Appendix A). Each trial was 8 s long, with the pulse in AS beginning 2 s from the start of data collection.

The participant's auditory masking input to the headphones was momentarily silenced, while they were instructed not to blink; the experimenter then waited for the randomly chosen wait of 1, 2 or 3 s before the trial was begun in the control software. Any trial during which the participant blinked was discounted, and a repeat of that trial was carried out at a later point in the sequence.

5.3 Data

Figures 5-1 and 5-2 show the AR to the pulses in AS, over the first 6 s of each trial. Figure 5-1 plots the absolute AR; Figure 5-2 plots the AR relative to its mean over the baseline period before the pulse in AS. The data were plotted using the "lattice" package (Sarkar, 2008) in R (R Development Core Team, 2012).

In this participant, for these trials, a variable lead of accommodation can be seen. The expected responses can also be seen, with gain close to 1, for the long pulses in AS. The briefer pulses appear to have stimulated less consistent responses than in the previous protocol (see section 4.3); the AR appears to be attenuated with decreasing AS pulse duration.

* Unlike the trial sequence of the previous chapter, in which the total sequence consisted of a succession of seven random permutations of the parameter space.

The higher level of activity in the AR, compared with the data of Figure 4-2, is attributed to the lower age of the participant, which is expected to result in stronger microfluctuations of accommodation (Heron and Schor, 1995).

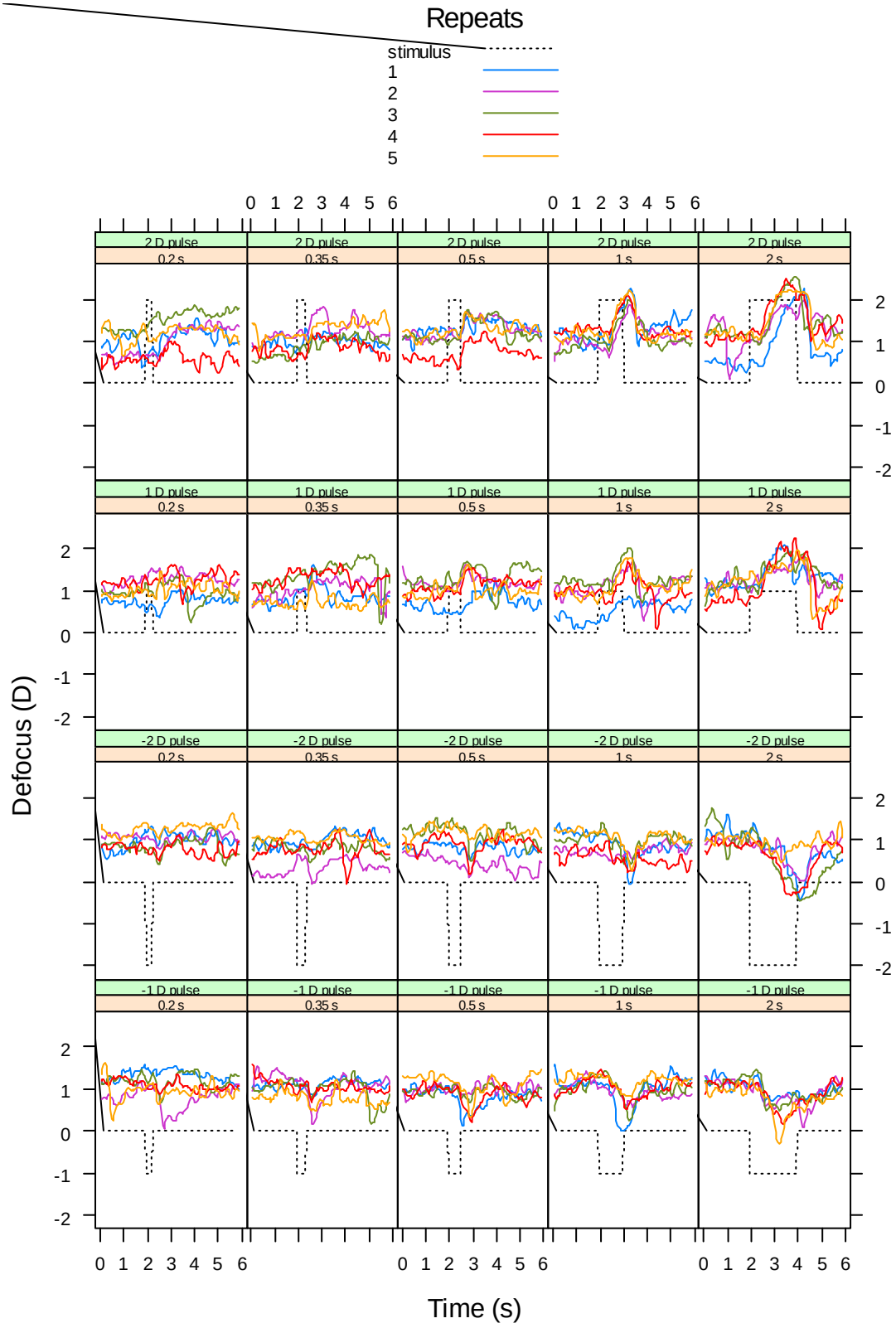

Figure 5-1: The time course of the AR recorded in all trials, at each of the stimulus conditions. The AS and AR are plotted relative to the baseline AS of 2 D.

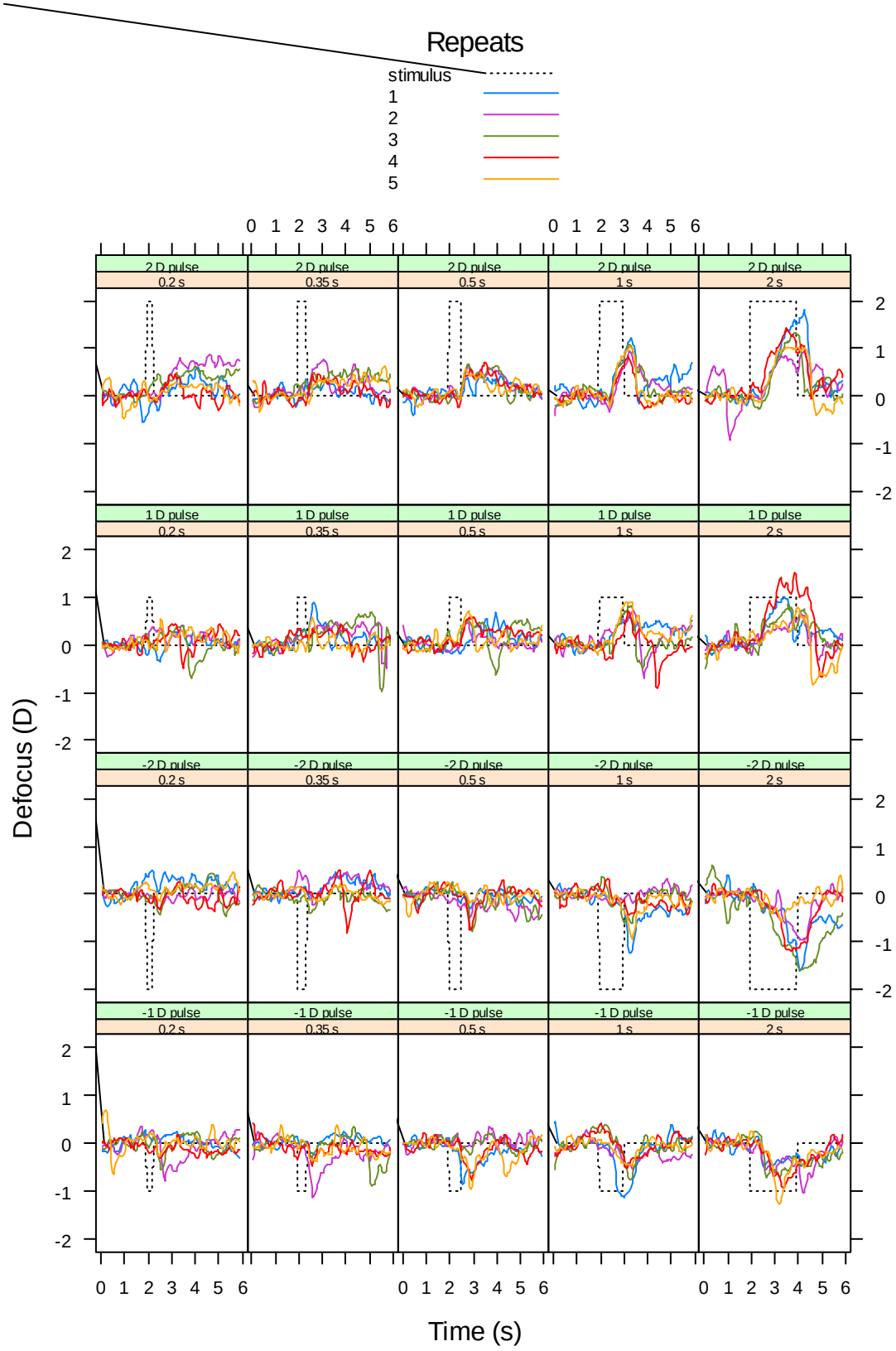

Figure 5-2: The time course of the AR recorded in all trials, relative to its mean baseline value (before the pulse in AS), at each of the stimulus conditions. The AS is plotted relative to the baseline AS of 2 D.

5.4 Discussion and conclusion

The consistent AR to very brief pulses in AS led to concerns of bias in the study of chapter 4. A consistent peak response of about 0.4 D was seen to AS pulses of 0.5 D, and all pulses in AR had similar duration, regardless of the AS pulse duration, contrary to the findings of Campbell and Westheimer (1960). It may be that the pulse durations covered a different regime in relation to accommodation control, but possible sources of bias were identified in the experimental procedure.

Also mentioned in section 4.4.2, a similar, consistent, pulsed AR was also observed when the participant was accidentally provided with a pulse in AS which changed the vergence of the stimulus at the eye from 0 to +0.5 or +1 D. This further implicated common cues for all trials in the protocol of chapter 4.

Following the modifications to the protocol reviewed in section 4.4.2, the data of section 5.3 show the AR to be attenuated as AS pulse duration decreases from 2.00 to 0.20 s, as expected. Positive and negative pulses in AR were also observed as expected, with decreased consistency as AS pulse duration decreased from 2.00 to 0.20 s.

It is assumed that the auditory cue from the DM and/or predictability of the timing of the AS were dominant cues in the highly consistent AR of chapter 4; an experiment is suggested in chapter 9, to explore the effect of an auditory cue on accommodation.

The improved data acquisition protocol appeared to provide useful measures of the AR to purely dioptric changes in stimuli, using the monocular AO apparatus

of chapter 3. A detailed investigation of the AR to rapid changes in AS was next carried out (chapter 6).

6 Experiment: The monocular accommodation response to a square wave stimulus during the latency and onset of accommodation

6.1 Introduction

With the monocular adaptive optics (AO) apparatus providing satisfactory stimulus control and aberrometry (chapters 3–5), and in the light of interesting indications from the pilot study of chapter 4, a detailed experiment was carried out on the accommodative response (AR) to rapid changes in dioptric accommodative stimulus (AS). This experiment particularly follows on from the work of Campbell and Westheimer (1960) and Khosroyani and Hung (2002), following Hung and Ciuffreda (1988), on the AR to pulses in AS. Their work was reviewed in sections 1.4.4, 4.1 and 4.4.1.3.

In control system models of accommodation (Khosroyani and Hung, 2002; Schor and Bharadwaj, 2006), upon processing of the retinal input, the controller passes a signal to the ciliary muscle, and the lens may then change shape. The finite response speed in deformation of the lens is taken into account with a transfer function which integrates back over the signal to describe the final action of accommodation. The confounding biomechanical response allows different descriptions of the accommodation control process to appear valid.

The aim of this experiment was to investigate the AR to changes in AS occurring within the latency period and during onset of accommodation. Starting from a baseline level of AS, each trial presented two conflicting levels of stimulus, and a return to the baseline, in quick succession. The AR to such stimuli was expected to provide new information about the accommodation control process.

Additionally, Mucke et al. (2008) found suppression of contrast sensitivity for high spatial frequencies (but not low spatial frequencies), during dynamic accommodation. It may be hypothesised that other sensitivities, such at that to retinal defocus, are suppressed during the latency or onset of accommodation.

Each stage of the AS was expected to produce a distinct AR, for time intervals between the stages longer than a critical value; following a step in AS, there was expected to be a minimum time window for sampling defocus, or during which further input is suppressed. It was also hypothesised that one of the two stages of the AR might dominate over the other: either suppression of input during accommodation may diminish the AR to a second change in AS, or the priority of the first stage of the AS may be decreased before onset by the imposition of the second stage. The timings of the AR would provide further opportunity for comparison with models of oculomotor control.

6.2 Methods

6.2.1 Data acquisition

There were six participants, all aged between 21 and 26 years (median: 25.5 years) and free of ocular disease. They are described further in Table 6-1 and Table 6-2. The experiment was approved by the Life Sciences Research Ethics Committee at the University of Bradford, and was carried out with informed consent of the participants.

The apparatus used was the monocular adaptive optics (AO) apparatus of chapter 3. The participants all used their right eye (dominant in all cases), wearing their habitual spectacle or contact lens correction. A bite bar maintained the participant in one position, so that the pupil image continuously covered the area of the sensor used for aberrometry.

Table 6-1: The spherocylindrical errors and corrections of the six participants.

Participant	Right eye			Left eye			Correction
	DS	DC	x	DS	DC	x	
1	−0.50	−0.25	180	−0.50	0.00	-	None
2	−1.00	−0.50	180	−1.25	−0.50	180	Contact lenses
3	+0.50	−0.75	12	+0.50	−0.75	10	None
4	+1.25	−1.50	95	+1.25	−1.50	95	Spectacles
5	−6.25	−0.25	30	−6.25	−0.25	135	Contact lenses
6	−0.50	−0.25	140	−0.50	−0.75	65	Contact lenses

Table 6-2: The genders and ages of the six participants.

Participant	Gender	Age
1	F	26
2	F	26
3	F	23
4	F	26
5	F	21
6	M	25

The deformable mirror (DM) was calibrated and set to cancel out aberrations of the apparatus in the DM channel, and the vergence of the stimulus at the eye was set to −2 D from the far point, as described in section 5.2.

The target (the black Maltese cross in Figure 2-4) appeared clear and had luminance 5 cd m^{-2}. One participant (Participant #1) reported that the triangles pointing vertically were clear while the horizontal triangles were a little blurred. This may have been due to sensitivity to the 0.3 DC residual aberration in the eye channel after cancelling the system aberrations (see section 3.3.1).

Participants were instructed to fixate on an edge of the target and attempt to keep it in focus while the DM altered its vergence at the eye.

The trials all started from the same baseline AS of 2 D. Following initiation of data collection, there was a 2 s period of baseline target vergence, before the DM effected one period of a square wave in AS. The mean of the square wave in the stimulus was the 2 D baseline; the initial step from the baseline was ±1 or ±2 D (positive values signifying an increase in accommodative demand). The period of the square wave was 0.1–1.0 s in steps of 0.1 s. The interval between changes in the stimulus (the inter-stimulus interval, ISI, see Figure 6-1) was therefore between 0.05 s and 0.50 s in steps of 0.05 s (half the period of the square wave).

Examples of the changes in AS and the consequent AR are shown in Figure 6-1. In the left-hand plot, the stimulus initially stepped 1 D further away from the participant, with ISI of 0.15 s. In the right-hand plot, the stimulus initially stepped 2 D closer to the participant, with ISI of 0.40 s. In both cases, the response followed both movements of the stimulus, after a latency period. The relative differences of the peaks in AR with the extrema of the baseline microfluctuations are also illustrated (max.diff and min.diff, used in section 6.3.1.2).

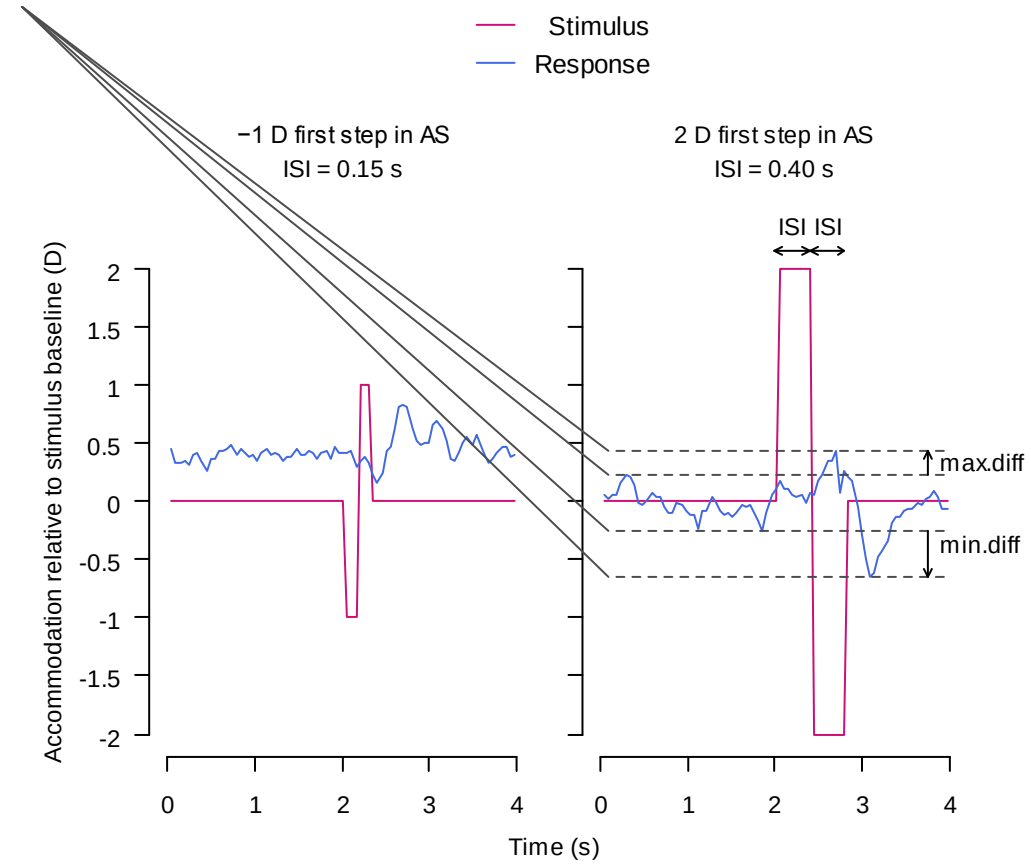

Figure 6-1: Examples of the stimulus and time course of the AR during two trials. Positive values on the vertical axis represent increased accommodative demand and response.

A record of background light was taken at the start of each experimental session. The software subtracted this background intensity pattern from the total intensity pattern during analysis of the Shack-Hartmann intensity distribution (see section 2.2). Noise from, and variations in, ambient light level at the sensor, mainly from leakage of outside light into the laboratory, were therefore not included in the data.

The instrument and the protocol aimed to remove cues to accommodate other than the blur induced by the change in vergence of the target at the eye. The size cue of a moving target was reduced by the Badal arrangement of the eye

and the closest parabolic mirror*. The improvements to the protocol of section 4.4.2 removed auditory cues and a memory cue for timing of the initial AR; the participant wore headphones with auditory input, and a randomly chosen time of 1, 2 or 3 s was interposed between asking the participant not to blink and beginning data collection. A memory cue for magnitude and direction of changes in AS was removed by randomising the trial sequence.

Randomisation of the trials and waiting times was carried out using an R (R Development Core Team, 2012) script (see Appendix A).

The participant was asked not to blink during each trial. If a participant blinked before 2 s after the dynamic stimulus had returned to baseline, the trial was rejected, and a trial with the same settings was inserted into the remainder of the trials to be completed.

For each of the six participants, five trials were carried out at each of the stimulus settings. Therefore a total of 30 trials were carried out at each stimulus setting.

The trials with ISI of 2 s and those with a static AS were used to continue to check the performance of the system. They also mitigated a conditioning cue to respond to the rapid square wave in AS. These trials showed the expected AR, including latency and gain (the record of accommodation during all of the trials can be seen in Appendix B.)

The infrared (IR) wavefront exiting the eye was analysed in terms of Zernike coefficients up to 5^{th} order (see sections 2.2.3 and 2.2.4) in each frame

* It was not quite eliminated. As the AS is changed from 0 D to 4 D, there is a change in magnification of approximately 16% in the image formed by the parabolic mirror furthest from the eye (from consideration of the object positions required for the closest parabolic mirror to provide the required stimuli).

captured by the camera. There were 160 frames over the trial, and the first step in target vergence occurred at the 40th frame (2 s from the start of data collection). The exposure time was typically 5 ms, which optimised the signal with respect to noise, and the frame time was 0.05 s. The best exposure time was reduced from 7 ms in chapter 5 by increasing the laser power at the eye from 0.33 mW to 0.40 mW, which is still well under the maximum permissible exposure of 0.7 mW for 8 hours' continuous viewing (British Standards Institution, 2009).

6.2.2 Data analysis

The Zernike coefficients corresponding to defocus and spherical aberration were extracted from the data and converted into AR in dioptres:

$$\mathrm{AR} = \frac{4\sqrt{3}}{R^2} \times c_4 - \frac{12\sqrt{5}}{R^2} \times c_{12}$$

where c_4 is the Zernike defocus coefficient and c_{12} is the Zernike coefficient for primary spherical aberration, both in microns*, and R is the radius of the circular aperture analysed, in mm (Thibos et al., 2002c; Thibos et al., 2004).

The 30 data points for a property of the AR (e.g. max.diff in Figure 6-1) were pooled for statistical analysis. Data distributions resembled normality (see the datasets in Appendix B), but many samples failed the Shapiro-Wilk test ($p < 0.1$). Therefore, non-parametric techniques were used; the median was used for statistical analysis of central tendencies among the data.

For one-tailed tests of a one-sample statistic (e.g. is the median of max.diff greater than zero?), bootstrap resampling of the data was used (Efron, 1979);

* As mentioned previously, there are also higher-order Zernike terms which could be included, but with decreasing contributions, in a complete calculation of the vergence of the aberrated light leaving the eye (López-Gil and Fernández-Sánchez, 2010).

assessment of statistical significance was based on a confidence interval for the statistic, calculated from its distribution among the bootstrapped samples. 10,000 replications of the samples (sampling with replacement) were used to generate the bootstrapped dataset. The BCa confidence interval of Efron (1987) was used, calculated by the “boot.ci” function in the “boot” package (Davison and Hinkley, 1997; Canty and Ripley, 2013) in R. Scripting of the bootstrap test followed the method of Rizzo (2008, pp. 197–207), and can be found in Appendix C.1.

For two-sample tests, Fisher’s permutation test (Pitman, 1937) was used to compare the medians (e.g. was max.diff greater when the first step in AS was positive or negative?). This test compares whether two samples are likely to be part of the same population, as identified by a chosen statistic (the difference between the medians in this case: ΔMed). That is, the two samples of 30 data points were pooled into a set of 60; two samples of 30 data points were randomly partitioned from within the set of 60 a large number of times (9,999); ΔMed was recorded for each of the 9,999 partitions. A distribution of ΔMed was therefore generated for random partitions of the 60 data points, also including the experimental difference between the two samples, ΔMed_{meas}. If ΔMed_{meas} fell within the outer ten centiles of the generated distribution of ΔMed, for instance, it would be concluded that there was 10% chance of being incorrect in stating that the two samples are from different populations, as identified by the difference between the medians. Simplifying this statement, the medians would have been found to be significantly different ($p < 0.1$).

Scripting of the permutation test followed the method of Rizzo (2008, pp. 217–219), and can be found in Appendix C.2.

Data were plotted using the “grid” (R Development Core Team, 2012) and “lattice” (Sarkar, 2008) packages, as well as the “base” package in R (the script of Appendix C.1 is also an example of production of a plot using the “grid” package).

6.3 Results

6.3.1 The AR to one or both stages of the stimulus

6.3.1.1 The time course of the AR

The mean time courses of the AR to the 40 stimulus conditions—over all participants and repeats—are shown in Figure 6-2. A mean response to all stages of the AS is apparent, even for some of the briefest stimuli (e.g. ISI = 0.05, 0.1 s). The time course for every trial can be seen in Appendix B.1.

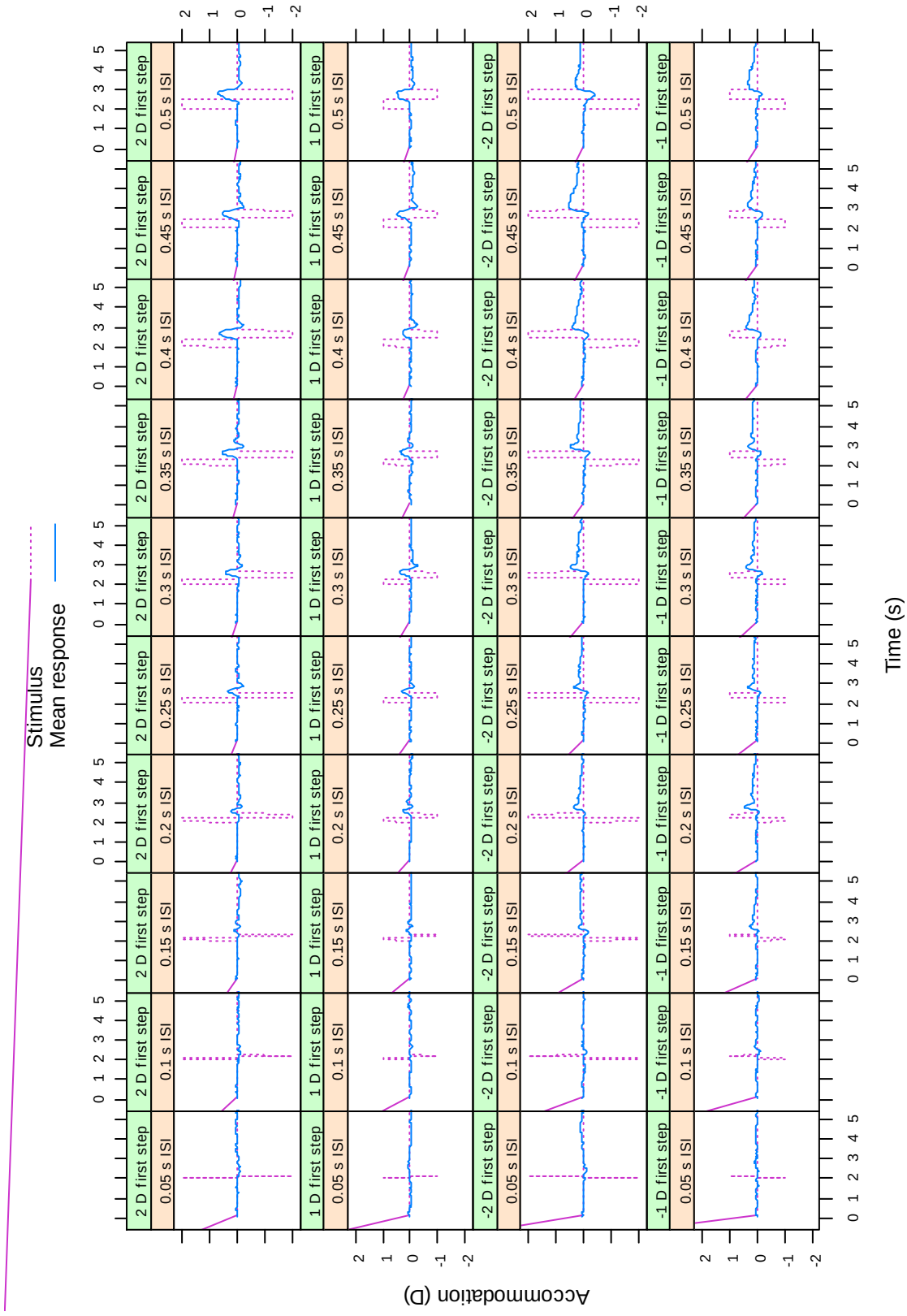

Figure 6-2: Mean time courses of the AR to the 40 different stimulus conditions. The AS is plotted relative to its baseline of 2 D. The AR in each trial was calculated relative to its mean baseline value, before the mean was taken over the 30 trials in each condition.

6.3.1.2 Statistically significant peaks

To judge whether peaks in AR were statistically significant, the maximum and minimum values were extracted for each trial. These were taken from the data beginning at the first change in AS and ending one second after the return to baseline, following the two stages of the dynamic AS. Evidence in Campbell and Westheimer (1960) shows that the AR to a brief pulse in AS reaches its peak in well under one second of the return to baseline, so this limit was considered sufficient.

For each trial, the maximum and minimum AR were calculated relative to the mean level of accommodation, with its fluctuations, in the 2 s baseline period before any change in AS. The differences between the peaks in AR and the extrema of the fluctuations in the baseline period were also calculated (max.diff and min.diff for each trial, as in Figure 6-1).

If, for any trial condition, bootstrap testing of the data from the 30 trials showed that the median of max.diff > 0, or the median of min.diff < 0, with 95% confidence, it was concluded that there was a significant AR in the relevant direction. A null result would indicate that the AR may have simply been a continuation of the baseline fluctuations.

The median peaks in AR, with respect to the average baseline value, are plotted in Figure 6-3. 95% confidence of a significant peak in AR is shown by an open square. A statistically significant response in at least one direction (any open square) was identified at all ISIs, from 0.05 s to 0.50 s. Significant responses were identified in both directions in 21 of the 40 stimulus conditions, at ISIs ranging from 0.15 s to 0.50 s, excluding 0.20 s (open squares for both maximum and minimum AR at any condition in Figure 6-3).

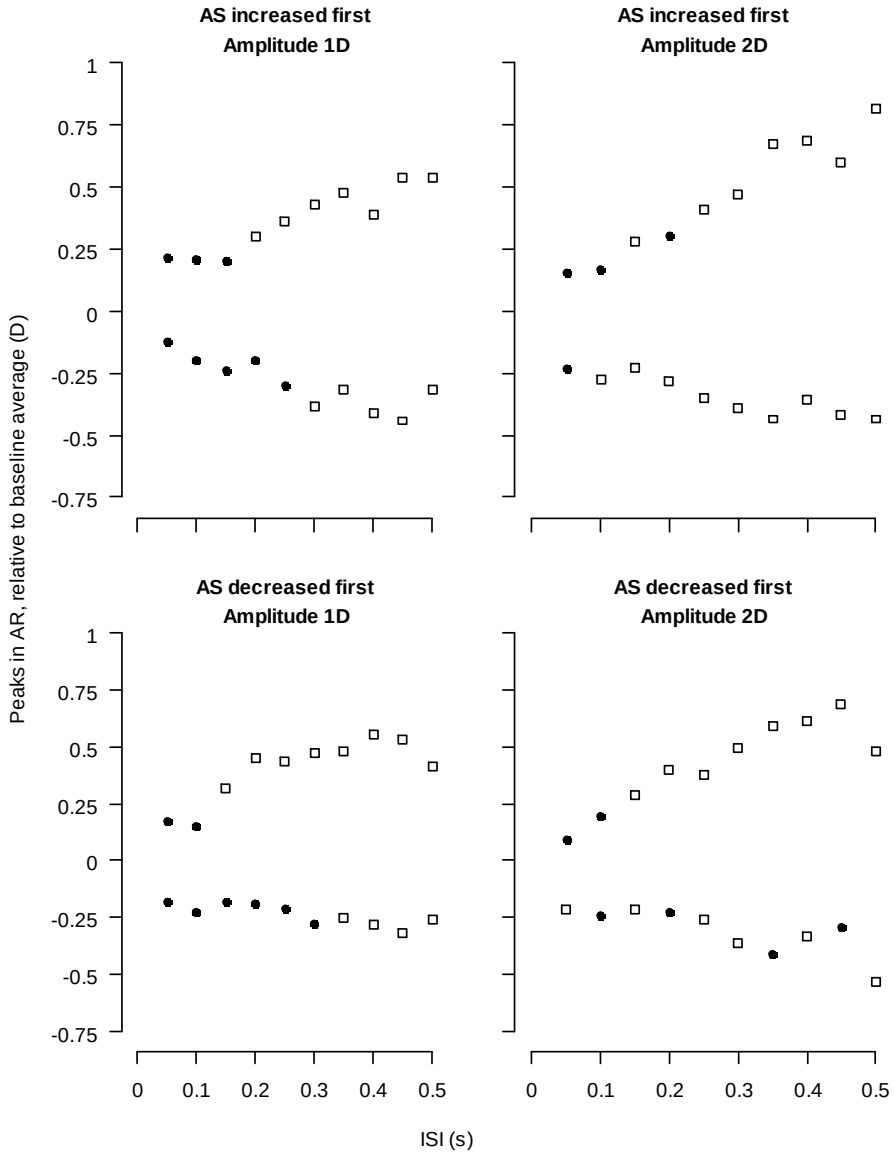

Figure 6-3: The median maxima and minima of accommodation in all trials. An open square indicates that the median peak in AR following the stimulus was found to be significantly outside the extremes of the baseline fluctuations of accommodation (*p* < 0.05, using bootstrap confidence intervals).

6.3.1.3 Categorisation of the AR in individual trials, by number and direction of peaks outside the baseline fluctuations

The number of peaks in AR beyond the baseline extrema (zero, one or two) was also found for each trial. The trials were categorised as illustrated in Figure 6-4; Figure 6-5 shows the relative contributions of the various categories of response.

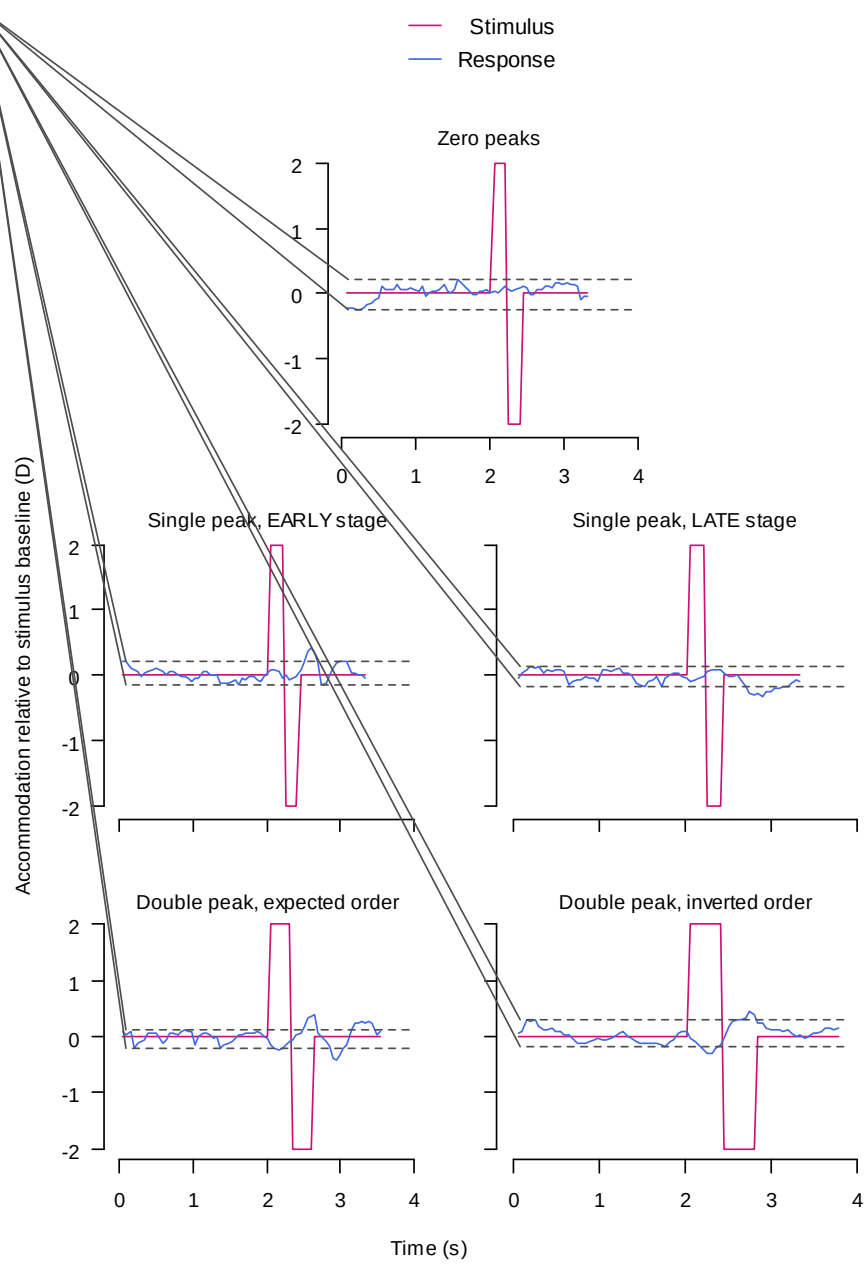

Figure 6-4: Examples of the categories of response, by number of peaks beyond the baseline fluctuations. The extrema of the baseline fluctuations are shown with dashed lines. The single responses are further categorised according to whether the single peak is in the direction of the EARLY or LATE stage of the AS. The double responses are further categorised according to whether the maximum and minimum are in the same order or inverted, with respect to the order of the levels of the AS.

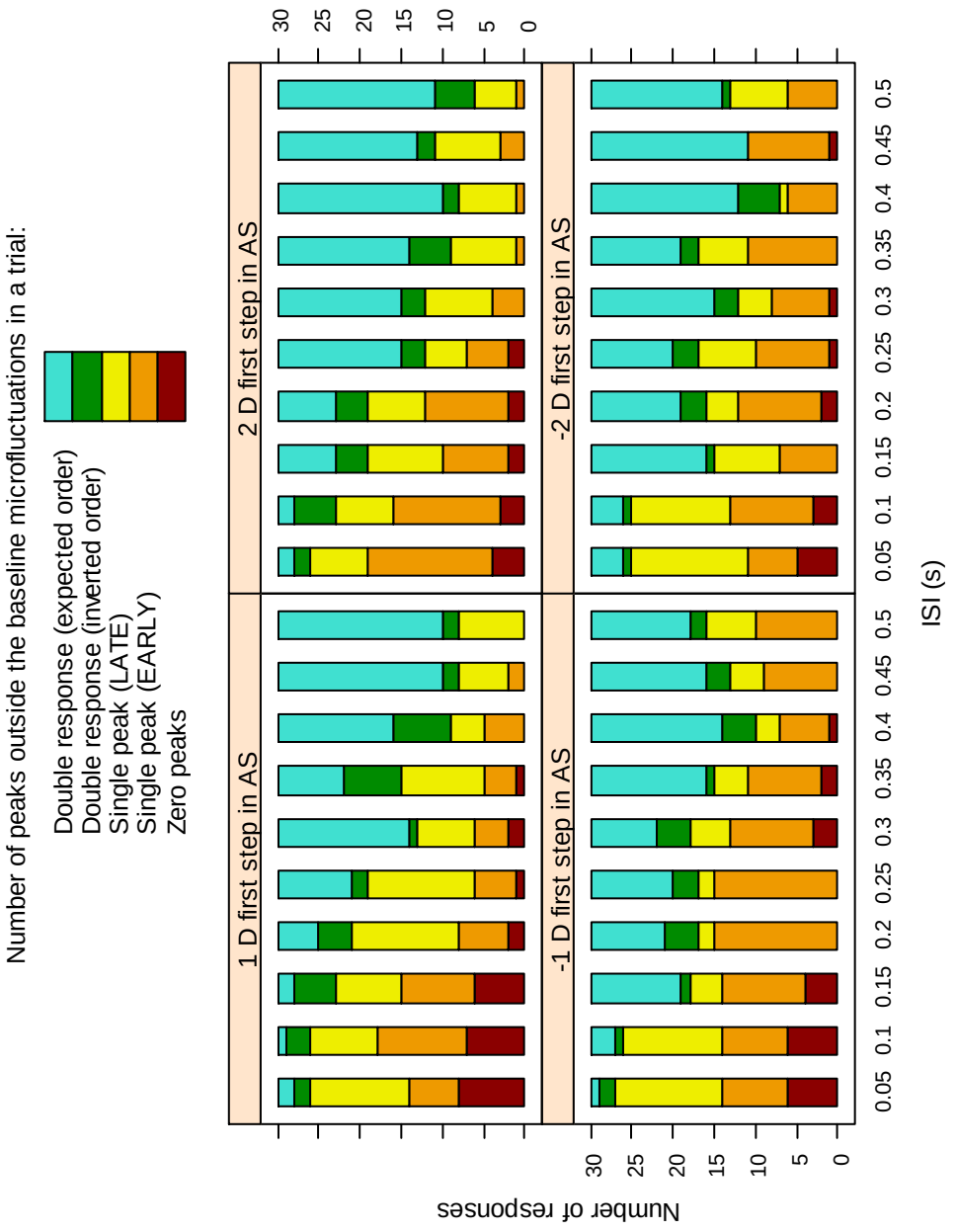

Figure 6-5: The numbers of trials with different numbers and orders of peaks in AR outside the baseline fluctuations. The legend is further explained in Figure 6-4. The relative proportions of the different types of response can be seen in the stacked bars.

In 14 of the 40 trial conditions, there were at least as many trials with a double response in the expected order ("correct double responses") as there were with all other types of response combined. All but one of these 14 conditions resulted in statistically significant peaks in AR to both stages of the stimulus

(see section 6.3.1.2). Double responses with inverted order ("incorrect double responses") were observed and will be discussed later (section 6.4.4).

6.3.1.4 Amplitudes of double and single responses

For the 21 conditions in which there were statistically significant responses in both directions (see Figure 6-3), the peaks of correct double responses were tested against the EARLY and LATE single responses. A significant result, using Fisher's permutation test, would indicate that the peaks of correct double responses did not share the same distribution with the EARLY or LATE single responses, as identified by a smaller median peak amplitude for the double responses.

In 10 out of the 21 conditions, one or both of the peaks of the double responses were significantly smaller than the corresponding single responses ($p < 0.1$; see section 6.4.3 for explanation of this significance threshold). In the other eleven conditions, neither peak of the double response was found to be significantly smaller than the corresponding single response ($p > 0.1$). In total, 12 of the 42 peaks (2 peaks × 21 trial conditions) revealed a significant difference. Table 6-3 shows a spread among durations of ISI and initial step in AS of conditions with a significant difference.

Table 6-3: The significant differences between peaks in single responses and correct double responses (Fisher's permutation test on the medians, $p < 0.1$). EARLY or LATE indicate that the single response was significantly stronger than the corresponding peak in the correct double response. The value in brackets is the difference between the medians. "N" indicates that neither single response was significantly stronger than the corresponding peak in the double response. Parameter settings with no statistical double response contain "/".

Stimulus interval (s)	First step in AS			
	-2 D	-1 D	+1 D	+2 D
0.15	LATE (0.15 D)	/	/	N
0.25	EARLY (0.21 D)	/	/	N
0.30	EARLY (0.13 D)	/	EARLY (0.18 D) LATE (0.44 D)	N
0.35	/	N	EARLY (0.19 D)	N
0.40	N	EARLY (0.24 D)	EARLY (0.27 D)	N
0.45	/	EARLY (0.25 D)	N	EARLY (0.19 D)
0.50	N	EARLY (0.28 D) LATE (0.29 D)	N	N

6.3.2 Effect of whether a given level of AS occurs EARLY or LATE

Among single responses, there were 278 EARLY responses in total, and 295 LATE responses. These counts are consistent with equal likelihood for single EARLY and single LATE responses. In a binomial test for a difference in likelihoods, no significant difference was found ($p = 0.50$).

The correct double responses were also tested for a difference in the AR to a level of AS occurring as either the EARLY or LATE stage in a trial. The EARLY maxima in AR (when the maxima in AS occurred first) were compared with the LATE maxima in AR (when the maxima in AS occurred second, i.e. when the two stages of the AS were reversed). Minima in AR were compared similarly.

Table 6-4 shows which position (EARLY or LATE) of the level of AS within a trial elicited a stronger peak in AR, when there was a significant difference between them (Fisher's permutation test, $p < 0.05$). A significant result indicates that the EARLY and LATE peak responses were found not to be part of the

same single distribution of peak responses, as identified by the difference of the medians.

Table 6-4: Tests for significant differences between peak responses to the levels of the AS, depending on whether that level of the AS was the first or second stage of the square wave. Only trials with a double response in the expected order were considered. "-" indicates there were fewer than five such trials for at least one of the trial conditions in each comparison. "ns**" indicates no significant difference. "LATE" and "EARLY" indicate a significant difference ($p < 0.05$) and which stage of the stimulus elicited the stronger median response. "**(LATE)**" indicates a difference approaching significance ($p < 0.1$). See text for details of the statistical test.**

Stimulus interval (s)	Level of AS, relative to baseline			
	-2 D	-1 D	+1 D	+2 D
0.05	-	-	-	-
0.10	-	-	-	-
0.15	ns	-	-	ns
0.20	**LATE**	ns	ns	ns
0.25	**LATE**	**LATE**	ns	(LATE)
0.30	ns	ns	ns	ns
0.35	**LATE**	**LATE**	ns	ns
0.40	ns	**LATE**	**LATE**	(LATE)
0.45	(LATE)	ns	ns	ns
0.50	ns	**LATE**	ns	**EARLY**

Before taking into account multiple comparisons, there were eight combinations of the level of AS and ISI at which the AR to the LATE stage AS was significantly different from ($p < 0.05$), and stronger than, that to the EARLY stage AS. This difference was found for both levels of the trials with amplitude 1 D and ISI 0.40 s. A further three stimulus levels and intervals approached a significant difference ($p < 0.1$); all had a greater median for the response to the LATE stage AS than the EARLY stage AS.

There was a small, but statistically significant, degree of correlation between the maxima and minima in each trial (Kendall's $\tau = 0.08$, $N = 1200$, $p < 0.01$, and see Figure 6-6). Therefore, they may have been partially dependent on each other. The two results at amplitude 1 D and ISI 0.40 s may be considered not

truly independent. There are therefore 7 truly independent findings as described above, and we may also consider 20 of the 40 possible tests to be independent.

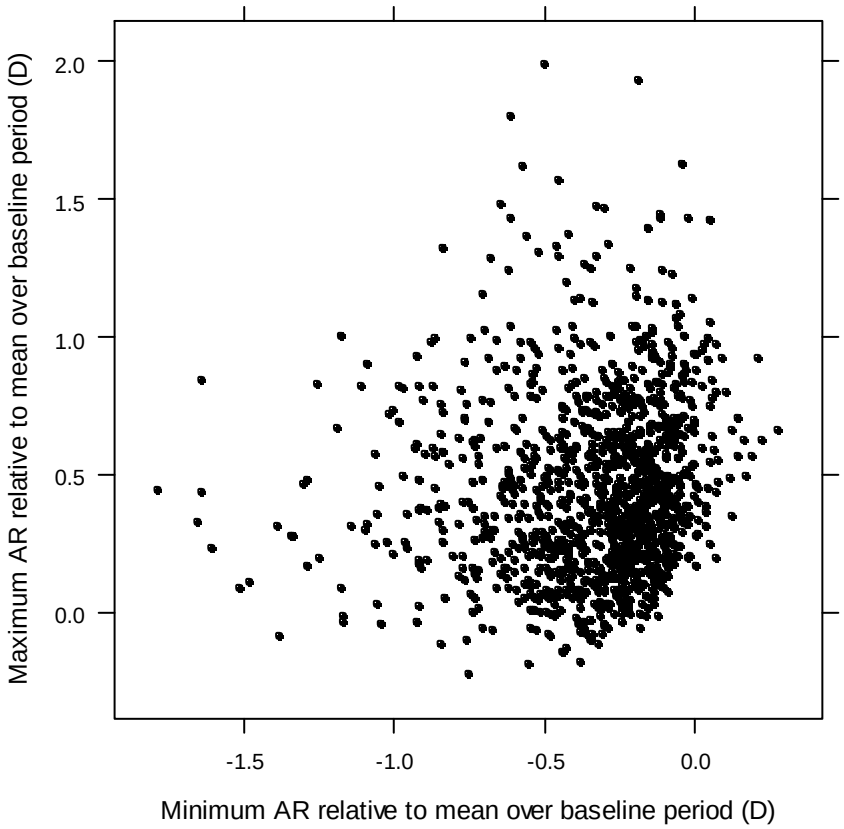

Figure 6-6: The maximum and minimum of AR, for every trial.

The likelihood of finding these significant differences by chance is therefore between that of at least 7 out of 20 independent findings and that of at least 8 out of 40, at $p < 0.05$, by chance, i.e. between

$$1 - \sum_{i=0}^{6}\left(0.05^{i} \times 0.95^{(20-i)} \times {}_{20}C_{i}\right) = 0.00003$$

and

$$1 - \sum_{i=0}^{7}\left(0.05^{i} \times 0.95^{(40-i)} \times {}_{40}C_{i}\right) = 0.0007$$

at most.

Therefore it is likely that a real difference between the LATE and EARLY stages of the correct double response has been found.

The single result where the response to the EARLY stage AS was greater (+2 D, 0.50 s) is not significant after similar correction for multiple comparisons (p > 0.5, using either the original significance threshold of 0.05 for P(type I error), or the exact probability of 0.027 in that case).

6.3.3 Timings of the AR

The response times of the different stages of the AR were also considered. Similarity of the small ARs with the baseline fluctuations made it difficult to examine the timing of the response to the first change in AS. However, the timings of the two peaks in a correct double response provided data on two response times (RT2, RT3) and the inter-response interval (IRI) illustrated in Figure 6-7. RT2 and RT3 were defined as the time interval between the second or third change in AS and the corresponding extremum of the AR; IRI was the time interval between the extrema of the AR.

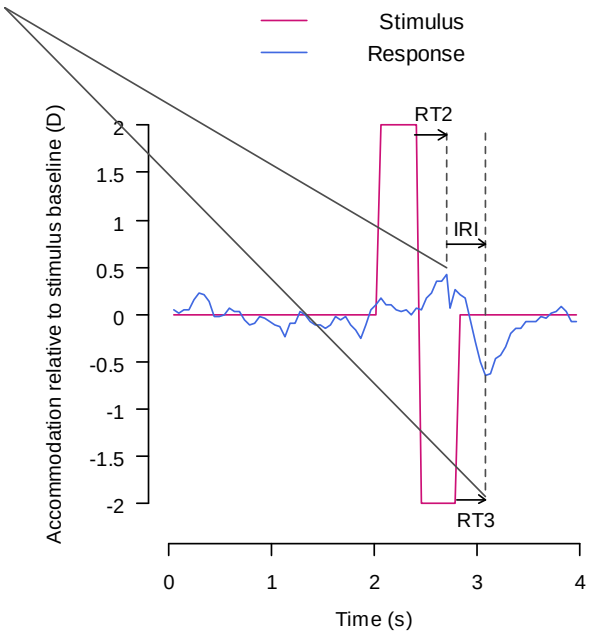

Figure 6-7: Definition of the second and third response times (RT2 and RT3) and inter-response interval (IRI) for a correct double response. The response times are defined to the peaks in AR caused by the second and third changes in AS.

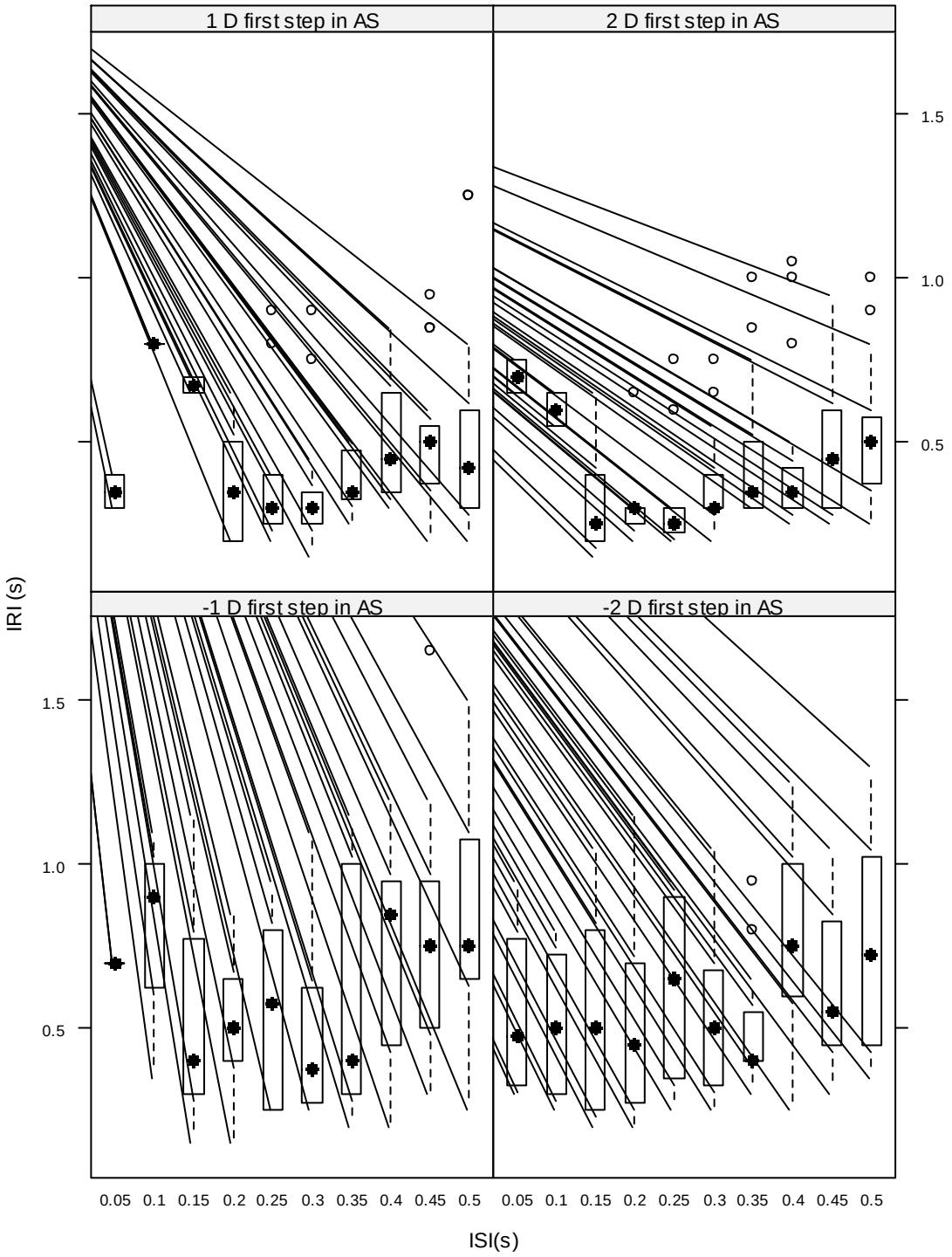

Figure 6-8: Box and whisker plot describing the IRI in trials with correct double responses. (All data points outside the standard whiskers are labelled with open circles.)

describes the IRI for correct double responses in each stimulus condition. The conditions where AS decreased in the first step resulted in much more varied results, and in general, longer IRI. When AS increased first, there appeared to

be trends where IRI decreased with decreasing ISI. These trends broke down at brief ISIs, where there were a low number of double responses.

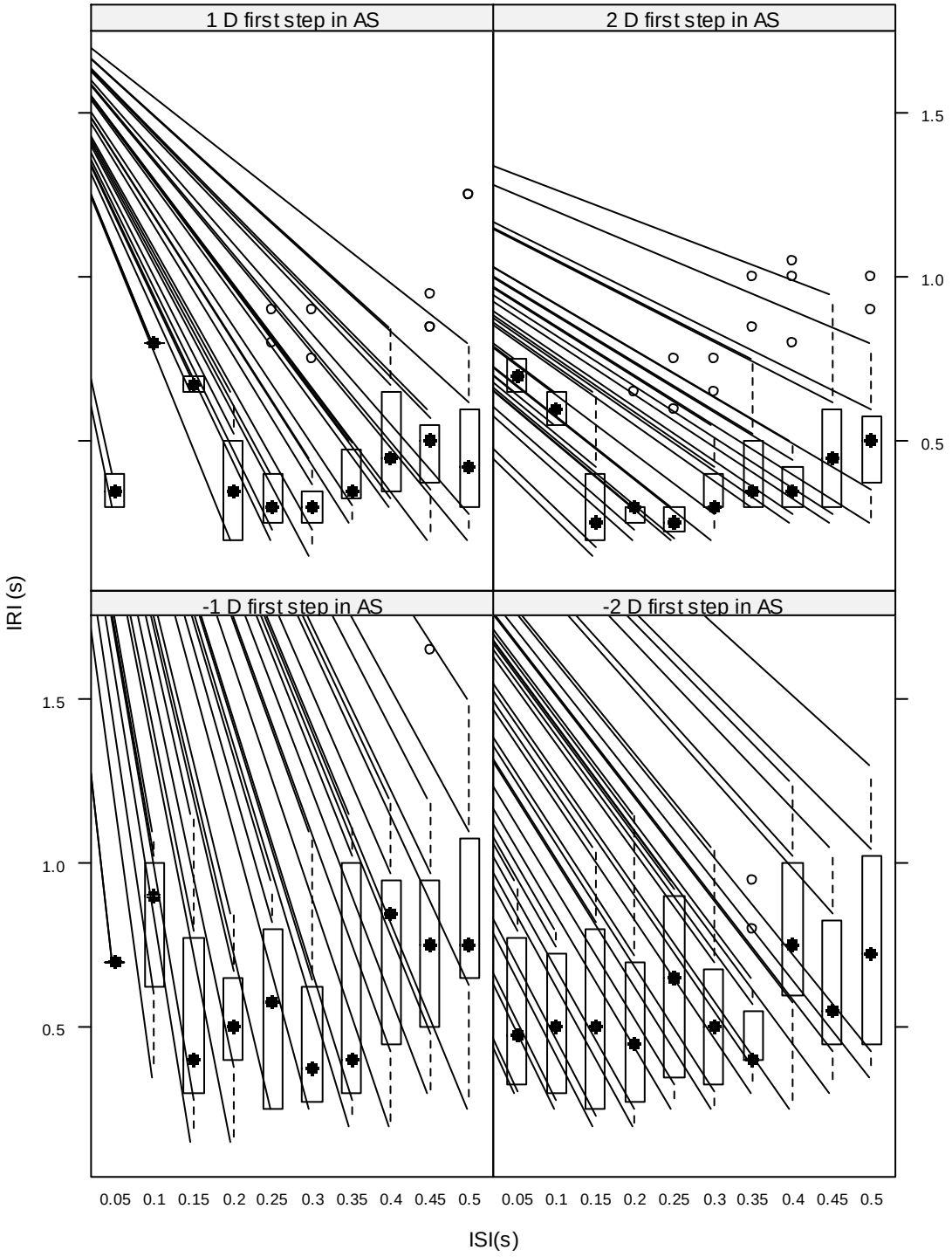

Figure 6-8: Box and whisker plot describing the IRI in trials with correct double responses. (All data points outside the standard whiskers are labelled with open circles.)

The most conditions with a statistically significant response to both stages of the AS were found when AS increased first, by a step of 2 D (top-right of Figure

6-3). These conditions also showed the clearest trend for IRI (top-right of Figure 6-8). A linear regression of the medians of these data, at ISI from 0.25 s to 0.5 s, found that

$$IRI = (0.95 \pm 0.11) \times ISI + 0.00 \pm 0.04$$

(R^2 = 0.94), where the confidence intervals are one standard error. This is consistent with IRI = ISI, although including ISI of 0.20 s and 0.15 s resulted in models not consistent with this relationship. (There was no statistically significant double response for an ISI of 0.20, 0.10 or 0.05 s, Figure 6-3).

The durations of RT2 and RT3 are plotted in Figure 6-9 and Figure 6-10. Figure 6-9 shows RT2 and RT3 in trials in which AS increased in its first step change; Figure 6-10 shows the same for trials with initial decreases in AS. In Figure 6-9, minimum response times are apparent which increase with decreasing ISI. Negative response times reveal the inclusion of some random fluctuations in the peaks of individual “double responses”. This was expected, hence the statistical analysis of section 6.3.1.2. A greater number of negative RT2s were found for stimuli with AS decreasing first (Figure 6-10).

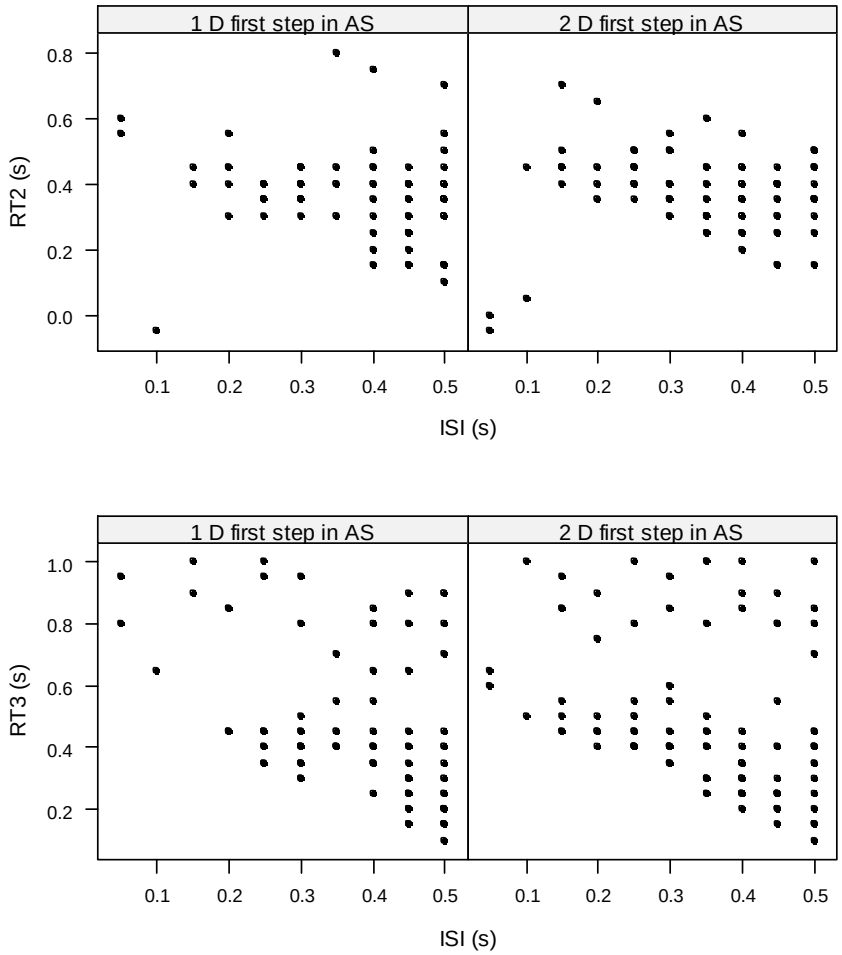

Figure 6-9: Scatterplots showing RT2 and RT3 against ISI, for trials in which the first step in AS was an increase, and which resulted in a correct double response. (The measurements have a time-resolution of 50 ms; several trials share the same response time in many cases.)

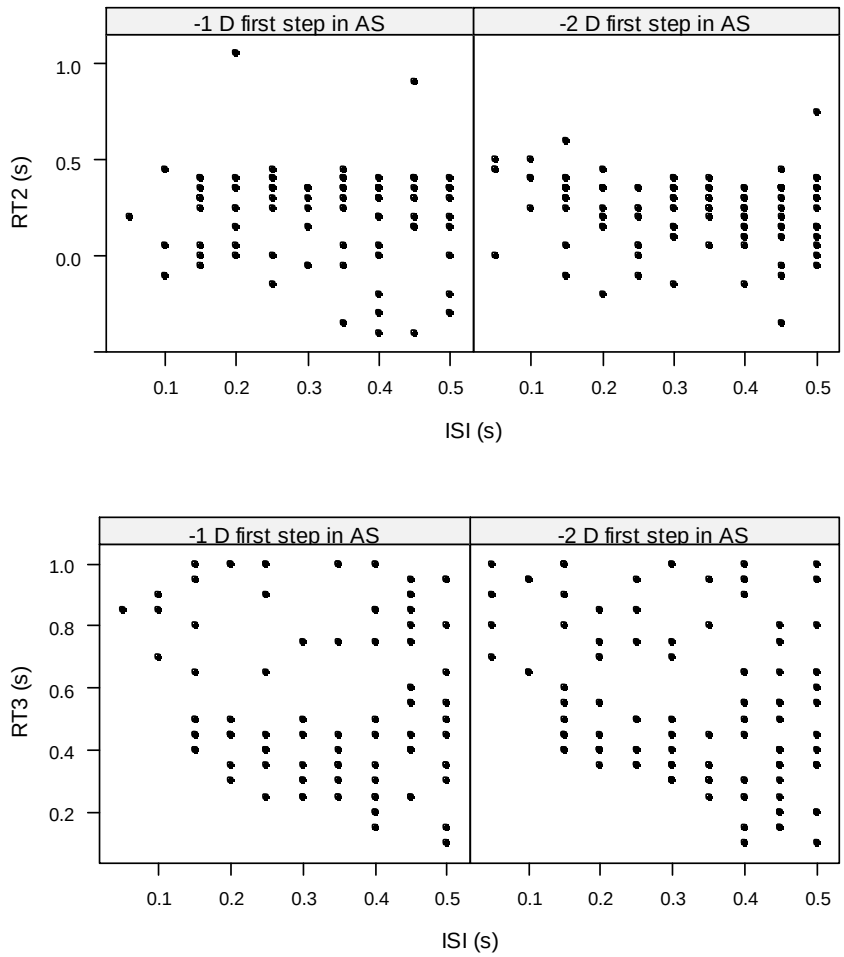

Figure 6-10: Scatterplots showing RT2 and RT3 against ISI, for trials in which the first step in AS was a decrease, and which resulted in a correct double response. (The measurements have a time-resolution of 50 ms; several trials share the same response time in many cases.)

Excluding the outliers in RT2 at ISI ≤ 0.1 s, Figure 6-9 demonstrates minimum response times which increase with decreasing ISI. Excluding the same outliers, (RT2 + ISI) had a minimum of either 0.55 s or 0.60 s in all conditions but three (one with 0.50 s and two with 0.65 s). (RT3 + ISI) also had a minimum of 0.60 s or 0.65 s in all conditions but four (all with a 1 D first step; these are apparent in the lower left of Figure 6-9).

The response times in Figure 6-10 show similar characteristics, with a minimum of 0.50–0.60 s in (RT3 + ISI), for ISI ≥ 0.15 s (excluding one point at first step: −1 D, ISI: 0.45 s). Analysis of RT2 in this case is confounded by the peaks incorrectly identified with very short or negative response times.

6.4 Discussion

6.4.1 The double-AR; continuous monitoring and parallel processing

The findings of Campbell and Westheimer (1960), using a single pulse in AS, suggested continuous monitoring by the accommodation system. However, when the duration of the single pulse in AS was 100 ms or shorter, or the pulse was a decrease in AS, some responses were absent. This may have indicated, first, minimum processing times for an AR, e.g. to trigger sampling of the AS and the sampling time itself. Second, decreases in AS may not be as strong a cue to accommodate as are increases.

In this experiment, one period of a square wave in AS was presented. Section 6.3.1 reported the statistical responses in both directions from the baseline, the prevalence of correct double responses in individual trials and the comparable strength of correct double responses and single responses. These results indicate that accommodation responded in both directions to the succession of conflicting stimuli, at least down to an ISI of 0.15 s.

At ISI of 0.15 s, and amplitude 2 D, both stages of the stimulus were completed within the usual latency of accommodation (0.37 s), and still elicited the AR in both directions. This result, in particular, supports the theory of continuous monitoring of the AS during processing of previous input, including stimuli more complex than a single pulse. By the time of the EARLY stage of the response, even the LATE stage of the stimulus was in the past, yet the LATE stage of the AR was still effected. The sampling of AS for the LATE response was carried out during the latency (preparation time) of the EARLY response. EARLY and LATE responses were therefore being prepared concurrently, likely at different stages of the preparation process. Becker and Jurgens (1979) performed a

similar, double-step experiment on the saccadic response and proposed this type of "parallel processing" of inputs in a control chain[*]. This aspect of accommodation control is discussed further in section 6.4.6 on response times.

Further, the LATE response appears to have taken the calculation for the EARLY response into account, in producing a significant peak beyond the baseline. (See also section 6.4.5 on relative strengths of the peaks in AR.)

One reason for the observed limit of double responses to ISI ≥ 0.15 s may be that the AR becomes indistinguishable from the fluctuations of accommodation using these methods. Another may be that this is close to a minimum time window for the sampling of retinal blur, once such sampling has been triggered. Similarly, Campbell and Westheimer (1960) found that responses were sometimes absent at single pulse durations of 100 ms or shorter.

From Figure 6-3, there were fewer conditions with a statistically significant double response with AS amplitude 1 D than with AS amplitude 2 D; there were also fewer when AS decreased first than when it increased first. The changes with amplitude 2 D thus provided clearer cues for the continuous monitoring than those at 1 D, and the same appears to be true for increases in dioptric stimulus, as opposed to decreases. The smaller decreases in AS when AS decreased first, as opposed to second, appeared to result in fewer ARs. This difference between the responses to increases and decreases in dioptric stimulus was also found by Campbell and Westheimer (1960).

Recent models of accommodation control have favoured a compound AR (Khosroyani and Hung, 2002; Schor and Bharadwaj, 2006). They contain a

[*] Becker and Jurgens called this capacity for a plurality of signals in the control chain "parallel processing", but an essential feature of their conclusions was that inputs cannot be processed simultaneously in the same component of the control chain.

rapid “open-loop” signal to change accommodation, following a large or rapid change in the stimulus, and a “closed-loop” response, continuously monitoring and following slower changes. The MATLAB/SIMULINK model of Khosroyani and Hung* predicts the double response found in this experiment, even down to ISI = 50 ms (see Figure 6-11). In that model, the acceleration at each change in the stimulus triggers a reset of the sampling for the rapid, open-loop response, allowing each state of the stimulus to produce such a response. The model of Schor and Bharadwaj relates only to single step-changes in AS and therefore cannot be closely compared with the data of this experiment.

Maximum and minimum AR in simulations using the control model of Khosroyani and Hung are in broad agreement with the data of sections 6.3.1.1 and 6.3.1.2. The parameters used successfully in their paper yielded the results of Figure 6-12, when the initial change in stimulus was an increase in accommodative demand. The general increase in peak responses with ISI was found, as in the experimental data plotted in Figure 6-3 (page 114). However, the gain of the peak responses is considerably higher in the simulation than in the experimental data, particularly with an AS amplitude of 2 D. The simulation also treats accommodation and disaccommodation symmetrically. Discussion of this control model continues in section 6.4.5.

* The MATLAB/SIMULINK model was kindly provided by Professor Hung, Rutgers University. The simulations were run and maxima and minima of accommodation extracted in MATLAB (Mathworks, 2008).

Figure 6-11: The double AR (green trace) predicted by Khosroyani and Hung (2002), in response to the 50 ms, 2 D stimulus of this experiment (dark blue square wave). The red trace is the accommodation signal generated by the "open-loop" component of the model. It follows the AS after a latency interval and is finally attenuated by the biomechanical response. The orange trace (at zero) is the signal generated by the "closed-loop" component of the model. In the case of such large and rapid changes, this component is not affected. (It does contribute to the simulated response to other stimuli from this experiment.)

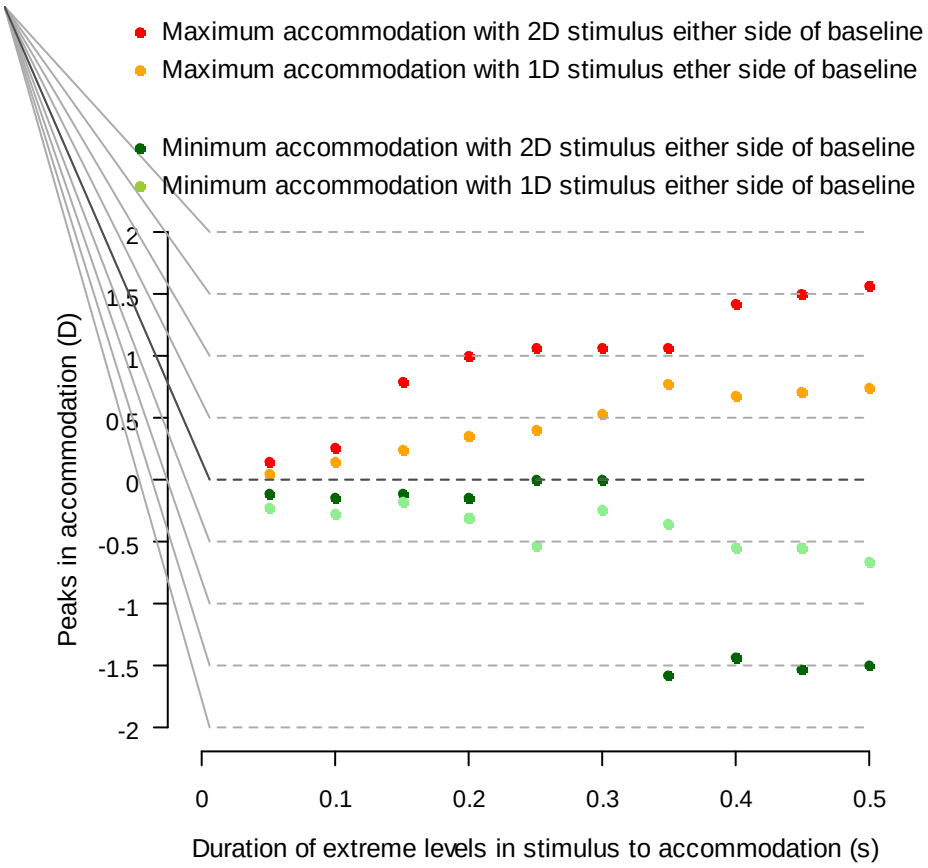

Figure 6-12: Data equivalent to that displayed in Figure 6-3 (page 114), from simulations using the model of Khosroyani and Hung (2002). These are the peaks when the initial step in the stimulus is an increase in demand. The AR is relative to the baseline level of AS (labelled zero in the model, although disaccommodation simulations are expected; see the original model paper).

6.4.2 Single responses and time-variance of the accommodation system

There also appeared to be responses to only a single stage of the stimulus. Both EARLY and LATE stages of the AS elicited single responses, with the other stage of the response apparently absent. Single responses were observed at all ISIs down to 0.05 s. Single responses were equally likely to be to the EARLY or LATE stage of the AS. There were also null responses, which did not exceed the baseline extrema.

There therefore appears to be a varying property in the accommodation system that causes identical changes in AS to result in different, or null, ARs. A link with the natural fluctuations of accommodation (visible in Figure 6-1 and Figure 6-7) is a candidate for further investigation.

6.4.3 Comparison of double and single responses

In nearly half of the conditions considered in section 6.3.1.4, single responses were significantly stronger than at least one stage of the correct double response. In just over half the conditions, this difference was not observed, and the median of a peak in the double response was sometimes higher than that in the single response. A stronger single peak may indicate that the single responses arise from a delay or failure in recognising the change in AS and signalling the halt to that stage of the AR. However, that no significant difference was observed in many conditions was interesting, particular in the case of the EARLY responses; in these single responses, the AR may have been halted as in the double response, but not instructed to follow the second stage of the AR. There may be more to learn about a difference between halting an AR during onset and initiating an AR towards a target level of AS.

The higher significance threshold ($p < 0.1$) was used to increase the likelihood of rejecting the interesting null hypothesis.

6.4.4 Incorrect double responses

The AR in some trials contained both maximum and minimum outside the range of the baseline fluctuations, but in opposite order to the levels presented in the AS (Figure 6-4 and Figure 6-5). The mean peaks of incorrect double responses were comparable in amplitude to those of correct double responses.

In the incorrect double responses, a decision has first been made to respond in the wrong direction, with respect to the stimulus. In the absence of many normal cues (size, disparity, relation with surroundings) this phenomenon has been observed before, particularly for steps of decreasing AS (Chin et al., 2009b). Secondly, however, either the direction error persists in the second stage of the

AR, or the accommodation system has realised the error and attempted to respond belatedly (the AS has returned to baseline by this time). The processing of these apparent, incorrect, double decisions also warrants further study.

6.4.5 Comparison of EARLY and LATE peaks in AR

In section 6.3.2, it was found, in correct double responses, that there was usually no significant difference between the AR to a given level of AS occurring either EARLY or LATE in a trial. When there was such a difference, the AR to the level of AS occurring LATE was likely to be greater than the AR to the same level of AS occurring EARLY (true for 8/40 conditions). In general, the LATE AR was not attenuated by the EARLY AR, at least not any more than the EARLY AR was attenuated by the LATE AR.

The models of both Khosroyani and Hung (2002) and Schor and Bharadwaj (2006) include a leaking of information over time, owing to the finite response speed, particularly of deformations of the crystalline lens. This leaking, integrating transfer function, between the signal to accommodate and the deformation of the lens, could result in an effective attenuation of obsolete signals to accommodate (the EARLY stage of the AS). However, these considerations alone do not automatically lead to the tendency to a stronger LATE response, as found in this study. In fact, the EARLY response could reduce the amplitude of the LATE response by modifying its starting point, combined with the slow transfer function of the biomechanics. This effect was observed when running the model of Khosroyani and Hung, as shown in Figure 6-12; the model treats the dynamics of accommodation and disaccommodation identically, so a weaker peak in disaccommodation than accommodation means

that the LATE response is weaker than the EARLY response. In this model, the LATE response was only greater than the EARLY response at four conditions out of twenty: ISI = 0.05, 0.1 and 0.25 s with amplitude 1 D, and ISI = 0.35 s with amplitude 2 D. At twelve out of twenty conditions, the EARLY response was stronger than the LATE response; in four conditions, the EARLY and LATE responses had similar amplitude.

The results of section 6.3.2 therefore reveal some disagreement between the control model of Khosroyani and Hung (2002) and the AR data, for the AS of this chapter.

During dynamic accommodation, Mucke et al. (2008) found a suppression of contrast sensitivity for high spatial frequencies, but not low spatial frequencies. It was hypothesised that input to accommodation would also be suppressed during accommodation onset. Again, however, the results of section 6.3.2 demonstrated no evidence for such a suppression of input to the accommodation system during dynamic accommodation. The opposite tendency was in fact observed in the correct double responses.

In order for the LATE response to not be significantly weaker than the EARLY response, the accommodation controller must use information both about what the accommodative state will be, or is, at the time of onset of the LATE response, and where the response should aim for. i.e., the step was deliberately made to start from the current, or estimated state, and was not relative to the baseline. If the LATE response was based solely on the defocus information from the LATE stage of the AS, the defocus errors for the EARLY and LATE responses would be roughly equal and opposite, particularly for ISI = 0.15 s. In that case, we would expect the responses to be roughly equal and opposite,

and the LATE response would return accommodation approximately to the baseline level. Especially for initial increases in AS, we would not expect the weaker response to the LATE decrease in AS—weaker because it is a decrease—to result in a peak beyond the baseline.

In their saccadic double-step experiment, Becker and Jurgens (1979) also found analogous “extra-retinal” error processing. The saccadic control system appeared to use an estimate of position in a first saccade in its accurate calculation of amplitude for a second saccade.

There are a few possible explanations for a tendency for the LATE peak AR to be stronger than the EARLY. One is that information from different periods during the latency interval and onset of accommodation is weighted with different priority. Conflicting information from later in the latency may be allowed higher importance because it is temporally closer to the actual response.

A related explanation is that the accommodation controller may integrate AS over a time window that can extend beyond a subsequent change in AS. In that case, inclusion of part of the LATE stage of the AS in the integration for the EARLY response could attenuate the EARLY response. That attenuation would be greater than the effect of including the final baseline AS in the integration for the LATE response.

Finally, the larger change in AS for the LATE response may have resulted in an increased velocity. Accommodation may have therefore progressed further beyond the baseline before it was checked by the final signal to return to baseline. It is already known that the magnitude of a step-change in

accommodation affects velocity and acceleration (Kasthurirangan and Glasser, 2005; Schor and Bharadwaj, 2006).

Exploration of these possibilities may lead to more precise understanding and more accurate models of accommodation control.

6.4.6 Timing

It was found in section 6.3.3 that for the strongest cues, eliciting the most double responses (2 D initial increase in AS) a clear trend was observed, where the IRI decreased with decreasing ISI. For longer ISI, the findings were consistent with IRI = ISI, and there may be a lower limit at 0.25 s for this relationship.

Also, the individual response times for the peaks in AR (RT2 and RT3) had minimum durations which increased with decreasing ISI, such that (RT2 + ISI) and (RT3 + ISI) appeared to have a consistent minimum of 0.50–0.65 s, independent of ISI. No exact data for such short pulses have been found in Campbell and Westheimer (1960) or elsewhere for comparison. However, this minimum appears to indicate a different regime from that observed by Campbell and Westheimer, where the onset of accommodation proceeded for a length of time approximately equal to the duration of the pulse in AS (see also the ARs and mean ARs in section 4.3).

These data are consistent with the existence of a minimum time interval for two changes in AS and two responses of accommodation. The increasing minima to RT2 and RT3, as ISI decreases, indicate that the second and third levels of AS took longer to pass through the control system as ISI decreased. The relationship IRI = ISI, with a possible lower limit at 0.25 s, may indicate that the longest process in the accommodation control chain for stimuli lasts

approximately 0.25 s. For ISI below this value, input may have to wait to enter this part of the control chain, just as the computing component in the saccadic model of Becker and Jurgens (1979) is free for new input after sending a command to generate an oculomotor signal.

There are complications to this theory, however. To account for the double responses at ISI = 0.15 s, a control chain with a longer limit to one of its processes (e.g. 0.25 s) must also allow storage of at least the defocus of the LATE stage of the AS. Furthermore, the short response times (< 0.25 s) at longer ISI are not accounted for by this simple theory, and appear to result from the predictive abilities of the accommodation system (Phillips et al., 1972).

It may be said that even including predictive effects, the shortest time in which an AR can be halted, once stimulated, appears to be about 0.6 s, for both "pulses" of the square-wave AS of this chapter. This limit may also contribute to explaining the timings of the AR in the pilot study of chapter 4. A further single-pulse experiment, using the improvements made to the protocol since the pilot study, could confirm the time limit to halting an AR, following stimulation (see section 9.3.1.2).

6.4.7 Limitations of the experiment

There was a risk that peaks in AR were missed by using the cut-off point of 1 s after the last change in stimulus for their detection. On the other hand, drifts in accommodation and blinks were more likely to be included by relaxing the cut-off. The data in Appendix B.1 show that the cut-off should not have caused many peaks to be missed, and at least responses would be clearly underway before the cut-off. It may be possible to design a better algorithm for searching

for peaks in the AR; a greater number of statistically significant responses may be found in that case.

Frames were captured every 0.05 s, and provided an analysis of the average wavefront over 7 ms. Measurements every 0.05 s should be sufficient to capture peaks in AR, but greater time-resolution would provide more accurate results.

Data on the velocity and acceleration of accommodation would have allowed further analysis of latencies and the role of feedback during the AR (Bharadwaj and Schor, 2005). It would also have allowed investigation with reference to the signals of acceleration and velocity of accommodation proposed by Schor and Bharadwaj (2006). Unfortunately, it was not possible to extract accurate velocities as responses to changes in AS, owing to the similarity of the brief AR to the baseline microfluctuations of accommodation, as seen in Figure 6-1 and Figure 6-7. Smoothing algorithms (running medians) were applied to attempt to distinguish the velocity of the response from that of the baseline fluctuations. Then, algorithms could be used to search for peak velocities of the response, rather than the high instantaneous velocities of the fluctuations. However, the timescale of the low-frequency component of the microfluctuations (around 0.5 s) is similar to the timescale of the AR, so smoothing of the microfluctuations also distorts the AR and prevents meaningful analysis (see also Appendix D, which shows an attempt to smooth over a briefer interval).

Future research should aim to find a solution to access the velocity and acceleration of such ARs. One option may be to use the mean time course of accommodation, such as is displayed in Figure 6-2. Fitting the AR to an analytical function without prior smoothing, as in Kasthurirangan and Glasser

(2005), may also be useful. Faster recording of the AR may also benefit the smoothing procedure (compare Appendix D and Bharadwaj and Schor, 2005), but it is limited here by the camera readout time.

Finally, an attempt has not been made to develop the computational simulation of accommodation. Further efforts are required to incorporate these findings into the models considered.

6.4.8 A possible follow-on study in accommodation dynamics and myopia

With respect to myopia, further studies could be carried out with the same instrument, to investigate differences in the AR to changes in AS within the latency and onset of accommodation. Together with other differences in accommodation between myopes and emmetropes (see section 1.4), a longer period of defocus may be required for myopes to register a change in AS. We may expect myopes to demonstrate a longer minimum ISI required for a statistically significant correct double response; differences in the timings of the AR may also be evident. Such experiments could include several each of emmetropes, early-onset myopes and late-onset myopes, and could contribute to the study of accommodation in myopes reviewed in section 1.4 (see also section 9.3.4).

6.5 Conclusions

A square wave in dioptric stimulus was observed by the six participants, under monocular conditions. Changes in AS took place within the latency and onset of accommodation. By analysing the AR, it was found firstly that sampling of the retinal input appears to take place over the course of the latency and onset of accommodation. The results of the sampling are carried over into a double

response, even when the two stages of the dynamic stimulus are completed within the latency of accommodation. There appeared to be a significant double response to such stimuli for ISI ≥ 0.15 s. The accommodation controller may respond in a similar way below this limit, but with the AR obscured by the microfluctuations of accommodation.

The first and second peaks of a double response were most likely not to be significantly different in amplitude as result of their order. However, 8 out of 40 of the stimulus levels and durations—a statistically significant proportion—resulted in a LATE peak which was significantly stronger than the corresponding EARLY peak. This may indicate a favouring of later information over earlier, for short ISI, either via a weighting function for defocus information over time or by integration over a certain time window. Alternatively, the effect may be due to the application of a high velocity of accommodation in response to the larger second step, to the extent that the second response is more extreme than the first, by the time the signal to return to baseline takes effect.

Two-stage models of accommodation, including an initial, rapid, open-loop response, appear to remain appropriate in the regime studied here. However, the literature did not predict the tendency towards a stronger LATE response.

The presence of single responses (equally likely to be EARLY or LATE) and null responses at various stimulus intervals indicates a time-variant starting condition for the accommodation control process. It is speculated that this may be linked to the natural microfluctuations of accommodation. Possibly also connected, incorrect decisions were sometimes taken as to the direction of response to two changes in AS in quick succession.

IRI decreased with decreasing ISI, and was approximately equal to it for the strongest stimuli. Response times to the second and third changes in AS increased as ISI decreased. This indicated, together with the double response at brief ISI, that the preparation for a later change in accommodation could begin during the preparation period for a prior change.

Longer response times at briefer ISI may indicate that defocus information is stored and has to wait until an occupied part of the control chain is vacant to enter it (e.g. sampling and computation of a signal). On the other hand, briefer response times at longer ISI indicate the role of predictive effects, which appear to shortcut stages of the control process which apply to brief stimuli. In total, including such predictive effects, the minimum time in which an AR can halted, following stimulation, appears to be about 0.6 s.

7 Binocular adaptive optics instrumentation and development

7.1 Design

7.1.1 Introduction

There has been interest in the relationships between aberrations of the eyes, accommodation and myopia for several years (see section 1.5), but it has only recently become possible to build and control binocular adaptive optics (AO) systems for aberration control and measurement. Binocular enhancement of contrast sensitivity (Campbell and Green, 1965) and enhancements of the accommodative response (AR) time, velocity and gain in binocular vision (Ibi, 1997) make it important to study the binocular AR in connection with manipulation of stimulus aberrations, not just the monocular AR. Binocular enhancement of visual acuity has also been found to increase with blur from simulations of higher-order aberrations (HOAs) (Fam and Lim, 2004), as well as with increasing defocus (Plainis et al., 2011). While monocular accommodation studies are useful for isolating cues to accommodate (e.g. retinal blur only, as in chapter 6), normal vision and accommodation are binocular, and binocular experiments must be undertaken to fully understand them.

Fernandez et al. (2009) and Sabesan et al. (2012) have constructed instruments which can be used to measure and control aberrations of both eyes, simultaneously, but do not have the facility to provide changes in lateral retinal disparity. This cue for the eyes to converge is essential for providing and studying the binocular dynamic AR. The apparatus of this chapter is the first instrument capable of both binocular AO control of stimulus aberrations, including dioptric stimulus to accommodate, and control of the retinal disparity cue to converge.

Figures 7-1 and 7-2 illustrate the AO apparatus developed for studying binocular accommodation dynamics, which includes a stereoscopic stimulus with variable horizontal image positions—using the scanning mirrors—and the capacity to perform aberrometry and AO experiments on converging eyes. For each eye, this apparatus features a visible stimulus, a deformable mirror (DM) as the AO element for stimulus control, a Shack-Hartmann wavefront sensor, and means to simultaneously control the visible stimulus and perform infrared (IR) aberrometry on the eye, as outlined in chapter 2. The wavefront measurements can be used as feedback for the stimulus control, e.g. in correction of the ocular aberrations.

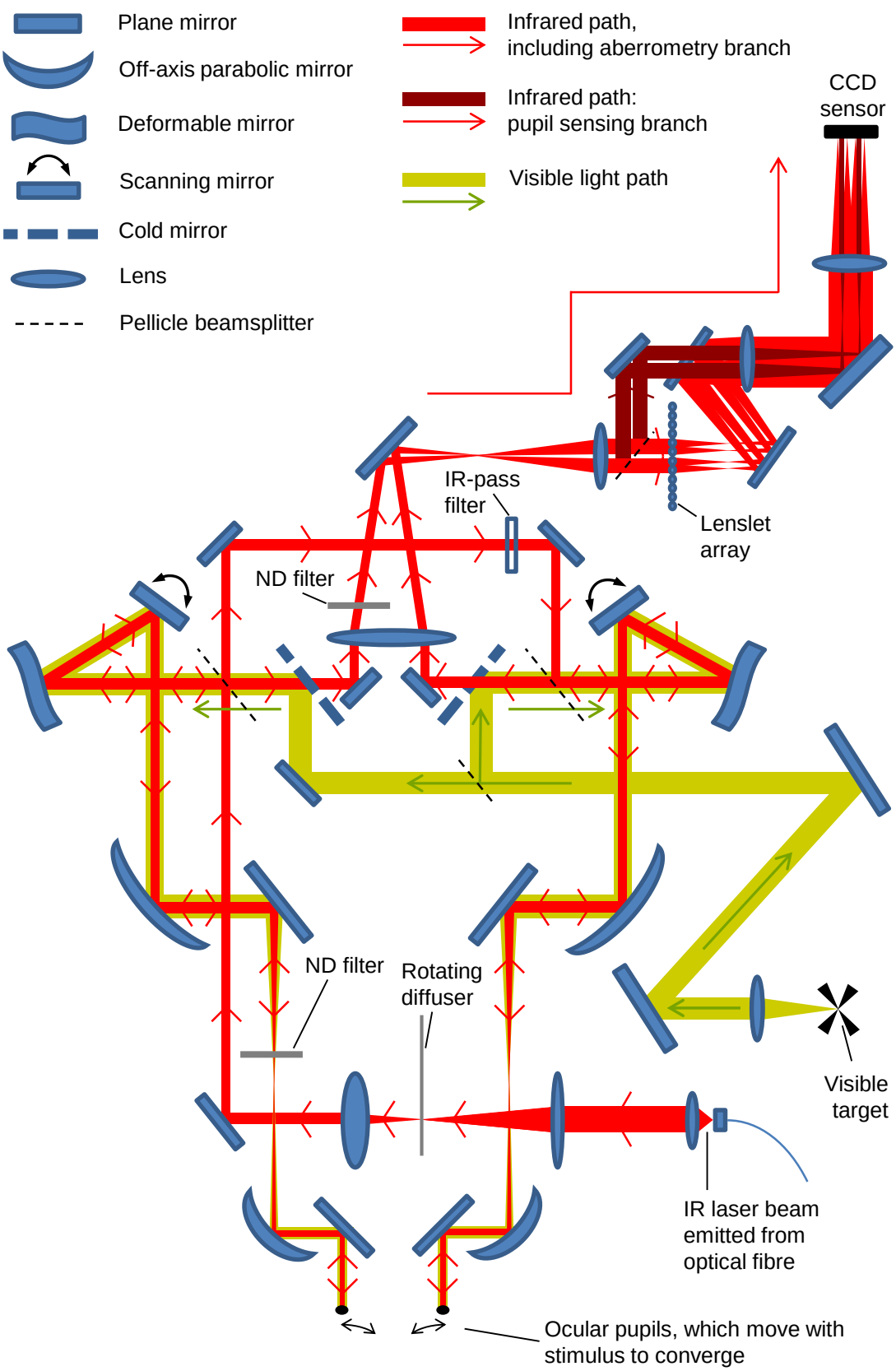

Figure 7-1: Diagram of the binocular AO apparatus. Pupil image planes are at the deformable mirrors and the lenslet array. The plane of the pupil sensing branch is raised upwards from the bench by a pellicle beamsplitter and a plane mirror. The plane of the aberrometry branch (from the lenslet array) is lowered towards the bench by two plane mirrors. The plane mirrors closest to the ocular pupils, marked "PD", are connected and move together on a rail. Focal lengths of the focussing elements are given in mm.

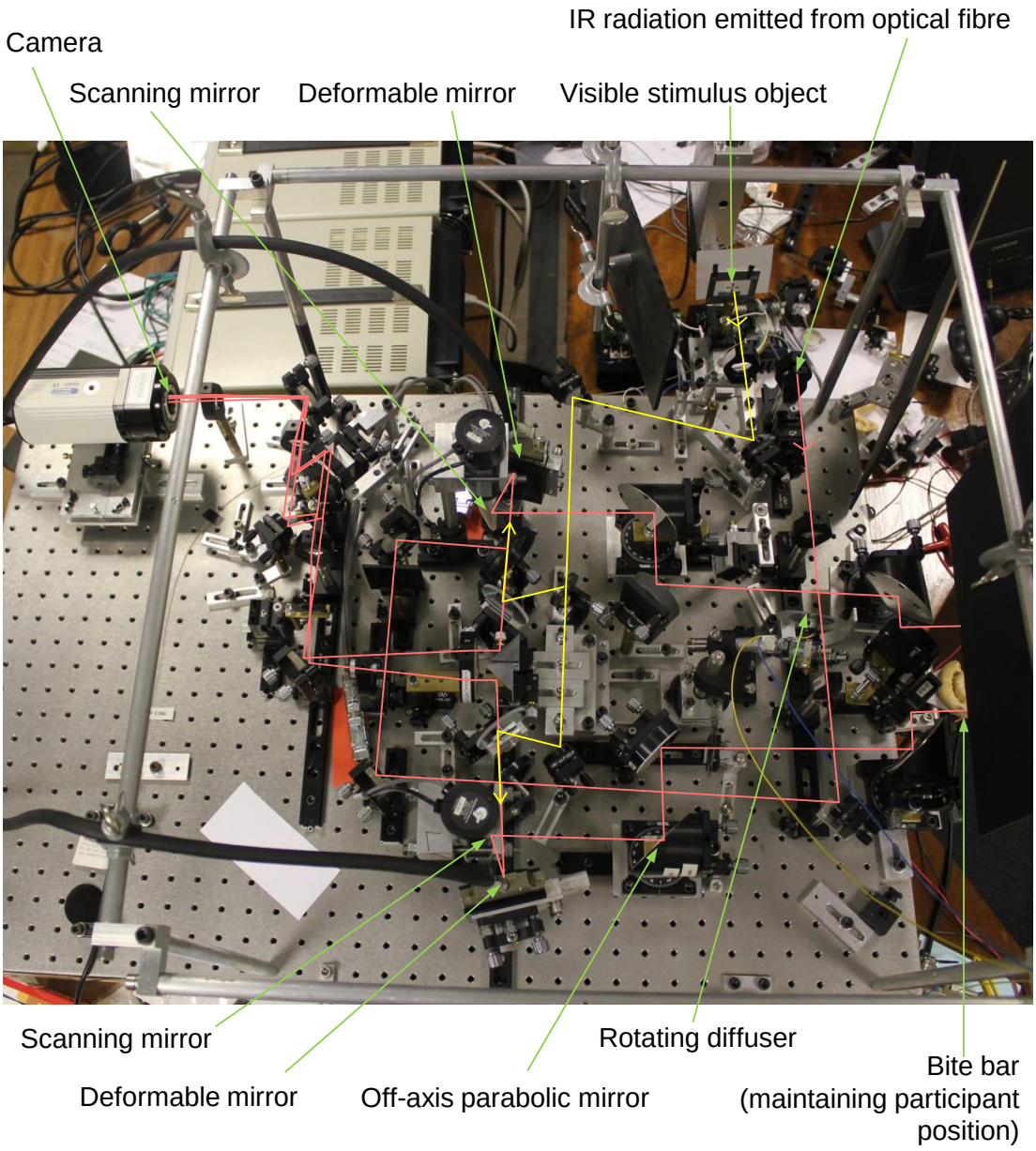

Figure 7-2: Photograph of the binocular AO apparatus. The IR paths (pink) and the start of the visible light paths (yellow) are traced over the photograph. The system is rotated 90° anti-clockwise, compared with the diagram of Figure 7-1.

Images of one stimulus object are presented in stereoscopic vision (see Figure 7-3) and may be manipulated identically or differently for the two eyes. The scanning (rotatable) mirrors move the stimulus images laterally, stimulating a change in convergence of the eyes*.

* While DMs can change the tilt of a wavefront, and therefore rotate a beam, the stroke is not sufficient for the rotations required for dynamic accommodation experiments. Roughly 1 mm of stroke would be required over the pupil image at the DM in this case to stimulate the convergence corresponding to a target at 0.25 m (or 4 D). Furthermore, a DM cannot be exactly conjugate to both the centre of rotation and the pupil plane of the eye (see section 7.1.3).

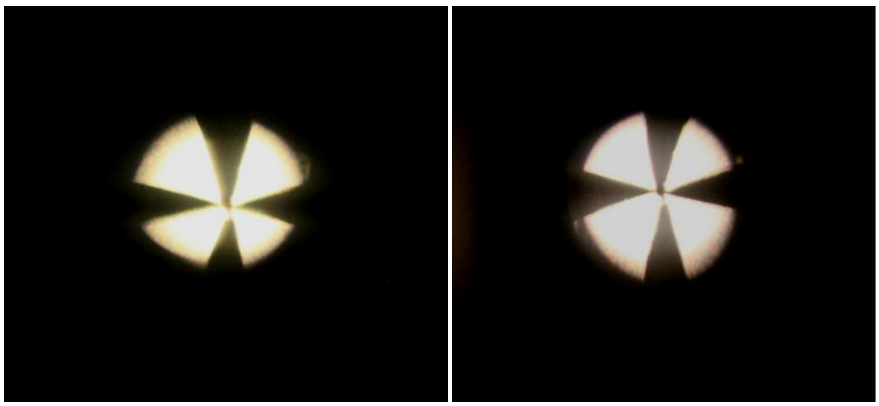

Figure 7-3: The stimuli which are fused by the participant for stereoscopic vision. The true contrast for the participant is higher than it appears here; glare from the camera is included in the black areas.

It is therefore possible to control both blur—from defocus or other aberrations—and lateral-spatial stimuli to accommodation and convergence, identically or differently for the two eyes, and to record the accommodation and convergence response, as well as the higher-order aberrations (HOAs) of the eyes. Four IR sensing channels are generated at the sensor: images for both pupil position and wavefront sensing are produced for each eye.

The system was designed by Dr. Karen Hampson at the University of Bradford, and minor modifications were made to the design as the instrument was developed. Modifications included the specific design of the visible stimulus input (see Figure 7-1 and section 7.2.6), the use of the IR-pass filter (see Figure 7-1 and section 7.1.3) and the removal of an aperture which was designed to filter out stray light, but which restricted measurements for moving ocular pupils. (This aperture was originally positioned where the beams cross, above the label “IR-pass filter” in Figure 7-1.)

All components of the apparatus were positioned and aligned, including the design and construction of custom optical mounts* (section 7.2). The performance of the system was checked, following calibration (section 7.3).

The control software was developed alongside the instrument by Dr. Hampson, with testing and small changes in code by the present author, as it became possible to test it in situ. Figure 7-4 shows the view on a monitor of the images formed at the CCD sensor in the four IR channels.

* Prof. Edward Mallen assisted by constructing and modifying some of the custom optical mounts, and providing components for others.

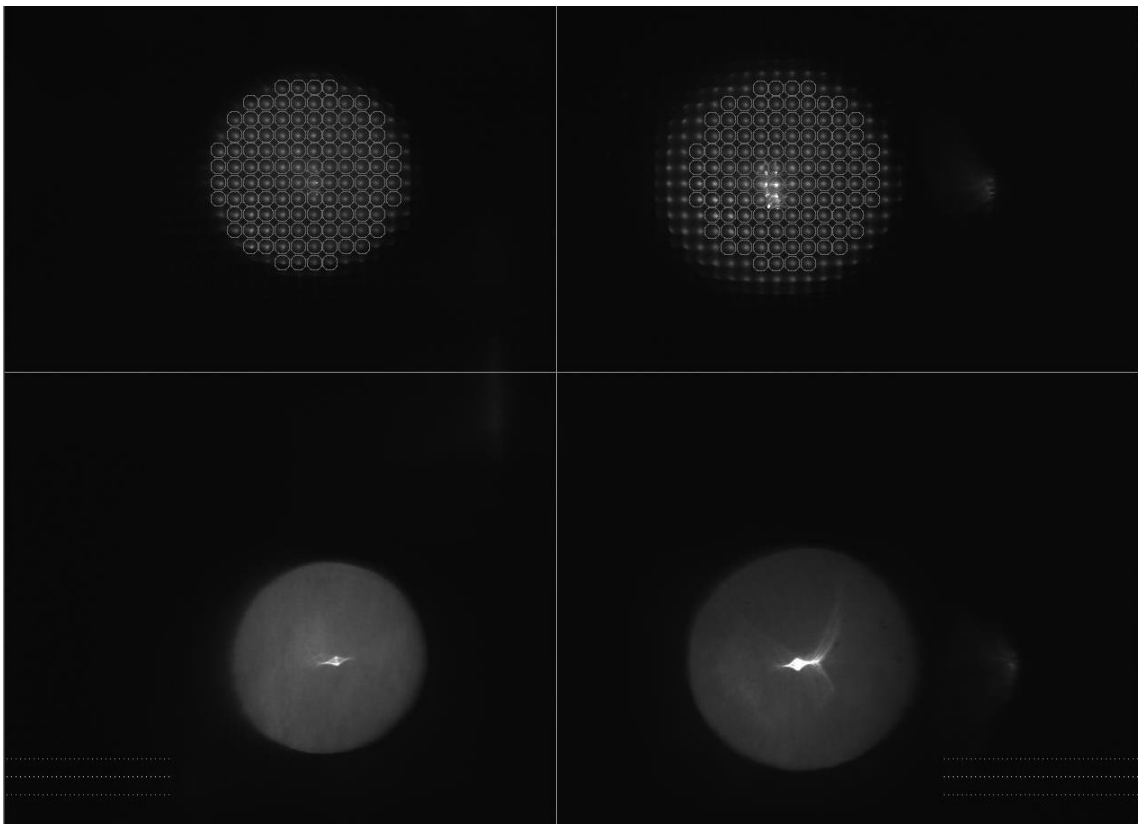

Figure 7-4: The pupil position (lower) and wavefront (upper) sensing images at the CCD sensor, as seen on a monitor by the experimenter. Right eye images are on the left-hand side and left eye images are on the right-hand side[*†]. The circular search blocks (see section 2.2.2) are visible with the wavefront sensing images. Some of the actuator voltages (all set at the midpoint) are visible in the bottom corners.

7.1.2 The deformable and scanning mirrors, and the CCD sensor

The DMs have 52 electromagnetic actuators each, behind a mirrored circular surface of diameter 15 mm (MIRAO 52, from Imagine Eyes S.A., France). They are specified to be able to generate a maximum change in relative phase of 50 μm, when applying tilt to an incident beam. Fernandez et al. (2006) investigated the performance of this DM and found that it was capable of applying changes in defocus of ±10 D to a stimulus, and accurately replicating desired levels of a given Zernike polynomial (see section 2.3), up to 5th order.

[*] A magnification difference is seen between the right and left pupil images in this figure, and in Figures 7-14 and 7-20. Such a magnification difference was not usually apparent; these screenshots were taken without the full calibration carried out prior to data collection (as in the protocol described in section 7.2.8).

[†] Purkinje-Sanson images are visible, generated by corneal reflexes. These images were found not to affect aberrometry measurements of trial lenses using the monocular instrument of chapter 3; they also do not affect the pupil centroiding process (which registers pixels as only either bright or dark, relative to a threshold).

However, because of the mechanical constraints of the membrane, coupling between adjacent actuators also sometimes resulted in extra, unintentional distortion of the mirror, revealed by the presence of other Zernike terms as well as the Zernike polynomial deliberately replicated. Dubra (2007) found the influence function of an actuator to be 60% at neighbouring actuators.

The scanning mirrors (Model 6880, Cambridge Technology, UK) are galvanometers specified to rotate between angle settings in approximately 0.9 ms, with a range of 40°.

The CCD sensor is a Retiga EXi Fast 1394 camera, from QImaging, Canada, as in the monocular apparatus of chapter 3.

7.1.3 Visible stimulus

A black Maltese cross on a colourless background (the “stimulus object”) is back-illuminated to provide the stimulus to binocular accommodation and convergence (see Figure 7-3). Images of the pattern are presented in stereoscopic vision, while the IR beam, camera and Shack-Hartmann sensor interrogate the optics of the eye.

Light from the stimulus object (see Figure 7-1) is collimated, folded into the system and split into two beams by a pellicle beam splitter (PBS). The beams carrying the stimulus for the left and right eyes are folded into the same paths as the IR beams by cold mirrors. The IR-pass filter prevents the left-eye beam from entering the right-eye path via the PBSs. In each eye, the plane wavefront of the visible beam is passed to a DM, then a scanning mirror, then through the off-axis parabolic mirrors (OAPMs) and finally to the eye. The neutral density (ND) filter between the OAPMs in the left eye channel balances the intensities

of the stimulus for the two eyes[*]. The OAPMs are designed for use with an angle of incidence of 45°.

The distance between the OAPMs is the sum of their focal lengths, and the lower-power OAPMs are one focal length (191 mm) from the DMs. The OAPMs therefore form an image of the wavefronts at the DMs in the pupil plane, which is one focal length (102 mm) from the nearest OAPMs to the eyes. Deformations of the DMs produce movement of the visible stimulus, towards or away from the participant, as in the monocular apparatus (section 3.1.2), or modulate other aberrations.

With the pupil of each eye at the focal point of its nearest OAPM, changes in the angular size of the observed target with dioptric stimulus are minimised. As the vergence at either eye changes from 0 to 2 D, the image is magnified by 11%; as the vergence at the eye changes from 0 to 4 D, the image is magnified by 22%.

The distances from the scanning mirrors to the eye are such that the scanning mirrors are conjugate with the centres of rotation of the eyes, and the beams are incident on the axes of rotation of the mirrors. When a scanning mirror rotates, the beam at the eye rotates in the opposite direction, with angular magnification ≈ the ratio of the focal powers of the OAPMs, but it still passes through the centre of the eye. The target therefore maintains visibility as lateral movement is provided, stimulating the eye to rotate by the magnified angle.

[*] ND filters passing 0.65 of the incident energy balanced the subjective brightness of the two stimulus images. The difference between the two eyes was a result of unequal transmission and reflection at the “40:40” pellicle beamsplitters (Edmund Optics, part 39-483; 20% of incident radiation is absorbed). In fact, it was found that these beamsplitters were asymmetric: they divided a beam much more equally when it was incident from one side; they were used in the more equally dividing orientation with reference to the IR beams.

The plane mirrors closest to the eyes are mounted on a rail, so that they can be moved towards or away from a participant. Thus, it is possible to adjust the distance between the beams carrying the stereoscopic presentation of the stimulus images, for participants with different interpupillary distance (PD).

7.1.4 Infrared aberrometry I: from laser, to eyes, to separation into pupil position and wavefront sensing channels

As in the monocular apparatus (chapter 3), the 830 nm radiation from a fibre-coupled diode laser (Access Pacific, UK) is emitted from the optical fibre and collimated. It is first focused onto a rotating diffuser, which causes the laser speckle pattern from the roughness of the retina to be rapidly varied over time, and averaged over the camera exposure time. This averaging prevents distortion of the positions of the intensity maxima at the camera, and misinterpretation of the intensity pattern, for instance in overestimation of total RMS aberration (Hofer et al., 2001).

Propagating on from the rotating diffuser, the beam is recollimated and passed on to a PBS which splits the input beam into left eye and right eye channels. The beam for the right eye is folded round to the right eye optics by plane mirrors and a further PBS.

The beams pass via the DMs, the scanning mirrors and the OAPMs, as described for the visible stimulus (section 7.1.3). The translatable mirrors marked “PD” in Figure 7-1 allow the separation of the IR beams to be varied appropriately to the participant, also as described for the stimulus in section 7.1.3.

Both the lenses either side of the rotating diffuser and the OAPMs minify the beams, to provide a small IR spot on the retina, as discussed with reference to the monocular apparatus (section 3.1.3).

The power of the IR beam at the left eye is 0.1 mW and at the right eye is 0.05 mW; these are much smaller than the maximum permissible exposure of the eye at this wavelength of 0.7 mW, for 8 hours' continuous viewing (British Standards Institution, 2009).

As in chapters 2 and 3, the IR beams are focussed to a spot on the retina of each eye, where the radiation is absorbed and scattered. Some of the scattered radiation passes back through the crystalline lens, the pupil and the cornea, exiting each eye as a beam. Each beam returns via the OAPMs, the scanning mirror and the DM, and is partially transmitted through a PBS, passing on through a cold mirror to the lens with focal length 200 mm. At this lens, the two eye beams are combined and share all remaining optics of the system. An ND filter following this combining lens balances the powers of the IR beams for sensing.

The combining lens is one focal length (200 mm) from the DMs. This lens and the next lens, with focal length 50.8 mm, are separated by the sum of their focal lengths. The beams from both eyes are spilt by a PBS after the latter lens, into pupil position and wavefront sensing channels.

7.1.5 Infrared aberrometry II: Pupil position sensing channels

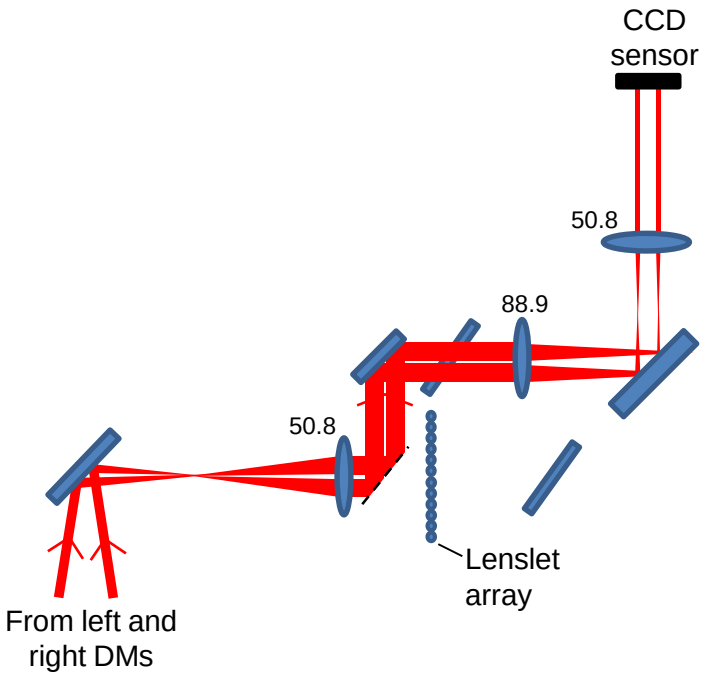

Figure 7-5: The beam paths for the pupil position sensing channels (symbols as in Figure 7-1). The beams are raised (upwards from the bench) by a PBS (dashed line) and a plane mirror, and pass above another plane mirror used for the wavefront sensing beams.

The pupil position sensing beams are raised slightly upwards from the bench by reflections at the PBS and a plane mirror in Figure 7-5. They enter the top-half of the lens marked 88.9; images of the beams exiting the ocular pupils are formed on the bottom half of the CCD sensor (see Figure 7-4). The separation between a pair of lenses is the sum of their focal lengths, and the CCD sensor is one focal length from the final lens.

A workstation analyses the intensity distributions in the lower quadrants of the CCD sensor. In each quadrant, pixel locations with intensity values above a threshold are collected, and the central pixel location is determined as the mean coordinates. (The procedures for intensity distribution analysis follow recording and subtraction of the background intensity distribution with no subject in place.)

The central horizontal position for each pupil determines the central coordinate of the Zernike polynomials used for wavefront analysis (see section 2.2.3), including where the search blocks (see also Figure 7-4) are positioned.

7.1.6 Infrared aberrometry III: Wavefront sensing and control channels

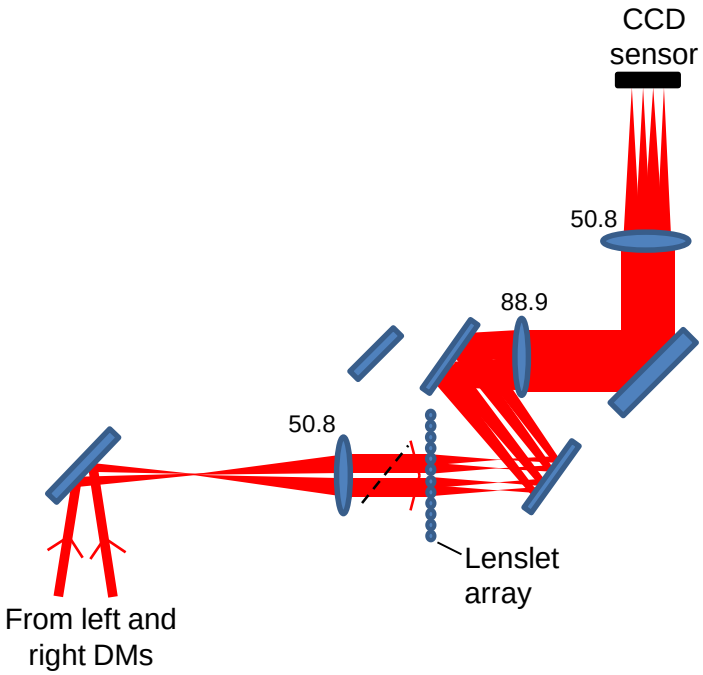

Figure 7-6: The beam paths for the wavefront sensing channels (symbols as in Figure 7-1). The beams are lowered (closer to the bench) by two plane mirrors, following the lenslet array.

The lenslet array (focal length 2.4 mm, pitch 200 µm, Advanced Microoptic Systems GmbH, Germany) is 50.8 mm (one focal length) from the lens preceding it (see Figure 7-6); an image of the wavefront at each DM is formed in the plane of the lenslets. Therefore, the wavefront exiting a pupil is eventually formed at the lenslet array. The lenslet array (focal length 2.4 mm) is separated from the next lens (focal length 88.9 mm) by the sum of their focal lengths, and so the wavefront can be analysed in the Shack-Hartmann sensor arrangement, using the workstation. (The remaining path lengths in the system were given in section 7.1.5.)

When the DMs are not flat, they modulate the aberrations at the wavefront sensor, as well as the aberrations of the stimulus. This effect must be taken into account when interpreting results, unlike in the eye channel of the monocular apparatus (section 3.1.3).

As well as providing aberrometry information on the eye, the analysis can be fed back as input to the following frame of an experimental trial, e.g. in correction of particular aberrations.

7.2 Optical and mechanical development

7.2.1 Introduction

The development of this instrument required solving many problems, repeatedly improving methods for aligning light beams, arranging mechanical components—including the very delicate PBSs (thickness 2 μm)—and testing and contributing to debugging of the control and measurement software. A handheld IR viewer and cameras connected to a monitor were used to observe the positions of the IR beams.

7.2.2 Laser power

The power of the fibre-coupled IR laser prepared for this apparatus was measured, and found to be lower than expected. The calibration table supplied with the laser indicated that 3.2 mW should have been emitted from the optical fibre using the chosen input setting (40 mA driving current[*]). However, only 0.2 mW was emitted from the fibre, as measured by the calibrated power meter (PM100D, with detector S130C, Thorlabs, Germany). It was necessary to provide approximately 0.1 mW to the eye, considering losses at optical surfaces and splitting of the beams, between the eye and the CCD sensor. The

[*] Indicated by a voltmeter reading of 400 mV across the readout terminals of the power supply.

unexpectedly low power of the laser was therefore a concern. Testing with a second laser revealed that the power supply was not at fault. The laser and fibre coupling were sent to the manufacturer for repair.

It was also necessary to characterise the loss of laser power on reflection at mirrors ready in the lab for use in the apparatus, since they had previously been mounted without labels or swapped in their mountings. They had coating either of type BD.1 or ER.2 (Newport, USA), causing losses of either 20% or 10% at 830 nm. It was desired to use as many ER.2 mirrors as possible, and as few BD.1 mirrors as possible. Each relevant mirror was placed in the path of the laser beam; the laser power before and after reflection at the mirror was measured; the mirrors were labelled for later use in the apparatus development.

7.2.3 Minification of the IR beam

It was desired, as in the monocular apparatus of chapter 3, to provide a small diameter IR beam with as little aberration as possible, for entry through the pupil of the eye, for focus on the retina.

The IR beam was first collimated following emission from the optical fibre. The core of the optical fibre coupled to the laser diode has diameter 5.5μm, and the collimating lens has focal length 1.65 mm. Therefore, the minimum tangent of the angle of divergence ($\tan \theta_{div}$) that could be achieved (see Figure 7-7, and neglecting diffraction) was therefore (5.5 / 2) / 1650, or 0.0017.

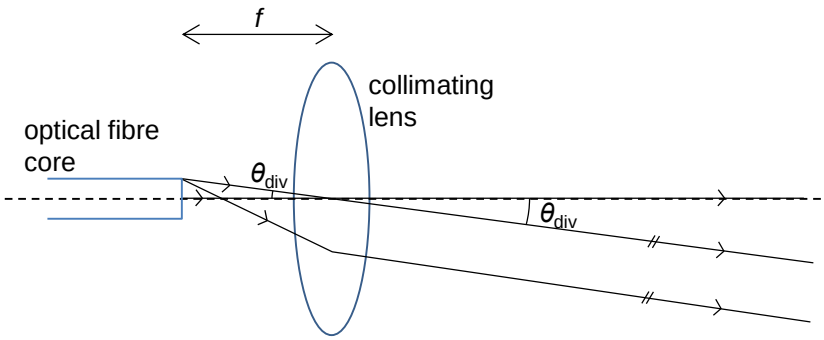

Figure 7-7: The angle of divergence (θ_{div}) of the collimated beam is limited by the range of angles of incidence at the collimating lens, i.e. by the size of the optical fibre core and the distance to the lens.

In fact, the beam diameter was measured as 5 mm, 1.45 m from the collimating lens, giving tan θ_{div} of (5 / 2) / 1450, or 0.0017. Therefore, the beam was optimally collimated by this lens.

The final beam size at the eye was 2 mm.

7.2.4 Rotating diffuser

The rotating diffuser was not introduced to the system until after much of the alignment described in section 7.2.7, so that the IR beams were more intense and easier to observe throughout the optical system. The rotating diffuser was positioned at the focal point of the lens preceding it in the beam, so that it did not introduce a spread of secondary IR sources across the beam. Such diffusion, away from the focal point, would have resulted in a greater angular range in the IR beam incident on the eyes, therefore in a larger IR source created at the retina, and finally in blurring of the Shack-Hartmann intensity pattern at the sensor. The final motor and diffuser arrangement are visible in Figure 7-2.

A screen was also added to the instrument, to shield the participant from a breeze generated by the rotating diffuser. The breeze increased the rate of tear film evaporation, causing participants to sense dryness of their eyes and

decrease the time between blinks. The screen is also observable in Figure 7-2, partly occluding the bite bar.

7.2.5 Model eyes

Model eyes (Figure 7-8) were constructed from lenses of diameter 0.5” and effective focal length 19.0 mm (PAC019.AR14, Newport, USA), and a white paper retina; the position of the retina, and so the axial length, was adjustable using a small translation stage. The model eyes were adjusted and measured to have plano refractive error (sphere and cylinder) using an autorefractor (NVISION-K 5001, Shin-Nippon, Japan). They were used for aligning and calibrating the apparatus.

A rail was mounted, projecting from the optical bench, which could hold the two model eyes in the place of a participant's eyes.

Further flexibility to the model eyes was added with a translation stage allowing vertical movement of the whole eye.

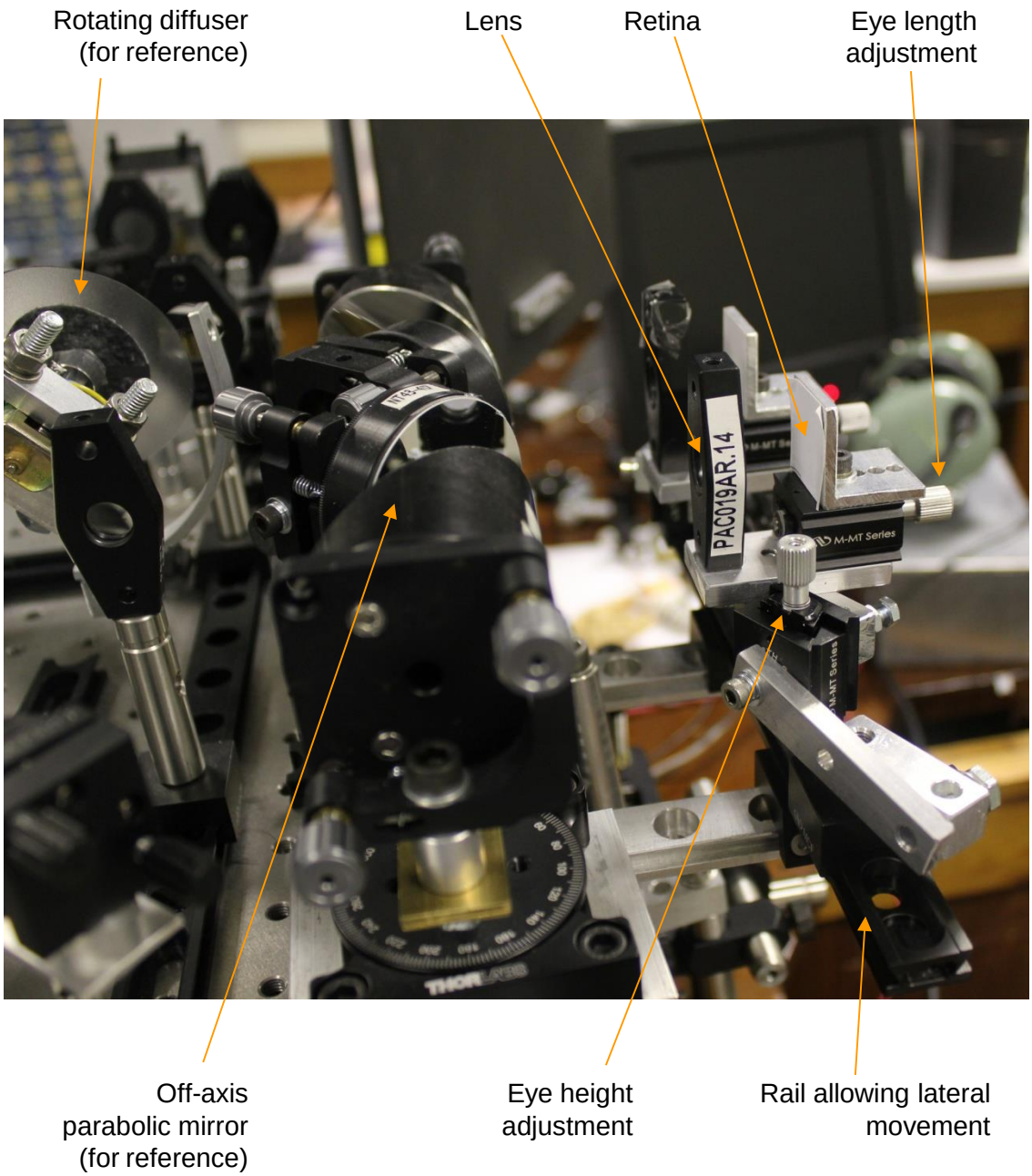

Figure 7-8: The model eyes mounted on the apparatus.

7.2.6 Design of the visible stimulus arrangement

The means of providing a visible stimulus to the participant was designed. It is illustrated in Figure 7-9. It was necessary to provide the stimulus to both eyes, via the DMs, scanning mirrors and OAPMs, with means of making the visible beams collinear with the IR beams; also see section 7.2.7.4 on rotations of the stimulus images. The relevant components were added to the system.

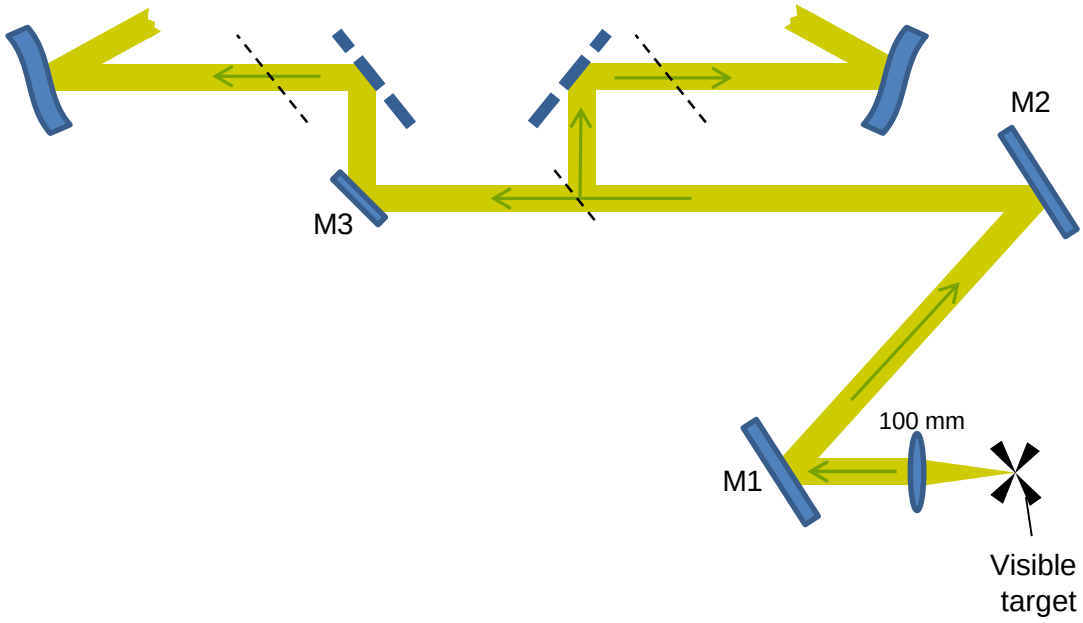

Figure 7-9: The means of providing a well-aligned visible stimulus in the binocular AO apparatus. Symbols are as in Figure 7-1. Plane mirrors are labelled for reference in section 7.2.7.4.

7.2.7 Alignment

7.2.7.1 Requirements, and diagnosis and solution of some problems

Full alignment of the apparatus included:

- Setting the correct distances between all optical elements for which distances were important (most of the elements).
- Achieving centrality of the beams on the DMs, OAPMs and scanning mirrors.
- Achieving clearance for the beams at all optical elements, including when moved by rotation of the scanning mirror and eyes.
- Making the IR and visible beams collinear, such that the calibrated aberration modulation (with the DMs) and rotation (with the scanning mirrors) of the IR beams would also predictably control the visible stimulus.

- Achieving the four images—two pupil images and two Shack-Hartmann intensity patterns—in the four quadrants of the sensing CCD chip at the end of the beam paths.

The alignment was required to result in the ability to calibrate the action of the DM actuators, via the Shack-Hartmann patterns at the sensor, such that aberrations could be reliably corrected and controlled. It was also required to result in the ability to detect the position of moving pupils at the sensor.

When an aspect of the system was modified, it was frequently required to realign a portion or all of the apparatus. It was also found that the system drifted out of alignment to some extent over time, so it was also necessary to realign the system, in part or in whole, for that reason. Vibrations from the rotating diffuser may be responsible for the gradual movement of some components.

A common cause for realignment, or improvement of alignment, was vignetting of the images at the sensor, as displayed on the monitor (e.g. as in Figure 3-5 with the monocular AO instrument). The optical element where the misalignment was occurring had to be identified and the system corrected.

The problematic part of the system was frequently the lens (focal length 200 mm) combining the two IR beams back into one path and/or the two mirrors just before this lens (see Figure 7-1 and Figure 7-10A). The two mirrors were each one coated surface of a right-angled prism. This allowed them to be positioned close to each other, so that they could bring the left eye and right eye IR beams close together, to both pass through the combining lens. Because of the frequent problems around this combining lens and the adjacent two mirrors, a new mount was designed and built for the mirrors. It is shown in Figure 7-10

and compared with the previous mount. Vignetting at the DMs and other elements was also common, during and following modifications and alignment.

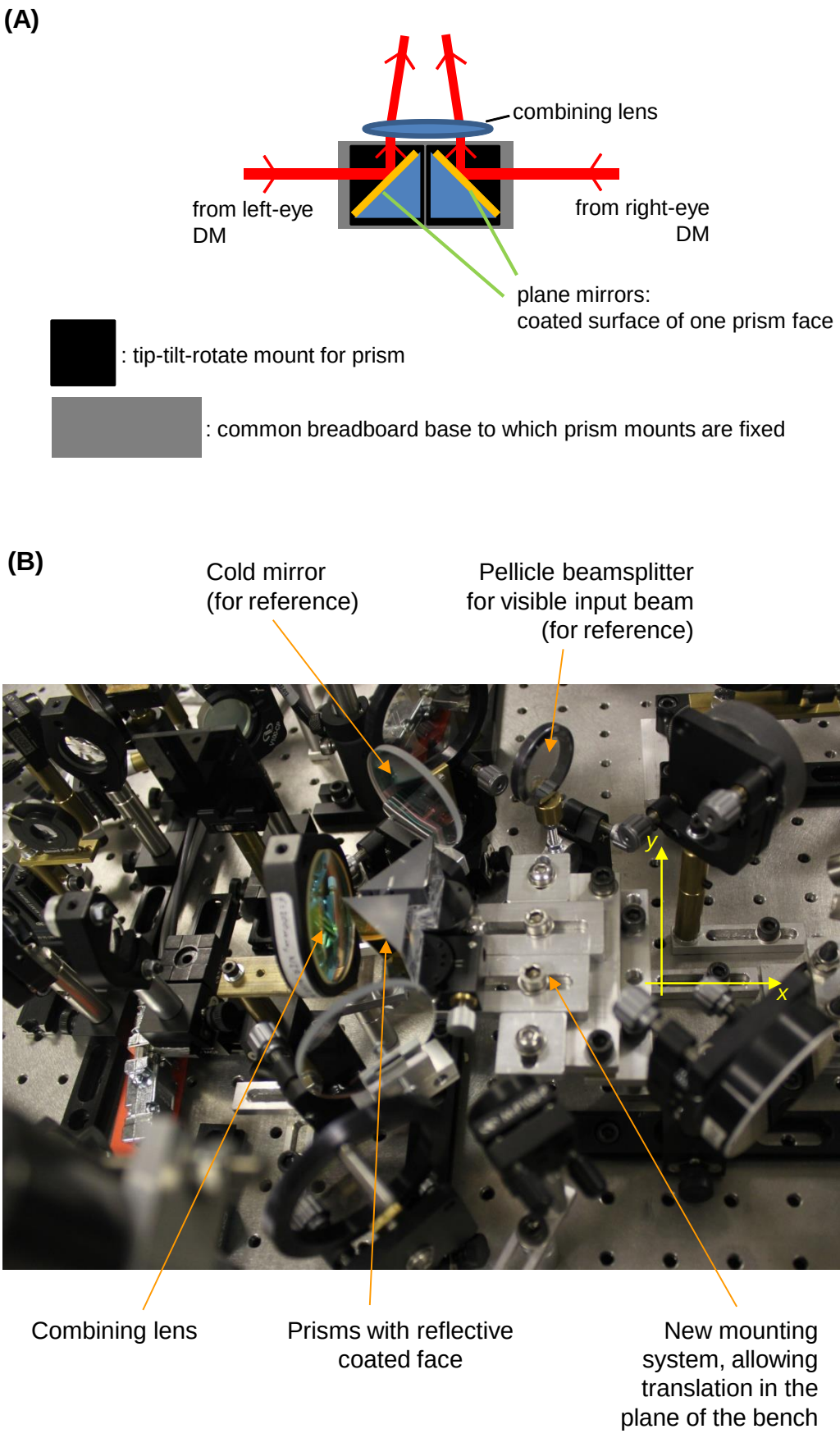

Figure 7-10: (A) The original mounting for the plane mirrors before the combining lens. (B) The mounting developed to allow greater tolerance on the alignment of the apparatus. The prisms can now be translated together in *y* and independently in *x*.

Distortion of the Shack-Hartmann intensity patterns, from encounters of the beam with the edge of an element, or possibly at an angle to its axis, also required diagnosis and solution of the problem. For example, the spots of the Shack-Hartmann pattern could appear dimmer in one corner of the image, or more blurred, possibly in a particular direction (e.g. astigmatism/coma).

When rotation of the beams was tested, with the scanning mirrors, a lack of clearance at some elements was also revealed. This resulted in many realignments of the apparatus, and such issues gave rise to the replacement of several components of diameter 1” with 1.5” (cold mirrors) or 2” (PBSs and combining lens) equivalents.

When components were damaged—for instance, the PBSs of thickness 2 μm—their replacement also necessitated realignment of at least part of the system.

7.2.7.2 Tools

For rough alignment of the system, a visible laser was used (625 nm, 0.9 mW laser diode module, part R83-836 from Edmund Optics, USA). It was possible to make the visible laser collinear, or approximately collinear, with the visible and/or IR beams of the apparatus, and therefore deduce the positions of the invisible IR beams and weak visible beams on the optical elements.

The visible laser was used in this way in three positions (which can be located in Figure 7-1): The beam was folded into the path of the IR laser from just after its initial collimation; the beam was split and aligned to match the path of light reflected from the eyes; the laser was placed in the position of the visible stimulus.

The visible laser beam was made collinear with the relevant apparatus beams by matching it with those beams' positions at two points, as accurately as

possible. Still, it did not result in fully successful alignments, as defined above; many alignment procedures relied upon IR viewers and cameras connected to a monitor.

Although the model eyes of section 7.2.5 were available, they were not highly reflective, and a brighter beam was useful for basic alignment of the beams, before considering the Shack-Hartmann intensity pattern. Plane mirrors were therefore used as model eyes to begin with. The reflected beam was made collinear with the incident beam, by making the two beams coincident at one point along the beam path (it being also coincident at the point of reflection). The path of reflected radiation could then be followed and aligned beyond the DM, through the combining lens and the four channel section leading to the sensor.

When the system appeared well aligned with use of the plane mirrors, the model eyes of section 7.2.5 were mounted onto the system. The system was aligned to result in clear pupil images and Shack-Hartmann intensity patterns in the beams reflected from the paper retinas and collimated by the lenses of the model eyes.

It was also necessary to align and calibrate the system for light reflected from rotated, converging eyes. A stepper motor (part 160-010-00500 with 4.2 A driver 160-020-00101, from Arc Euro Trade Ltd., UK) was used to rotate a model eye and check for vignetting of the images at the sensor (as observed on a monitor), and for calibrating the rotation of the scanning mirrors and aberrations of the system for particular angles of ocular convergence (see section 7.3.5). Figure 7-11 shows a model eye mounted on a rotating column controlled by the

stepper motor. Step sizes of 0.450° and 0.900° were used for testing and calibration (the closest steps available to 0.5° and 1°).

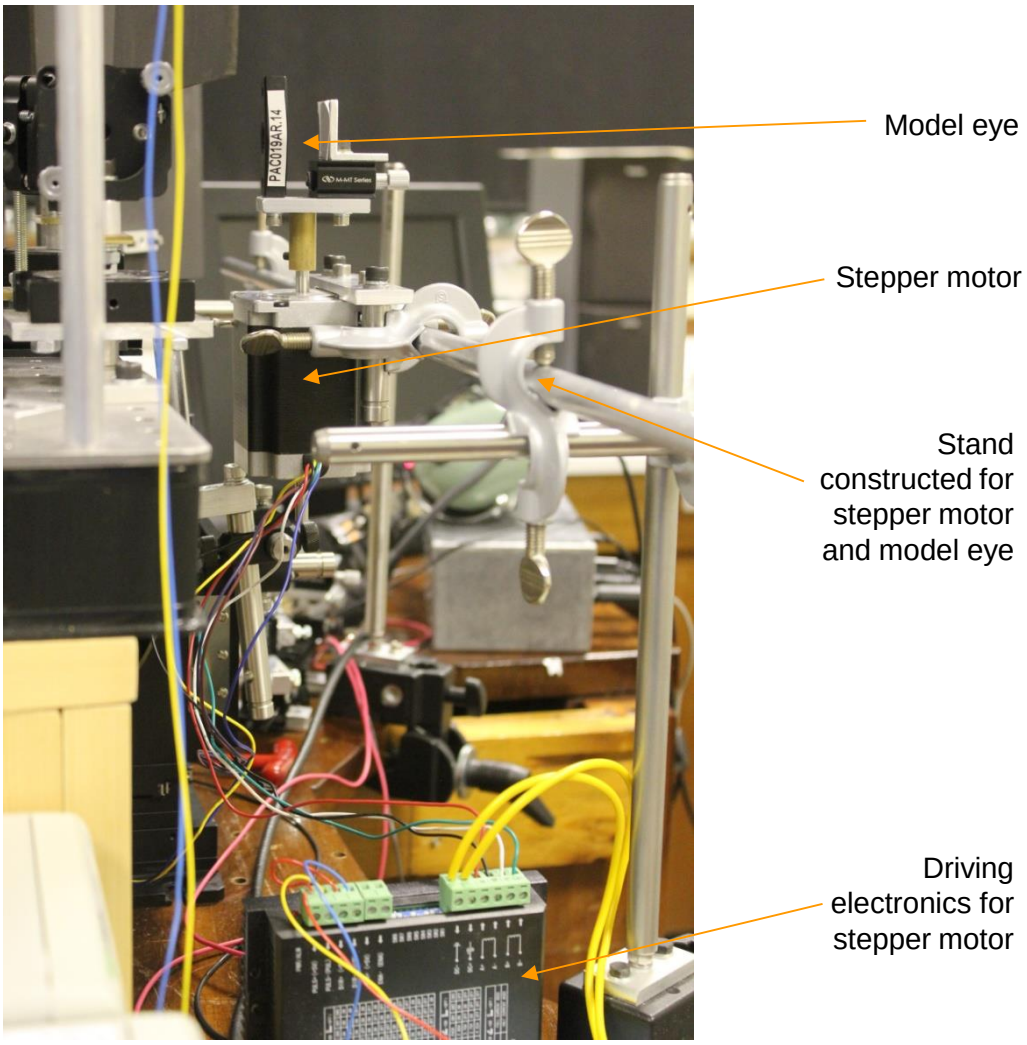

Figure 7-11: The model eye, mounted on the stepper motor, for testing and calibrating the apparatus with respect to eye rotation.

7.2.7.3 Four-channel section

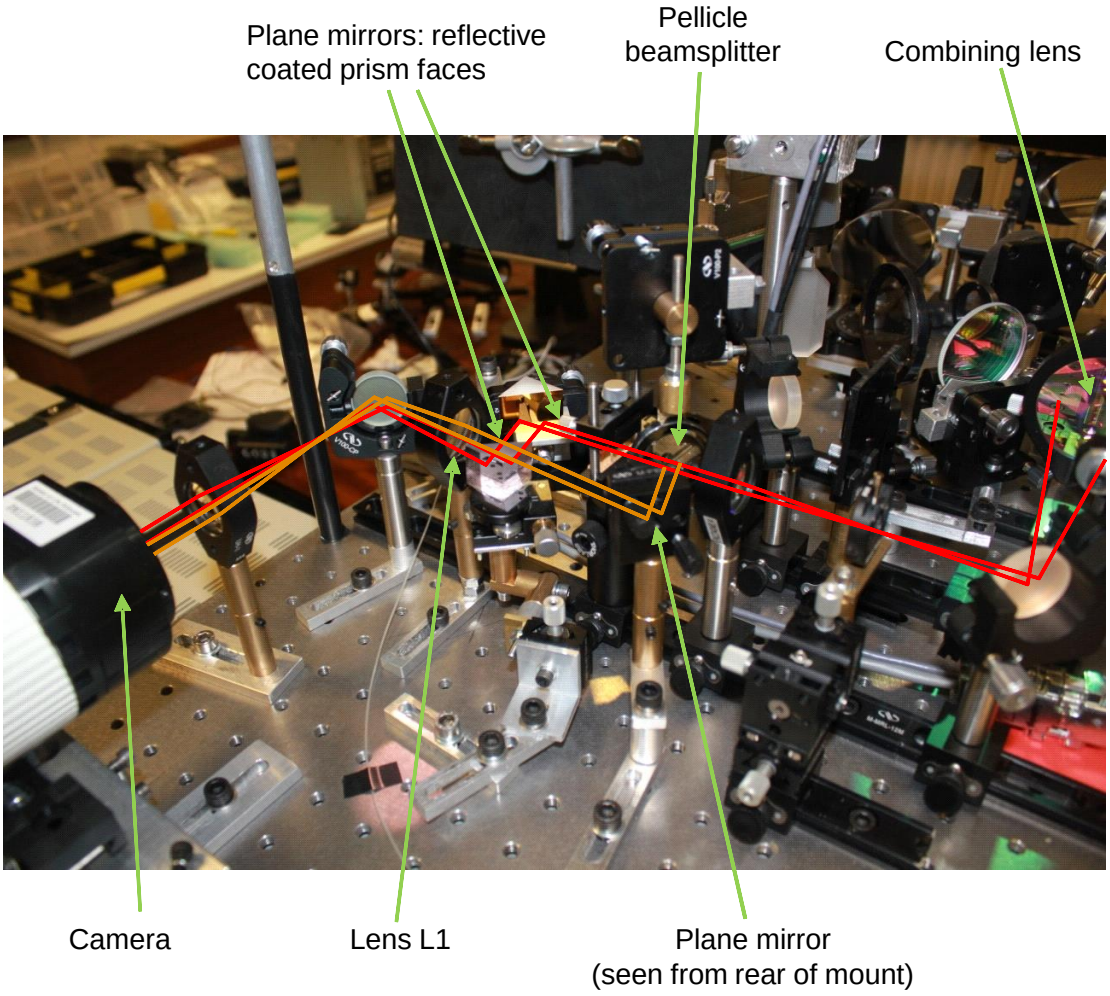

Figure 7-12: The four-channel section of the apparatus. The beams arriving from the combining lens are split at the pellicle beamsplitter into pupil position (orange) and wavefront (red) sensing channels.

As discussed in sections 7.1.5 and 7.1.6, the left eye and right eye beams are both split into pupil position and wavefront sensing beams. This section is shown again in Figure 7-12. To minimise system aberrations, and provide an image in each quadrant of the sensor, with room for pupil movement, it is necessary to send all four beams through lens L1, parallel to its axis, and separated by the correct distances. Their lateral separation is determined by the position of the beams on the mirrors before the combining lens (see Figure 7-10). The direction and vertical separation are controlled by the angles of the pellicle beamsplitter and plane mirrors.

The vertical separation was found and adjusted for using graph paper and an IR camera and monitor. A vertical separation of 2.5 mm was chosen at the camera chip, which implied a vertical separation of 5 mm at L1.

It was ensured that all of the beams were parallel to the axis, before meeting L1, by removing the plane mirror after L1 and making the beams all coincident with a target at its focal point.

Finally, the plane mirror after L1 or the camera could be moved as appropriate for symmetry of the four image positions in the quadrants of the sensor, as observed on a monitor (e.g. in Figure 7-4).

7.2.7.4 Rotational disparity and final alignment of visible stimuli

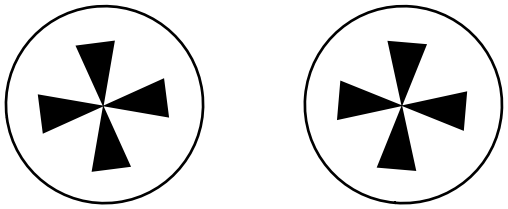

Figure 7-13: Relative rotation of the stimuli for each eye, before improvements in visible beam alignment.

When the stereoscopic visible stimulus was inspected for the first time, it was observed that the two images were rotated relative to each other, as illustrated in Figure 7-13. The images were brought to the same angle by ensuring that the visible beams were not being twisted as they were folded into the same path as the IR beams. The beam folding arrangement is shown in Figure 7-1 and Figure 7-9. (The peripheries of the images in Figure 7-3 also display a curvature in opposite directions, but before this correction of the system the whole images were rotated.)

The feature causing the rotation of the image was a vertical component to the beam direction from M2 to M3, through the pellicle beamsplitter (Figure 7-9). To fold the non-horizontal beam into the horizontal plane of the apparatus, the

normals to the reflectors were required not to be in the horizontal plane. However, unless the normal to a reflector has either zero azimuthal angle or zero angle of elevation, with respect to the normal to the object plane, the image will be rotated about a horizontal axis. (This can be demonstrated by drawing two object points, a reflector and two image points on a piece of paper, with the line between the object points not parallel to the reflector. When the paper is folded slightly along the line of the reflector, introducing an elevation to its normal, the heights of the two image points become different. There is also a vertical component to the axis of rotation, but this would have little effect on the stimulus, when its effects are compared with the distance to the eye.) The perpendicular orientations of the cold mirrors for the left eye and right eye beams produced images with opposite angles of rotation.

The rotation disparity was therefore corrected by making the beam from M2 to M3 purely horizontal, at the same height as beams from the DMs to the OAPMs. Since it was very difficult to see the dim beam of the visible stimulus, the visible laser was matched with its path (see section 7.2.7.2) and used to align M1 and M2 appropriately.

Finally, vertical disparity of the two visible stimulus images could be removed by slightly adjusting M3 (and the pellicle beamsplitter, if necessary). This was sometimes done in combination with adjustment of the plane mirrors closest to the eyes to counter small drifts between sessions in IR beam alignment.

7.2.8 Data collection protocol

A data collection protocol was developed for consistent optical performance of the system. Firstly, bite bars were used for each participant, to maintain pupil positions during data collection. Then, it was desired to use the same regions of

the DMs between participants, despite participants having slightly different vertical positions for their pupils. To achieve this consistency, the head of each participant was rotated, using the mounting for the bite bar which held them in position, to set their pupil heights such that IR beams reflected from their eyes fell upon the previously calibrated areas of the DMs. The plane mirrors closest to the eyes were also moved towards or away from the eyes to set the reflected beams to the correct separation, reflecting from the retinas and falling upon the previously calibrated areas of the DMs. The on-screen search blocks for the Shack-Hartmann spots showed the experimenter the required positions for the beams, illustrated in Figure 7-14.

Calibration of the action of the DMs (see section 7.3.2) was found not to be always reliable from day to day. Data collection was therefore arranged later in the day, allowing time for checking the calibration and recalibrating in the morning.

Participants were instructed to keep the target clear and asked whether it was possible to fuse the images of the stimulus, and whether the stimulus was clear and remained clear. Their answers provided guidance as to whether further alignment or recalibration was necessary.

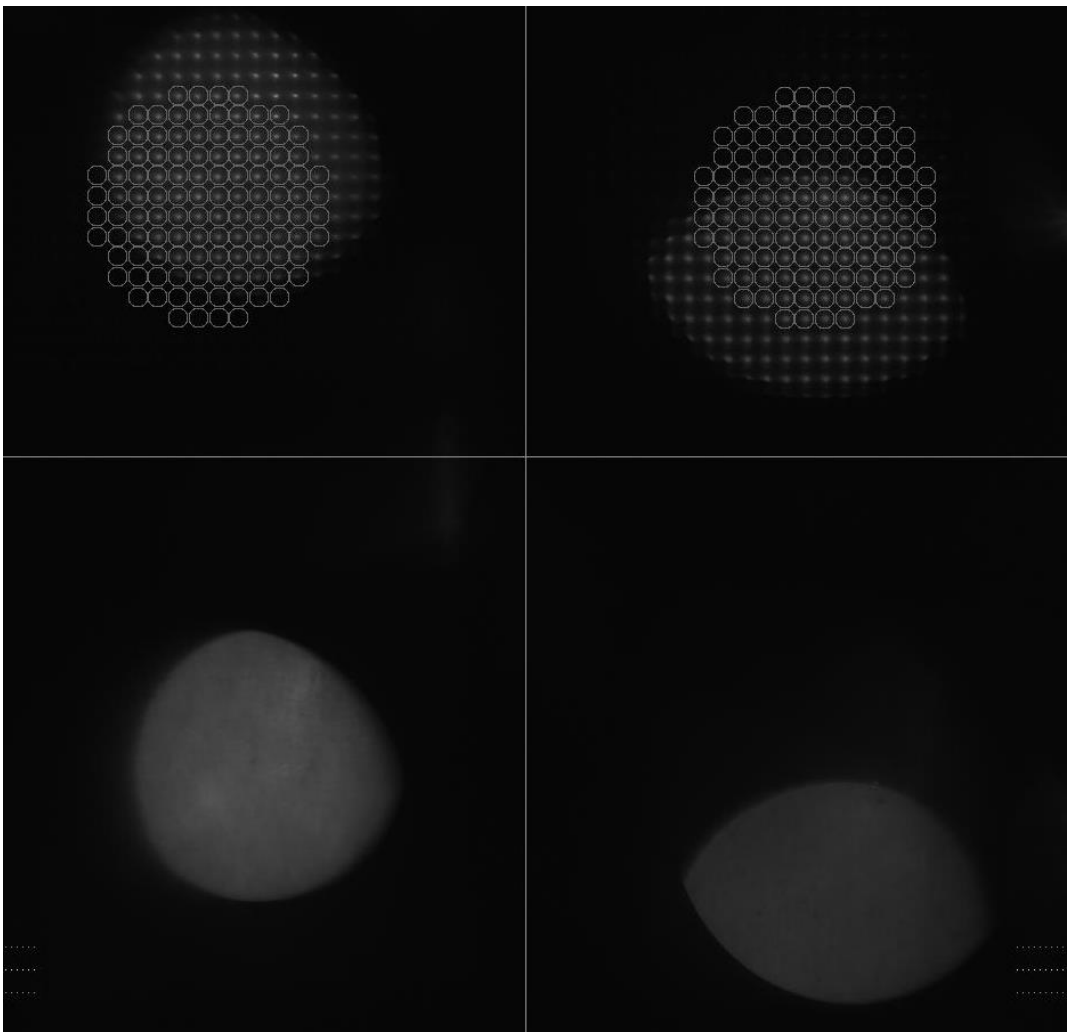

Figure 7-14: Misalignment of the participant, requiring rotation of the bite bar to level the images vertically, and movement of the closest plane mirrors to the participant, to decrease the separation of the beams entering the eyes. The participant was aligned following the capture of this image, to provide the aligned pupils of Figure 7-4.

7.3 Testing and calibration

7.3.1 Effect of trial lenses

As with the monocular instrument of chapter 3, the effects of spherical and cylindrical trial lenses, placed in front of the model eyes, were recorded.

The effect of spherical trial lenses on defocus in either eye is shown in Figure 7-15. They show a linear response of the system, with gain near unity.

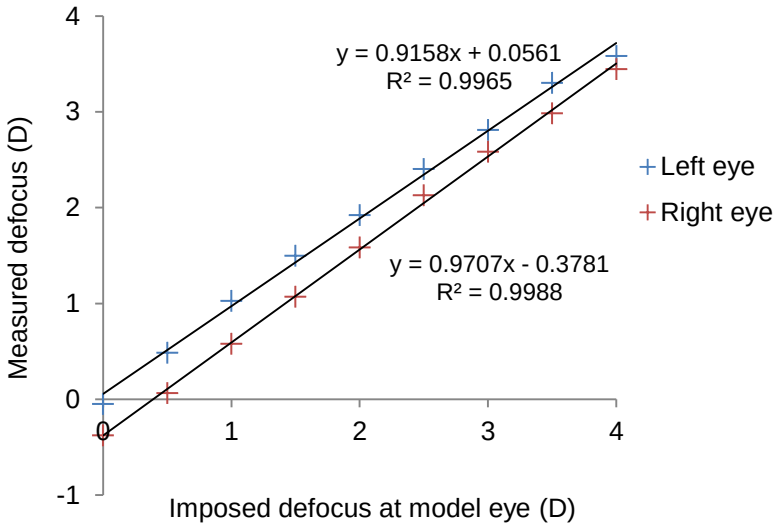

Figure 7-15: Measurements of defocus, using the wavefront sensing channels, of levels of defocus applied to the beams reflected from the model eyes.

Table 7-1 relates a largely accurate response of the system to cylindrical lenses of power −2 D, as in section 3.3.1 for the monocular system. However, some variability was found (up to 0.7 D discrepancy in astigmatism in some other measurements), and appeared to vary with fine adjustment of the position of the model eye. These effects most likely indicate a criticality of alignment of the beams with the centres of the off-axis parabolic mirrors, which are expected to cause astigmatism when the beams are not perfectly centred on them. The fine alignment of the model eyes with respect to the beams was not fixed as it is in the monocular system; the necessity for adjustment of lateral position of the pupils took priority up to this stage in the development.

At present, the precision of cylindrical measurement and correction with the system may be limited; even after thorough alignment using the bite bar, it is found that a participant's head may still move slightly, before and during the few seconds of a data collection trial.

Table 7-1: Response of the apparatus to imposition of cylindrical defocus on the beam reflected from the model eyes. It shows close agreement with the predicted spherocylindrical aberrations, to about 0.1 D, apart from the left eye result at plano/−2.00x45.

		Spherocylindrical error	
	Introduced by trial lens	Predicted	Measured
Left eye	Plano (No trial lens)	-	−0.10/−0.32x31
	Plano/−2.00x45	−0.09/−2.30x44	−0.03/−2.65x41
	Plano/−2.00x135	−0.40/−1.70x137	−0.48/−1.57x141
Right eye	Plano (No trial lens)	-	0.41/−0.78x35
	Plano/−2.00x45	0.40/−2.46x43	0.43/−2.57x44
	Plano/−2.00x135	−0.05/−1.56x138	−0.03/−1.61x138

7.3.2 Calibration, and correction of inherent aberrations

To calibrate the wavefront control of the stimulus for each eye, each actuator of the relevant DM is moved forwards and backwards from its central, “biased” setting. The effect of the DM on the wavefront returning from the model eye is recorded as the change in coefficients of the first 44 Zernike polynomials (up to and including 8^{th} order).

Following calibration, for either eye, the system performs singular value decomposition (Tyson, 1997, pp. 252–255) on the effects of the actuators, which provides a set of orthogonal “mirror modes” (combinations of actuator voltages) for controlling the wavefront. The various actuators can then be used to control aberrations of the stimulus. In particular, they can be used to provide a step in defocus, or to correct the ocular aberrations, which are calculated for every frame (approximately every 100 ms). A gain value is chosen, which is the fraction of the aberration measured in frame i which will be corrected in frame $(i + 1)$.

To cancel out inherent aberrations of the system, correction of the beam reflected from the model eye was initiated, using a chosen number of mirror modes and a gain value (typically 0.3). Correction was allowed to continue until the actuator voltages (displayed on the monitor) became stable. When correction was then halted, a note was made of the spherocylindrical error remaining in the system, and the actuator positions were stored as the “flat” reference position for the DMs. Before correction, the spherocylindrical error of the system was about −0.1 DS/−1.5 DC (1 d.p.) for each model eye. The magnitude of the residual spherocylindrical error after correction was less than 0.1 D in each eye, in all of defocus, astigmatism and spherical equivalent of their combination*.

Control of a greater number of mirror modes is useful for more precisely affecting the wavefront, but the potential for undesired coupling between modes, due to constraints on the mirror surface and pupil area, is then increased (see section 7.4.1). When the system was less well set up, the number of usable mirror modes was reduced. For example, failure to record a background exposure before calibration would increase noise and reduce the number of modes it was possible to correct. Attempting to use an unfeasible number of modes resulted in diverging actuator voltages (see section 7.4.1). Typically, it was possible to correct the beams using 21 mirror modes.

7.3.3 Model eye measurements during stimulus control

It was possible to observe the effect of a DM on the visible stimulus to an eye by its effect on the wavefront returning from a model eye. For instance, the DM could be instructed to change the vergence of the stimulus at the eye by −2 D;

* Spherical equivalent = Defocus + (Astigmatism / 2)

the wavefront returning from the model eye would still be collimated[*], so the same −2 D should be observable as a change at the lenslet array, using the Shack-Hartman arrangement (and a magnification factor in the software).

Results of testing stimulus control were variable, and often revealed a necessity to adjust and recalibrate the apparatus. When steps in defocus only were instructed, astigmatism was also introduced, as revealed in Table 7-2. Undesirable coupling between defocus and other Zernike modes was also observed, as shown in Figure 7-16. Jumps in many of the Zernike modes are visible at the point where the DM was instructed to modify only defocus[†]. Furthermore, vertical coma and higher aberrations were introduced as the left-eye channel attempted to correct the wavefront, before the step. However, the correction of the strong astigmatism inherent to the system was performed well, in the first few frames, in both eyes.

Table 7-2: Responses achieved to steps of −2 D and −4 D in defocus, as input instructions to the DMs. The responses are as measured in the wavefront sensing channels, and show directly the effect of the DMs on the beams reflected by the model eyes. The "Other responses" are the results achieved when calibrating for the data collection of chapter 8.

Step in defocus (instruction to DM)	Best response achieved		Other responses	
	Left eye	Right eye	Left eye	Right eye
−2 D	−1.90/0.05x52	−1.91/0.05x99	−1.98/−0.55x72 −2.14/−0.36x84	−1.75/−0.15x99 −2.07/−0.08[‡]
−4 D	−3.87/−0.04x95	−3.63/−0.18x95	Not typically used	Not typically used

[*] Although the retinal IR "source" would be very slightly larger.
[†] Multiplying by the normalisation factor (see section 2.2.3), the defocus measured in the right eye channel changed in this case by 1.6 D, and that in the left eye channel by 2.0 D.
[‡] Axis not recorded.

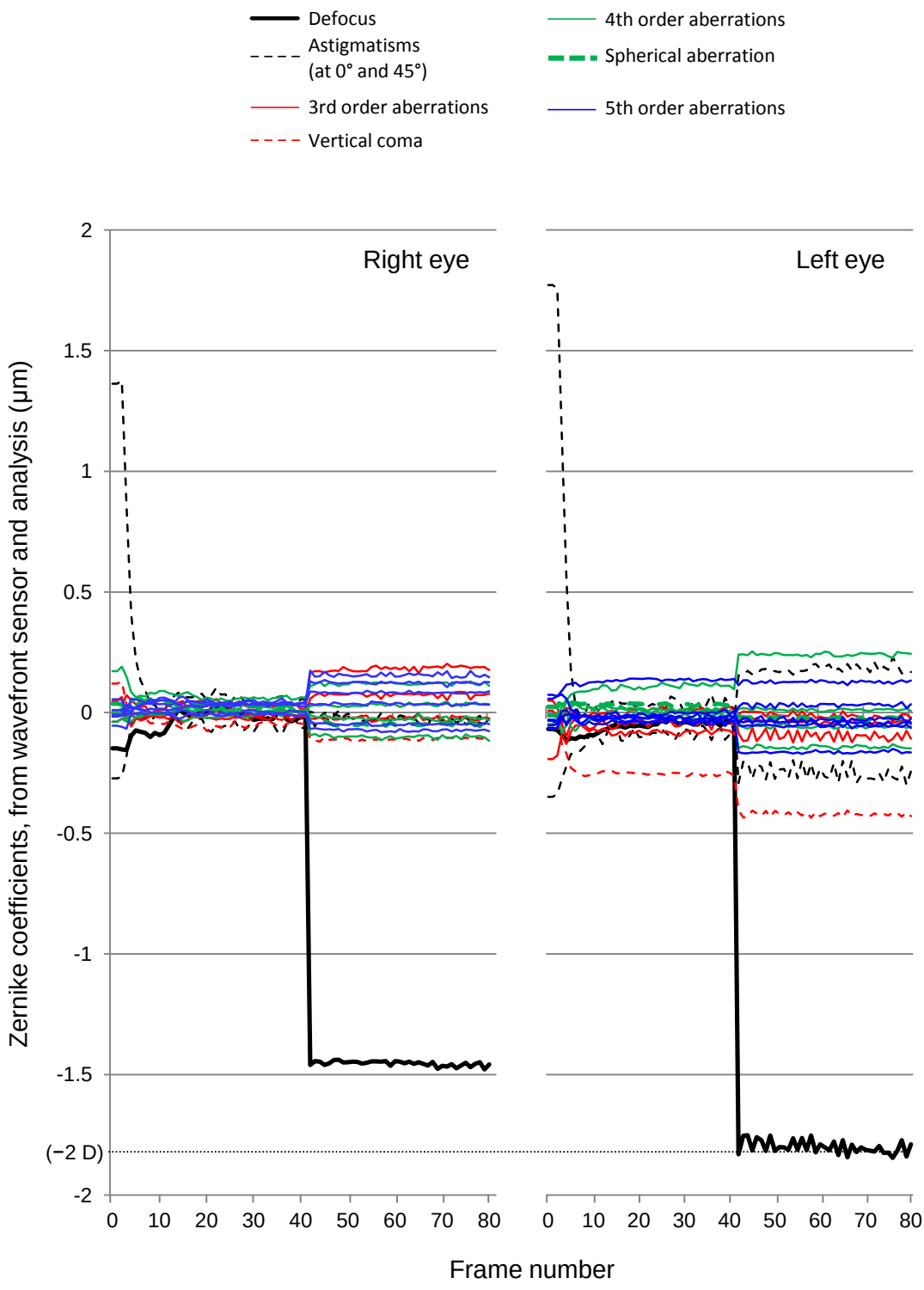

Figure 7-16: Zernike aberrations recorded when correcting the beam reflected from the model eyes for forty frames (approximately 4 s), followed by input to the DM for a −2 D step in defocus in the stimulus. Zernike aberrations of different order are marked in different colours; some aberrations within these orders are marked with dashed lines. Vertical coma is identified as showing the worst coupling, during wavefront correction and following the instruction to step only defocus (see left eye). Spherical aberration is identified as of interest in accommodation studies, and demonstrates little coupling. The dotted black line shows the −1.83 µm Zernike defocus coefficient expected (for this 5.04 mm pupil detection aperture) following the −2 D step.

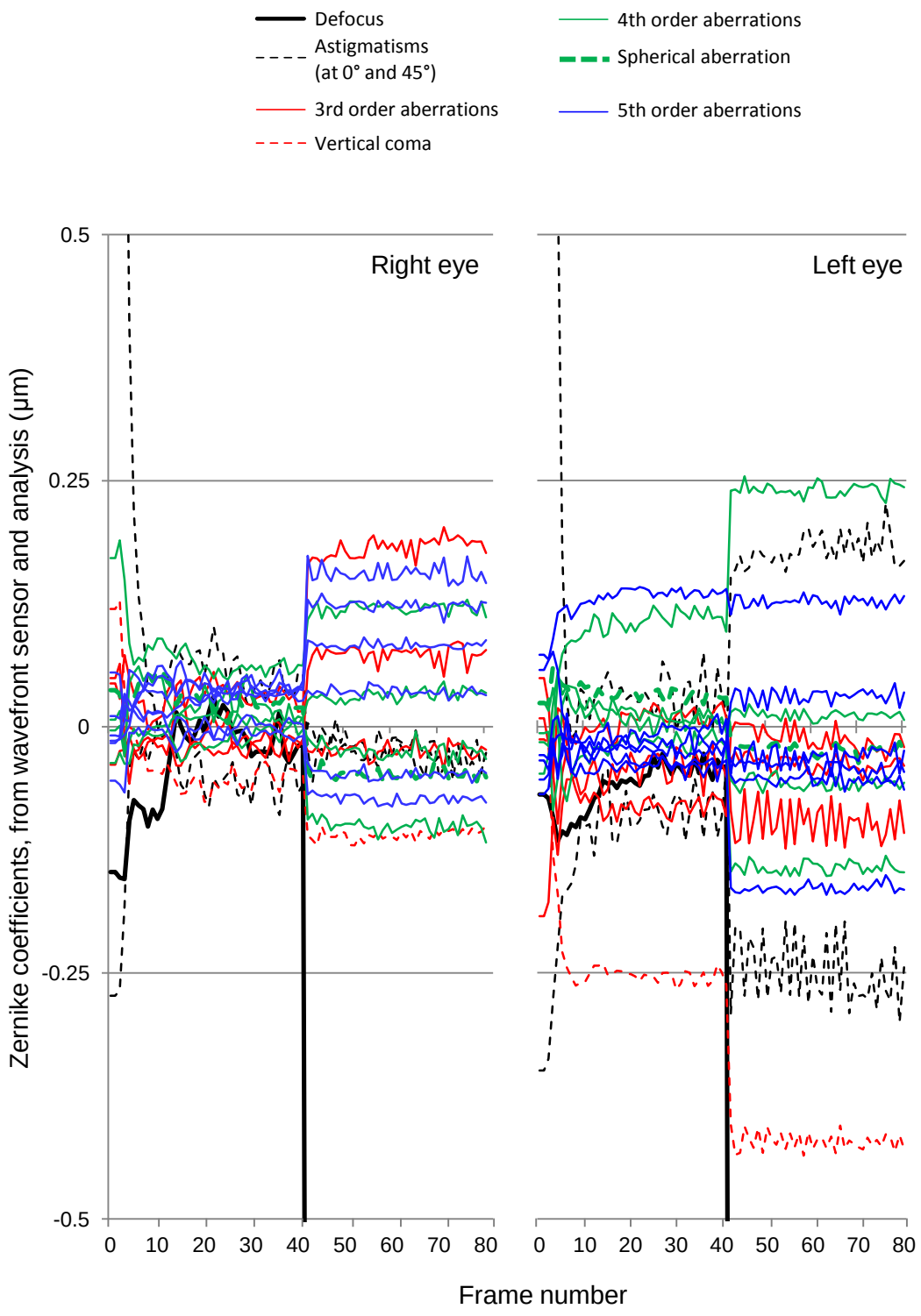

Figure 7-17: The Zernike coefficients of Figure 7-16, with a magnified scale, for clarity.

The coupling between Zernike modes during DM control indicates room for improvement in the apparatus and its calibration. Particular issues and suggestions are discussed in section 7.4.

Despite the coupling, it was possible to provide steps of −2 D to both eyes, such that participants could fuse them, with clear binocular vision (see section 7.3.6).

7.3.4 Pupil position sensing

Testing of the pupil position sensing capability of the apparatus in particular resulted in much development of the control software. Several improvements were made, of which some are described below.

First, testing of correct calculation and processing of pupil-centre positions was carried out using file input of a model intensity distribution.

Second, the use of pupil tracking during data collection was found to increase the frame time to several seconds. This required modification of the control software such that the calculations introducing the delay were performed before attempting to collect data[*].

When the tracking speed was improved, wavefront sensing data showed large jumps in aberrations, corresponding to jumps of the search blocks (see section 2.2.2 and Figure 7-4) as they followed the pupil centre. These jumps are shown in Figure 7-18. The software was again improved by Dr. Hampson, to result in smooth tracking data, as in Figure 7-19 (note the change in defocus scale).

[*] They generated lookup tables of the derivatives of Zernike coefficients (see section 2.2) at the search block positions, based on ten different reference coordinates for the pupil centre, across the width of a search block. Detection of the centre position of the pupil image determined the relevant lookup table for the calculations of the Zernike coefficients.

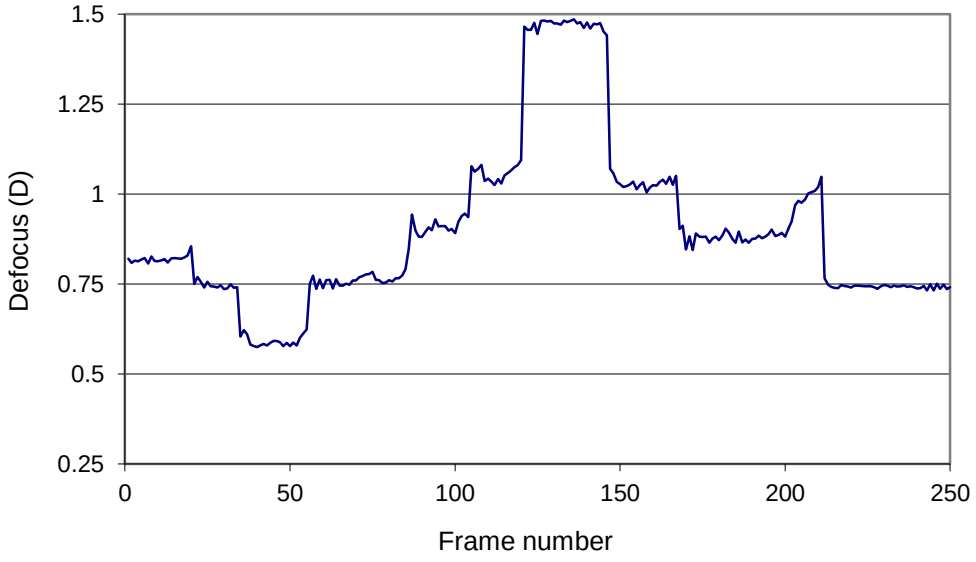

Figure 7-18: Measurements of defocus as a model eye (plus a +1 D trial lens) was slid across a rail, perpendicularly to the IR beam (see Figure 7-8).

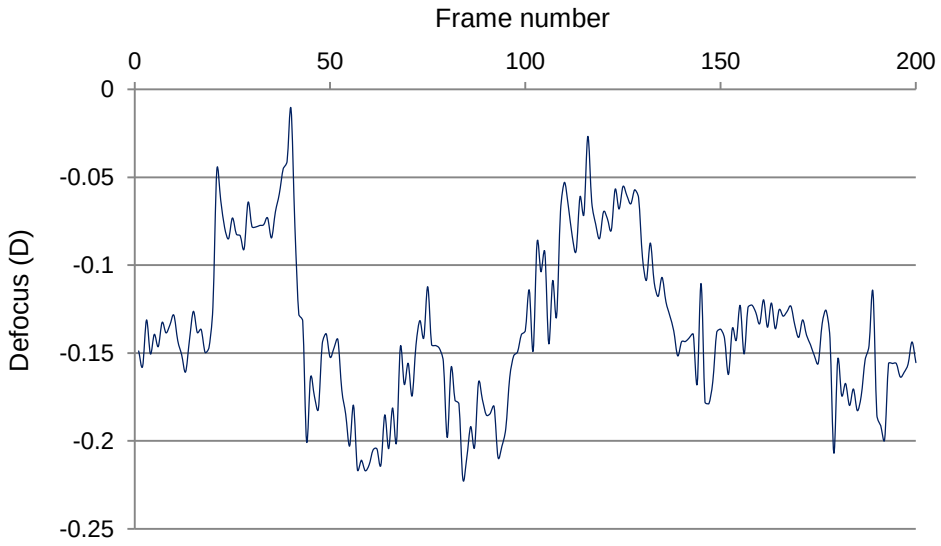

Figure 7-19: Measurements of defocus as a model eye was slid across a rail, similarly to the procedure for Figure 7-18, following development of the aberrometry and pupil tracking code. Note that the defocus scale here is expanded by a factor of five, relative to Figure 7-18.

7.3.5 Scanning mirror control and beam angle

The linearity of beam rotation with scanning mirror voltage was checked, in case a more complicated calibration function was required for angular control. The data are shown in Figure 7-20 and did show good linearity.

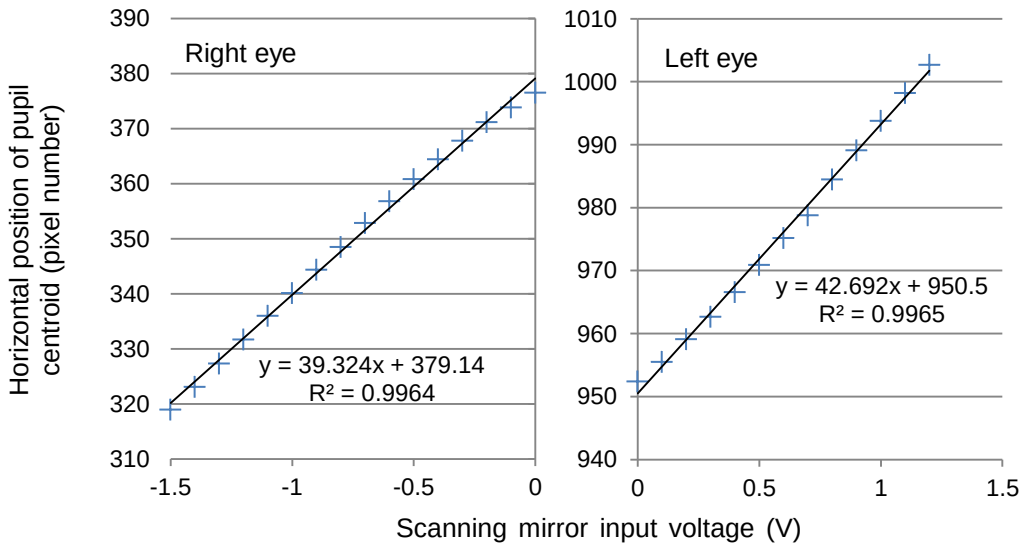

Figure 7-20: Linearity of pupil image position (i.e. beam rotation through small angles) at the sensor with input voltage to the scanning mirror, using the model eyes. Beam rotation at the eye is approximately 4 × input voltage, including the magnification through the off-axis parabolic mirrors. Negative and positive voltages were required to stimulate convergence of the right and left eyes, respectively. The angular range of data collection was limited by vignetting of the pupil image at the sensor.

It was also necessary to measure the intrinsic aberrations of the system with beam rotation, so that the ocular aberrometry could take such changes into account as the eyes converged. For these measurements, the model eye was mounted on a stepper motor (section 7.2.7.2). Following correction of the system aberrations, the eye was rotated inwards in steps of 0.45°; each time, the pupil image was returned to its original position at the sensor by rotating the scanning mirror, and a record of the aberrations was taken. These data were taken from 0° to beyond 6.8° of convergence (equating to a stimulus ¼ m from the eye, with PD 60 mm), for both eyes, and stored in the software. They are shown, up to fourth order modes, in Figure 7-21. Most aberration components remain small, but defocus and horizontal astigmatism increase in amplitude as the beam moves across the parabolic mirrors. Vertical coma (one of the third order aberrations) also increased noticeably with angle in the right eye.

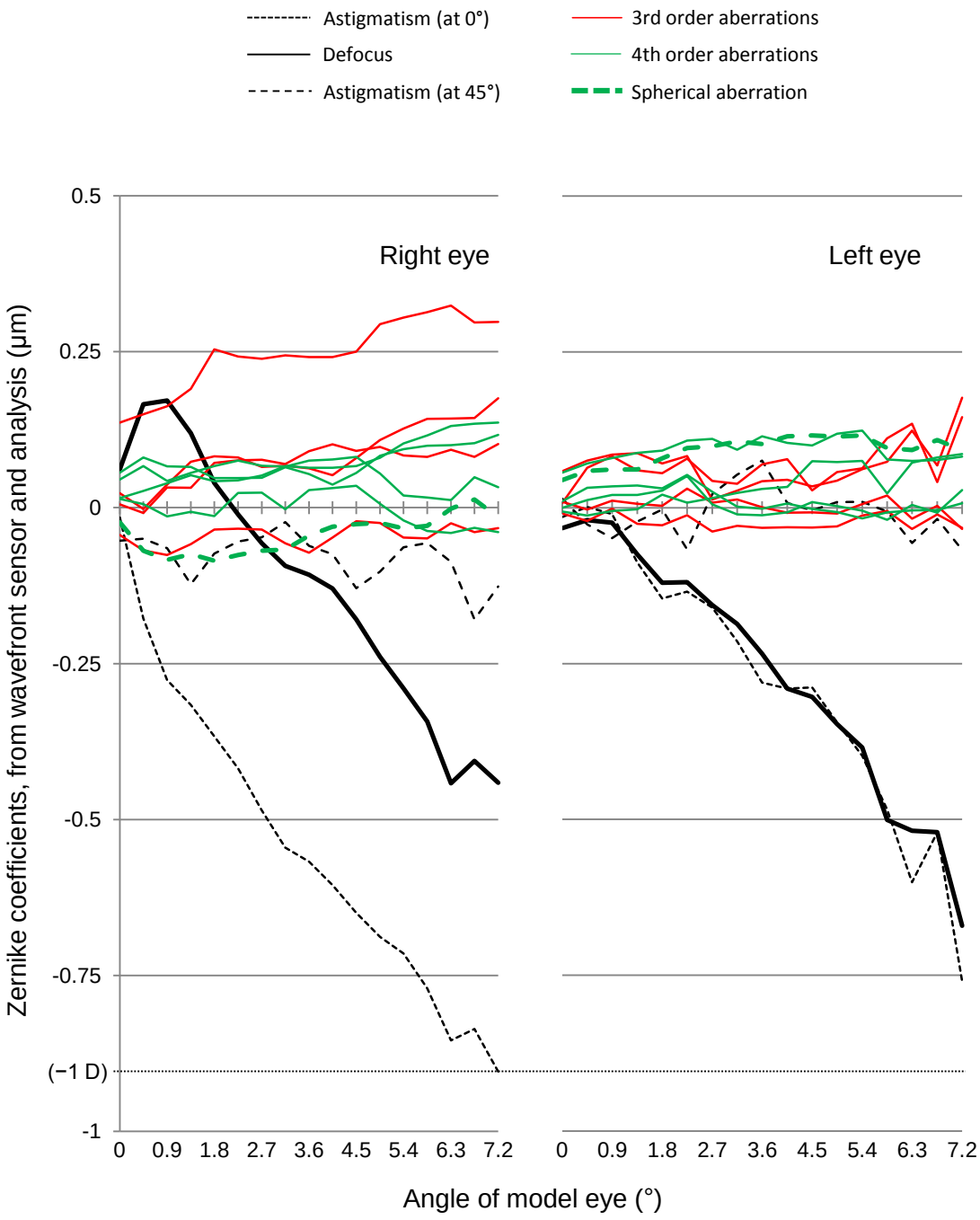

Figure 7-21: The Zernike aberrations recorded at different beam angles through the system, up to fourth order. The dotted reference line shows the Zernike defocus coefficient corresponding to −1 D of defocus (0.91 µm).

While preparing to take these measurements, it was noticed that the input voltage required to move the beam through a particular angle appeared to be twice the value expected from the scanning mirror specification. This observation was checked using graph paper, positioned 12 cm from the scanning mirrors and observing the IR beam movement using a camera. For

both scanning mirrors, with an input of 5 V, the mirror rotated to provide 2.0 cm of beam movement, corresponding to 1 V per mechanical degree, or 0.5 V per degree of beam rotation. This compared with the specification of “0.5 V per mechanical degree” in the mirror manual. The control software was modified accordingly.

7.3.6 Perception of images with and without stimulus control

At various stages of the development of this apparatus, participants observed the stimulus, while maintained in position using a bite bar, and reported the clarity of the images. Earlier in the development work, static images were checked, with no action either of the DMs or scanning mirrors. As progress was made, the images were checked during correction of aberrations with a static accommodative stimulus of 0, 1 or 2 D, with no stimulation of convergence. Finally, participants viewed steps in accommodative stimulus from 0 to 2 D, with appropriate rotation of the scanning mirrors to provide the congruent cue to convergence.

When images were unclear, or became unclear as a result of the stimulus control, in at least one eye, work continued on developing the apparatus and protocol for collecting reliable data. Also, it was necessary to check for and correct vertical disparity of the two images, which could vary between days or weeks.

The instrument was finally able to provide clear stereoscopic stimuli (as reported by fellow researchers from the department) with either no movement of the DMs or during HOA correction, and following a 2 D increase in the stimulus to accommodate, with a corresponding stimulus to converge. Data from participants viewing these stimuli are provided and discussed in chapter 8.

7.4 Limitations and suggested improvements

7.4.1 Deformable mirror performance

As noted above (section 7.3.2), it was typically only possible to use up to about 21 mirror modes for wavefront correction. Beyond this number, attempts to initially correct the intrinsic aberrations of the apparatus often failed (resulting in diverging actuator positions) and even around this number, a serious amount of astigmatism was sometimes introduced to a beam when only wishing to control defocus (see section 7.3.3).

The electronics supplied to convert voltage signals from the workstation into control of the DM actuators also frequently failed to start up correctly, which slowed down progress on the apparatus. One of the control modules was eventually replaced by the manufacturer, which reduced the frequency of this failure.

Dubra (2007) investigated the performance of the MIRAO 52 and another DM; he found the influence function of an actuator in the MIRAO 52 to be approximately 60% of its peak value at neighbouring actuators. The influence function of an actuator in the other DM (“Multi-DM”, Boston Micromachines, USA) was only 26% at its neighbouring actuators. The strong coupling between actuated regions of the MIRAO 52 may limit the features of surfaces which can be produced by the DM for aberration control over the pupil area.

For use with human participants, it was necessary to reduce the pupil size for aberrometry to approximately 5 mm, particularly when using near stimuli, which stimulated miosis. Rotation of the beams, with convergence of the eyes, also narrowed the pupil images at the sensor, due to movement of the beams on the

off-axis parabolic mirrors (see Figure 7-22, where the images of the converged pupils no longer fill the search blocks).

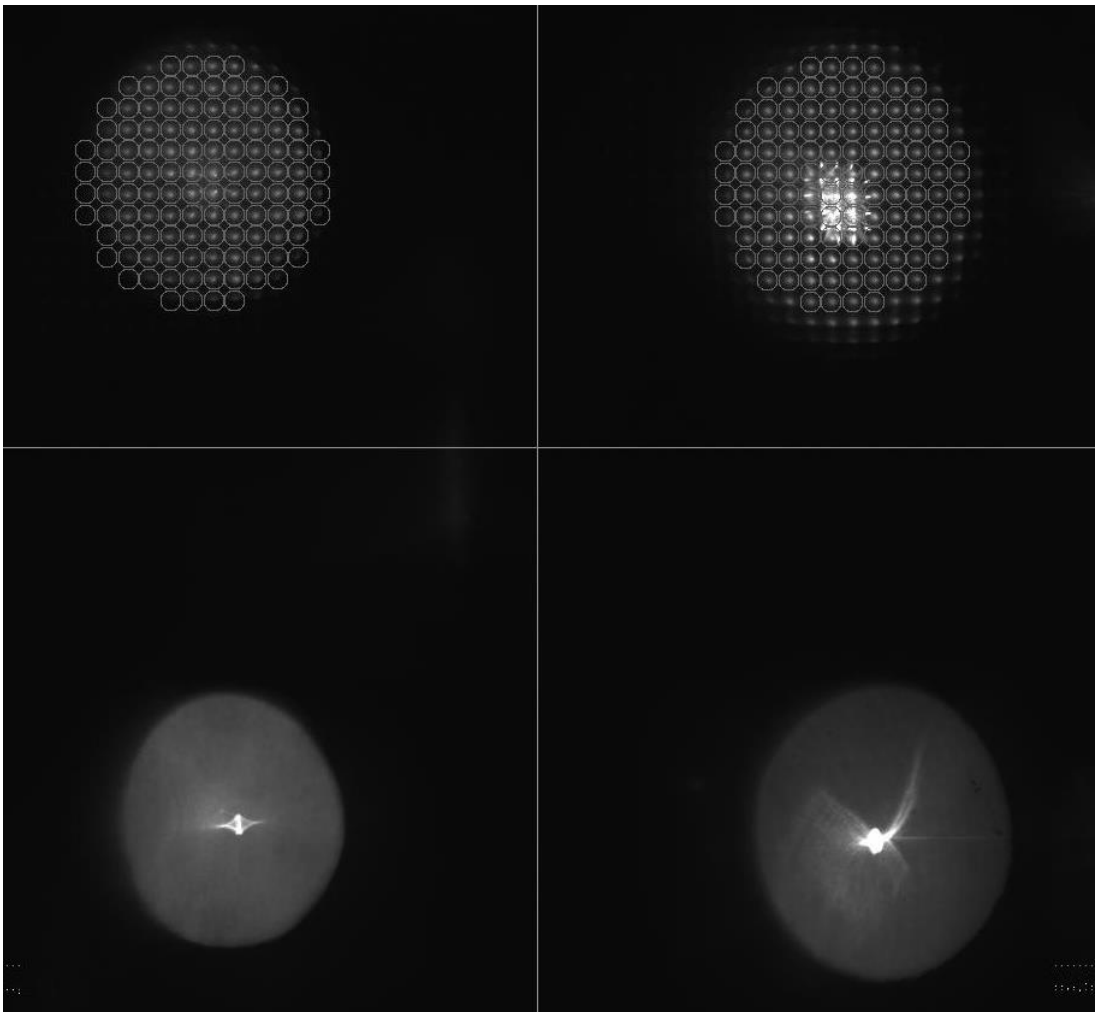

Figure 7-22: Images at the CCD sensor when the accommodative stimulus for Figure 7-4 was moved to a vergence of −2 D at the eye, with agreement in the stimulus to convergence. The pupil images are narrower in the horizontal dimension, and no longer fill the area of the search blocks, for this participant.

Larger pupil sizes were originally considered in the design of the apparatus; limitation to 5 mm for practical reasons effectively reduced the number of actuators acting on the wavefront. Fernandez et al. (2006) considered a 11.89 mm pupil image at the DM useful for wavefront control; this size excluded the outermost actuators, to allow greater control of slopes at the edge of the pupil image. The pupil images used in this and the following chapter, for wavefront sensing and control, have diameter 9.45 mm at the DMs. They

exclude more actuators than did the images of Fernandez et al. (2006), and the outermost ring of actuators now appears nearly redundant. Figure 7-23 shows these various dimensions, and the arrangement of mirror actuators, to scale. The reduction in the number of effective actuators may have limited the number of truly independent mirror modes it was possible to use for wavefront control.

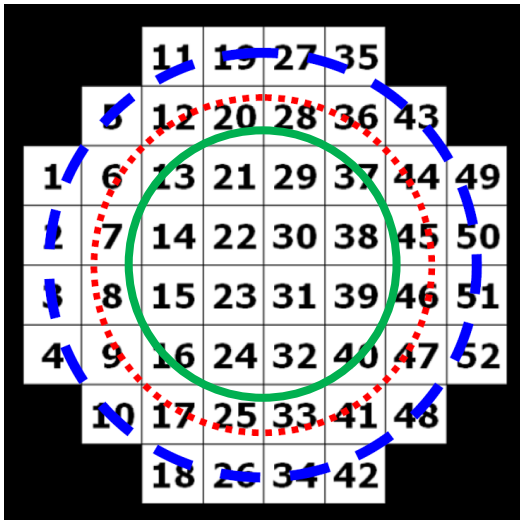

Figure 7-23: The size of the aperture for wavefront sensing and control, at the DM, in the apparatus of this chapter (green circle), relative to the mechanical DM aperture of 15 mm (blue dashed circle) and pupil image size considered by Fernandez et al. (2006) (red dotted circle). The dimensions are to scale and relative to the square grid of actuators controlling the DM (numbered). Adapted from Fernandez et al. (2006).

The positions of the ND filters in the beam path for the left eye can be improved. A plate in a converging beam gives rise to spherical aberration, coma, and when the plate is tilted, astigmatism. Bearing this mind, aberrations introduced by the ND filters in their originally designed positions may be causing difficulties in calibration of the left-eye channel (see section 7.3.3).

It was also found that aberration correction was performed more effectively via the minimisation of the specific Zernike coefficients, rather than simple minimisation of wavefront slope errors, which does not require such calculations. It was possible to use a greater number of mirror modes when correcting “via Zernikes”, and for the same number of mirror modes, better

wavefront correction was achieved “via Zernikes”. This difference is not yet understood, and may provide interest for further research into AO control, but it may also be linked to the attempt to generate and use mirror modes over only a limited portion of the mirror.

Improvements which may benefit the system are the use of a different DM, with a greater number of actuators, possibly with a narrower influence function; the magnification of a practical pupil size to fill more of the aperture of the DM; the movement of the ND filters such that they are always normal to constantly collimated beams.

7.4.2 Shape of pupil segments for calculation of Zernike polynomial derivatives

The control software currently compares the average wavefront slope over a lenslet with the average slopes of the Zernike polynomials over circular apertures, corresponding to lenslet positions within the pupil image. However, the lenslets are square; comparing the wavefront slopes with average slopes of the Zernike polynomials over square apertures may yield slightly different results. An investigation into the difference this would make to the system is planned as part of the future development of the instrument.

7.4.3 Frame rate

The frame rate is currently limited to 9.7 frames s^{-1} by the readout time of the CCD camera. The frame rate was increased by a factor of two when using an option to bin groups of four camera pixels together, as used in the monocular AO apparatus of chapters 3–6. However, the attempt to use binning in this binocular system resulted in unhelpful intensity fluctuations of the binned images. The fluctuations were possibly connected with the use of the rotating diffuser and briefer exposure times, combined with the convoluted path from the

diffuser to the eyes, particularly via the off-axis parabolic mirrors. Attempts to reduce the brightness fluctuations when binning pixels together would be beneficial.

7.4.4 Unknown aberrations through sections of the apparatus

The ocular aberrations, and the effect of the DM on stimulus aberrations, are observed very indirectly, via many optical components. There are few checks on the performance of different sections of the apparatus, although the formation of Shack-Hartmann spots and pupil images at the sensor (e.g. Figure 7-4), the linear measurements with respect to imposed defocus (Figure 7-15, section 7.3.1) and the perceived clarity of images (section 7.3.6) are good indicators for the whole apparatus.

To ensure accuracy of the alignment and calibration of the apparatus, it would be beneficial to employ a further Shack-Hartmann sensor, or other aberrometer, as a testing instrument at different points in the system. Use of such a sensor at the eye positions (see Figure 7-1) would directly reveal the effect of the action of the DM on the stimulus. Use of such a sensor after the combining lens (Figure 7-10A) would provide data on the aberrations after the off-axis transmission through the combining lens, and before the final relay of the four channel system (also used off-axis). Results may, for example, shed further light on the coupling of defocus with astigmatism and coma seen in sections 7.3.1 and 7.3.3.

8 Test data from the binocular adaptive optics instrument: human participants viewing dynamic stimuli

8.1 Method

The apparatus described in chapter 7 was used to collect data with two participants, as a test of its performance. Data collection was approved by the Life Sciences Research Ethics Committee at the University of Bradford, and was carried out with informed consent of the participants.

The stimulus (luminance ≈ 20 cd m^{-2}) began at distance (0 D and parallel gaze); a −2 D step in defocus, with a concordant change in horizontal positions of the stimulus images, was instructed after the 40^{th} frame (after about 4 s). Data collection then continued for a further 40 frames. −2 D corresponds to a Zernike defocus coefficient of 1.83 μm, for the experimental pupil size of 5.04 mm.

From the start of each trial, the system was instructed to either perform no aberration correction, or correct 44 Zernike aberration modes (up to and including 8^{th} order, see sections 2.2 and 2.3) in both eyes (section 8.2.1), or correct 44 Zernike aberration modes in one eye only, with the other uncorrected (section 8.2.2). Following the step change, aberrations were recorded, but not corrected. Pupil image tracking was carried out in order to maintain consistent aberrometry over the pupil aperture, before and after the stimulus step, and consistent aberration correction before the step.

The data of sections 8.2.1 and 8.2.2 were each collected in one day, with recalibration (see section 7.3.2) performed before data collection, on the same day (as described in section 7.2.8). The participants were aligned on the system as described in section 7.2.8.

In chapter 4 (see section 4.4.2), it was noted that elimination of audible cues from the action of the DM was required for clear investigation of the accommodation response (AR) to blur. In the apparatus of chapter 7, and this chapter, the electromagnetic actuators of the DMs do not generate sounds, but the galvanometer scanning mirrors do. Similarly to the protocol of chapters 5 and 6, the two participants wore headphones with audio input, such that the rotating mirrors were inaudible.

8.2 Results and discussion

8.2.1 Aberration correction in both eyes

Figures 8-1 and 8-2 show the effect of instructing the apparatus to correct the aberrations of both eyes, before the step change in the stimulus. Figure 8-1 reports trials with aberration correction, with a gain of 0.1, using 21 mirror modes (see section 7.3.2). Figure 8-2 reports trials with no aberration correction. The participant (P1) was female, aged 22 years and free from ocular disease (refractive errors: right eye −6.25/−0.25x30, left eye −6.25/−0.25x135, distance PD: 62 mm). She wore her habitual contact lens correction.

Trials were rejected in which the pupil tracking did not result in sufficient movement of the aberrometry search blocks (see section 2.2.2) to maintain a Shack-Hartmann spot in every search block, i.e. when the pupil image area was allowed to leave the region of the search blocks. Trials were also rejected when the participant blinked within the data collection period. Five trials were required to acquire the four binocular datasets of Figure 8-1. Four trials were required to acquire the four binocular datasets of Figure 8-2.

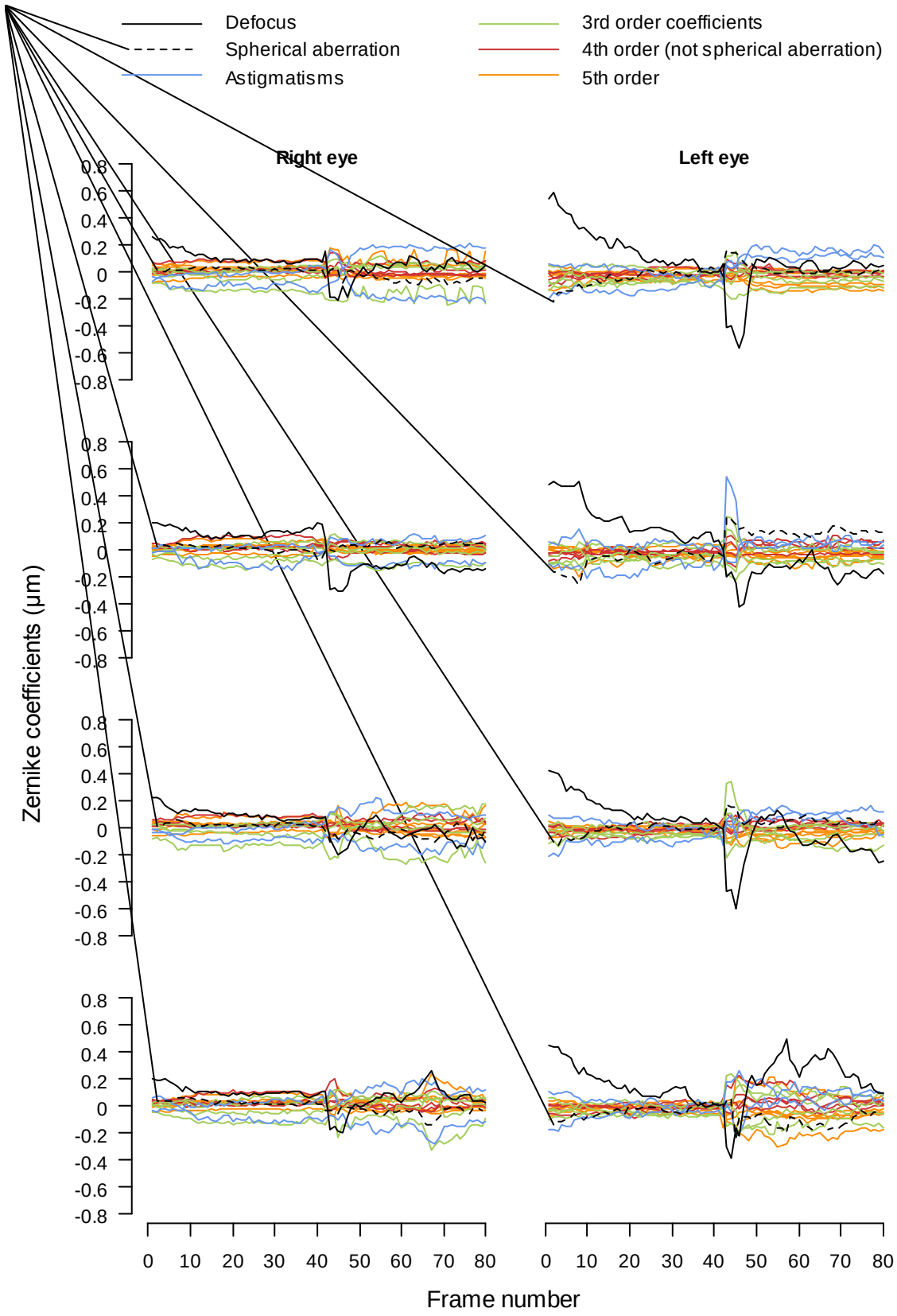

Figure 8-1: The four datasets recorded with participant P1, when 44 Zernike terms were corrected with gain 0.1, before the stimulus step (frame 40). The Zernike coefficients are plotted up to 5th order (the first twenty modes), and distinguished according to the legend. Each horizontal pair of plots describes one trial.

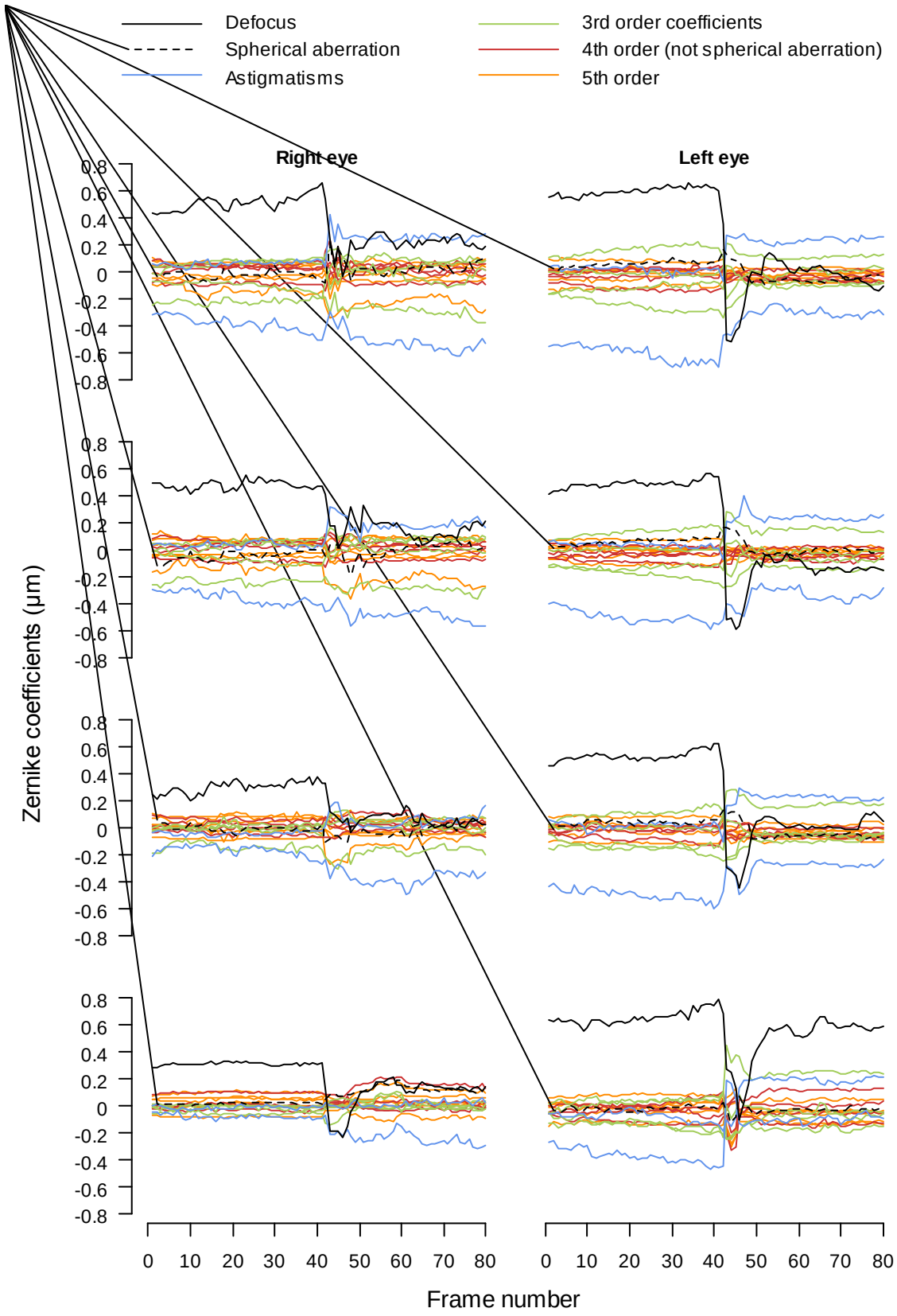

Figure 8-2: The four datasets recorded with participant P1, when no aberration correction was performed. The stimulus step was instructed at frame 40. The Zernike coefficients are plotted up to 5th order (the first twenty modes), and distinguished according to the legend. Each horizontal pair of plots describes one trial.

In Figure 8-1, aberration correction is seen, particularly in defocus, which decreases towards zero over the first 40 frames. It is particularly evident in defocus because of the initial lead of accommodation at distance. In the left eye, all aberrations appear to be well-corrected towards zero. The right eye appears to show less complete aberration correction, probably owing to undesired coupling between mirror modes (see sections 7.3.3 and 7.4.1).

In Figure 8-2, the lead of accommodation is visible in the frames before the step in AS, and is reduced after the step in AS. The mean initial lead of accommodation, over the first 40 frames in each trial, was between 0.33 and 0.56 D in the right eye and between 0.53 and 0.71 D in the left eye. These values are consistent with the results of Abbott et al. (1998), discussed in section 1.4.1.1. In the right eye, the lead of accommodation reduced by between 0.18 and 0.37 D after the step in AS (using the mean lead before the step and the mean lead/lag following stabilisation of defocus after the step, taken from the 55^{th} frame). In the left eye, the lead of accommodation reduced by between 0.08 and 0.68 D. The vergence of the wavefronts leaving the DMs was approximated by the Zernike defocus coefficient, multiplied by the appropriate conversion factor (see section 2.2.3).

Introducing spherical aberration (SA) to the calculations of vergence, as indicated by Thibos et al. (2004) and used in chapter 6, resulted in noisy defocus measurements incompatible with the clear vision reported by the participant. This was the case for the inclusion of primary (4^{th} order); primary and secondary (6^{th} order); and primary, secondary and tertiary (8^{th} order) SA. The normalisation factors for these components are large—from $12\sqrt{5} \div (\text{radius in mm})^2$ for primary to $120 \div (\text{radius in mm})^2$ for tertiary SA—so

small departures from zero and fluctuations have a dramatic effect on the calculations. It appears this apparatus is not currently sufficiently precise to use these aberrations in the analysis of accommodation*. Figure 8-3 and Figure 8-4 show the pupil image motion at the DMs, for the trials of Figure 8-1 and Figure 8-2. Figure 8-4 zooms in on the frames immediately following the 40th frame, at which the scanning mirrors are instructed to turn. The displacements of the pupil images from their initial locations are recorded in pixels, and can be multiplied by the pixel size and magnification from the CCD sensor to the DMs for this purpose. From Figure 8-4, most of the motion of the scanning mirrors occurs between the 42nd and 43rd frames, indicating a latency in the control of the mirrors of approximately 0.2 s (1 frame = 0.1 s). Following this change in the positions of the stimulus images, the pupils converge back towards their original image positions on the DMs, starting between the 44th and 45th frames, with some slight motion visible just before the 44th frame. The latency of convergence is therefore also approximately 0.2 s. The time to stabilisation of the final level of convergence is approximately 0.9 s (also from inspection of the graphs). These timings are as expected from Rashbass and Westheimer (1961), who found intervals of about 160 ms and 800 ms, respectively.

* When analysing the data of chapter 6, including primary spherical aberration (4th order) in the calculation of accommodative power did not make an obvious difference to the results, compared with the use of Zernike defocus only; it was considered a refinement to the analysis.

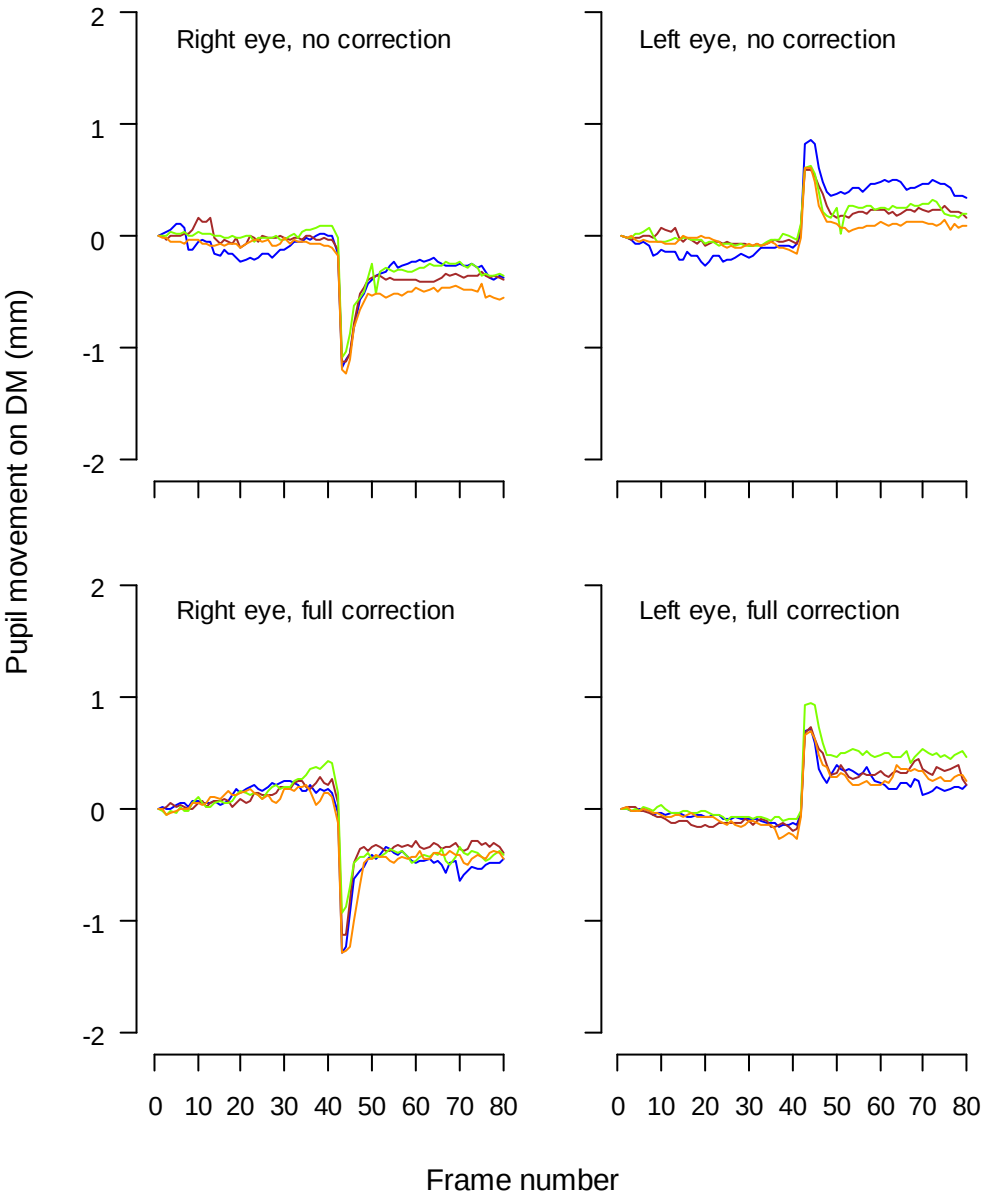

Figure 8-3: Pupil image motion on the DMs, during the trials of Figures 8-1 and 8-2.

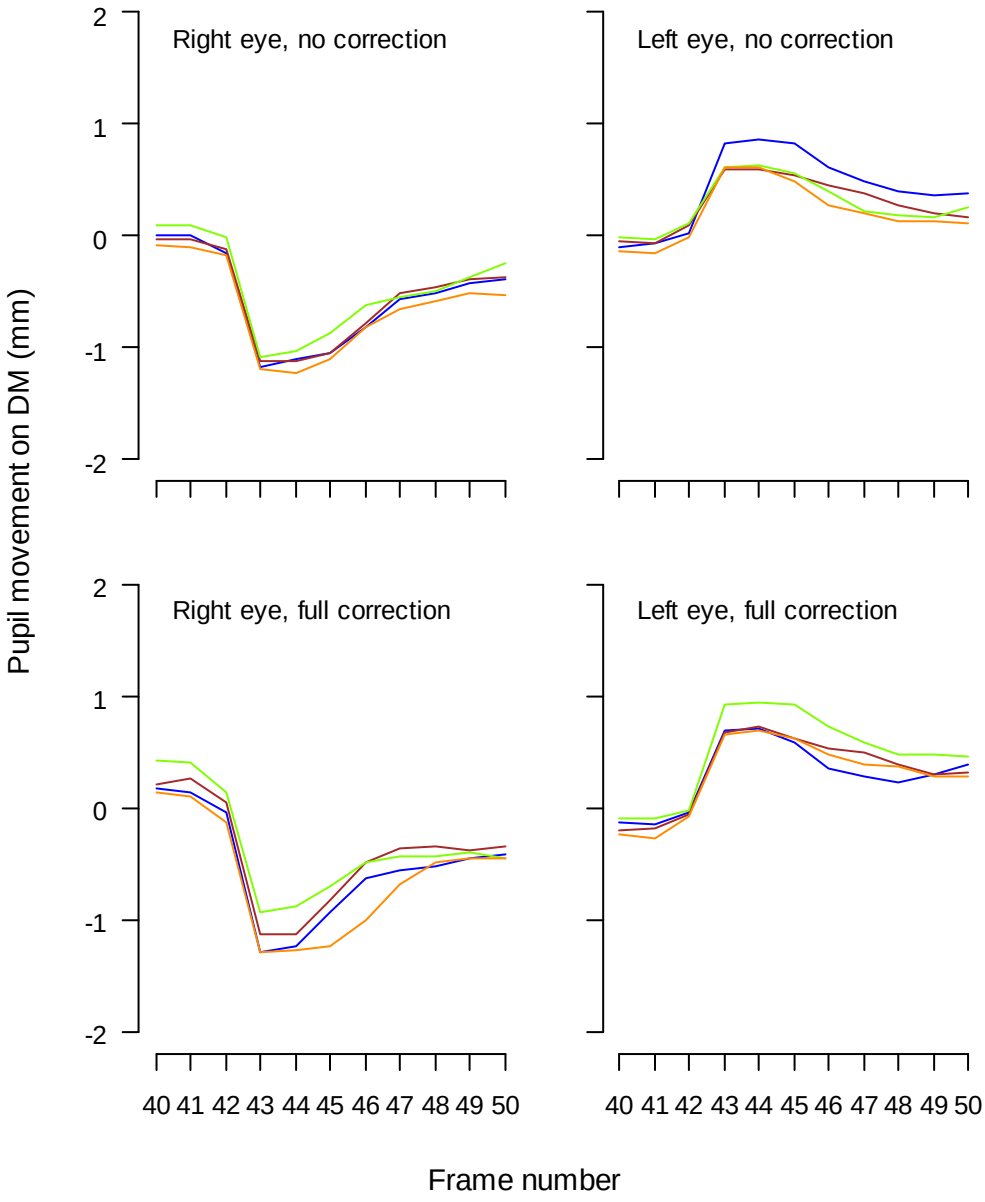

Figure 8-4: Pupil image motion of Figure 8-3, zooming in on the period containing the convergence stimulus and response.

In the brief time before the eyes converge to fixate on the stimulus at 2 D, the pupil images are moved from their initial positions on the DMs. When the eyes turn to fixate correctly on the target, the images return to close to their original positions on the DMs. The effect on the wavefront of the portions of the DM outside the calibrated pupil area is not known, and may result in a possible initial error in aberrometry immediately following a stimulus to converge.

The accommodation response times observable in Figures 8-1 and 8-2 are very similar to the timings of pupil image motion on the DMs. With the system not calibrated for different beam locations—while it is calibrated for beam angle (see section 7.3.5)—it is not possible to discern precisely how fast accommodation is responding during the 1 s following the step in AS. However, comparing pupil image motion and accommodation during this period (Figure 8-5) appears to show that accommodation lags behind convergence, as expected (Wilson, 1973; Maxwell et al., 2010).

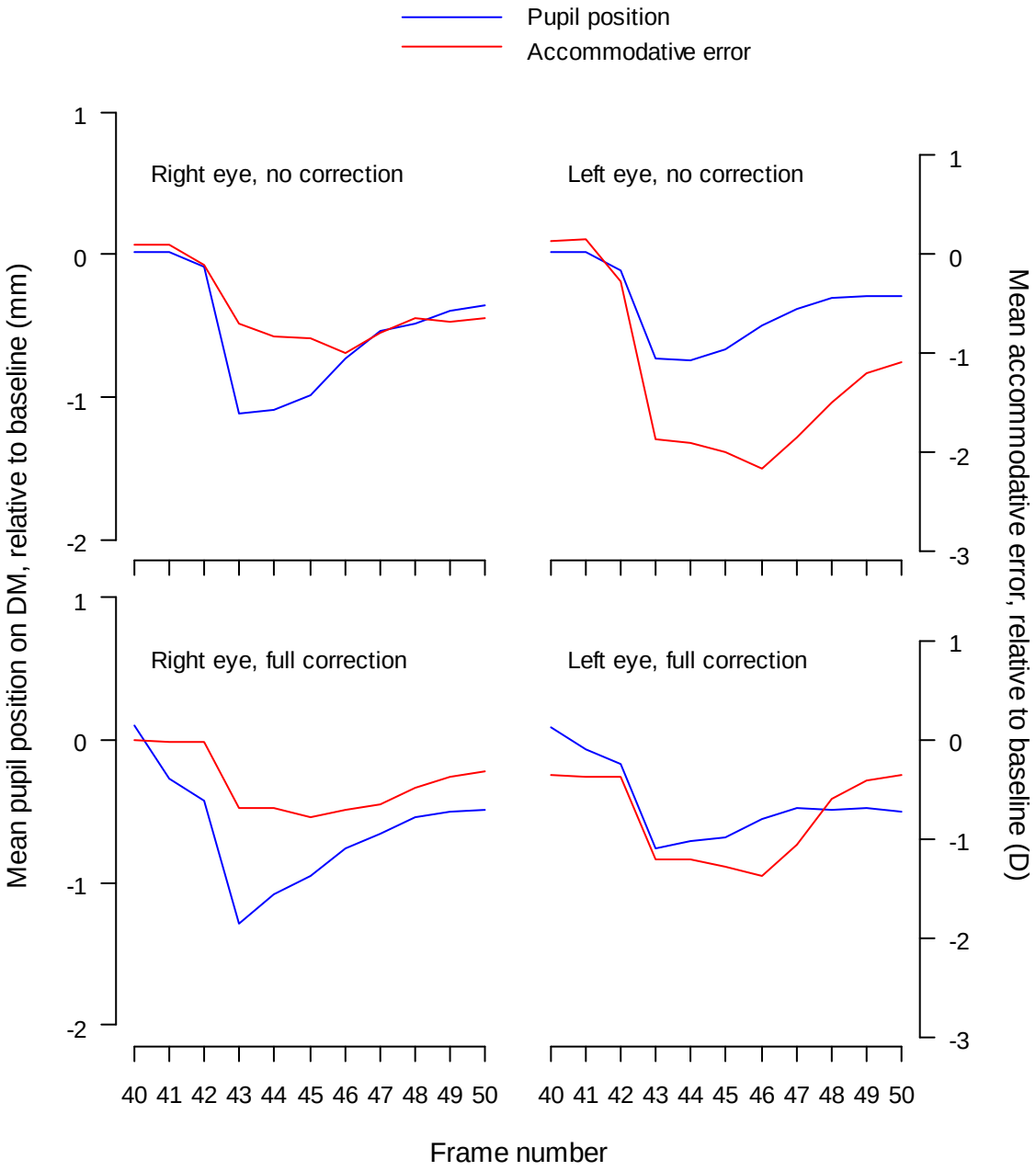

Figure 8-5: Pupil position and accommodative error, scaled such that they would be plotted at the same value, if convergence and accommodation were in perfect agreement, for participant P1. Negative pupil position thus corresponds to outward image movement at the DM. Mean baseline values over frames 1–40 were calculated for each trial, before finding the mean deviation from the baseline over four trials.

8.2.2 Aberration correction in one eye

Figure 8-6 shows the effect of instructing the apparatus to correct the aberrations of the left eye only, before the step change in the stimulus, with the right eye uncorrected. The participant in these trials (P2) was female, aged 26 years and free from ocular disease (refractive errors: right eye −1.00/−0.50x180, left eye −1.25/−0.50x180, PD: 66 mm). She wore her habitual

spectacle correction. Aberrations were corrected with a gain of 0.1, using 21 mirror modes.

All Zernike coefficients for the left eye are seen to decrease towards zero over the first 40 frames, in each trial.

Similarly to section 8.2.1, Figures 8-7 to 8-10 describe the aberrations in trials for this participant carried out with no correction, pupil image motion at the DM, and comparison with the timings of accommodation.

Four trials were required to acquire the four binocular datasets of Figure 8-6. Five trials were required to acquire the four binocular datasets of Figure 8-7. Pupil tracking failed in one trial because of strong reflections from the spectacle lenses. The spectacles were tilted slightly on the participants head to remove these reflections from the pupil images. Trials were rejected for inadequate pupil tracking, as in section 8.2.1, but not for blinks after the step in the stimulus (as in one of the trials in Figure 8-6), since quantitative analysis was not planned for this period.

Decreases in the lead of accommodation, following the stimulus step, can be seen in the left eye in trials with no AO correction of aberrations (black traces, Figure 8-7). The right-eye responses of this participant do not show the same obvious decrease in lead, although the steps in defocus and accommodative responses are visible.

Pupil image motion (Figures 8-8 and 8-9) and the relative timings of convergence and accommodation (Figure 8-10) are similar to that described in section 8.2.1.

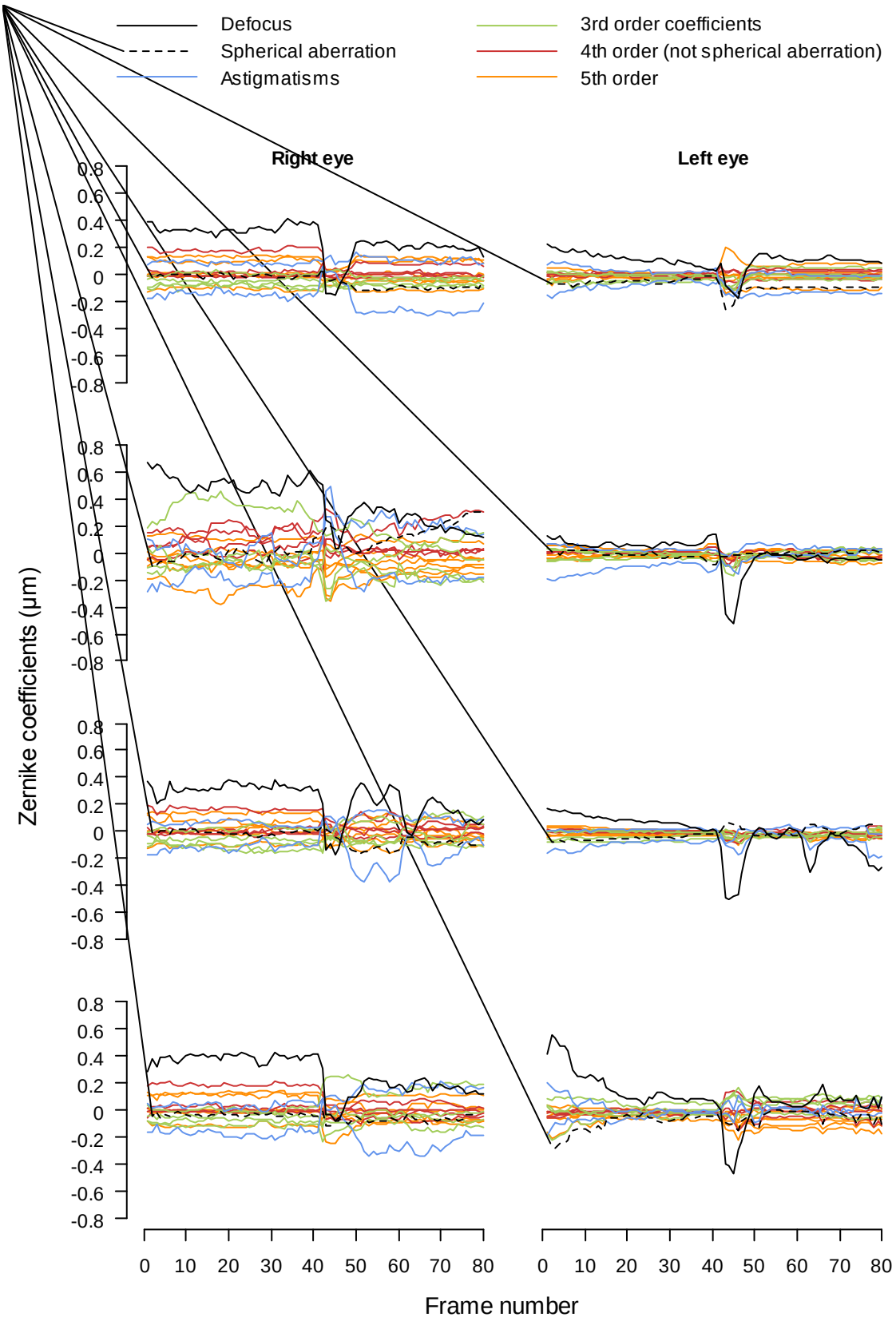

Figure 8-6: The four datasets recorded with participant P2, when 44 Zernike terms were corrected with gain 0.1, for the left eye, before the stimulus step (frame 40); the right eye was uncorrected. The Zernike coefficients are plotted up to 5th order (the first twenty modes), and distinguished according to the legend. Each horizontal pair of plots describes one trial.

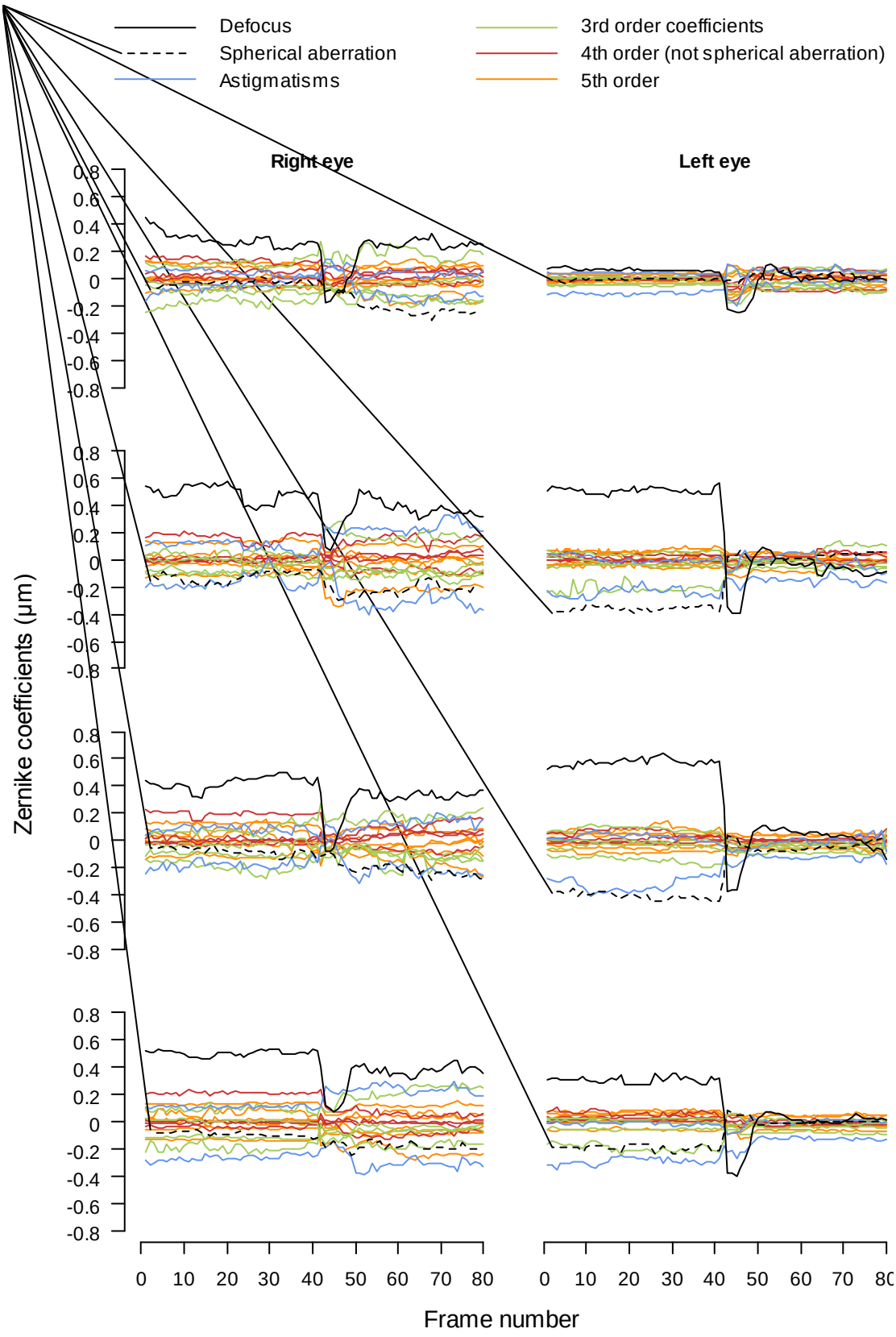

Figure 8-7: The four datasets recorded with participant P2, when no aberration correction was performed. The stimulus step was instructed at frame 40. The Zernike coefficients are plotted up to 5th order (the first twenty modes), and distinguished according to the legend. Each horizontal pair of plots describes one trial.

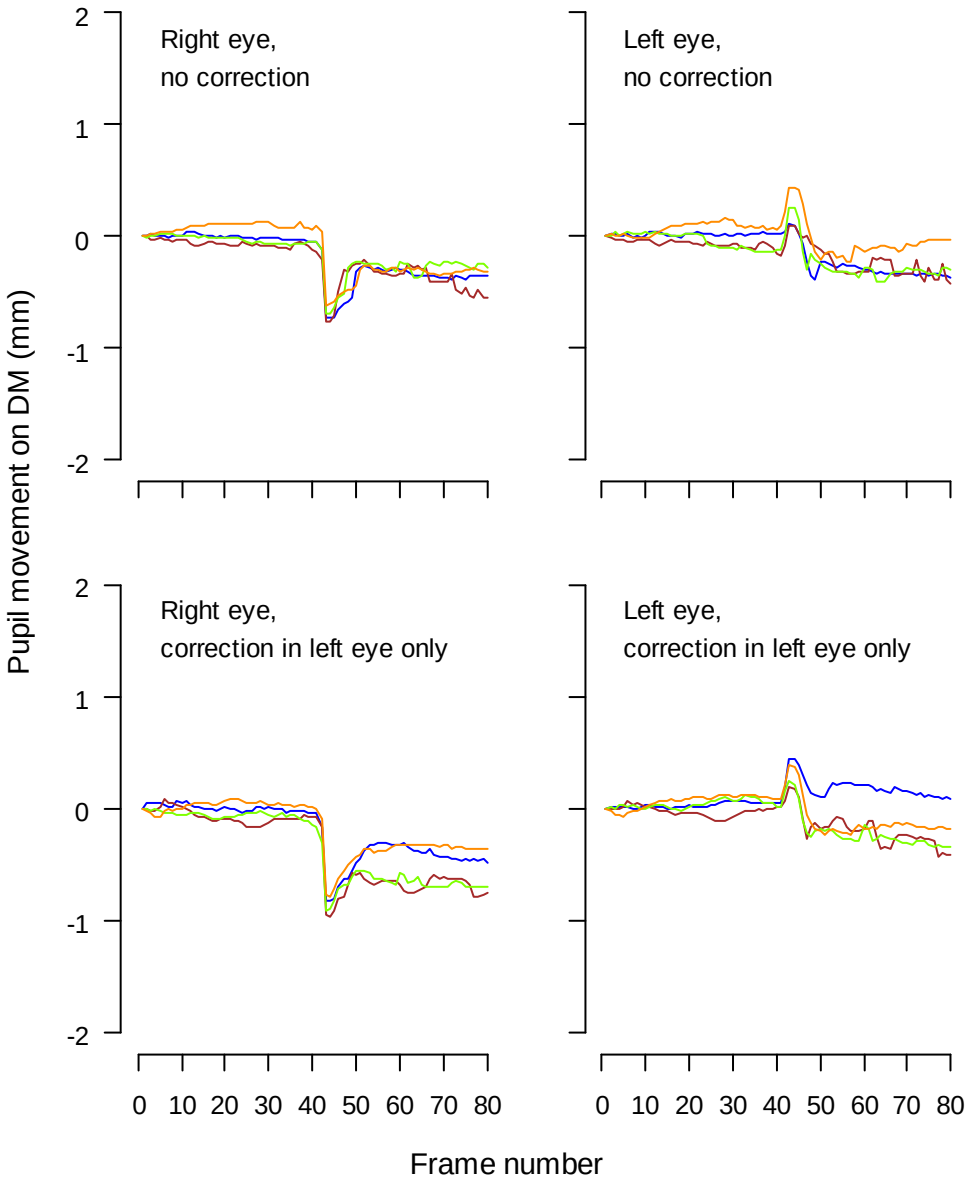

Figure 8-8: Pupil image motion on the DMs, during the trials of Figures 8-6 and 8-7.

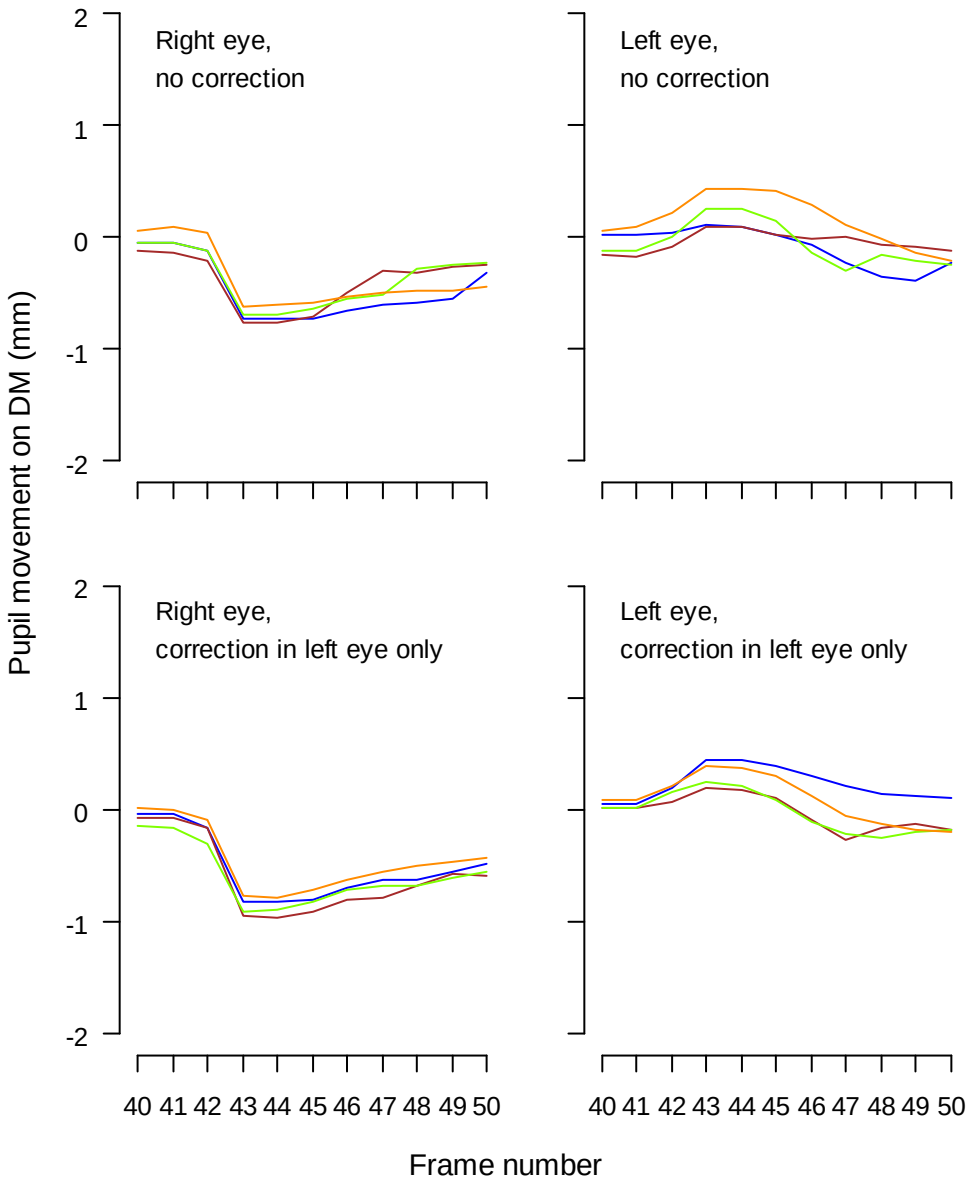

Figure 8-9: Pupil image motion of Figure 8-8, zooming in on the period containing the convergence stimulus and response.

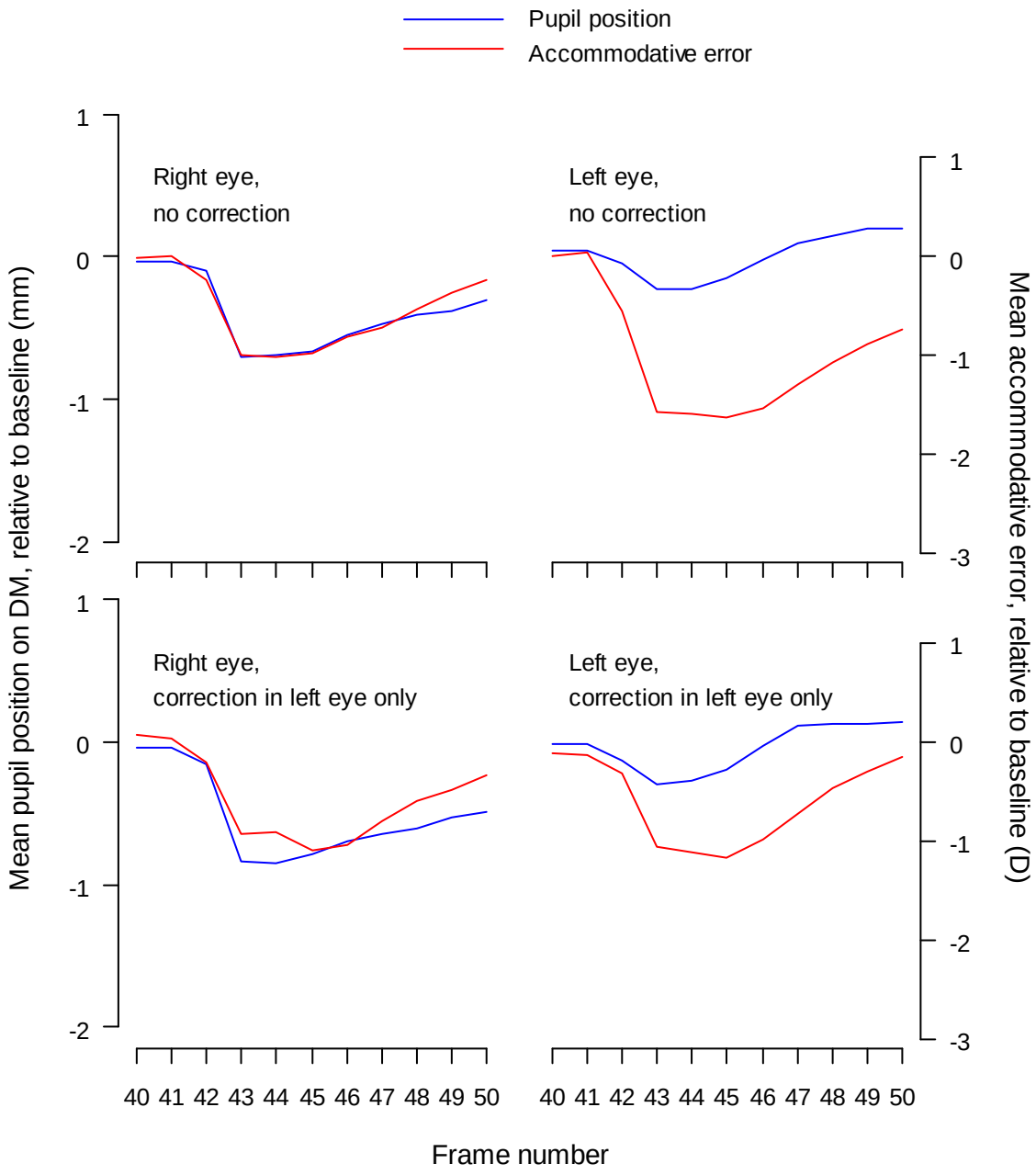

Figure 8-10: Pupil position and accommodative error, scaled such that they would be plotted at the same value, if convergence and accommodation were in perfect agreement, for participant P2. Negative pupil position thus corresponds to outward image movement at the DM. Mean baseline values over frames 1–40 were calculated for each trial, before finding the mean deviation from the baseline over four trials.

8.3 Assessment and potential improvement of data quality

8.3.1 Summary of stimuli and data collected

Data have been collected, using the apparatus of chapter 7 to provide a visible stimulus to participants and perform binocular aberrometry. A 2 D increase in the dioptric stimulus to accommodate was effected using the DMs; horizontal

positions of the stereoscopic image, stimulating convergence, were concordantly stepped using the galvanometer scanning mirrors. The pupil image positions were detected, to provide dynamic reference coordinates on the CCD sensor, on which to base aberrometry of the beams returning from the eyes. In half of all of the trials, correction of the first 44 Zernike aberration modes (up to 8^{th} order) was performed over the 40 frames before the stimulus step. In half of the trials with aberration correction (section 8.2.1), the aberrations were corrected in both eyes during this period. In the remaining trials with aberration correction (section 8.2.2), the aberrations were corrected in the left eye only, with the right eye uncorrected, testing this facility of the apparatus control software.

The values of the 44 Zernike coefficients were recorded in every trial, as were the pupil image positions at the CCD sensor. The coefficient for defocus was converted into approximate vergence of the beam returning from the eyes, after reflection at the DM; it revealed the lead or lag of accommodation, rather than the absolute accommodation response. The pupil image positions at the CCD sensor were converted into image positions at the DMs.

8.3.2 Perception of the stimuli

The two participants perceived the stimulus to be initially clear and remain clear, although they reported an unusual sensation during aberration correction, including a perception that the stimulus was moving towards them. This is currently ascribed to the gradual (gain = 0.1) dynamic correction of the lead of accommodation at distance, which is expected to gradually increase the dioptric stimulus until the participant demonstrates an accurate accommodation response.

8.3.3 Aberration correction

The data showed that aberration correction was performed as instructed, although it may be limited in some cases by coupling between mirror modes of the DMs (see sections 7.3.3 and 7.4.1).

As discussed in section 7.4.1, the use of a larger pupil at the DMs, covering a greater number of actuators, may result in improved (decreased) coupling between mirror modes, during aberration correction. If movement of the pupil images then required a larger DM aperture, a DM with a greater number of actuators would be useful.

8.3.4 Timing and accuracy of the convergence stimulus and response

Pupil image positions were stepped as expected by the movement of the scanning mirrors before the convergence response returned them approximately to their original positions on the DMs.

A latency of approximately 0.2 s was found in the control of the scanning mirrors, i.e. most of the motion of the mirrors occurred 2 frames after the instruction to rotate (see section 8.2.1). Following this rotation, a latency of approximately 0.2 s and a total response time of approximately 0.9 s was found in the convergence response, which corresponded well with the data of Rashbass and Westheimer (1961) (about 160 ms and 800 ms, respectively).

The pupil images returned close to their original positions on the DMs (as detected by the centroiding algorithm, see section 7.1.5), as shown in Figures 8-3, 8-4, 8-8 and 8-9. There is room for improvement, however in the final pupil image positions. This is possibly due to slight misalignment of the beams on the centres of the scanning mirrors. It may not be possible to improve this alignment much further, because of the imprecision in judging beam position on the

mirrors, using an IR camera from an oblique angle, with a beam size of a few millimetres. It may be necessary to calibrate the DM and system aberrations for different beam locations and DM settings, as discussed below in section 8.3.5.

The inaccuracy of the final response could also be due to imprecision in the distance from the final off-axis parabolic mirrors (see Figure 7-1) to the eyes. Strictly speaking, the centre of the rotation of the eye should be conjugate with the centre of the scanning mirror; the first nodal point of the eye should be one focal length from the nearest parabolic mirror. These distances are difficult to assess externally. A rule is currently used to measure from a point just behind the participant's pupils to a point on the nearest plane mirror; the bite bar mounting is adjusted accordingly.

Participant alignment could be improved by testing steps between stimuli at 0 and 2 D, with convergence, and adjusting participant position (using the bite bar mounting) until the pupil image positions are identical for the two stimulus levels.

8.3.5 The accommodation response and implications

The form of the defocus response was as expected, with a negative step in the measurements at the point of the stimulus step, as the DM added −2 D of vergence to both the stimulus and the beam returning from the eye (compare with the non-accommodating model eye in section 7.3.3). As accommodation responded, the defocus measurement returned towards its original value, but usually stabilised at a lower level than that before the stimulus step. The difference in defocus levels before and after the step is expected, since there is a lead of accommodation at distance, which decreases with increasing stimulus and becomes a lag of accommodation at near (Abbott et al., 1998).

The timings of the accommodation response (latency and total response time) are close to that of the convergence response, with a brief lag. Until the convergence response is complete, the pupil image is displaced from the calibrated region of the DM; the aberrometry is not calibrated to take into account the relevant beam paths in the system (although it is calibrated to take into account different beam paths, from eye rotation, that result in the same pupil image position). Therefore, accommodation cannot be precisely analysed during this interval. Such analysis would require further calibration of the intrinsic system aberrations at different pupil image locations, also with eye rotation at these positions. The calibration should cover the different DM settings used ("flat" and −2 D defocus, in this case).

Such calibration is possible in principle, but with the drifts observed in the alignment of the system over time, it would be unfeasible to perform it before every data collection session. It may be possible to improve the stability of the apparatus, and therefore the efficiency of time spent on calibration, by mechanically isolating the rotating diffuser from the optical bench. They are already connected with a sprung mount which dampens vibration, but further isolation may be useful. The current mounting for the scanning mirrors may also possibly allow the rapid changes in their angular momentum to result in some slight slippage, and incremental changes in alignment; this possible effect should be measured.

Inclusion of spherical aberration (SA) in the calculation of vergence of the beams leaving the eye (as in chapter 6) should give more accurate results than Zernike defocus alone (Thibos et al., 2004). However, analyses of AR including SA were inconsistent with expected data and with the clear vision reported,

while the simple defocus measurements—without SA—gave the expected accommodation results. It may be that coupling between defocus and SA, combined with the change in SA of the eye during accommodation (see section 1.5.5.1) confounded the subsequent measurements. The coupling between modes should be addressed as discussed in section 7.4.1 and mentioned again above in section 8.3.3.

9 Conclusions and continuations

9.1 Motivation and relevance

As introduced in chapter 1, the purpose of this work was to contribute towards the research effort concerning myopia. Epidemiological surveys (sections 1.2 and 1.3), genetic studies (section 1.2.1) and animal research (section 1.2.2.4, also in 1.3.3 and 1.3.4) are all providing valuable insight into the recent dramatic increase in prevalence and severity of myopia, particularly in East and South-East Asia. The research of this thesis includes and facilitates contributions to detailed optometric investigation, another area of great activity in the effort to understand and control myopia (sections 1.3, 1.4 and 1.5).

The accommodation response—both static and dynamic—has been intensively studied for its possible role in myopia development and progression (sections 1.4.1–1.4.3). Differences have been found among emmetropic, early-onset myopic and late-onset myopic eyes, and among emmetropic, stable myopic and progressing myopic eyes. Since animal models indicate so strongly the role of defocus in emmetropisation, inaccuracies of accommodation, including static properties (lag of accommodation at near) and transient properties (latency and response time of accommodation, accommodative adaptation, microfluctuations) have been of great interest. The axial lengthening of the eye during accommodation may also be linked to myopia development.

A more recent area of interest has been the role of aberrations of the eye, considered in more detail than spherocylindrical error (section 1.5). Such higher-order aberrations (HOAs), measured as wavefront errors (see chapter 2), appear to be more severe in myopic eyes than emmetropic eyes. HOAs

have also been observed as a cue to accommodation, with its importance varying between subjects.

In order to contribute to research in these areas, two adaptive optics (AO) instruments were developed, which can provide a dynamic stimulus to accommodate (a monocular system) or accommodate and converge (a binocular system). They can simultaneously record the accommodative response (AR) and correct or perform other modifications to the HOAs of the eye, using aberrometry (see chapter 2 for the general principle).

Data collection protocols were developed and a detailed investigation of the AR to one period of a square wave in dioptric accommodative stimulus (AS) was carried out. New characteristics of the AR to rapid changes in AS were identified.

As the understanding of accommodation, HOAs, and links between them become more complete, the understanding of differences between refractive groups, as mentioned above, will increase. Finally, these areas will combine with other topics discussed in chapter 1 to indicate possibilities for the control of the myopia “epidemic”. It should be noted that some promise is already shown in the area of the correction of peripheral refractive errors (Bullimore, 2014).

9.2 Instruments

9.2.1 Monocular adaptive optics instrument

The monocular adaptive optics (AO) instrument of chapter 3 was based on a previously existing instrument (Hampson et al., 2009), which was thoroughly realigned and modified, following prior removal from the laboratory for building work. The instrument was improved by the use of off-axis parabolic mirrors, reducing stray light from reflections at lens surfaces, and through the

development of new mounting hardware and alignment procedures for the optics. It was possible to test and calibrate the instrument over a range of 4 D of defocus, compared with the previous range of 1.5 D (Chin, 2009; Hampson et al., 2009). The stimulus was also reported to appear clearer by participants who had observed it before and after these developments.

This instrument is capable of closed-loop and open-loop control of aberrations, including defocus (to stimulate accommodation) and higher-order Zernike aberrations (see chapter 2).

As well as the pilot experiment of chapter 4 (findings included in section 9.3.1), chapters 4 and 5 describe developments of the data collection protocol. To isolate blur of the retinal image as the cue to accommodate, it was necessary to mask the noise of the deformable mirror (DM)—the AO element—using headphones with audio input, so that it could not provide an auditory signal.

The monocular AO apparatus allowed the experiment of chapter 6 to be carried out, the results of which have also been peer-reviewed and published in an international journal (Curd et al., 2013a). The apparatus appears reliable and can be used for many further experiments testing the monocular AR, also including open- or closed-loop control of HOAs. Some such investigations had begun, before the improvements described here (Chin et al., 2009a; Chin et al., 2009b; Hampson et al., 2010).

As used in Curd et al. (2013a), the DM provides an excellent means of manipulating an AS, including rapid changes within 1 ms (Flexible Optical B.V., 2014). It would be useful to further probe the speed of the DM using a high

speed camera, with a Shack-Hartmann sensor in place of the participant on this instrument, for instance.

9.2.2 Binocular adaptive optics instrument

The binocular AO instrument, described in chapters 7 and 8, was a new instrument. Like the monocular instrument, it is capable of closed-loop and open-loop control of aberrations, including defocus and higher-order Zernike aberrations, but it also provides horizontal movement of the target images provided to the eyes, for stimulation of convergence. The aberrations and horizontal stimulus position can be modified independently for the two eyes. This instrument is the only known apparatus capable of aberration correction (or other manipulation) and convergence control.

Following the developments reported in this thesis, it was possible to provide a step in AS to a participant, with a concordant change in the horizontal image positions, stimulating convergence. The HOAs of the participants could be corrected, up to the 8^{th} order Zernike modes, in either one or both eyes.

The current design and specification of the AO components of the instrument (the DMs) appear to result in coupling between aberration modes, resulting in imperfections of the calibration of aberration control. Steps in Zernike defocus were found also to alter other aberrations, astigmatism in particular; instructions to correct all aberrations sometimes resulted in stable, non-zero Zernike coefficients. Changes were suggested in sections 7.4 and 8.3 that could reduce this coupling and improve the performance of the system.

The alignment of the instrument also appeared to drift over time, resulting in frequent repetition of the calibration procedure. It is also desired to investigate the extension of the calibration procedure to cover more pupil image positions

at the DM (allowing calibrated aberrometry during the convergence response). Modifications have been suggested that may improve the stability of the alignment, and make it practical to perform a more comprehensive calibration of the system.

Despite these needs for further development, participants reported that the stimuli in the test trials (chapter 8) appeared clear, and they consistently fused the stereoscopic image. A 2 D step in accommodation and convergence was stimulated, with and without HOA correction before the step. The defocus term (describing dynamic accommodation) was recorded as expected, as was pupil motion at the DM (describing dynamic convergence). Correction of HOAs was observed, where it was instructed.

Work should be continued on this instrument, as suggested, since it is a unique apparatus and will be able to answer questions about ocular accommodation and HOAs in true, binocular vision. It would be possible to begin optometric experiments at this stage, since stimuli are clear, aberrations can be controlled, and data can be collected, but the imprecision of calibration and aberration control may introduce much uncertainty to measurements. Reducing such uncertainty would be beneficial before attempting detailed investigations.

9.3 Experiments

9.3.1 Accommodation and rapid changes in dioptric stimulus

9.3.1.1 Findings

A single period of a square wave in AS was presented monocularly to six participants (chapter 6). The interval between changes in AS (the inter-stimulus interval, ISI) was between 0.05 s and 0.50 s.

The trials with ISI ≥ 0.15 s produced statistically significant peaks in the AR to both levels of the square wave ($p < 0.05$). Even when the second stage of the AS was in the past by the time of the response to the first stage of the AS, both response stages were elicited sequentially. Retinal input can therefore be sampled for processing during the latency and onset of accommodation, with more than one distinct output level derived from this input.

The response to a particular level of AS, with a particular ISI, did not usually depend on whether the level of AS occurred first or second in the trials (comparing one square wave with its inversion). However, there was a statistically significant tendency for the response to be significantly stronger ($p < 0.05$) when the level of AS occurred second, rather than first (8 out of 40 parameter settings: $p < 0.0007$). This tendency may be related to relative weighting of information over the latency interval, or limits on the time window for integration of defocus input. Alternatively, it may be a result of the higher velocity of accommodation known to result from a larger step in AS (the second step in the square wave sequence being double the first). Models of accommodation in the literature do not yet predict this tendency.

The AR to the single square wave period sometimes only consisted of a single peak, as opposed to the double responses described above. Also, there were some trials with a double response, but with directions of movements in the AR inverted with respect to the AS (“incorrect double responses”). These different responses suggest a time-variant starting condition for the accommodation controller, which it is speculated is linked with the natural microfluctuations of accommodation.

Returning to the “correct” double responses, timings of the AR to the second and third changes in the square wave AS indicated that information can be stored by the accommodation controller, until a component in the control chain is free to process it. For instance, if a process which cannot deal with more than one input lasts 250 ms, a second stimulus level calculated after 150 ms would be stored for 100 ms before being admitted to that process. This theory was previously applied to saccade control, following a related double-step experiment (Becker and Jurgens, 1979).

On the other hand, there are brief response times (< 0.25 s) to stimuli with longer ISI, which indicate the role of predictive effects, as found by Phillips et al. (1972).

Including predictive effects, minimum response times indicated that an AR cannot be halted, following stimulation, until about 0.6 s has elapsed, although this protocol was not designed to test for such a minimum halting interval. Such a minimum halting interval disagrees with the understanding, following the work of Campbell and Westheimer (1960), that the duration of a pulse in AR has about the same duration as the pulse in AS. The ISI is briefer in this experiment, and may reveal a different regime of AR from that studied by Campbell and Westheimer. The pilot study of chapter 4 had given similar, general indications.

9.3.1.2 Further experiments on timing

As well as providing its main findings, the data and analysis of chapter 6 also suggest further accommodation studies.

The suggested minimum halting time of 0.6 s (see end section 9.3.1.1), even including predictive effects reducing the response time, is particularly interesting, as it would reveal new limits to the accommodation control process.

If it is a real minimum interval, including with predictive effects, it would require new explanations of how rapid successions of signals to accommodate are dealt with. In this case, the mechanism for producing an AR would be delayed by the processing of previous input, but could accept an instruction prepared by the predictive component of accommodation control, providing a shortcut of the normal latency period. Such findings may combine with models such as that of Khosroyani and Hung (2002) in explaining the components of accommodation control, their functions and durations.

An experiment to test for a minimum halting time for an AR, once it has been stimulated, has been designed. Three conditions may be examined. First, single stimulus pulses of unpredictable onset time, step size and duration may be provided, and the halting times found from the temporal location of the peak in AR (case 1 in Figure 9-1). Second, single pulses in AS can be provided, with unpredictable onset time, but with predictable pulse amplitude, direction and duration (case 2 in Figure 9-1). This second condition may reveal a minimum halting time including with some predictive effects, as indicated by the results of chapter 6. Thirdly, pulses in AS of predictable onset time, step size and duration would allow comparison with previous data such as those of Phillips et al. (1972), in further examination of the AR to highly predictable stimuli (case 3 in Figure 9-1).

These experiments should be carried out both monocularly and binocularly, to also test any additional effect of convergence input on the response times.

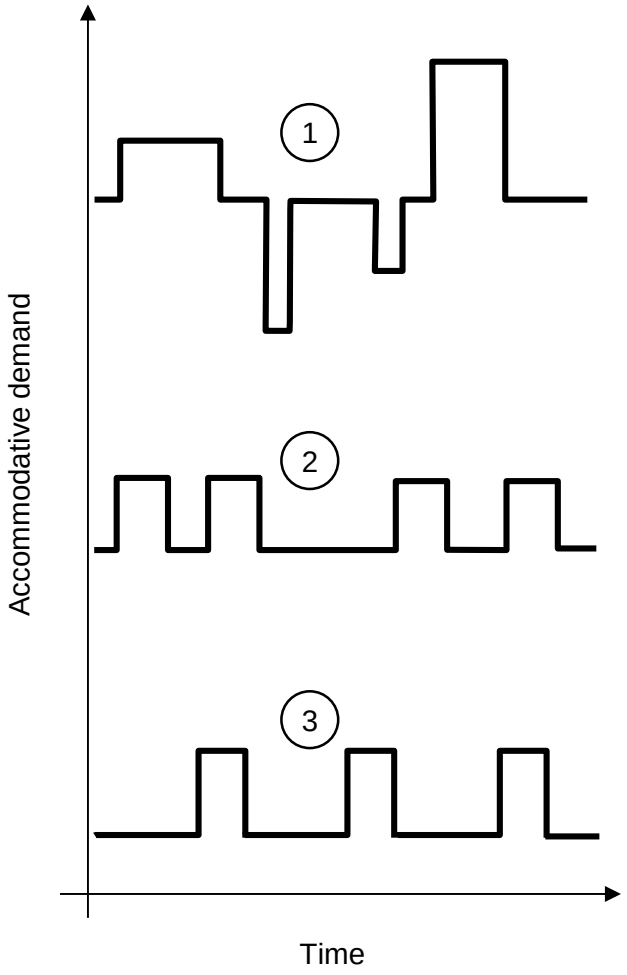

Figure 9-1: A suggestion for variation between classes of trial in an experiment on limits to accommodation timing. Predictability increases from case 1 to case 3 (see main text), revealing properties of accommodation with respect to different levels of predictability. Brief pulses can be used, as in chapters 4–6, to find lower limits to accommodation timing.

9.3.1.3 Analysis of the mode of accommodation

Accessing velocity and acceleration data of the AR to rapid changes in AS would provide information about the use of feedback during the changes in accommodation, as in Bharadwaj and Schor (2005), who considered single steps in AS. Constant pulses in the acceleration of accommodation, irrespective of the total AR, indicated an open-loop initiation of the response, while a closed-loop process completed the response.

Further analysis of the data of chapter 6, or in the experiment proposed above, may include the use of analytical functions, such as that used by

Kasthurirangan and Glasser (2005), to model the AR. Time derivatives may then be extracted from the fitted models[*]. The mean time courses of the AR can also provide a starting point for exploring these properties.

9.3.1.4 Further experiments on incorrect responses

In chapter 6, and previously (Chin et al., 2009b), accommodation has been found to respond in the incorrect direction, compared with the change in AS. It is speculated here that there may be a connection with the state of the microfluctuations of accommodation. The appearance of many single-peaked responses in chapter 6, as opposed to the double response under main consideration, also indicated a time-variant state of accommodation which affects the initial response.

The different types of response to the square wave AS confound analysis of "incorrect" or null decisions by the accommodation system. A single response, for example, may be either in the correct or incorrect direction, depending on the stage of the AS to which it truly corresponds.

Therefore, a single pulse experiment is proposed, in which the direction and position of the microfluctuations of accommodation[†] at the time of the pulse in AS would be tested for an association with incorrect decisions as to the direction of the AR. Unpredictable onset time, step size and duration should be used for the single pulses in AS. It would also be interesting to test for an association between the direction and position of the microfluctuations and the variable latency interval for single step stimuli.

[*] Velocity and acceleration analysis would also allow estimates of the latency periods of the ARs considered (Schor et al., 1999; Bharadwaj and Schor, 2005).
[†] The low-frequency component.

9.3.1.5 Further experiments on weighting of information over the latency period

One explanation for the tendency for the response to the second half of the square wave AS to be stronger than the response to the first half was that information is deliberately weighted such that earlier information is given less importance by the time of the response. An inclusion of a brief period of the next—(i + 1)th—stage of the AS at the end of an integration time window triggered for the previous—ith—stage would be another explanation. Alternatively, the tendency may owe to the high velocity of accommodation triggered by the large change between the two levels of the square wave in AS, particularly when combined with a minimum halting time as discussed in sections 9.3.1.1 and 9.3.1.2.

An experiment which would test the differential weighting theory could provide a stimulus with an initial step of, say 1 D, with an additional pulse of another 1 D added to the step function at a varying time relative to the initial step (Figure 9-2). How the temporal location of the extra pulsed level of AS affected the peak AR would reveal information about how the retinal defocus input is weighted following the initial step in AS.

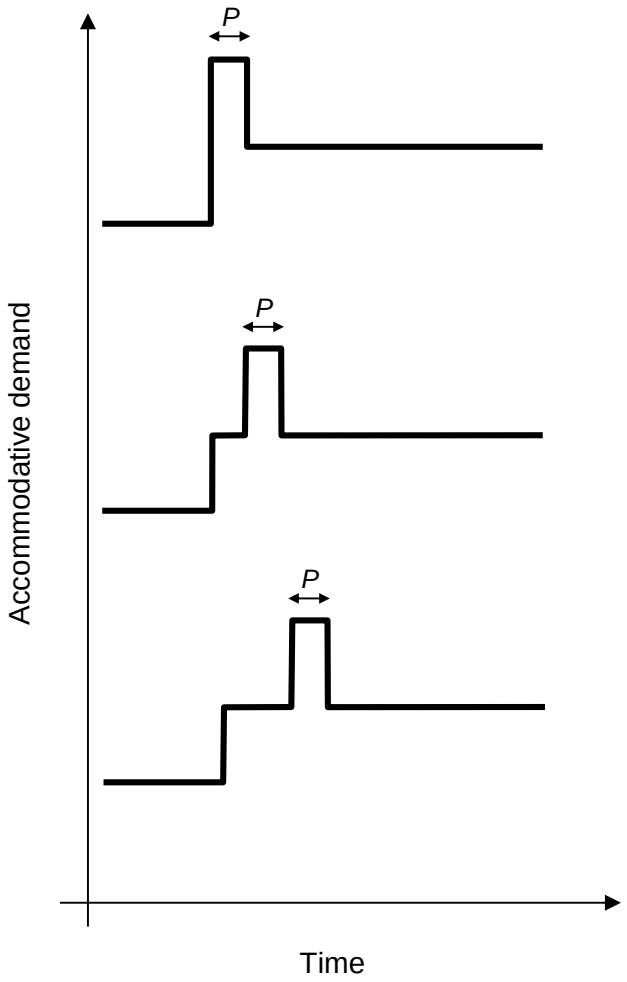

Figure 9-2: Example trials for the experiment on time-weighting of input suggested in the main text. *P* could be 100 ms, for example. If the trials in which the extra pulse in AS occurs earlier demonstrate a weaker peak response, that may indicate that retinal input is weighted, such that earlier information is given less priority than later information, during the latency and onset of accommodation.

The peak AR for a single pulse in AS could also be recorded, for various post-pulse levels of AS (Figure 9-3). Differences in peak AR between the post-pulse levels could reveal inclusion of the post-pulse level of AS in the integration for the response to the intra-pulse level.

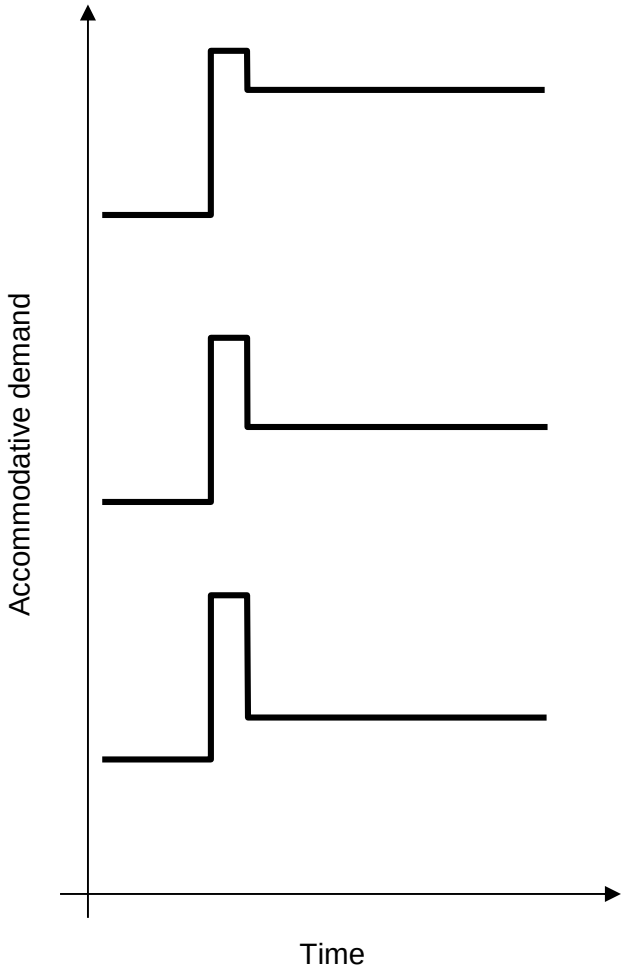

Figure 9-3: Example trials, testing the extent of inclusion of the post-pulse stimulus level in the response of the accommodation system to the pulse in AS.

A minimum halting time for accommodation, combined with an open-loop pulse in acceleration or velocity (see 9.3.1.2 and 9.3.1.3) could explain the stronger response to the second stage of the AS, regardless of the other properties considered here.

9.3.1.6 Further experiments on the effect of auditory cues

In the pilot study of chapter 4, even very brief pulses in AS (duration 0.05 s) were consistently found to elicit a pulse in AR. Further, all AS pulse durations (0.05–0.40 s) unexpectedly resulted in similar durations of the pulse in AR. Pulses providing positive vergence at the eye also stimulated the same,

consistent result. It was suspected that the auditory cue from movements of the DM actuators was playing an important role in these responses.

It would now be simple to test the AR with and without this possible cue, using the masking auditory input through headphones. When the auditory cue of the headphones is masked, the AR is expected to follow the direction of the pulse in AS, and to become weaker or absent for the briefest pulse in AS, compared with the data of chapter 4.

The participant may be conditioned by the auditory cue to the extent that accommodation could be stimulated by auditory input alone, without any change in AS. It may be possible to test this by recording the sound of the DM as the actuators are controlled, and playing the recording back to the participants. Trials with only playback of the recording would be randomly interspersed within control trials where the DM provides a pulse in AS. The participants should be unaware of the hypothesis. It may be that the recording of the sound generated by the DM is not sufficiently representative. Instead, the workstation could provide audio input which was simultaneous with changes in the AS during control trials, and identical input, without changes in AS, in the experimental trials.

9.3.2 Future experiments on accommodation and aberration manipulation

The binocular instrument of chapters 7 and 8 was designed with three initial areas of experimentation in mind. Two of these are analogous to the monocular work of Chin (2009), some of which is reported in Chin et al. (2009a), Chin et al. (2009b) and Hampson et al. (2010). They involve the modification (correction, inversion and doubling) of aberrations of one eye, while the fellow eye remains

uncorrected. Binocular summation when defocus (Plainis et al., 2011) and simulated HOAs (Fam and Lim, 2004) are imposed suggest that HOAs affect true, binocular vision, including accommodation, in as yet unidentified ways. These investigations are currently only possible using the binocular AO instrument of this thesis.

In one set of experiments, the static AR is measured with the various modifications to the aberrations of one eye. The effect on the static accommodative error, and microfluctuations (RMS amplitude, frequency components) would be observable. Correction of the HOAs may lead to more accurate accommodation. On the other hand, the HOAs may be part of useful feedback from microfluctuations of accommodation. If these cues are incongruous between the eyes, the result may be an increase in the RMS amplitude of the fluctuations, as previously observed for weaker cues from accommodative stimuli (see section 1.4.3). It is hypothesised that the state of HOAs in the dominant eye will have a stronger effect on the AR.

In the second set of experiments, the aberrations of one eye (apart from defocus) are to be modified during dynamic accommodation. Steps and sinusoidal oscillations are planned for the AS. Response timings, gain and phase (for sinusoidal stimuli) of the AR would be analysed. Again, the HOAs may be part of useful information for the accommodative system, as found monocularly for some subjects by Chen et al. (2006) and Chin et al. (2009b). They are hypothesised to be more important in the dominant eye. Correcting the HOAs of both eyes is also planned, and a stronger effect on the response properties is expected.

The third set of experiments involved putting the retinal blur (accommodation) and horizontal image positions (convergence) into conflict, and measuring the effect on the accommodation system. A degree of static accommodative error is expected to arise from the connection between convergence and accommodation control. It will be useful to measure this defocus, considering the recent introduction of handheld devices for displaying stereoscopic and autostereoscopic images and video, and the general trend towards increased use of 3-D images and video. Increases in the amplitude of the microfluctuations are expected, in defocus and in HOAs, as an indicator of stress on the accommodative system. Correcting HOAs in this conflicting situation may be detrimental to stable accommodation, leading to increased fluctuations, since HOAs increase the depth of field of the eye (Marcos et al., 1999) and therefore tolerance to defocus.

In the future, it should be confirmed that the monocular and binocular AO instruments of this thesis produce the same results when experiments are transferred between them (in monocular vision). Accommodation properties found in monocular vision can be tested for their relevance to normal, binocular vision. On the other hand, where monocular data are found to usefully reflect results from binocular vision, use of the eye channel of the two-channel monocular system may be beneficial for more direct interpretation of the accommodation response, including HOAs.

9.3.3 New experiment on the function of microfluctuations

The low frequency component of the natural microfluctuations of accommodation is assumed to provide constant feedback to accommodation

control. Exploring their effect on null or incorrect decisions of accommodation has been suggested above (section 9.3.1.4).

Using the AO instruments of this thesis, it is possible to cancel out the effect of the microfluctuations on retinal blur and observe the consequent AR. The DMs can provide the opposite change in defocus to that resulting from the microfluctuations. In static accommodation, this may result in large drifts, as the fluctuations increase in amplitude, seeking feedback. If the oscillations of the fluctuations are directly controlled in a closed-loop, blur-driven feedback system, they may no longer oscillate.

Furthermore, the effect of defocus changes from the microfluctuations can be cancelled out during the beginning of the application of a ramp in AS. If $AS_0(f)$ is a reference dynamic AS, f is frame number, and $AR(f)$ describes the measured accommodation, the following algorithm generates cancellation of the fluctuations in defocus from the microfluctuations:

$$AS_{exp}(f + 1) = AR(f) – AS_0(1) + AS_0(f + 1),$$

where $AS_{exp}(f)$ is the experimentally produced variation of vergence at the eye, using the DM. The required reference AS (static, then ramp) is simply added to the current AR, which includes the microfluctuations. Cancellation of the microfluctuations must lag one frame behind the actual properties, although the monocular system of chapter 3 has a frame time of 0.05 s, which may be adequate.

Realistically,

$$AS_{exp}(f + 1) = g\cdot[AR(f) - AS_0(1)] + AS_0(f + 1),$$

where *g* is the gain (< 1) chosen experimentally for the AO arrangement, resulting in stability of the system, but less perfect correction of defocus.

When accommodation began to respond to the ramp in $AS_0(f)$, a positive feedback loop would be set up. The system would soon become unable to support the required increases in AS_{exp} and the trial would be stopped. However, the study of Hung and Ciuffreda (1988) displayed interesting step and ramp behaviour in the response to ramps in AS, with different latency periods for AR, depending on the slope of the ramp (see section 1.4.4). In this experiment, it would be possible to test the role of changing defocus from the low-frequency microfluctuations in the decision to respond to discrepancies in defocus. Deprived of the more rapid information from the fluctuations—modulations of defocus, or rate of change of defocus (Gray et al., 1993)—initial responses to ramped stimuli may be delayed.

So, with either a static or dynamic AS, it may be possible to observe a change in AR as a direct result of cancelling out (or otherwise modifying) defocus modulations provided by the microfluctuations.

9.3.4 Experiments including refractive error

Investigations following immediately from this work would appear to concern more accurate understanding of accommodation in general. However, it is desired to contribute to the effort to understand myopia prevalence and severity, and therefore future work should also address associations of variations in accommodation control with refractive error.

For instance, are HOAs more or less important to myopes than to emmetropes as a cue to accommodation? Do myopes demonstrate more incorrect or null accommodation decisions than emmetropes? Do the timings of the responses

to rapid changes in stimulus differ between refractive groups? Section 1.4 reviews some examples of the relative inaccuracy of accommodation in myopes, in different ways. Comparisons of progressing and late-onset myopes with stable and early-onset myopes, respectively (again in section 1.4), also reveal interesting properties; characteristics of progressing and late-onset myopes are considered to be more closely or more recently linked to environmentally induced refractive error.

9.4 Final summary

In the pursuit of understanding of myopia onset and progression—with a current myopia “epidemic” in East Asia, and increasing prevalence in much of the world—research into accommodation control was undertaken.

Two instruments have been developed to this end, which use adaptive optics to measure ocular aberrations, including changes in the power of the accommodating eye. They simultaneously provide control of visual stimuli which can include changes in dioptric stimulus, stimulus to convergence, and modification of HOAs (e.g. correction of the HOAs of the eye).

One was a monocular instrument; development involved modifications and realignment which improved a previously functioning apparatus (Hampson et al., 2009). It is now of increased use for investigations of the accommodation response, including with modifications of HOAs. It was used for the experiment of chapter 6, also published as Curd et al. (2013a), with preliminary findings presented as Curd et al. (2013b).

The other was a new, unique, binocular instrument, providing a stereoscopic stimulus, also including horizontal motion of stimulus images, providing a cue to

converge. The stimuli for the two eyes can be manipulated independently. This system was developed from a rough layout on an optical bench to a functioning apparatus, taking data on human participants. There remain improvements to be made, in order to perform experiments with the same reliability as the monocular apparatus, but it allows many interesting investigations of accommodation, ocular HOAs, and convergence, in binocular vision.

An interesting pilot study and a detailed experiment were carried out on the accommodation response to rapid changes in dioptric stimulus. In the pilot study, on single pulses in dioptric stimulus, it appeared that auditory signals can be strong cues to accommodate, and also that there may be more to learn about the responses to such stimuli. The pulses in the accommodation response did not appear to have the same duration as the stimulus pulses, contrary to previous research, which mostly involved pulses of longer duration.

The detailed experiment explored the response to one period of a square wave in dioptric stimulus. There were several interesting findings; not all of the details will be summarised in this final section.

Firstly, accommodation responded to both halves of the square wave stimulus, even when the whole period was 300 ms (briefer than the latency period). This, combined with the timings of the responses, indicated that different levels of input could be gathered within the latency period, and that a second input could be stored in the accommodation system until a component (e.g. calculation of a signal to send to the ciliary muscle) was free to process it.

Secondly, the response to the second half of the square wave stimulus had a tendency to be sometimes stronger than the first; explanations and further experiments were suggested.

Third, accommodation sometimes occurred in the opposite directions to the changes in stimulus, and sometimes to only one or neither stage of the stimulus. A possible connection with the microfluctuations was speculated upon and an experiment proposed.

Finally, a minimum halting time for an accommodation response, once it has been triggered, may have been indicated, at about 0.6 s. A further experiment is also proposed to test for this limit to the control system.

Several questions are now open to investigation as continuation of this research. Some arise from the experimental studies of this thesis; some remain outstanding as the motivation for the design of the binocular AO instrument; some new possibilities suggest themselves, as the combined properties of these instruments and ocular accommodation are considered. It is hoped that the work of these chapters may contribute in some small, but significant, way to the future understanding of accommodation, and eventually myopia.

References

Abbott, M. L., Schmid, K. L. & Strang, N. C. (1998) Differences in the accommodation stimulus response curves of adult myopes and emmetropes. *Ophthalmic Physiol Opt.* 18**,** 13–20.

Adams, D. W. & McBrien, N. A. (1992) Prevalence of myopia and myopic progression in a population of clinical microscopists. *Optom Vis Sci.* 69**,** 467–473.

Adler, D. & Millodot, M. (2006) The possible effect of undercorrection on myopic progression in children. *Clin Exp Optom.* 89**,** 315–321.

Applegate, R. A., Ballentine, C., Gross, H., Sarver, E. J. & Sarver, C. A. (2003) Visual acuity as a function of Zernike mode and level of root mean square error. *Optom Vis Sci.* 80**,** 97–105.

Artal, P., Benito, A. & Tabernero, J. (2006) The human eye is an example of robust optical design. *J Vis.* 6(1): 1. DOI: 10.1167/6.1.1

Artal, P., Berrio, E., Guirao, A. & Piers, P. (2002) Contribution of the cornea and internal surfaces to the change of ocular aberrations with age. *J Opt Soc Am A Opt Image Sci Vis.* 19**,** 137–143.

Artal, P., Chen, L., Fernandez, E. J., Singer, B., Manzanera, S. & Williams, D. R. (2004) Neural compensation for the eye's optical aberrations. *J Vis.* 4(4): 4. DOI: 10.1167/4.4.4.

Artal, P., Guirao, A., Berrio, E. & Williams, D. R. (2001) Compensation of corneal aberrations by the internal optics in the human eye. *J Vis.* 1(1): 1. DOI: 10.1167/1.1.1.

Association of Optometrists (2014) *Vision Standards*. Available from *http://www.aop.org.uk/practitioner-advice/vision-standards*. Accessed 13 Jan 2014.

Atchison, D. A. & Smith, G. (2004) Possible errors in determining axial length changes during accommodation with the IOLMaster. *Optom Vis Sci.* 81**,** 283–286.

Baird, P. N., Schache, M. & Dirani, M. (2010) The GEnes in Myopia (GEM) study in understanding the aetiology of refractive errors. *Prog Retin Eye Res.* 29**,** 520–542.

Becker, W. & Jurgens, R. (1979) An analysis of the saccadic system by means of double step stimuli. *Vision Res.* 19**,** 967–983.

Bharadwaj, S. R. & Schor, C. M. (2005) Acceleration characteristics of human ocular accommodation. *Vision Res.* 45**,** 17–28.

Bharadwaj, S. R. & Schor, C. M. (2006a) Dynamic control of ocular disaccommodation: First and second-order dynamics. *Vision Res.* 46**,** 1019–1037.

Bharadwaj, S. R. & Schor, C. M. (2006b) Initial destination of the disaccommodation step response. *Vision Res.* 46**,** 1959–1972.

Bharadwaj, S. R., Vedamurthy, I. & Schor, C. M. (2009) Short-term adaptive modification of dynamic ocular accommodation. *Invest Ophthalmol Vis Sci.* 50**,** 3520–3528.

British Standards Institution (2009) *BS EN 60825-1:2007 Safety of laser products — Part 1: Equipment classification and requirements*. London: British Standards Institution.

Buehren, T., Collins, M. J. & Carney, L. G. (2005) Near work induced wavefront aberrations in myopia. *Vision Res.* 45**,** 1297–1312.

Buehren, T., Iskander, D. R., Collins, M. J. & Davis, B. (2007) Potential higher-order aberration cues for sphero-cylindrical refractive error development. *Optom Vis Sci.* 84**,** 163–174.

Bullimore, M. A. (2014) Myopia control: the time is now. *Ophthalmic Physiol Opt.* 34, 263–266.

Campbell, F. W. (1960) Correlation of accommodation between the two eyes. *J Opt Soc Am.* 50**,** 738.

Campbell, F. W. & Green, D. G. (1965) Monocular versus binocular visual acuity. *Nature.* 208**,** 191–192.

Campbell, F. W., Robson, J. G. & Westheimer, G. (1959) Fluctuations of accommodation under steady viewing conditions. *J Physiol.* 145**,** 579–594.

Campbell, F. W. & Westheimer, G. (1960) Dynamics of accommodation responses of the human eye. *J Physiol.* 151**,** 285–295.

Canty, A. & Ripley, B. (2013) *boot: Bootstrap R (S-Plus) Functions. R package version 1.3–9*. Available from http://cran.rproject.org/web/packages/boot/index.html. Accessed 27 Apr 2014.

Carroll, J. P. (1981) Regression curves for the optical parameters of the eye. *Am J Optom Physiol Opt.* 58**,** 314–323.

Castejon-Mochon, J. F., Lopez-Gil, N., Benito, A. & Artal, P. (2002) Ocular wave-front aberration statistics in a normal young population. *Vision Res.* 42**,** 1611–1617.

Chen, L., Kruger, P. B., Hofer, H., Singer, B. & Williams, D. R. (2006) Accommodation with higher-order monochromatic aberrations corrected with adaptive optics. *J Opt Soc Am A Opt Image Sci Vis.* 23**,** 1–8.

Chen, X., Sankaridurg, P., Donovan, L., Lin, Z., Li, L., Martinez, A., Holden, B. & Ge, J. (2010) Characteristics of peripheral refractive errors of myopic and non-myopic Chinese eyes. *Vision Res.* 50**,** 31–35.

Cheng, X., Bradley, A., Hong, X. & Thibos, L. N. (2003) Relationship between refractive error and monochromatic aberrations of the eye. *Optom Vis Sci.* 80**,** 43–49.

Chin, S. S. (2009) *Adaptive optics, aberration dynamics and accommodation control.* PhD Thesis. Bradford School of Optometry and Vision Science, School of Life Sciences, University of Bradford.

Chin, S. S., Hampson, K. M. & Mallen, E. A. H. (2008) Binocular correlation of ocular aberration dynamics. *Opt Express.* 16**,** 14731–14745.

Chin, S. S., Hampson, K. M. & Mallen, E. A. H. (2009a) Effect of correction of ocular aberration dynamics on the accommodation response to a sinusoidally moving stimulus. *Opt Lett.* 34**,** 3274–3276.

Chin, S. S., Hampson, K. M. & Mallen, E. A. H. (2009b) Role of ocular aberrations in dynamic accommodation control. *Clin Exp Optom.* 92**,** 227–237.

Chung, K., Mohidin, N. & O'Leary, D. J. (2002) Undercorrection of myopia enhances rather than inhibits myopia progression. *Vision Res.* 42**,** 2555–2559.

Ciuffreda, K. J. & Wallis, D. M. (1998) Myopes show increased susceptibility to nearwork aftereffects. *Invest Ophthalmol Vis Sci.* 39**,** 1797–1803.

Collins, M. J., Buehren, T. & Iskander, D. R. (2006) Retinal image quality, reading and myopia. *Vision Res.* 46**,** 196–215.

Cordain, L., Eaton, S. B., Brand Miller, J., Lindeberg, S. & Jensen, C. (2002) An evolutionary analysis of the aetiology and pathogenesis of juvenile-onset myopia. *Acta Ophthalmol Scand.* 80**,** 125–135.

Cubalchini, R. (1979) Modal wavefront estimation from phase derivative measurements. *J Opt Soc Am.* 69**,** 973–977.

Curd, A. P., Hampson, K. M. & Mallen, E. A. (2013a) Processing blur of conflicting stimuli during the latency and onset of accommodation. *Vision Res.* 92**,** 75–84.

Curd, A., Hampson, K. & Mallen, E. (2013b) Suppression in the accommodative response to short-duration changes in dioptric stimulus. *Invest Ophthalmol Vis Sci.* 54**,** ARVO E-Abstract 4262.

Dandona, R., Dandona, L., Naduvilath, T. J., Srinivas, M., McCarty, C. A. & Rao, G. N. (1999) Refractive errors in an urban population in Southern India: the Andhra Pradesh Eye Disease Study. *Invest Ophthalmol Vis Sci.* 40**,** 2810–2818.

Dandona, R., Dandona, L., Srinivas, M., Sahare, P., Narsaiah, S., Munoz, S. R., Pokharel, G. P. & Ellwein, L. B. (2002) Refractive error in children in a rural population in India. *Invest Ophthalmol Vis Sci.* 43**,** 615–622.

Davison, A. C. & Hinkley, D. V. (1997) *Bootstrap Methods and Their Applications*. Cambridge: Cambridge University Press.

Day, M., Seidel, D., Gray, L. S. & Strang, N. C. (2009) The effect of modulating ocular depth of focus upon accommodation microfluctuations in myopic and emmetropic subjects. *Vision Res.* 49**,** 211–218.

Day, M., Strang, N. C., Seidel, D., Gray, L. S. & Mallen, E. A. (2006) Refractive group differences in accommodation microfluctuations with changing accommodation stimulus. *Ophthalmic Physiol Opt.* 26**,** 88–96.

Dirani, M., Chamberlain, M., Shekar, S. N., Islam, A. F., Garoufalis, P., Chen, C. Y., Guymer, R. H. & Baird, P. N. (2006) Heritability of refractive error and ocular biometrics: the Genes in Myopia (GEM) twin study. *Invest Ophthalmol Vis Sci.* 47**,** 4756–4761.

Dirani, M., Tong, L., Gazzard, G., Zhang, X., Chia, A., Young, T. L., Rose, K. A., Mitchell, P. & Saw, S. M. (2009) Outdoor activity and myopia in Singapore teenage children. *Br J Ophthalmol.* 93**,** 997–1000.

Drexler, W., Findl, O., Schmetterer, L., Hitzenberger, C. K. & Fercher, A. F. (1998) Eye elongation during accommodation in humans: differences between emmetropes and myopes. *Invest Ophthalmol Vis Sci.* 39**,** 2140–2147.

Drexler, W., Morgner, U., Ghanta, R. K., Kartner, F. X., Schuman, J. S. & Fujimoto, J. G. (2001) Ultrahigh-resolution ophthalmic optical coherence tomography. *Nat Med.* 7**,** 502–507.

Dubra, A. (2007) Wavefront sensor and wavefront corrector matching in adaptive optics. *Opt Express.* 15**,** 2762–2769.

Ebenholtz, S. M. (1983) Accommodative hysteresis: a precursor for induced myopia? *Invest Ophthalmol Vis Sci.* 24**,** 513–515.

Edwards, M. H. (1998) Myopia: definition, classifications and economic implications. In Rosenfield, M. & Gilmartin, B. (eds.) *Myopia and nearwork*. Oxford: Butterworth-Heinemann.

Efron, B. (1979) Bootstrap methods: another look at the jackknife. *Ann Stat.* 7**,** 1–26.

Efron, B. (1987) Better bootstrap confidence intervals. *J Am Stat Assoc.* 82**,** 171–185.

Ehrlich, D. L. (1987) Near vision stress — vergence adaptation and accommodative fatigue. *Ophthalmic Physiol Opt.* 7**,** 353–357.

Ehsaei, A., Mallen, E. A., Chisholm, C. M. & Pacey, I. E. (2011) Cross-sectional sample of peripheral refraction in four meridians in myopes and emmetropes. *Invest Ophthalmol Vis Sci.* 52**,** 7574–7585.

Fam, H. B. & Lim, K. L. (2004) Effect of higher-order wavefront aberrations on binocular summation. *J Refract Surg.* 20**,** S570–575.

Faria-Ribeiro, M., Queiros, A., Lopes-Ferreira, D., Jorge, J. & Gonzalez-Meijome, J. M. (2013) Peripheral refraction and retinal contour in stable and progressive myopia. *Optom Vis Sci.* 90**,** 9–15.

Fernandez, E. J. & Artal, P. (2005) Study on the effects of monochromatic aberrations in the accommodation response by using adaptive optics. *J Opt Soc Am A Opt Image Sci Vis.* 22**,** 1732–1738.

Fernandez, E. J., Prieto, P. M. & Artal, P. (2009) Binocular adaptive optics visual simulator. *Opt Lett.* 34**,** 2628–2630.

Fernandez, E. J., Vabre, L., Hermann, B., Unterhuber, A., Povazay, B. & Drexler, W. (2006) Adaptive optics with a magnetic deformable mirror: applications in the human eye. *Opt Express.* 14**,** 8900–8917.

Fincham, E. F. (1951) The accommodation reflex and its stimulus. *Br J Ophthalmol.* 35**,** 381–393.

Fincham, E. F. (1953) Factors controlling ocular accommodation. *Br Med Bull.* 9**,** 18–21.

Flexible Optical B.V. (2014) *Piezoelectric DM*. Available from *http://www.okotech.com/pdm*. Accessed 25 Apr 2014.

Foulds, W. S., Barathi, V. A. & Luu, C. D. (2013) Progressive myopia or hyperopia can be induced in chicks and reversed by manipulation of the chromaticity of ambient light. *Invest Ophthalmol Vis Sci.* 54**,** 8004–8012.

Gambra, E., Sawides, L., Dorronsoro, C. & Marcos, S. (2009) Accommodative lag and fluctuations when optical aberrations are manipulated. *J Vis.* 9(6): 4. DOI: 10.1167/9.6.4.

Garner, L. F., Owens, H., Kinnear, R. F. & Frith, M. J. (1999) Prevalence of myopia in Sherpa and Tibetan children in Nepal. *Optom Vis Sci.* 76**,** 282–285.

Goldschmidt, E. (1968) On the etiology of myopia. An epidemiological study. *Acta Ophthalmol (Copenh).* 98**,** Suppl. 1–172.

Goldschmidt, E. (2003) The mystery of myopia. *Acta Ophthalmol Scand.* 81**,** 431–436.

Gray, L. S., Winn, B. & Gilmartin, B. (1993) Effect of target luminance on microfluctuations of accommodation. *Ophthalmic Physiol Opt.* 13**,** 258–265.

Grosvenor, T. (2003) Why is there an epidemic of myopia? *Clin Exp Optom.* 86**,** 273–275.

Gwiazda, J., Thorn, F., Bauer, J. & Held, R. (1993) Myopic children show insufficient accommodative response to blur. *Invest Ophthalmol Vis Sci.* 34**,** 690–694.

Gwiazda, J., Hyman, L., Hussein, M., Everett, D., Norton, T. T., Kurtz, D., Leske, M. C., Manny, R., Marsh-Tootle, W. & Scheiman, M. (2003) A randomized clinical trial of progressive addition lenses versus single vision lenses on the progression of myopia in children. *Invest Ophthalmol Vis Sci*. 44, 1492–1500.

Hampson, K. M., Chin, S. S. & Mallen, E. A. H. (2009) Dual wavefront sensing channel monocular adaptive optics system for accommodation studies. *Opt Express.* 17**,** 18229–18240.

Hampson, K. M., Chin, S. S. & Mallen, E. A. H. (2010) Effect of temporal location of correction of monochromatic aberrations on the dynamic accommodation response. *Biomed Opt Express.* 1**,** 879–894.

Han, W., Kwan, W., Wang, J., Yip, S. P. & Yap, M. (2007) Influence of eyelid position on wavefront aberrations. *Ophthalmic Physiol Opt.* 27**,** 66–75.

Harb, E., Thorn, F. & Troilo, D. (2006) Characteristics of accommodative behavior during sustained reading in emmetropes and myopes. *Vision Res.* 46**,** 2581–2592.

Hartwig, A. & Atchison, D. A. (2012) Analysis of higher-order aberrations in a large clinical population. *Invest Ophthalmol Vis Sci.* 53**,** 7862–7870.

Hayashi, K., Ohno-Matsui, K., Shimada, N., Moriyama, M., Kojima, A., Hayashi, W., Yasuzumi, K., Nagaoka, N., Saka, N., Yoshida, T., et al. (2010) Long-term pattern of progression of myopic maculopathy: a natural history study. *Ophthalmology.* 117**,** 1595–1611.

He, J. C., Burns, S. A. & Marcos, S. (2000) Monochromatic aberrations in the accommodated human eye. *Vision Res.* 40**,** 41–48.

He, J. C., Gwiazda, J., Thorn, F. & Held, R. (2003) Wave-front aberrations in the anterior corneal surface and the whole eye. *J Opt Soc Am A Opt Image Sci Vis.* 20**,** 1155–1163.

Heron, G. & Schor, C. (1995) The fluctuations of accommodation and aging. *Ophthalmic Physiol Opt*. 15, 445–449.

Ho, M., Liu, D. T., Chan, V. C. & Lam, D. S. (2013) Choroidal thickness measurement in myopic eyes by enhanced depth optical coherence tomography. *Ophthalmology.* 120**,** 1909–1914.

Hofer, H., Artal, P., Singer, B., Aragon, J. L. & Williams, D. R. (2001) Dynamics of the eye's wave aberration. *J Opt Soc Am A Opt Image Sci Vis.* 18**,** 497–506.

Hubel, D. H., Wiesel, T. N. & LeVay, S. (1976) Functional architecture of area 17 in normal and monocularly deprived macaque monkeys. *Cold Spring Harb Symp Quant Biol.* 40**,** 581–589.

Hung, G. K. & Ciuffreda, K. J. (1988) Dual-mode behaviour in the human accommodation system. *Ophthalmic Physiol Opt.* 8**,** 327–332.

Ibi, K. (1997) Characteristics of dynamic accommodation responses: Comparison between the dominant and non-dominant eyes. *Ophthalmic Physiol Opt.* 17**,** 44–54.

Iribarren, R., Morgan, I. G., Chan, Y. H., Lin, X. & Saw, S. M. (2012) Changes in lens power in Singapore Chinese children during refractive development. *Invest Ophthalmol Vis Sci.* 53**,** 5124–5130.

Irving, E. L., Callender, M. G. & Sivak, J. G. (1991) Inducing myopia, hyperopia, and astigmatism in chicks. *Optom Vis Sci.* 68**,** 364–368.

Jiang, B. C. & Morse, S. E. (1999) Oculomotor functions and late-onset myopia. *Ophthalmic Physiol Opt.* 19**,** 165–172.

Jones, L. A., Mitchell, G. L., Mutti, D. O., Hayes, J. R., Moeschberger, M. L. & Zadnik, K. (2005) Comparison of ocular component growth curves among refractive error groups in children. *Invest Ophthalmol Vis Sci.* 46**,** 2317–2327.

Jones-Jordan, L. A., Mitchell, G. L., Cotter, S. A., Kleinstein, R. N., Manny, R. E., Mutti, D. O., Twelker, J. D., Sims, J. R. & Zadnik, K. (2011) Visual activity before and after the onset of juvenile myopia. *Invest Ophthalmol Vis Sci.* 52**,** 1841–1850.

Kasthurirangan, S. & Glasser, A. (2005) Influence of amplitude and starting point on accommodative dynamics in humans. *Invest Ophthalmol Vis Sci.* 46**,** 3463–3472.

Kasthurirangan, S., Vilupuru, A. S. & Glasser, A. (2003) Amplitude dependent accommodative dynamics in humans. *Vision Res.* 43**,** 2945–2956.

Kelly, J. E., Mihashi, T. & Howland, H. C. (2004) Compensation of corneal horizontal/vertical astigmatism, lateral coma, and spherical aberration by internal optics of the eye. *J Vis.* 4(4): 2. DOI: 10.1167/4.4.2.

Kempen, A. H., Mitchell, P., Lee, K. E., Tielsch, J. M., Broman, A. T., Taylor, H. R., Ikram, M. K., Congdon, N. G., O'Colmain, B., Friedman, D. S. (2004) The prevalence of refractive errors among adults in the United States, Western Europe, and Australia. *Arch Ophthalmol.* 122**,** 495–505.

Khosroyani, M. & Hung, G. K. (2002) A dual-mode dynamic model of the human accommodation system. *Bull Math Biol.* 64**,** 285–299.

Kiefer, A. K., Tung, J. Y., Do, C. B., Hinds, D. A., Mountain, J. L., Francke, U. & Eriksson, N. (2013) Genome-wide analysis points to roles for extracellular matrix remodeling, the visual cycle, and neuronal development in myopia. *PloS Genet.* 9(2): e1003299. DOI: 10.1371/journal.pgen.1003299.

Kollbaum, P. S., Jansen, M. E. & Rickert, M. E. (2012) Comparison of patient-reported visual outcome methods to quantify the perceptual effects of defocus. *Cont Lens Anterior Eye.* 35**,** 213–221.

Lee, T. T. & Cho, P. (2013) Relative peripheral refraction in children: twelve-month changes in eyes with different ametropias. *Ophthalmic Physiol Opt.* 33**,** 283–293.

Lee, Y. Y., Lo, C. T., Sheu, S. J. & Lin, J. L. (2013) What factors are associated with myopia in young adults? A survey study in taiwan military conscripts. *Invest Ophthalmol Vis Sci.* 54**,** 1026–1033.

Lim, L. S., Gazzard, G., Low, Y. L., Choo, R., Tan, D. T., Tong, L., Yin Wong, T. & Saw, S. M. (2010) Dietary factors, myopia, and axial dimensions in children. *Ophthalmology.* 117**,** 993–997.e4.

Lopez-Gil, N. & Fernandez-Sanchez, V. (2010) The change of spherical aberration during accommodation and its effect on the accommodation response. *J Vis*. 10(13): 12. DOI: 10.1167/10.13.12.

Lopez-Gil, N., Rucker, F. J., Stark, L. R., Badar, M., Borgovan, T., Burke, S. & Kruger, P. B. (2007) Effect of third-order aberrations on dynamic accommodation. *Vision Res.* 47**,** 755–765.

Ma, F., Dai, J. & Sun, X. (2014) Progress in understanding the association between high myopia and primary open-angle glaucoma. *Clin Exp Ophthalmol.* 42**,** 190–197.

Mallen, E. A., Gammoh, Y., Al-Bdour, M. & Sayegh, F. N. (2005) Refractive error and ocular biometry in Jordanian adults. *Ophthalmic Physiol Opt.* 25**,** 302–309.

Mallen, E. A., Kashyap, P. & Hampson, K. M. (2006) Transient axial length change during the accommodation response in young adults. *Invest Ophthalmol Vis Sci.* 47**,** 1251–1254.

Marcos, S., Moreno, E. & Navarro, R. (1999) The depth-of-field of the human eye from objective and subjective measurements. *Vision Res.* 39**,** 2039–2049.

Marcus, M. W., de Vries, M. M., Junoy Montolio, F. G. & Jansonius, N. M. (2011) Myopia as a risk factor for open-angle glaucoma: A systematic review and meta-analysis. *Ophthalmology.* 118**,** 1989–1994.

Mathworks (2008) *MATLAB 7.7.0.471*. Natick: The MathWorks, Inc.

Mathworks (2011) *MATLAB 7.12.0*. Natick: The MathWorks, Inc.

Matsumura, H. & Hirai, H. (1999) Prevalence of myopia and refractive changes in students from 3 to 17 years of age. *Surv Ophthalmol.* 44**,** S109–115.

Maxwell, J., Tong, J. & Schor, C. M. (2010) The first and second order dynamics of accommodative convergence and disparity convergence. *Vision Res.* 50**,** 1728–1739.

McBrien, N. A. & Millodot, M. (1987) The relationship between tonic accommodation and refractive error. *Invest Ophthalmol Vis Sci.* 28**,** 997–1004.

Mira-Agudelo, A., Lundstrom, L. & Artal, P. (2009) Temporal dynamics of ocular aberrations: monocular vs binocular vision. *Ophthalmic Physiol Opt*. 29, 256–263.

Morgan, I. G. (2003) The biological basis of myopic refractive error. *Clin Exp Optom.* 86**,** 276–288.

Morgan, I. G., Ohno-Matsui, K. & Saw, S. M. (2012) Myopia. *Lancet.* 379**,** 1739–1748.

Morgan, I. & Rose, K. (2005) How genetic is school myopia? *Prog Retin Eye Res.* 24**,** 1–38.

Morgan, R. W., Speakman, J. S. & Grimshaw, S. E. (1975) Inuit myopia: an environmentally induced "epidemic"? *Can Med Assoc J.* 112**,** 575–577.

Mucke, S., Manahilov, V., Strang, N. C., Seidel, D. & Gray, L. S. (2008) New type of perceptual suppression during dynamic ocular accommodation. *Curr Biol.* 18**,** R555–556.

Murthy, G. V., Gupta, S. K., Ellwein, L. B., Munoz, S. R., Pokharel, G. P., Sanga, L. & Bachani, D. (2002) Refractive error in children in an urban population in New Delhi. *Invest Ophthalmol Vis Sci.* 43**,** 623–631.

Mutti, D. O., Hayes, J. R., Mitchell, G. L., Jones, L. A., Moeschberger, M. L., Cotter, S. A., Kleinstein, R. N., Manny, R. E., Twelker, J. D. & Zadnik, K. (2007) Refractive error, axial length, and relative peripheral refractive error before and after the onset of myopia. *Invest Ophthalmol Vis Sci.* 48**,** 2510–2519.

Mutti, D. O., Mitchell, G. L., Moeschberger, M. L., Jones, L. A. & Zadnik, K. (2002) Parental myopia, near work, school achievement, and children's refractive error. *Invest Ophthalmol Vis Sci.* 43**,** 3633–3640.

Mutti, D. O., Mitchell, G. L., Sinnott, L. T., Jones-Jordan, L. A., Moeschberger, M. L., Cotter, S. A., Kleinstein, R. N., Manny, R. E., Twelker, J. D. & Zadnik, K. (2012) Corneal and crystalline lens dimensions before and after myopia onset. *Optom Vis Sci.* 89**,** 251–262.

Mutti, D. O., Sinnott, L. T., Mitchell, G. L., Jones-Jordan, L. A., Moeschberger, M. L., Cotter, S. A., Kleinstein, R. N., Manny, R. E., Twelker, J. D. & Zadnik, K. (2011) Relative peripheral refractive error and the risk of onset and progression of myopia in children. *Invest Ophthalmol Vis Sci.* 52**,** 199–205.

Napper, G. A., Brennan, N. A., Barrington, M., Squires, M. A., Vessey, G. A. & Vingrys, A. J. (1995) The duration of normal visual exposure necessary to prevent form deprivation myopia in chicks. *Vision Res.* 35**,** 1337–1344.

Niwa, K. & Tokoro, T. (1998) Influence of spatial distribution with blur on fluctuations in accommodation. *Optom Vis Sci.* 75**,** 227–232.

Pan, C. W., Ramamurthy, D. & Saw, S. M. (2012a) Worldwide prevalence and risk factors for myopia. *Ophthalmic Physiol Opt.* 32**,** 3–16.

Pan, C. W., Zheng, Y. F., Wong, T. Y., Lavanya, R., Wu, R. Y., Gazzard, G. & Saw, S. M. (2012b) Variation in prevalence of myopia between generations of migrant Indians living in Singapore. *Am J Ophthalmol.* 154**,** 376–381.

Paquin, M. P., Hamam, H. & Simonet, P. (2002) Objective measurement of optical aberrations in myopic eyes. *Optom Vis Sci.* 79**,** 285–291.

Parssinen, O. (2012) The increased prevalence of myopia in Finland. *Acta Ophthalmol.* 90**,** 497–502.

Phillips, S., Shirachi, D. & Stark, L. (1972) Analysis of accommodative response times using histogram information. *Am J Optom Arch Am Acad Optom.* 49**,** 389–400.

Pitman, E. J. G. (1937) Significance tests which may be applied to samples from any populations. *Suppl J R Stat Soc.* 4**,** 119–130.

Plainis, S., Ginis, H. S. & Pallikaris, A. (2005) The effect of ocular aberrations on steady-state errors of accommodative response. *J Vis.* 5(5): 7. DOI: 10.1167/5.5.7.

Plainis, S., Petratou, D., Giannakopoulou, T., Atchison, D. A. & Tsilimbaris, M. K. (2011) Binocular summation improves performance to defocus-induced blur. *Invest Ophthalmol Vis Sci.* 52**,** 2784–2789.

Platt, B. C. & Shack, R. (2001) History and principles of Shack-Hartmann wavefront sensing. *J Refract Surg.* 17**,** S573–577.

Porter, J., Guirao, A., Cox, I. G. & Williams, D. R. (2001) Monochromatic aberrations of the human eye in a large population. *J Opt Soc Am A Opt Image Sci Vis.* 18**,** 1793–1803.

Quek, T. P., Chua, C. G., Chong, C. S., Chong, J. H., Hey, H. W., Lee, J., Lim, Y. F. & Saw, S. M. (2004) Prevalence of refractive errors in teenage high school students in Singapore. *Ophthalmic Physiol Opt.* 24**,** 47–55.

R Development Core Team (2012) *R: A language and environment for statistical computing.* Vienna: R Foundation for Statistical Computing.

Rabin, J., Van Sluyters, R. C. & Malach, R. (1981) Emmetropization: A vision-dependent phenomenon. *Invest Ophthalmol Vis Sci.* 20**,** 561–564.

Rashbass, C. & Westheimer, G. (1961) Disjunctive eye movements. *J Physiol.* 159**,** 339–360.

Read, S. A., Collins, M. J. & Sander, B. P. (2010) Human optical axial length and defocus. *Invest Ophthalmol Vis Sci.* 51**,** 6262–6269.

Read, S. A., Collins, M. J., Vincent, S. J. & Alonso-Caneiro, D. (2013) Choroidal thickness in myopic and nonmyopic children assessed with enhanced depth imaging optical coherence tomography. *Invest Ophthalmol Vis Sci.* 54**,** 7578–7586.

Rizzo, M. L. (2008) *Statistical computing with R*. Boca Raton: Chapman & Hall/CRC.

Roorda, A. (2011) Adaptive optics for studying visual function: a comprehensive review. *J Vis.* 11(5): 6. DOI: 10.1167/11.5.6.

Rose, K. A., Morgan, I. G., Ip, J., Kifley, A., Huynh, S., Smith, W. & Mitchell, P. (2008) Outdoor activity reduces the prevalence of myopia in children. *Ophthalmology.* 115**,** 1279–1285.

Rose, K. A., Morgan, I. G., Smith, W. & Mitchell, P. (2002) High heritability of myopia does not preclude rapid changes in prevalence. *Clin Exp Ophthalmol.* 30**,** 168–172.

Rosenfield, M. (1998) Accommodation and myopia. In Rosenfield, M. & Gilmartin, B. (eds.) *Myopia and nearwork*. Oxford: Butterworth-Heinemann.

Rosenfield, M. & Abraham-Cohen, J. A. (1999) Blur sensitivity in myopes. *Optom Vis Sci.* 76**,** 303–307.

Rosenfield, M. & Gilmartin, B. (eds.) (1998) *Myopia and nearwork*. Oxford: Butterworth-Heinemann.

Sabesan, R., Zheleznyak, L. & Yoon, G. (2012) Binocular visual performance and summation after correcting higher order aberrations. *Biomed Opt Express.* 3**,** 3176–3189.

Santodomingo-Rubido, J., Mallen, E. A. H., Gilmartin, B. & Wolffsohn, J. S. (2002) A new non-contact optical device for ocular biometry. *Br J Ophthalmol.* 86**,** 458–462.

Sarkar, D. (2008) *Lattice: multivariate data visualization with R*. New York: Springer.

Saunders, K. J. (1995) Early refractive development in humans. *Surv Ophthalmol.* 40**,** 207–216.

Saw, S. M. (2003) A synopsis of the prevalence rates and environmental risk factors for myopia. *Clin Exp Optom.* 86**,** 289–294.

Saw, S. M., Chua, W. H., Hong, C. Y., Wu, H. M., Chan, W. Y., Chia, K. S., Stone, R. A. & Tan, D. (2002) Nearwork in early-onset myopia. *Invest Ophthalmol Vis Sci.* 43**,** 332–339.

Saw, S. M., Gazzard, G., Shih-Yen, E. C. & Chua, W. H. (2005) Myopia and associated pathological complications. *Ophthalmic Physiol Opt.* 25**,** 381–391.

Schache, M., Richardson, A. J., Mitchell, P., Wang, J. J., Rochtchina, E., Viswanathan, A. C., Wong, T. Y., Saw, S. M., Topouzis, F., Xie, et al. (2013) Genetic association of refractive error and axial length with 15q14 but not 15q25 in the Blue Mountains Eye Study cohort. *Ophthalmology.* 120**,** 292–297.

Schor, C. M. & Bharadwaj, S. R. (2005) A pulse-step model of accommodation dynamics in the aging eye. *Vision Res.* 45**,** 1237–1254.

Schor, C. M. & Bharadwaj, S. R. (2006) Pulse-step models of control strategies for dynamic ocular accommodation and disaccommodation. *Vision Res.* 46**,** 242–258.

Schor, C. M., Lott, L. A., Pope, D. & Graham, A. D. (1999) Saccades reduce latency and increase velocity of ocular accommodation. *Vision Res.* 39**,** 3769–3795.

Seet, B., Wong, T. Y., Tan, D. T., Saw, S. M., Balakrishnan, V., Lee, L. K. & Lim, A. S. (2001) Myopia in singapore: taking a public health approach. *Br J Ophthalmol.* 85**,** 521–526.

Seidel, D., Gray, L. S. & Heron, G. (2003) Retinotopic accommodation responses in myopia. *Invest Ophthalmol Vis Sci.* 44**,** 1035–1041.

Seidel, D., Gray, L. S. & Heron, G. (2005) The effect of monocular and binocular viewing on the accommodation response to real targets in emmetropia and myopia. *Optom Vis Sci.* 82**,** 279–285.

Shao, Y., Tao, A., Jiang, H., Shen, M., Zhong, J., Lu, F. & Wang, J. (2013) Simultaneous real-time imaging of the ocular anterior segment including the ciliary muscle during accommodation. *Biomed Opt Express.* 4**,** 466–480.

Siegwart, J. T., Jr. & Norton, T. T. (1998) The susceptible period for deprivation-induced myopia in tree shrew. *Vision Res.* 38**,** 3505–3515.

Simensen, B. & Thorud, L. O. (1994) Adult-onset myopia and occupation. *Acta Ophthalmol (Copenh).* 72**,** 469–471.

Skeller, E. (1954) *Anthropological and ophthalmological studies on the Angmagssalik Eskimos*. Copenhagen: C.A. Reitzel.

Smith, E. L., 3rd (1998a) Environmentally induced refractive errors in animals. In Rosenfield, M. & Gilmartin, B. (eds.) *Myopia and nearwork*. Oxford: Butterworth-Heinemann.

Smith, E. L. (1998b) Spectacle lenses and emmetropization: the role of optical defocus in regulating ocular development. *Optom Vis Sci.* 75**,** 388–398.

Smith, E. L. (2013) Optical treatment strategies to slow myopia progression: effects of the visual extent of the optical treatment zone. *Exp Eye Res.* 114**,** 77–88.

Smith, E. L., Huang, J., Hung, L. F., Blasdel, T. L., Humbird, T. L. & Bockhorst, K. H. (2009a) Hemiretinal form deprivation: evidence for local control of eye growth and refractive development in infant monkeys. *Invest Ophthalmol Vis Sci.* 50**,** 5057–5069.

Smith, E. L., 3rd, Hung, L. F. & Huang, J. (2009b) Relative peripheral hyperopic defocus alters central refractive development in infant monkeys. *Vision Res.* 49**,** 2386–2392.

Smith, E. L., Hung, L.-F. & Huang, J. (2012) Protective effects of high ambient lighting on the development of form-deprivation myopia in rhesus monkeys. *Invest Ophthalmol Vis Sci.* 53**,** 421–428.

Smith, E. L., Hung, L. F., Huang, J., Blasdel, T. L., Humbird, T. L. & Bockhorst, K. H. (2010) Effects of optical defocus on refractive development in monkeys: evidence for local, regionally selective mechanisms. *Invest Ophthalmol Vis Sci.* 51**,** 3864–3873.

Smith, E. L., 3rd, Hung, L. F., Kee, C. S. & Qiao, Y. (2002) Effects of brief periods of unrestricted vision on the development of form-deprivation myopia in monkeys. *Invest Ophthalmol Vis Sci.* 43**,** 291–299.

Smith, E. L., 3rd, Kee, C. S., Ramamirtham, R., Qiao-Grider, Y. & Hung, L. F. (2005) Peripheral vision can influence eye growth and refractive development in infant monkeys. *Invest Ophthalmol Vis Sci.* 46**,** 3965–3972.

Sng, C. C. A., Lin, X. Y., Gazzard, G., Chang, B., Dirani, M., Lim, L., Selvaraj, P., Ian, K., Drobe, B., Wong, T. Y. & Saw, S. M. (2011) Change in peripheral refraction over time in Singapore Chinese children. *Invest Ophthalmol Vis Sci.* 52**,** 7880–7887.

Sorsby, A., Benjamin, B. & Sheridan, M. (1961) *Refraction and its components during the growth of the eye from the age of three*. London: HMSO.

Sorsby, A. & Leary, G. A. (1970) *A longitudinal study of refraction and its components during growth*. London: HMSO.

Stark, L. R. & Atchison, D. A. (1997) Pupil size, mean accommodation response and the fluctuations of accommodation. *Ophthalmic Physiol Opt.* 17**,** 316–323.

Stone, R. A., Pendrak, K., Sugimoto, R., Lin, T., Gill, A. S., Capehart, C. & Liu, J. (2006) Local patterns of image degradation differentially affect refraction and eye shape in chick. *Curr Eye Res.* 31**,** 91–105.

Tarrant, J., Roorda, A. & Wildsoet, C. F. (2010) Determining the accommodative response from wavefront aberrations. *J Vis.* 10(5): 4. DOI: 10.1167/10.5.4.

Thibos, L. N., Applegate, R. A., Schwiegerling, J. T., Webb, R. & V.S.I.A Standards Taskforce Members (2002a) Standards for reporting the optical aberrations of eyes. *J Refract Surg.* 18**,** S652–S660.

Thibos, L. N., Bradley, A. & Hong, X. (2002b) A statistical model of the aberration structure of normal, well-corrected eyes. *Ophthalmic Physiol Opt.* 22**,** 427–433.

Thibos, L. N., Hong, X., Bradley, A. & Applegate, R. A. (2004) Accuracy and precision of objective refraction from wavefront aberrations. *J Vis.* 4(4): 9. DOI: 10.1167/4.4.9.

Thibos, L. N., Hong, X., Bradley, A. & Cheng, X. (2002c) Statistical variation of aberration structure and image quality in a normal population of healthy eyes. *J Opt Soc Am A Opt Image Sci Vis.* 19**,** 2329–2348.

Thibos, L. N., Wheeler, W. & Horner, D. (1997) Power vectors: an application of Fourier analysis to the description and statistical analysis of refractive error. *Optom Vis Sci.* 74**,** 367–375.

Troilo, D. & Nickla, D. L. (2005) The response to visual form deprivation differs with age in marmosets. *Invest Ophthalmol Vis Sci.* 46**,** 1873–1881.

Troilo, D. & Wallman, J. (1991) The regulation of eye growth and refractive state: an experimental study of emmetropization. *Vision Res.* 31**,** 1237–1250.

Tyson, R. K. (1997) *Principles of adaptive optics.* 2nd edition. San Diego: Academic Press.

Vera-Diaz, F. A. & Doble, N. (2012) The human eye and adaptive optics. In Tyson, R. K. (ed.) *Topics in adaptive optics*. InTech. DOI: 10.5772/31073.

Vera-Diaz, F. A., Strang, N. C. & Winn, B. (2002) Nearwork induced transient myopia during myopia progression. *Curr Eye Res.* 24**,** 289–295.

Verhoeven, V. J. M., Hysi, P. G., Wojciechowski, R., Fan, Q., Guggenheim, J. A., Hohn, R., MacGregor, S., Hewitt, A. W., Nag, A., Cheng, C. Y., et al. (2013) Genome-wide meta-analyses of multiancestry cohorts identify multiple new susceptibility loci for refractive error and myopia. *Nat Genet.* 45**,** 314–318.

Vincent, S. J., Collins, M. J., Read, S. A. & Carney, L. G. (2013) Retinal and choroidal thickness in myopic anisometropia. *Invest Ophthalmol Vis Sci.* 54**,** 2445–2456.

Vitale, S., Cotch, M. F., Sperduto, R. & Ellwein, L. (2006) Costs of refractive correction of distance vision impairment in the United States, 1999-2002. *Ophthalmology.* 113**,** 2163–2170.

Vitale, S., Sperduto, R. D. & Ferris, F. L., 3rd (2009) Increased prevalence of myopia in the United States between 1971-1972 and 1999-2004. *Arch Ophthalmol.* 127**,** 1632–1639.

Walline, J. J., Lindsley, K., Vedula, S. S., Cotter, S. A., Mutti, D. O. & Twelker, J. D. (2011) Interventions to slow progression of myopia in children. *Cochrane Database Syst Rev* 2011, Issue 12. DOI: 10.1002/14651858.CD004916.pub3.

Wallman, J., Gottlieb, M. D., Rajaram, V. & Fugate-Wentzek, L. A. (1987) Local retinal regions control local eye growth and myopia. *Science.* 237**,** 73–77.

Wang, B. & Ciuffreda, K. J. (2006) Depth-of-focus of the human eye: theory and clinical implications. *Surv Ophthalmol.* 51**,** 75–85.

Webb, R. H., Albanese, M. J., Zhou, Y., Bifano, T. & Burns, S. A. (2004) Stroke amplifier for deformable mirrors. *Appl Opt.* 43**,** 5330–5333.

Wei, W. B., Xu, L., Jonas, J. B., Shao, L., Du, K. F., Wang, S., Chen, C. X., Xu, J., Wang, Y. X., Zhou, J. Q. & You, Q. S. (2013) Subfoveal choroidal thickness: the Beijing Eye Study. *Ophthalmology.* 120**,** 175–180.

Wildsoet, C. F. (1998) Structural correlates of myopia. In Rosenfield, M. & Gilmartin, B. (eds.) *Myopia and nearwork*. Oxford: Butterworth-Heinemann.

Wilson, B. J., Decker, K. E. & Roorda, A. (2002) Monochromatic aberrations provide an odd-error cue to focus direction. *J Opt Soc Am A Opt Image Sci Vis.* 19**,** 833–839.

Wilson, D. (1973) A centre for accommodative vergence motor control. *Vision Res.* 13**,** 2491–2503.

Winn, B. & Gilmartin, B. (1992) Current perspective on microfluctuations of accommodation. *Ophthalmic Physiol Opt.* 12**,** 252–256.

Wolffsohn, J. S., Gilmartin, B., Thomas, R. & Mallen, E. A. (2003) Refractive error, cognitive demand and nearwork-induced transient myopia. *Curr Eye Res.* 27**,** 363–370.

Wu, H. M., Seet, B., Yap, E. P. H., Saw, S. M., Lim, T. H. & Chia, K. S. (2001) Does education explain ethnic differences in myopia prevalence? A population-based study of young adult males in Singapore. *Optom Vis Sci.* 78**,** 234–239.

Wu, J. F., Bi, H. S., Wang, S. M., Hu, Y. Y., Wu, H., Sun, W., Lu, T. L., Wang, X. R. & Jonas, J. B. (2013) Refractive error, visual acuity and causes of vision loss in children in Shandong, China. The Shandong Children Eye Study. *PLoS ONE* 8(12): e82763. DOI: 10.1371/journal.pone.0082763.

Xiang, F., He, M. & Morgan, I. G. (2012a) The impact of parental myopia on myopia in Chinese children: population-based evidence. *Optom Vis Sci.* 89**,** 1487–1496.

Xiang, F., He, M. & Morgan, I. G. (2012b) The impact of severity of parental myopia on myopia in Chinese children. *Optom Vis Sci.* 89**,** 884–891.

Zadnik, K. & Mutti, D. O. (1998) Prevalence of myopia. In Rosenfield, M. & Gilmartin, B. (eds.) *Myopia and nearwork*. Oxford: Butterworth-Heinemann.

Zheng, Y. F., Pan, C. W., Chay, J., Wong, T. Y., Finkelstein, E. & Saw, S. M. (2013) The economic cost of myopia in adults aged over 40 years in singapore. *Invest Ophthalmol Vis Sci.* 54**,** 7532–7537.

Zhou, X., Lu, F., Xie, R., Jiang, L., Wen, J., Li, Y., Shi, J., He, T. & Qu, J. (2007) Recovery from axial myopia induced by a monocularly deprived facemask in adolescent (7-week-old) guinea pigs. *Vision Res.* 47**,** 1103–1111.

Zhu, M., Collins, M. J. & Robert Iskander, D. (2004) Microfluctuations of wavefront aberrations of the eye. *Ophthalmic Physiol Opt.* 24**,** 562–571.

Zhu, M., Collins, M. J. & Robert Iskander, D. (2006) The contribution of accommodation and the ocular surface to the microfluctuations of wavefront aberrations of the eye. *Ophthalmic Physiol Opt*. 26, 439–446.

Zylbermann, R., Landau, D. & Berson, D. (1993) The influence of study habits on myopia in Jewish teenagers. *J Pediatr Ophthalmol Strabismus.* 30**,** 319–322.

Appendix A: Random trial orders generated in R

A.1 The script

This is the script used to generate the sequence of trials for the data of chapter 5. The trial order for chapter 6 was produced similarly. Appendix A.2 contains the sequence generated.

```
# ##random.trials.R

# Trial parameters
durations <- c(0.2,0.35,0.5,1,2)
heights <- c(-2,-1,1,2)
repeats <- 1:5
lengths <- 8
waits <- 1:3

# Columns of parameters,
# providing a trial at each parameter setting and repeat
# (not at each wait)
Dur <- rep(durations, times=length(heights)*length(repeats))
Dur.fs <- Dur/0.05
Amp <- rep(heights, each=length(durations), times=length(repeats))
Rep <- rep(repeats, each=length(durations)*length(heights))
Length <- rep(lengths, length.out=length(Rep))
Wait <- sample(waits, length(Dur), replace=T)

# Length of trial in frames
L.fs <- Length/0.05

# Bind all columns into one data frame
trials <- data.frame(Durn=Dur.fs, Amp, Rep, No.frames=L.fs, Wait)

# Create random order for trials
o <- sample(length(Dur), length(Dur))

# Put trials in the random order
trials <- trials[o,]

# Output to file
write.table(trials, file="Pulse trials 2012-09-05.txt",
        quote=F, sep=" ", row.names=F)
```

A.2 The list of trials

On the next page is the list of trials generated for input of parameters into the GUI, trial by trial, for control of the monocular AO system, for the data collection of chapter 5. A similar list was produced and followed with each subject in the data collection of chapter 6.

“Wait” was counted by the experimenter, not input to the GUI, and “Length” was set at the start of the data collecting session.

Trials were ticked off in a text file as a session progressed. Rejected trials (for blinking) were marked for repetition and run again by the experimenter at a later point in the sequence of trials.

Durn	Amp	Rep	No.frames	Wait	Durn	Amp	Rep	No.frames	Wait
40	1	1	160	2	10	2	2	160	2
4	-2	5	160	1	4	2	3	160	2
40	-1	3	160	1	10	2	1	160	3
10	-2	1	160	2	4	-2	4	160	3
40	2	1	160	1	7	-2	1	160	2
4	-2	3	160	3	4	1	5	160	2
4	-1	2	160	2	10	-1	5	160	2
40	-1	1	160	3	7	1	5	160	1
40	-2	2	160	1	20	2	4	160	2
7	-1	4	160	2	10	-2	4	160	2
20	-1	2	160	3	40	-2	1	160	3
4	-1	4	160	1	4	-1	1	160	3
7	-1	3	160	2	20	-1	4	160	1
4	2	5	160	1	20	2	1	160	3
20	-2	1	160	2	4	2	4	160	3
10	-1	3	160	3	20	-1	1	160	1
40	-2	4	160	3	10	1	3	160	3
4	1	2	160	1	7	1	1	160	3
40	1	2	160	1	4	-2	1	160	1
40	-2	3	160	2	4	-1	3	160	3
20	1	3	160	3	20	1	1	160	2
40	-2	5	160	3	40	2	4	160	3
20	-2	5	160	3	20	1	5	160	3
7	1	4	160	1	7	-2	3	160	3
10	2	3	160	1	10	-1	2	160	1
10	1	4	160	2	10	-1	4	160	3
20	-2	4	160	1	7	2	1	160	1
40	-1	5	160	3	7	2	2	160	1
7	2	5	160	2	20	-2	2	160	3
4	2	2	160	1	20	-1	3	160	1
7	1	3	160	2	7	2	3	160	2
40	1	4	160	2	10	-1	1	160	2
10	2	4	160	3	4	-1	5	160	2
10	-2	2	160	3	40	-1	2	160	2
10	1	5	160	2	20	2	2	160	1
10	-2	3	160	1	4	-2	2	160	2
20	1	4	160	3	10	2	5	160	1
4	1	3	160	2	10	-2	5	160	1
7	1	2	160	3	4	1	1	160	1
40	2	3	160	1	20	2	5	160	2
40	1	5	160	2	20	-2	3	160	2
10	1	1	160	2	7	-2	5	160	3
7	-1	5	160	2	20	-1	5	160	2
7	-2	4	160	1	10	1	2	160	2
40	2	5	160	2	20	2	3	160	3
7	-1	2	160	3	4	1	4	160	1
4	2	1	160	1	20	1	2	160	3
7	-1	1	160	3	40	2	2	160	1
7	2	4	160	2	7	-2	2	160	1
40	-1	4	160	3	40	1	3	160	2

Appendix B: Accommodation data processed in chapter 6

B.1 Raw AR data

The next six pages contain the accommodation recorded in all trials of chapter 6, including the extra trials with no steps in AS (ISI = 0) and with ISI = 2 s. These extra trials were included as checks on the system and to reduce the predictability of the stimuli.

The plots were conveniently created using the “lattice” package in R (Sarkar, 2008). After sorting the accommodation data into a data frame, the following code generates one of the plots below. There are blank, redundant cells in the array of graphs.

```
timeplots.abs <-
        xyplot(defocus ~ time |
        paste(as.factor(Duration), "s ISI") * paste(as.factor(-Step), "D first step"),
                groups=Repeat, data=timeplot.abs.results,
                type="l",
                scales=list(cex=0.7),
                par.strip.text=list(cex=0.6, lines=1),
                col.line=line.cols,
                auto.key=list(text=c("","","Responses","","","Stimulus"), lineheight=0.7,
cex=10/12, lines=T, points=F),
                xlab=list(label="Time / s", cex=11/12),
                ylab=list(label="Accommodation, relative to stimulus baseline / D",
cex=11/12),
                xlim=c(-0.2,8.2),
                )

pushViewport(viewport(width=unit(22, "centimetres"), height=unit(15, "centimetres"),
gp=gpar(fontsize=10)))

print(timeplots.abs, newpage=F)
```

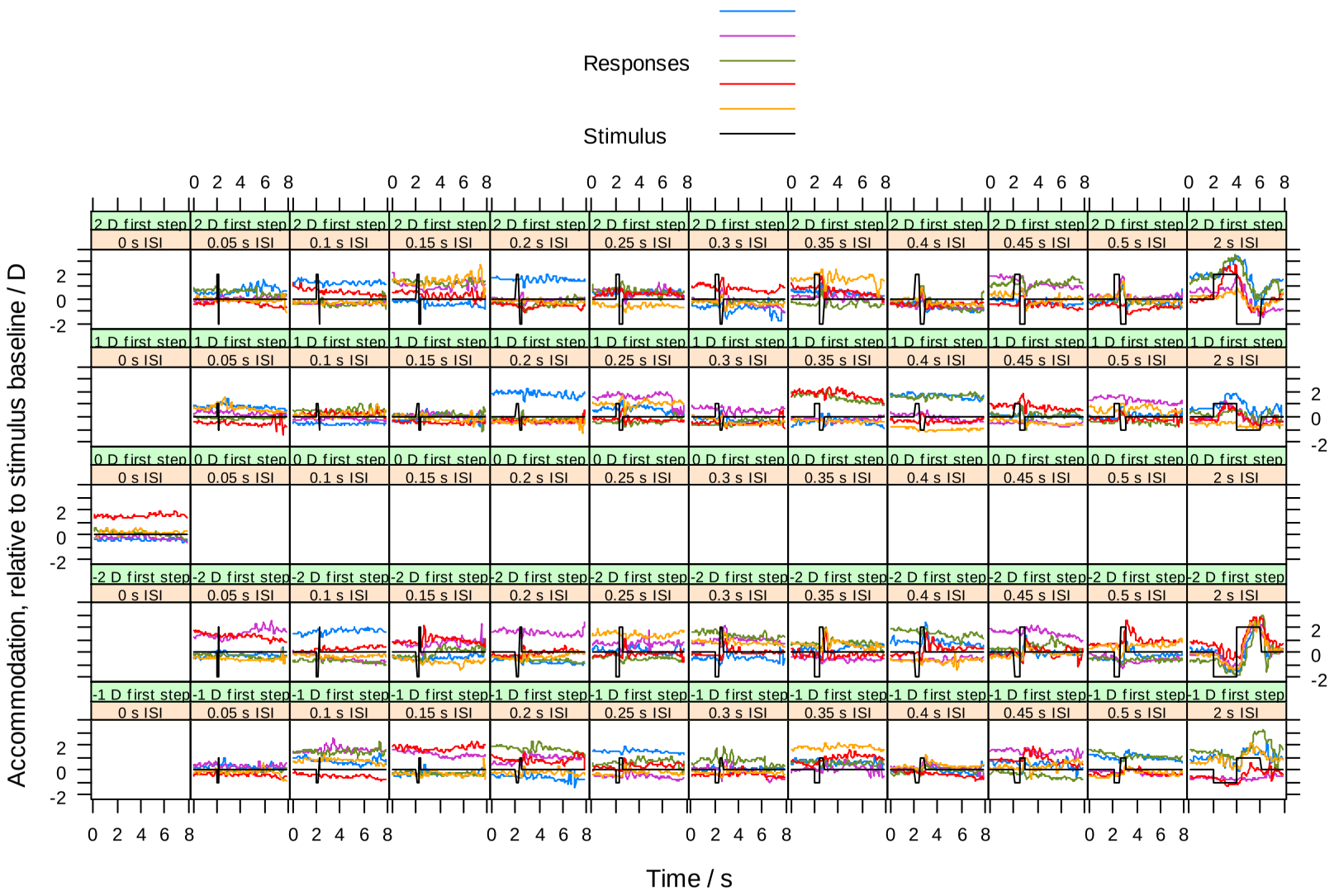
Responses
Stimulus
Accommodation, relative to stimulus baseline / D
Time / s
2 D first step
1 D first step
0 D first step
-2 D first step
-1 D first step
0 s ISI
0.05 s ISI
0.1 s ISI
0.15 s ISI
0.2 s ISI
0.25 s ISI
0.3 s ISI
0.35 s ISI
0.4 s ISI
0.45 s ISI
0.5 s ISI
2 s ISI

Participant 2

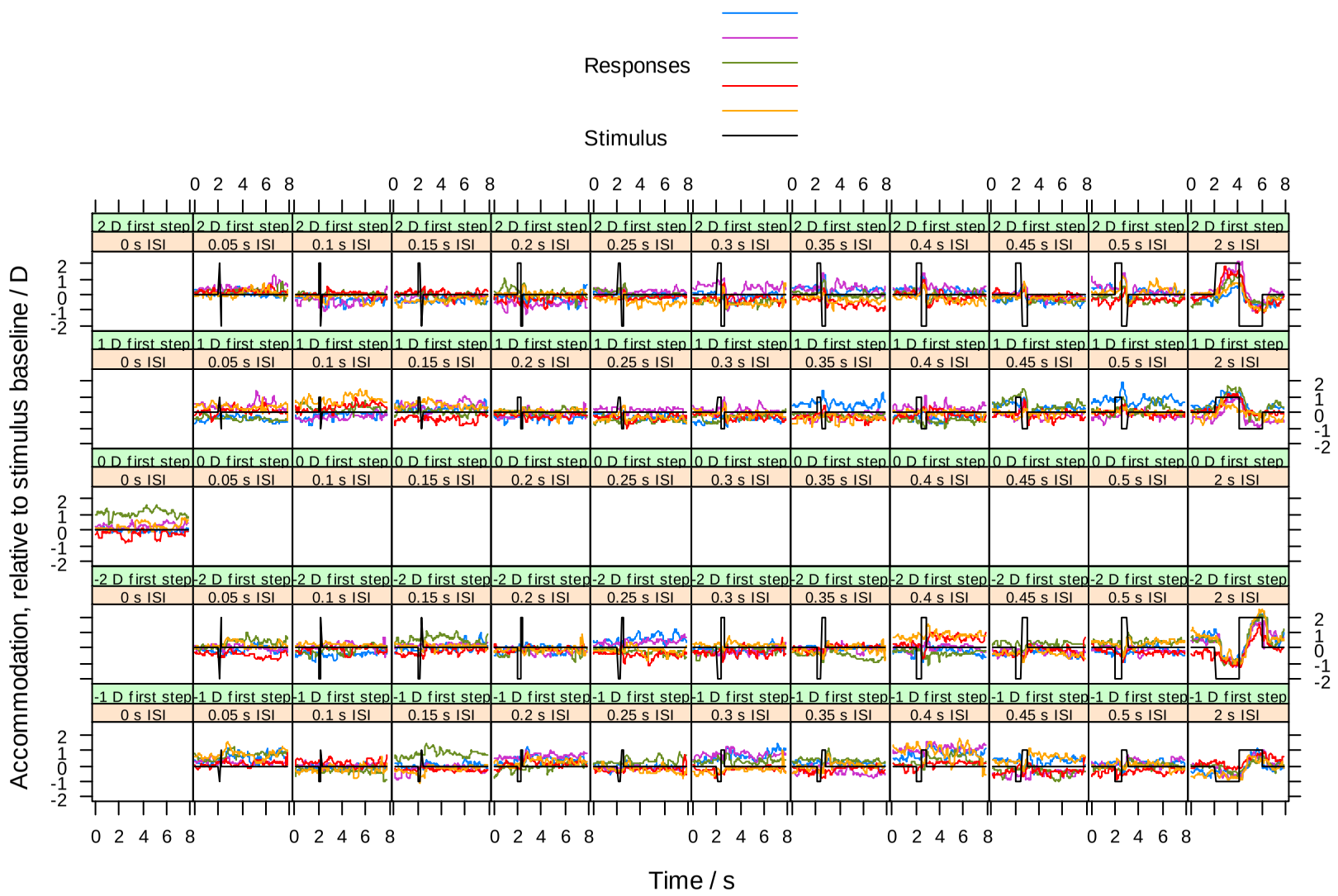

Participant 3

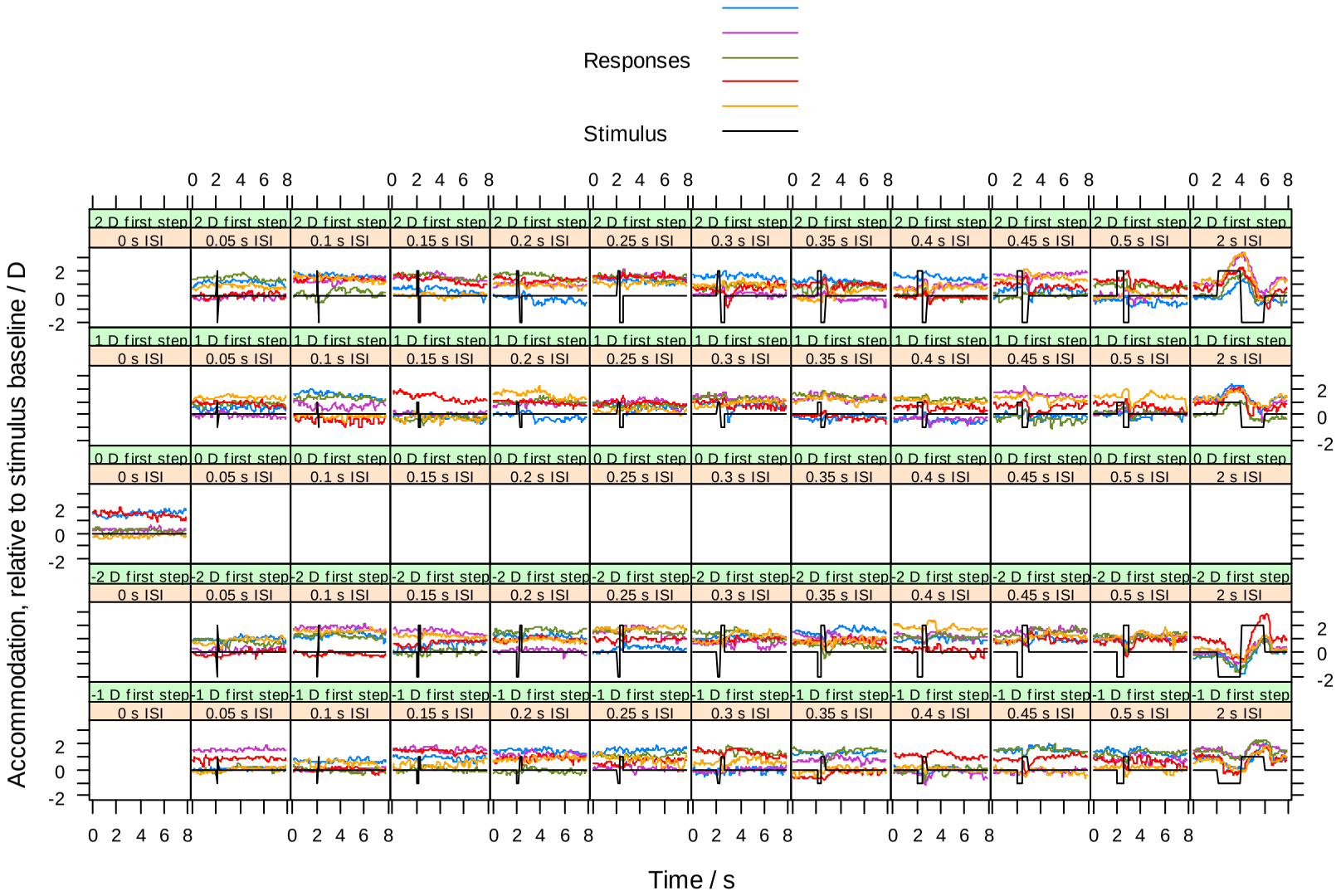

Participant 4

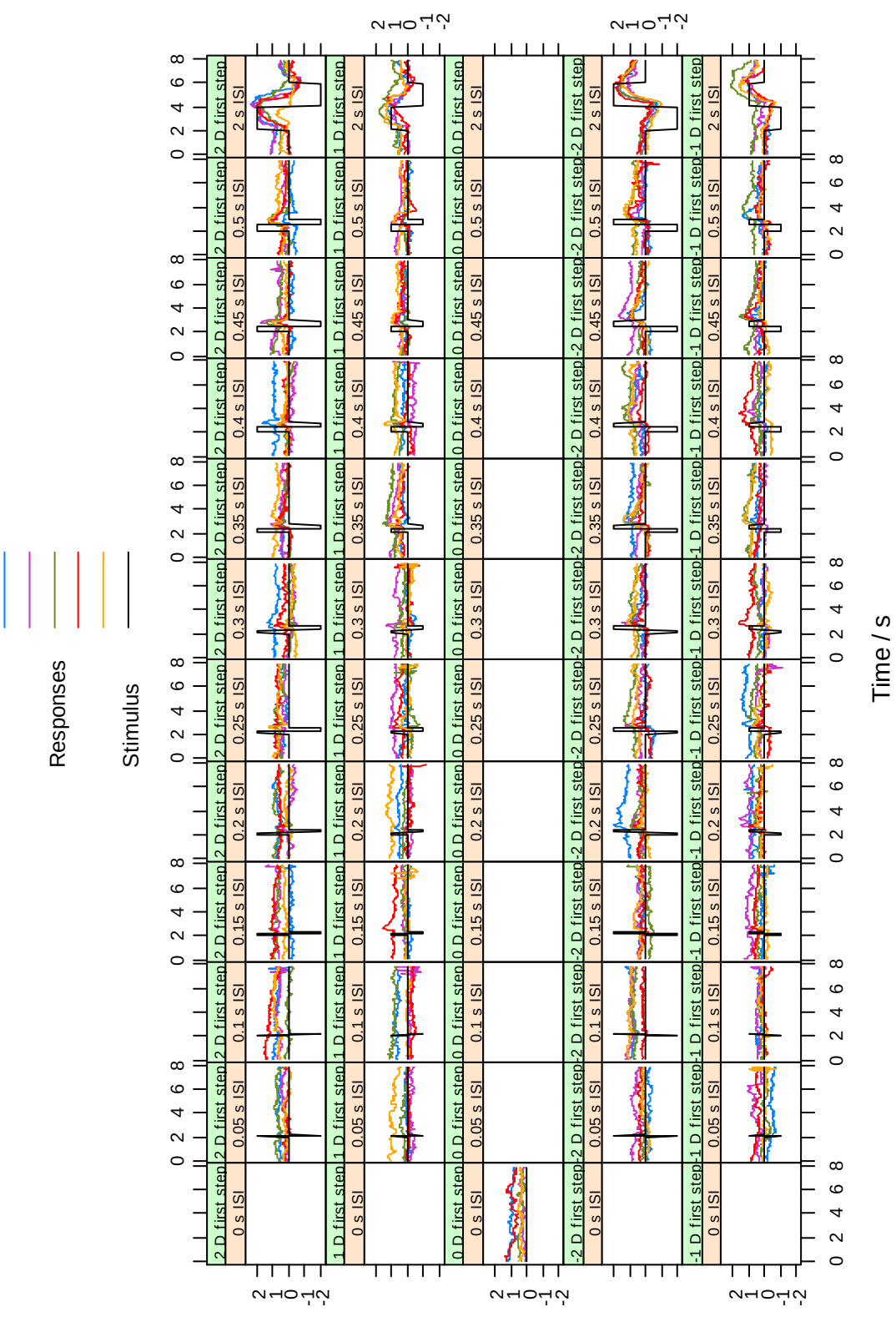

Participant 5

Participant 6

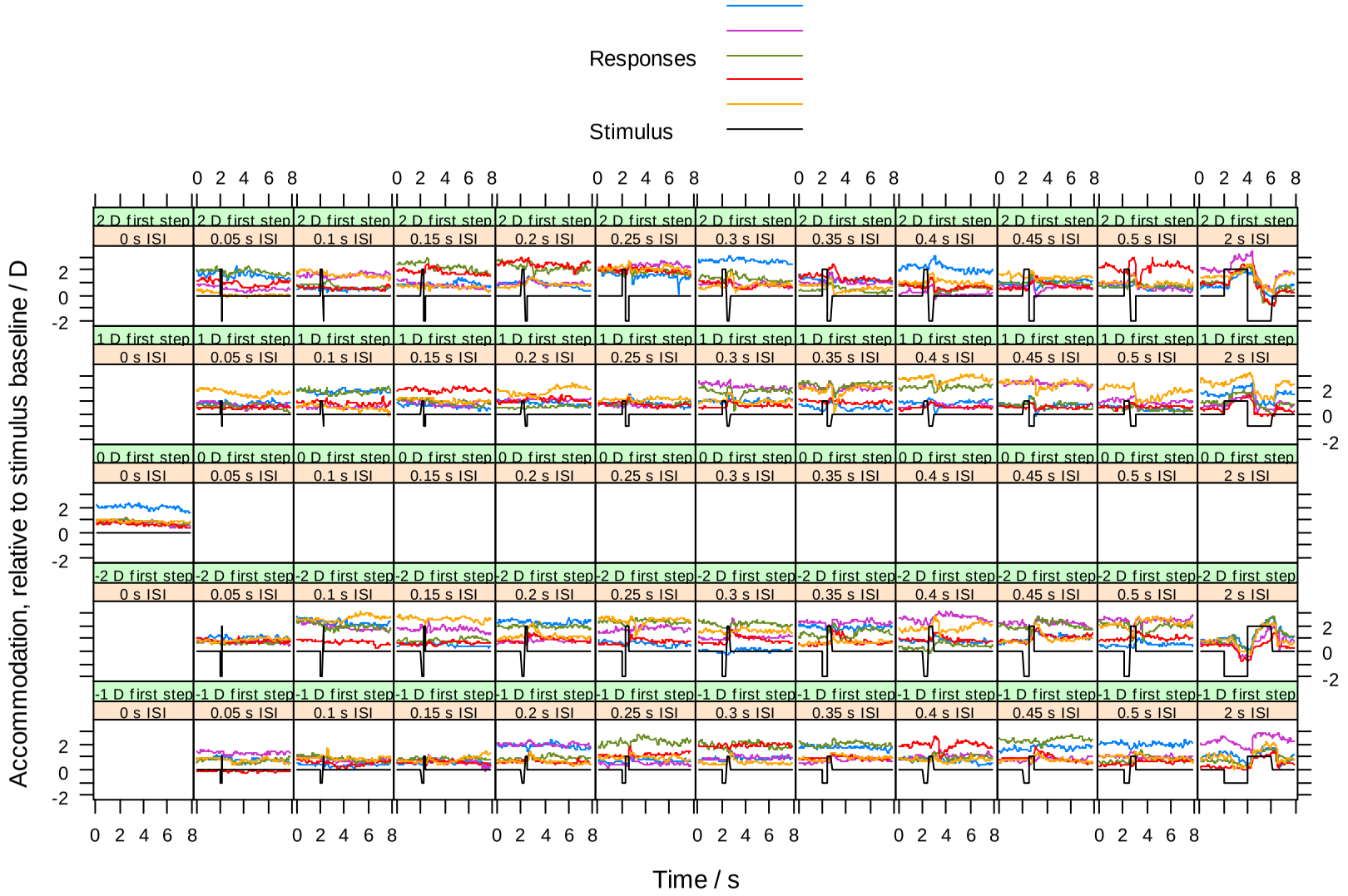

B.2 Histograms of peak AR

Below are the histograms of the peaks in AR, relative to their mean value over the 2 s baseline period, for the square wave in AS. As mentioned in section 6.2.2, there is a resemblance to normality in the distributions of the data (but many samples failed the Shapiro-Wilk test, with $p < 0.1$).

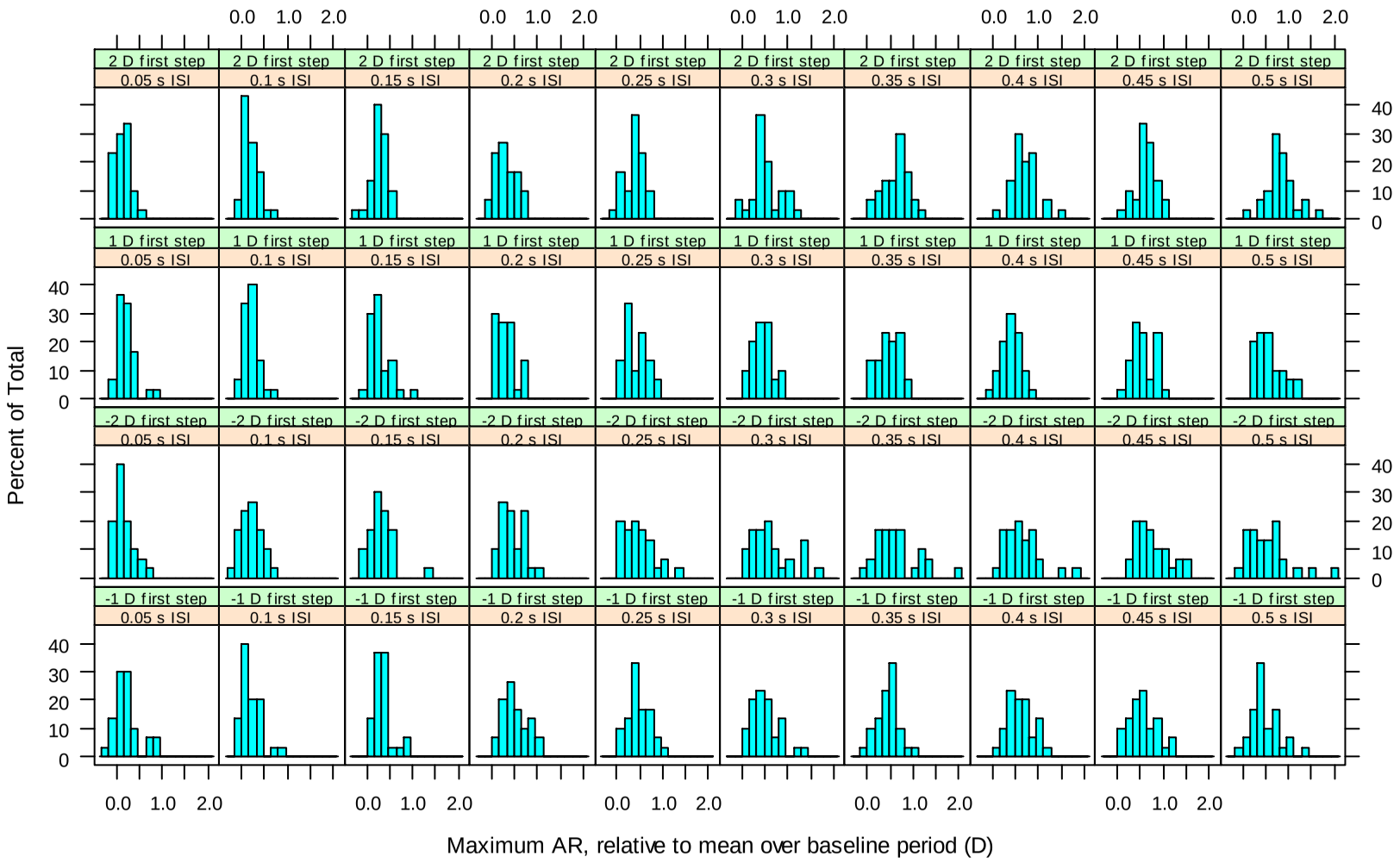
2 D first step
0.05 s ISI
0.1 s ISI
0.15 s ISI
0.2 s ISI
0.25 s ISI
0.3 s ISI
0.35 s ISI
0.4 s ISI
0.45 s ISI
0.5 s ISI
1 D first step
-2 D first step
-1 D first step
0.0 1.0 2.0
0 10 20 30 40
Percent of Total
Maximum AR, relative to mean over baseline period (D)

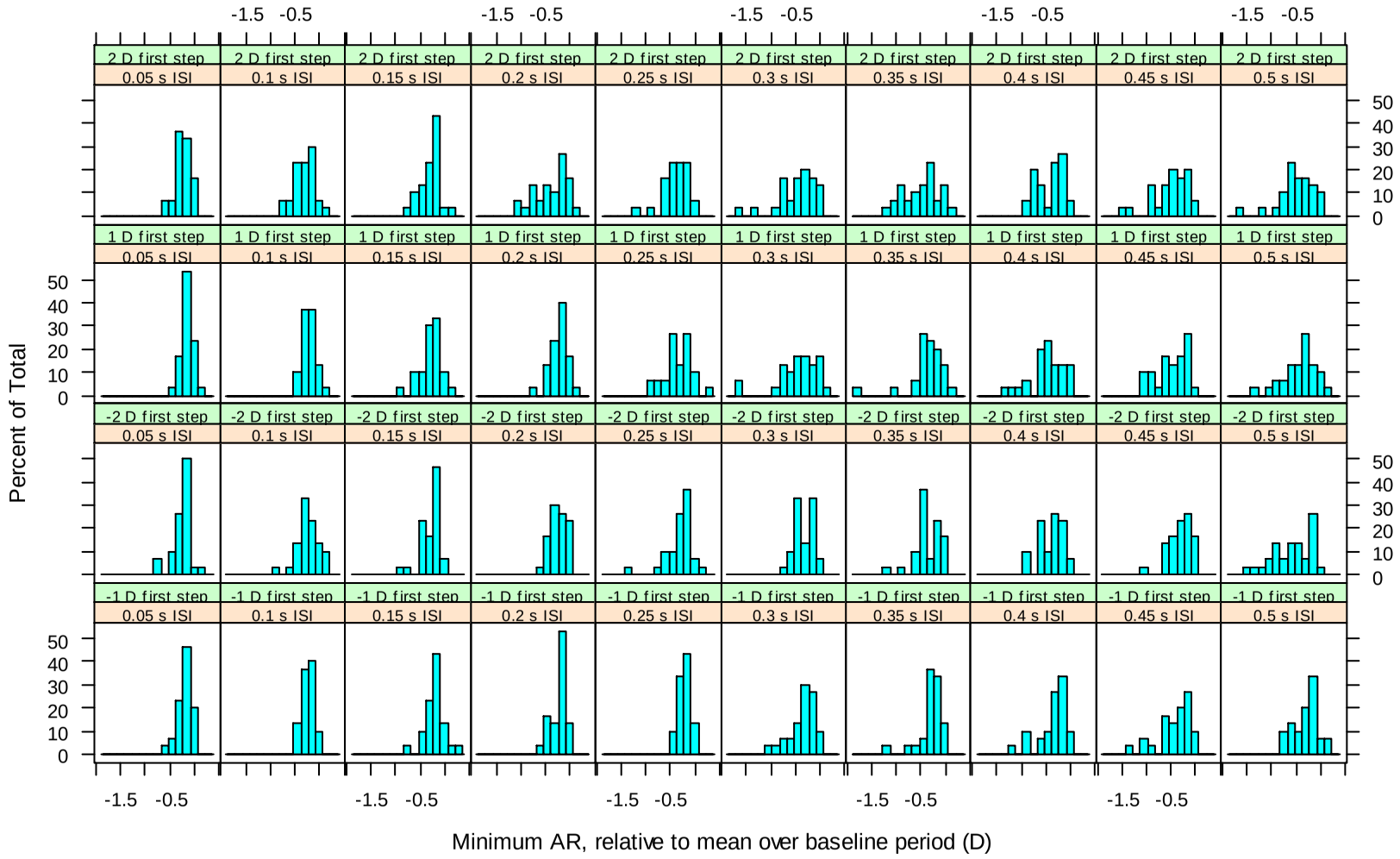
2 D first step
0.05 s ISI
2 D first step
0.1 s ISI
2 D first step
0.15 s ISI
2 D first step
0.2 s ISI
2 D first step
0.25 s ISI
2 D first step
0.3 s ISI
2 D first step
0.35 s ISI
2 D first step
0.4 s ISI
2 D first step
0.45 s ISI
2 D first step
0.5 s ISI
1 D first step
0.05 s ISI
1 D first step
0.1 s ISI
1 D first step
0.15 s ISI
1 D first step
0.2 s ISI
1 D first step
0.25 s ISI
1 D first step
0.3 s ISI
1 D first step
0.35 s ISI
1 D first step
0.4 s ISI
1 D first step
0.45 s ISI
1 D first step
0.5 s ISI
-2 D first step
0.05 s ISI
-2 D first step
0.1 s ISI
-2 D first step
0.15 s ISI
-2 D first step
0.2 s ISI
-2 D first step
0.25 s ISI
-2 D first step
0.3 s ISI
-2 D first step
0.35 s ISI
-2 D first step
0.4 s ISI
-2 D first step
0.45 s ISI
-2 D first step
0.5 s ISI
-1 D first step
0.05 s ISI
-1 D first step
0.1 s ISI
-1 D first step
0.15 s ISI
-1 D first step
0.2 s ISI
-1 D first step
0.25 s ISI
-1 D first step
0.3 s ISI
-1 D first step
0.35 s ISI
-1 D first step
0.4 s ISI
-1 D first step
0.45 s ISI
-1 D first step
0.5 s ISI
-1.5
-0.5
0
10
20
30
40
50
Percent of Total
Minimum AR, relative to mean over baseline period (D)

Appendix C: Implementation of statistical tests using data resampling

C.1 Bootstrap (and plotting with “grid”)

The principle of the bootstrap method of statistical testing was given in section 6.2.2. The script below was used calculate the probabilities of incorrectly rejecting the null hypothesis (max.diff $\not>$ 0 or min.diff $\not<$ 0), before plotting Figure 6-3.

In the control code, and in analysis below, negative step heights increase accommodative demand; the DM is instructed to decrease defocus, to increase the vergence at the eye of light from the stimulus. In the plots and the text of this thesis, this convention is inverted, and positive step heights increase accommodative demand.

```
###### RelAR.stat.peaks.R

##########################################
############# GET DATA FROM FILES! #################
##########################################

library(grid)     # loads “grid “ and “boot” packages
library(boot)     #

# Set up subjects and their directories

subjects <- c("AA", "BB", "CC", "DD", "EE", "FF") # Anonymised
parent.dir <- "C:/Documents and Settings/apcurd/My          Documents/R/DoublePulse"
dirs <- paste(parent.dir, "/", subjects, " 2P 2012-09-18", sep="")

# Get maxima and minima, from start of the stimulus to 1s after,
# and their difference with baseline fluctuations before the stimulus
# Concatenate the data frames of all participants

for(s in 1:length(subjects)) {
        setwd(dirs[s])
        source("load.defocus.array.R")
        source("get.relative.defocus.array.R")
        setwd(parent.dir)
        source("ar.stats.R")            # ar.stats gathers max.diff and min.diff, and
                                        # other results—e.g. response times—
                                        # for each trial
```

```
	plot.data.subj <- cbind(plot.data, subject=subjects[s])
	results.subj <- cbind(results, subject=subjects[s])
	if (s==1) {
		plot.data.main <- plot.data.subj
		results.main <- results.subj
		}
		else {
			plot.data.main <- rbind(plot.data.main, plot.data.subj)
			results.main <- rbind(results.main, results.subj)
		}
}
setwd(parent.dir)
results.main$Durn.s <- results.main$Durn.fs*0.05
results.main <- subset(results.main, Durn.s > 0 & Durn.s < 2)


############## SIGN TEST for median max.diff > 0 or median min.diff < 0
############## not currently used in plotting #############
sign.test.max <- function(peaks) {
		successes <- sum(peaks > 0) # number of "successes" as far as the
binomial test is concerned, i.e. max.diff > 0
		no.trials <- length(peaks)
		p.val <- binom.test(successes, no.trials, alt="g")$p.value # Probability of
finding this many successes (vs. failures) within this many trials, by chance
}

sign.test.min <- function(peaks) {
		successes <- sum(peaks < 0) # number of "successes" as far as the
binomial test is concerned, i.e. min.diff < 0
		no.trials <- length(peaks)
		p.val <- binom.test(successes, no.trials, alt="g")$p.value # Probability of
finding this many successes (vs. failures) within this many trials, by chance
}


################ BOOTSTRAP TEST  for medians #######
## Use percentile intervals as not symmetric #######
## Use 0.9 as “boot” is two-tailed and gives confidence bounds######


# First. a function to use on the medians in bootstrap.
# Simply because boot requires two arguments,
# and indices can be one of them.

med.for.boot <- function(dat,ind) {
	median(dat[ind])
}

# Now, is zero outside the relevant end of the 90% confidence interval?
# If so, change the point symbol for the graph

boot.test <- function(dat, type) {
	boot.obj <- boot(dat, med.for.boot, R=10000)
	bounds <- boot.ci(boot.obj, type="bca", conf=0.9)$bca
		# first used type="perc"
```

```
                # $percent gives conf, rank_lower quantile, rank_upper quantile, lower
bound conf int , upper bound conf int
                # $bca the same, but when using "bca"

        if (type=="max") {
                if (bounds[4] > 0) pch <- 0
                else pch <- 19 # pch is the point symbol for the graph
        }
        else {
                if (bounds[5] < 0) pch <- 0
                else pch <- 19
        }
}

########### POINT SYMBOLS FOR GRAPHS ############
## i.e. if p < 0.05, give it the significant symbol ##
## Not currently used in plotting ##

pch.func <- function(p.value){
        if(p.value < 0.05) pch <- 0
        else pch <- 19
}


### PUT STATISTICS IN TABLE

# Take medians, combining participants

med.max.AR <- aggregate(ar.maxima ~ Durn.s * Amp, data=results.main,
        median) # aggregate has default: na.action=na.omit
med.min.AR <- aggregate(ar.minima ~ Durn.s * Amp, data=results.main,   median)

# Do sign tests (the sign test results are currently unused)

p.max.diff.med <- aggregate(max.diff ~ Durn.s * Amp, data=results.main,
        sign.test.max)
p.min.diff.med <- aggregate(min.diff ~ Durn.s * Amp, data=results.main,
        sign.test.min)

# Convert p.values to point symbols
# (again, these are not used in the end, but the columns have stayed in,
# so that all.peaks.with.p works (just below),
# and contains the info if desired later)

p.max.diff.med <- cbind(p.max.diff.med, pch=sapply(p.max.diff.med$max.diff,
        FUN=pch.func))
p.min.diff.med <- cbind(p.min.diff.med, pch=sapply(p.min.diff.med$min.diff,
        FUN=pch.func))

# Set up data frame with medians and ready for p-values from bootstrap test

all.peaks.with.p <- cbind(med.max.AR,         p.max.diff.med=p.max.diff.med$max.diff,
        p.max.diff.pch=p.max.diff.med$pch, pch.max.boot=0,
        ar.minima=med.min.AR$ar.minima,   p.min.diff.med=p.min.diff.med$min.diff,
        p.min.diff.pch=p.min.diff.med$pch, pch.min.boot=0)
```

```
# Do bootstrap tests

for (r in 1:dim(all.peaks.with.p)[1]) {

        # On max.diff

        dat <- subset(results.main,
                Amp==all.peaks.with.p$Amp[r] &
                Durn.s==all.peaks.with.p$Durn.s[r])$max.diff

        all.peaks.with.p$pch.max.boot[r] <- boot.test(dat, "max")

        # On min.diff

        dat <- subset(results.main,
                Amp==all.peaks.with.p$Amp[r] &
                Durn.s==all.peaks.with.p$Durn.s[r])$min.diff

        all.peaks.with.p$pch.min.boot[r] <- boot.test(dat, "min")
}

##############################################
############# PLOT!! ####################
##############################################

plot.data <- all.peaks.with.p

####### Main viewport
pushViewport(viewport(name="main", width=unit(14, "centimetres"),
        height=unit(19, "centimetres"), gp=gpar(fontsize=10)))
#grid.rect()

## Heights of graph viewports in centimetres
height.top <- 9
height.bottom <- 9

##### Four viewports - one for each graph
pushViewport(viewport(width=unit(7, "centimetres"), height=unit(height.bottom,
        "centimetres"), x=unit(1, "npc"), y=unit(0,"npc"), just=c("right","bottom"),
        name="rightbottom")) # create viewport for the right-hand cell of the
        layout
#grid.rect()
upViewport() # return to main viewport

pushViewport(viewport(width=unit(7, "centimetres"), height=unit(height.bottom,
        "centimetres"), x=unit(0, "npc"), y=unit(0,"npc"),  just=c("left","bottom"),
        name="leftbottom")) # create viewport for the left-hand cell of the layout
#grid.rect()
upViewport()

pushViewport(viewport(width=unit(7, "centimetres"), height=unit(9,
        "centimetres"), x=unit(0, "npc"), y=unit(height.bottom, "centimetres"),
        just=c("left", "bottom"), name="lefttop"))
#grid.rect()
upViewport()
```

```
pushViewport(viewport(width=unit(7, "centimetres"), height=unit(9,
        "centimetres"), x=unit(1, "npc"), y=unit(height.bottom, "centimetres"),
        just=c("right", "bottom"), name="righttop"))
#grid.rect()

margins <- c(5,4.5,0,0)
xrange <- c(0,0.5)
xax <- seq(0,0.5,by=0.1)
yrange <- c(-0.75,1)
yax <- seq(-.75,1,by=0.25)
no.xpoints <- 10 # 10 for no 0 or 40 frame-point

pushViewport(plotViewport(margins=c(3.5,2.5,0,0), name="RTplotarea"))
        # create plot area with margins at right-top
pushViewport(dataViewport(xrange, yrange, name="RTaxes")) # axes area

seekViewport("rightbottom") # go to the RB
pushViewport(plotViewport(margins=c(5,2.5,0,0), name="RBplotarea"))
pushViewport(dataViewport(xrange, yrange, name="RBaxes"))

seekViewport("leftbottom") # go to the LB
pushViewport(plotViewport(margins=margins, name="LBplotarea"))
pushViewport(dataViewport(xrange, yrange, name="LBaxes"))

seekViewport("lefttop") # go to the LT
pushViewport(plotViewport(margins=c(3.5, 4.5,0,0), name="LTplotarea"))
pushViewport(dataViewport(xrange, yrange, name="LTaxes"))


############# SOME PARAMETERS TO BE USED LATER ##################

letteringsize <- 9
titlepos <- unit(yrange[2]+0.05,"native")
titlegpar <- gpar(fontsize=letteringsize, fontface="bold")
#plot.data$Durn.s <- plot.data$Durn.fs*0.05
pointsymbol <- 19
pointsize <- unit(5, "points")
xlabel <- "ISI (s)"
ylabel <- paste("Peaks in AR, relative to baseline average (D)")
axisgpar <- gpar(fontsize=letteringsize, lwd=0.5)
labgpar <- gpar(fontsize=letteringsize)
pointsgpar <- gpar(lwd=0.5)
minus.sign <- intToUtf8(0x2212)


# get data into best order for plotting
plot.data.neg1 <- subset(plot.data, Amp==-1)
pointsymbol.neg1 <- c(plot.data.neg1$pch.max.boot,
        plot.data.neg1$pch.min.boot)

plot.data.neg2 <- subset(plot.data, Amp==-2)
pointsymbol.neg2 <- c(plot.data.neg2$pch.max.boot,
        plot.data.neg2$pch.min.boot)

plot.data.pos1 <- subset(plot.data, Amp==1)
```

```
pointsymbol.pos1 <- c(plot.data.pos1$pch.max.boot,
        plot.data.pos1$pch.min.boot)

plot.data.pos2 <- subset(plot.data, Amp==2)
pointsymbol.pos2 <- c(plot.data.pos2$pch.max.boot,
        plot.data.pos2$pch.min.boot)

#########################################################################
###############
#############********** Left-top: 1D, towards first (-1D)
*****************##################
#########################################################################

seekViewport("LTaxes")
# Set LHS axes for NEGATIVE INITIAL PULSE
grid.xaxis(at=xax, label=F, name="LTxaxis", gp=axisgpar)
grid.yaxis(at=yax, name="LTyaxis", gp=axisgpar)

# y-label for whole set of graphs
grid.text(ylabel, x=unit(-4.5, "lines"), y=unit(0, "npc"), rot=90, name="ylabel",
        gp=labgpar) # y label

# x points
x <- rep(plot.data.neg1$Durn.s, times=2)

# Draw points
grid.points( x, c(plot.data.neg1$ar.maxima, plot.data.neg1$ar.minima),
        default.units="native",
        pch=pointsymbol.neg1, size=pointsize,
        gp=pointsgpar
        )

# Add title
grid.text("AS increased first\nAmplitude 1D", y=titlepos, just="bottom",      gp=titlegpar)

#########################################################################
###############
#############********** Right-top: 2D, towards first (-2D)
*****************##################
#########################################################################

seekViewport("RTaxes")
# Set LHS axes for NEGATIVE INITIAL PULSE
grid.xaxis(at=xax, label=F, name="RTxaxis", gp=axisgpar)
grid.yaxis(at=yax, label=F, name="RTyaxis", gp=axisgpar)

# Draw points
grid.points( x, c(plot.data.neg2$ar.maxima, plot.data.neg2$ar.minima),
        default.units="native",
        pch=pointsymbol.neg2, size=pointsize,
        gp=pointsgpar
        )

# Add title
grid.text("AS increased first\nAmplitude 2D", y=titlepos, just="bottom",      gp=titlegpar)
```

```
##########################################################################
#############
#############********** Left-bottom: 1D, away first (+1D)
*****************##################
##########################################################################

### Set RHS axes for POSITIVE INITIAL PULSE
seekViewport("LBaxes")
grid.xaxis(at=xax, name="LBxaxis", gp=axisgpar)
grid.yaxis(at=yax, name="LByaxis", gp=axisgpar)

# Add title
grid.text("AS decreased first\nAmplitude 1D", y=titlepos, just="bottom",      gp=titlegpar)

# Draw points
grid.points( x, c(plot.data.pos1$ar.maxima,plot.data.pos1$ar.minima),
          default.units="native",
          pch=pointsymbol.pos1, size=pointsize,
          gp=pointsgpar
          )

upViewport()

# x-label for whole set of graphs
grid.text(xlabel, x=unit(1, "npc"), y=unit(-3.5,"lines"), name="xlabel",          gp=labgpar)
# x label

##########################################################################
#############
#############********** Right-bottom: 2D, away first (+2D)
*****************##################
##########################################################################

### Set RHS axes for POSITIVE INITIAL PULSE
seekViewport("RBaxes")
grid.xaxis(at=xax, name="RBxaxis", gp=axisgpar)
grid.yaxis(at=yax, label=F, name="RByaxis", gp=axisgpar)

# Add title
grid.text("AS decreased first\nAmplitude 2D", y=titlepos, just="bottom",      gp=titlegpar)

# Draw points
grid.points( x, c(plot.data.pos2$ar.maxima,plot.data.pos2$ar.minima),
          default.units="native",
          pch=pointsymbol.pos2, size=pointsize,
          gp=pointsgpar
          )
```

C.2 Permutation tests

This function was written to perform the permutation test described in section 6.2.2.

```
perm.test.medians <- function(y0, y1) {

        med.diff0 <- median(y1) - median(y0)
        conc <- c(y0,y1)
        index <- 1:length(conc)
        reps <- numeric(R)
        for ( i in 1:R) {
                choice <- sample(index, size=length(y0), replace=F)
                yA <- conc[choice]
                yB <- conc[-choice]
                reps[i] <- median(yB)-median(yA)
                }
        p <- mean( c(med.diff0, reps) <= med.diff0)
        if (p<=0.5) p <- 2*p
                else p <- 2*(1-p)

}
```

Appendix D: Smoothed velocity of accommodation

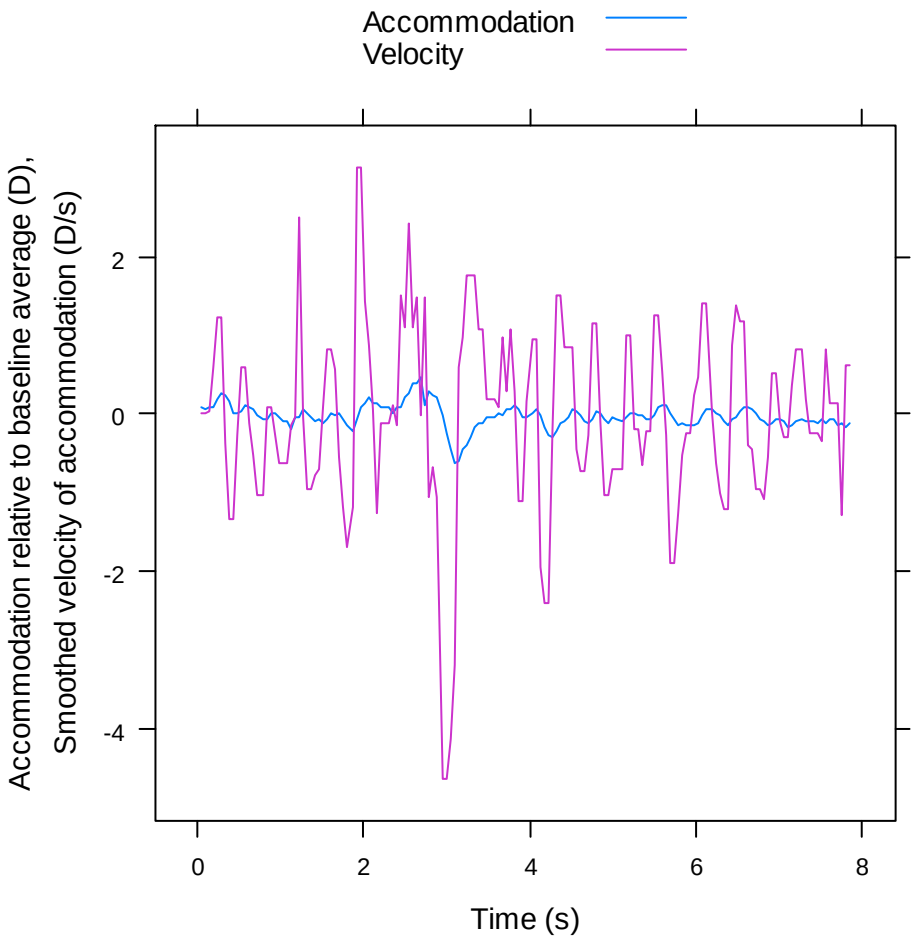

This is the AR in the trial of Figure 6-1 (right-hand side), also with a smoothed velocity trace (time course of accommodative stimulus: one period of a square wave lasting 0.4 s, starting at 2 D; initial step of +2 D occurring at 2 s). The instantaneous velocities were calculated and then smoothed over 0.1 s, as in Bharadwaj and Schor (2005). A running median of three frames was used for the smoothing. (The accommodation data of Bharadwaj and Schor were collected at 200 Hz, allowing more effective smoothing over 100 ms than with our data taken at 20 Hz.)

This trial produced a clear double response in accommodation, but the maximum in smoothed positive velocity still occurred at just before 2 s through

the trial. I.e. it appears within the baseline microfluctuations and is not relevant to the response to the square wave stimulus. The maximum in smoothed negative velocity in this case occurred in the expected interval, between the two peaks in accommodation.

In other trials, the maxima and minima in smoothed velocity were also found in the natural microfluctuations after the stimulus and accommodative response had returned to their baseline level. The peak velocity between the two peaks in the accommodation response was sometimes weaker than peaks during the natural microfluctuations.

It was decided that extracting peaks in these smoothed velocities may not represent the true velocities very well. In the extreme case, trials with no real response to the stimulus would still produce high velocities within the natural fluctuations of accommodation.

Smoothing over a longer time period is unsatisfactory, since it would smooth over significant intervals compared with the timescale of the responses. Fitting the accommodation response with an analytical function, and calculating velocity from that function (Kasthurirangan and Glasser, 2005), may be more satisfactory. Choosing the appropriate function may be challenging.